Understanding the Molecular Basis of Disease Resistance Against Septoria Tritici Blotch in Wheat

Christopher Stephens (MSc)

Thesis submitted to the University of Nottingham for the degree of

Doctor of Philosophy

November 2021

Acknowledgements

First of all, I would like to share my sincere thanks for the tireless patience, advice, direction and support of my supervisors Jason Rudd and Kostya Kanyuka. It has been a privilege to work with you and with the Wheat Pathogenomics Team. There are too many other researchers and students at Rothamsted and elsewhere who have helped and advised me over the course of my project to name here, but I hope I have adequately acknowledged their contributions within the individual chapters. Thanks also to the other PhD students within the WPT team: Claire Kanja, Alina Igna, Catherine Walker, my fellow PhD cohort members Tania Chancellor and Hannah Blyth, for all their support, friendship and technical help over the years.

Thanks to all of my colleagues at Rothamsted for providing a wonderful atmosphere in which to work and live. I am very happy to say that I have made lifelong friendships here and I like to think that we have all left our mark on the institute. Again, there are too many of you to name everyone here, but special mentions should go to Niall and Dana MacGregor, Ewan Richardson and Tom David, as well as Sarah Foster, Erika Kroll and Chiara Zafferri for taking over various sports and social clubs. I hope to see you all over a board game, football pitch or a pint very soon.

Finally, I would like to thank some of my best friends. George, Liam, Avani, Sara, Andy, Charlie and Tristram I feel incredibly fortunate to have you all as friends. To my family and my wonderful partner Helen, thank you for feigning interest for all the hours that I have bored you with science-talk, and for encouraging me to finish this project. I could not have done it without you.

Abstract

Zymoseptoria tritici, a fungal pathogen of wheat and the causal agent of Septoria Tritici Blotch (STB), is a particular challenge to wheat production on a global level, causing crop losses of up to 50% in some cases. Genetic resistance presents an effective way of controlling STB in wheat, with numerous resistance loci having been identified. *Stb6*, which encodes a wall-associated kinase-like protein and confers resistance to *Z. tritici* isolates expressing the corresponding AvrStb6 effector, has recently been cloned. However, many questions regarding *Stb6*-mediated resistance remain unanswered. The global frequency of avirulence *AvrStb6* alleles in modern *Z. tritici* populations remains unknown. The role that AvrStb6 plays in *Z. tritici* pathogenicity, the nature of its interaction with Stb6 and the mechanism by which *Stb6* confers resistance are also yet to be elucidated.

In the following thesis, I present data indicating a dramatic shift in the frequency of virulence AvrStb6 isoforms in modern *Z. tritici* populations, relative to previous studies. Transient expression of fluorophore-tagged Stb6 and AvrStb6 in the tobacco species *Nicotiana benthamiana* also revealed that AvrStb6 localises to the apoplast. Stb6 displays an unusual cellular localisation pattern, being present in both the plasma membrane but also identified in the cell wall and in hectian strands adjoining the two. Expression of Stb6 in *N. benthamiana* induces a kinase-dependent cell death phenotype, which is independent of the co-receptor BAK1. I also report on the identification of candidate protein interactors for Stb6 and AvrStb6. Both interactors are predicted to be chloroplast-localised. These findings present an intriguing hypothesis as to the possible mechanism of *Stb6*-mediated resistance. This study therefore represents an important contribution to our understanding of evolutionary genetics in a plant pathogen, provides a putative mechanism for AvrStb6 in pathogenicity and has also potentially identified a completely novel resistance mechanism for an immune receptor protein. Research such as this plays a role in helping develop more productive crop plants with improved genetic resistance to pathogens.

Table of contents

List of Figures

List of Tables

List of abbreviations

3-AT = 3-amino-1,2,4-triazol

Avr gene/protein = Avirulence gene/protein

BSA = Bovine serum albumin

BSMV = *Barley stripe mosaic virus*

CDPK = calcium-dependant protein kinase

Co-IP = Co-immunoprecipitation

CSIR = Cell surface-localised immune receptor

cv. = Cultivar

CWDE = Cell wall-degrading enzyme

DAMP = Damage-associated molecular pattern

dpi = Days post inoculation

EGF = Epidermal growth factor domain

EGF-Ca = Epidermal growth factor, calcium-binding domain

ETI = Effector-triggered immunity

ETS = Effector-triggered susceptibility

GC = Guanylyl cyclase motif

GFP = GREEN FLUORESCENT PROTEIN

GUB_WAK_bind = Galacturonan-binding domain

hpi = Hours post inoculation

HR = Hypersensitive response

HST = Host-specific toxin

IIR = Intracellular immune receptor

IP = Immunoprecipitation

LRR = Leucine-rich repeat

LysM = Lysin motif

MAPK = Mitogen-activated protein kinase

mRFP = Monomeric RED FLUORESCENT PROTEIN

NB-LRR (or NLR) = Nucleotide-binding leucine-rich repeat protein

NLP = NECROSIS AND ETHYLENE-INDUCING PEPTIDE 1-LIKE PROTEIN

OGs = Oligogalacturonides

PAMP = Pathogen-associated molecular pattern

PCD = Programmed cell death

PRR = Pattern recognition receptor

PSI/II = Photosystem I/II

PTI = PAMP-triggered immunity

R gene/protein = Resistance gene/protein

RD = Arginine-aspartate motif

RIPS = Repeat-induced point mutations

RLCK = Receptor-like cytoplasmic kinase

RLK = Receptor-like protein kinase

RLP = Receptor-like protein

ROS = Reactive oxygen species

RT-qPCR = Reverse transcriptase-quantitative polymerase chain reaction

SC-LT/LTH = Complete supplement media lacking leucine and tryptophan/leucine, tryptophan and histidine

SDS-PAGE = Sodium dodecyl sulphate-polyacrylamide gel electrophoresis

SP = Signal peptide

STB = Septoria tritici blotch

TBS = TRIS-buffered saline

TE = Transposable element

Thf1 = THYLAKOID FORMATION 1 (*syn*. ToxABP)

TILLING = Targeting induced local lesions In genome

TM = Transmembrane domain

ToxABP = TOXA-BINDING PROTEIN 1

VIGS = Virus-induced gene silencing

VOX = Virus-induced overexpression

WAK = Wall-associated receptor-like kinase

Y2H = Yeast two-hybrid

Chapter 1: General Introduction

1.1 Summary

With the requirement to breed ever more productive crop plants to feed a growing global population, compounded by increasingly wide-spread resistance to pesticides exhibited by pathogens, plant immunity is becoming an increasingly important area of research. Of the genes that confer or contribute to disease resistance, the wall-associated receptor-like kinases (WAKs) are increasingly shown to play a major role, in addition to their contribution to plant growth and development or tolerance to abiotic stresses. Being transmembrane proteins, WAKs form a central pillar of a plant cell's ability to monitor and interact with their extracellular environments. WAKs contribute to plant immunity in a variety of ways. Some act as cell surface-localised immune receptors recognising either pathogen- or plant-derived invasion molecules (e.g. effectors or damage-associated molecular patterns, respectively). Others promote innate immunity through cell wall modification and strengthening, thus limiting pathogen intrusion. A recently identified WAK-like gene in wheat, *Stb6*, confers resistance to the fungal pathogen *Zymoseptoria tritici* in a gene-for-gene manner. However, the breadth of effectiveness of *Stb6* in field conditions globally, whether Stb6 directly interacts with the corresponding *Z. tritici* effector AvrStb6 and what mechanisms *Stb6*-mediated defence utilises are all currently unknown.

1.2 Acknowledgment of contributions

Sections 1.3 to 1.4.7 of this chapter are adapted from the manuscript "WAKsing plant immunity, waning diseases" published by the Journal of Experimental Botany in September 2021 (https://doi.org/10.1093/jxb/erab422). Editing and feedback on the structure of this review was provided by Kostya Kanyuka and Kim E. Hammond-Kosack.

1.3 Plant immunity

Phytopathogens are an endemic issue in modern agriculture, accounting for a significant proportion of lost yield, estimated to be up to 15% of crop production in some cases (Schwessinger *et al.*, 2015). Recent restrictions on pesticide use (Jess et al., 2014) and the emergence of resistance to those pesticides (Cools and Fraaije, 2008), combined with the requirement to feed a growing global population, make the study of plant immunity an area of increasing importance. The genetic basis for immunity in plants was first demonstrated by Flor *et al.* (1971) with the characterisation of the gene-for-gene interaction between a plant disease resistance gene and a corresponding pathogen avirulence gene. The cloning of genetic factors underpinning immunity began in the 1990s with the isolation of *Hm1* in maize, which confers resistance to a race of the fungus *Cochliobolus carbonum* (Johal and Briggs, 1992). Discoveries such as this led to the formulation of the zig-zag model (Jones & Dangl, 2006), which proposed two seemingly distinct branches of immunity: pathogen-associated molecular pattern (PAMP) triggered immunity (PTI) and effector-triggered immunity (ETI). PTI is moderated by extracellular pattern recognition receptors (PRRs) which detect conserved molecules such as fungal chitin and bacterial flagellin, and provides broad spectrum resistance to non-adapted potential pathogens. By contrast, ETI is conferred by cytoplasmic resistance proteins which detect pathogen-specific secreted effector proteins either directly or through modifications of host proteins targeted by effectors (van der Biezen and Jones, 1998), and provides resistance to adapted pathogens.

In recent years this binary model of plant immunity has been challenged (Thomma *et al.*, 2011), with the discovery of conserved effectors such as Ecp2 and narrowly distributed PAMPs such as Pep-13 (Brunner *et al.*, 2002, Lauge *et al.*, 2000). New discoveries such as this has inspired the proposal of revised models. Cook *et al.* (2015) proposed to recognise all microbial and host damage-derived molecules as invasion patterns, which are detected by the invasion pattern receptors, with all interactions existing on a spectrum of invasion pattern conservation and the strength of the immune response. This

model has since been further refined to include a spatial dimension for the recognition of invasion molecules by immune receptors in the apoplast vs cytosol, and simplified to cover interactions of plants only with their adapted pathogens (Kanyuka & Rudd, 2019). This Spatial Invasion Model elevated the importance of Cell Surface-localised Immune Receptors (CSIRs), membrane-bound proteins with extracellular domains involved in the recognition of apoplastic invasion molecules, above the level of a first line of defence, as the diversity and complexity of this class of proteins becomes better understood.

The first CSIR identified was Xa21 of rice, a receptor-like protein kinase (RLK) which confers resistance to the bacterial pathogen *Xanthomonas oryzae* pv. *oryzae* (*Xoo*; Song *et al.*, 1995). The model plant *Arabidopsis thaliana* (hereafter referred to as Arabidopsis) RLKs, such as FLAGELLIN-SENSITIVE 2 (FLS2; Gomez-Gomez & Boller, 2000) and ELONGATION FACTOR TU RECEPTOR (EFR; Zipfel *et al.*, 2006) were shown to interact with flg22 and elf18 peptides derived from the conserved bacterial proteins FLAGELLIN and ELONGATION FACTOR THERMO UNSTABLE (EF-Tu), respectively. Meanwhile, CHITIN ELICITOR RECEPTOR KINASE 1 (CERK1) in Arabidopsis (Miya *et al.*, 2007) and CHITIN ELICITOR-BINDING PROTEIN (CEBiP) in rice (Kaku *et al.*, 2006) recognise fungal chitin-derived oligosaccharides. Numerous RLKs and receptor-like proteins (RLPs), which are similar to RLKs but possess no intracellular kinase domain, have now been identified as CSIRs that recognise a wide range of invasion molecules. CSIRs could be grouped into several classes primarily based on the presence of specific motifs in their extracellular domains, including leucine-rich repeat (LRR) containing receptors (e.g. FLS2) which detect proteinaceous invasion molecules, lysin motif (LysM) containing receptors (e.g. CERK1) which bind carbohydrates, and G-type lectin-containing receptors (e.g. I-3) which are capable of binding both glycans and proteins (Bouwmeester & Govers, 2009).

Detection of invasion molecules by CSIRs and the corresponding immune response mechanisms they activate are complex and highly regulated. In Arabidopsis, FLS2 and EFR require SOMATIC EMBRYOGENESIS RECEPTOR-LIKE KINASE (SERK) coreceptors such as BRASSINOSTEROID INSENSITIVE 1-ASSOCIATED RECEPTOR KINASE 1 (BAK1; Roux *et al.*,

2011) for immune signalling. Signalling pathways for some CSIRs have been very well characterised and involve signal transfer to RECEPTOR-LIKE CYTOPLASMIC KINASES (RLCKs; Lu *et al.*, 2010) and propagation by MITOGEN-ACTIVATED PROTEIN KINASE (MAPK) cascades (Asai *et al.*, 2002), influx of Ca^{2+} and associated activation of CALCIUM-DEPENDENT PROTEIN KINASES (CDPKs; Ranf *et al.*, 2014) leading to the induction of reactive oxygen species (ROS; Kadota *et al.*, 2014) and WRKY transcription factors (Lal *et al.*, 2018) and upregulation of immune-related genes (Albert *et al.*, 2020). Stable genetic transformation (Schwessinger *et al.*, 2015) or engineering chimeric CSIR proteins (Holton *et al.*, 2015, Thomas *et al.*, 2018, Wu *et al.*, 2019) has been utilised to express CSIRs from model plants in crop species to engineer increased disease resistance. This has demonstrated the versatility and breadth of CSIR-mediated immunity and its potential utility in providing resistance to plant pathogens in agriculture.

One class of CSIRs, wall-associated kinases or WAKs, are a class of RLKs only now coming into focus as major players in plant immunity (Kanyuka & Rudd, 2019). A greater understanding of this gene family can help further elucidate the role of CSIRs in plant immunity, as well as providing a host of new candidate genes for contribution to disease resistance.

1.4 Wall-associated kinases (WAKs)

WAKs represent a significant sub-group of the RLK family. As for other RLKs, WAKs possess an intracellular kinase domain, a transmembrane helix and an extracellular region characterised by the presence of sub-group specific domains including those potentially mediating interactions with the cell wall. Some WAKs have functions in plant immunity, while others play roles in growth and development (Wagner & Kohorn, 2001) or in tolerance to abiotic stresses such as heat, salt and heavy metals (Hou *et al.*, 2005, Sivaguru *et al.*, 2003, Wang *et al.*, 2019, Yin & Hou, 2017, Zhang *et al.*, 2019). Here, we will focus primarily on the role played by WAKs in defence against pathogens.

Arabidopsis *WALL-ASSOCIATED KINASE-1* (*AtWAK1*) was the first WAK-encoding gene identified (He *et al.*, 1996) and is part of a small gene cluster

located on chromosome 1 (He *et al.*, 1999). A total of 22 genes were found to encode WAKs in the Arabidopsis genome (Verica & He, 2002). The AtWAK1 protein was isolated from fractions of digested cell wall, suggesting a strong cell wall interaction *in vivo* (He *et al.*, 1996). It was subsequently demonstrated that the extracellular domain of AtWAK1 is indeed covalently linked with the pectin component of the cell wall (Anderson *et al.*, 2001). This direct connection between the cell wall and the cytosol, through the kinase domain, along with a short rosette leaves phenotype observed in the transgenic antisense *AtWAK1* and *WALL-ASSOCIATED KINASE-2* (*AtWAK2*) Arabidopsis plants, revealed a role for these genes in leaf cell expansion (Anderson *et al.*, 2001, Lally *et al.*, 2001, Kohorn *et al.*, 2006, Wagner & Kohorn, 2001). AtWAK1 was also shown to bind with high affinity to oligogalacturonides (OGs), oligomers of α-1,4–linked galacturonic acid, derived from cell wall pectin and released during cell wall loosening and expansion, or due to the action of pathogen-derived cell wall degrading enzymes (CWDEs) during infection (Decreux & Messiaen, 2005). OGs have long been understood as elicitors of plant defence, acting as damage-associated molecular patterns (DAMPs; Nothnagel *et al.*, 1983), and downstream defence signalling in response to OGs has been a subject of intense research (Ferrari *et al.*, 2013). Expression of *AtWAK1* was also shown to be upregulated by salicylic acid (SA) and wounding (He *et al.*, 1998, Wagner & Kohorn, 2001). The direct interaction between AtWAK1 and OGs and the important role for AtWAK1 in plant immunity was first demonstrated in elegant experiments involving transgenic Arabidopsis plants expressing a chimeric receptor-like protein comprising an AtWAK1 ectodomain and a cytoplasmic EFR kinase domain (Brutus *et al.*, 2010). Treatment of these plants with OGs induced an EFR kinase-mediated defence response. Furthermore, transgenic Arabidopsis plants ectopically expressing *AtWAK1* had enhanced resistance to the necrotrophic fungus *Botrytis cinerea* compared to the wild-type, confirming a role for *AtWAK1* in plant immunity (Brutus *et al.*, 2010). Two other WAKs identified in Arabidopsis are strongly implicated in plant immunity. One is RESISTANCE TO FUSARIUM OXYSPORUM-1 (RFO1), which was shown to confer quantitative resistance to necrotrophic root pathogens *Fusarium oxysporum* and *Verticillium longisporum* (Diener & Ausubel, 2005). The other is WALL-ASSOCIATED KINASE-LIKE-10 (AtWAKL10), which contributes to

resistance to *Pseudomonas syringae*, with transgenic Arabidopsis lacking this WAK demonstrating increased susceptibility to this bacterial pathogen compared to the wild-type (Bot *et al.*, 2019).

Immunity-related WAKs have been identified in other model and crop plant species, including the dicots tomato (*Solanum lycopersicum*), cotton (*Gossypium hirsutum*) and oilseed rape (*Brassica napus*), and the monocot crops wheat (*Triticum aestivum*), rice (*Oryza sativa*), maize (*Zea mays*) and barley (*Hordeum vulgare*) (Table 1.1). Several of these confer resistance to Ascomycete fungi of the Dothideomycetes class, which have either hemibiotrophic or latent necrotrophic lifestyles. However, WAKs conferring resistance to bacteria or fungal pathogens belonging to other classes have also been identified. The pathogens controlled by WAKs may have broad host ranges, (e.g. *P. syringae*; Rosli *et al.*, 2013) or are restricted to a single plant species (e.g. *Sporisorium reilianum*; Zuo *et al.*, 2015). Moreover, WAKs were shown to be involved in defence against both extracellular pathogens (Saintenac *et al.*, 2018) and those which penetrate host cells (Li *et al*., 2009). A WAK-mediated resistance against the floral diseases such as Fusarium head blight (Gadaleta *et al*., 2019), root diseases such as blackleg (Larkan *et al*., 2020), and foliar diseases such as Northern corn leaf blight (Hurni *et al*., 2015) have all been documented (Table 1.1).

1.4.1 Domain architecture of WAK proteins

Similar to other proteins belonging to the RLK superfamily, WAKs comprise an extracellular region, a transmembrane-spanning domain and an intracellular kinase domain (Figure 1.1). The extracellular regions of the WAK family show the highest diversity (Verica *et al.*, 2003) and contain the galacturonan-binding (GUB_WAK_bind) domain and, frequently, one or more additional domains. The intracellular regions of WAK proteins, which contain a kinase domain, appear to be more conserved.

The GUB_WAK_bind domain is implicated in the binding to pectin in the extracellular cell wall matrix. Indeed, AtWAK1 has been shown to form both covalent and ionic bonds with pectin and to remain firmly bound to the cell wall following plasmolysis. Some WAKs characterised from other plant species,

such as rice WALL-ASSOCIATED KINASE-1 (OsWAK1; Li *et al.*, 2009), WALL-ASSOCIATED KINASE-25 (OsWAK25; Jo *et al.*, 2011) and XANTHOMONAS ORYZAE PV. ORYZAE RESISTANCE 4 (Xa4; Hu *et al*., 2017), have also been shown to localise to the cell wall. However, other WAK proteins, such as WALL-ASSOCIATED KINASE-5 (TaWAK5) of wheat (Yang *et al*., 2014) and WALL-ASSOCIATED KINASE-RECEPTOR LIKE KINASE-1 (ZmWAK-RLK1/ZmHtn1; Yang *et al.*, 2019) and WALL-ASSOCIATED KINASE (ZmWAK/qHSR1; Zuo et al., 2015) of maize, have been shown to separate from the cell wall and retract with the plasma membrane following plasmolysis, suggesting a lack of covalent binding to the cell wall pectin. Interestingly, the rice WALL-ASSOCIATED KINASE-91 (OsWAK91/OsDEES1; Wang *et al*., 2012) could be found in both the plasma membrane and the cell wall, as well as within the hectian strands connecting the two following plasmolysis. The exact mechanism by which WAKs and pectin interact, and what determines strong binding with the cell wall, is yet to be fully understood (Kohorn, 2016) although amino acids such as lysine and arginine are suggested to be important in homogalacturonan-binding (Decreux *et al.*, 2006). The GUB_WAK_bind domain may play other important roles in WAKs. For example, susceptibility isoforms of the oilseed rape RESISTANCE TO LEPTOSPHAERIA MACULANS-9 (Rlm9), a WAK involved in the race-specific resistance against *Leptosphaeria maculans*, contain amino-acid changes in the GUB_WAK_bind domain relative to the resistance isoform (Larkan *et al*., 2020), suggesting a possible role for this protein domain in effector recognition.

WAKs possess a diverse combination of domains between the N-terminal GUB_WAK_bind domain and the transmembrane helix (Figure 1.1). Many WAKs contain one or more copies of epidermal growth factor (EGF)-like domain, some of which have been characterised as calcium-binding. Others have been shown to possess a Wall-associated receptor kinase, C-terminal domain (WAK_assoc_C), which often lies C-terminal to the GUB_WAK_bind domain. All of these domains are cysteine-rich. EGF-like domains have been shown to form disulphide bridges stabilising the secondary protein structure (Sampoli Benitez & Komives, 2000). In animals, EGF-like domains have been implicated in protein-protein interactions (Yarden & Sliwkowski, 2001). Calcium-

binding EGF domains are very similar, but have been shown to bind a single calcium ion that is required for ligand binding (Selander-Sunnerhagen *et al.*, 1992). Calcium is essential for many interactions with receptor ligands, with the ectodomains of AtWAK1 and *Brachypodium distachyon* WALL-ASSOCIATED KINASE-1, -10 and -42 (BdWAK1, BdWAK10, and BdWAK42) shown to bind OGs in a calcium-dependent manner (Decreux & Messiaen, 2005, Wu *et al*., 2020). EGF-mediated protein-protein interactions may be a common mode of action for WAKs that function in pathogen surveillance. However, some characterised immunity-related WAKs do not have EGF-like domains, including the wheat Stb6 (Saintenac *et al.*, 2018) and maize ZmWAK-RLK1/ZmHtn1 (Hurni *et al*., 2015) proteins which confer resistance to the fungal pathogens *Zymoseptoria tritici* and *Exserohilum turcicum*, respectively. Analyses of WAK-encoding genes in oilseed rape, *B. distachyon,* tomato, and poplar (*Populus trichocarpa*), also identified those that encode proteins with no EGF-like domains (Larkan *et al.*, 2020, Sun *et al*., 2020, Tocquard *et al.,* 2014, Wu *et al.*, 2020).

Immunity-related WAKs could be classified as RLK/Pelle serine-threonine kinases (Lehti-Shiu & Shiu, 2012). Some WAKs involved in pathogen defence contain a conserved arginine immediately preceding the catalytic aspartate in the catalytic loop of the kinase domain, and thus are classified as RD kinases. Both residues play vital roles in RD kinase activity, with aspartate acting as the catalytic residue, and the arginine being essential for orientation of the catalytic site and phosphotransfer to the kinase substrate (Krupa et al., 2004). Defence-related RD WAKs include Arabidopsis AtWAK1, RFO1 and AtWAKL10, as well as oilseed rape Rlm9, cotton WALL-ASSOCIATED KINASE-5A (GhWAK5A) and WALL-ASSOCIATED KINASE-7A (GhWAK7A), rice OsWAK1, 14, 21.2, 25, 91, 92 and 112d, and tomato WALL-ASSOCIATED KINASE-1 (SlWAK1). However, RD kinases are more commonly linked to roles in growth and development, whereas all non-RD kinases characterised to date, including PRRs such as FLS2, have been implicated in host immunity (Dardick *et al*., 2012). To date, only non-RD WAKs related to plant immunity have been characterised from monocots. These include ZmWAK/qHSR1 and ZmWAK-RLK1/ZmHtn1 of maize, Xa4 of rice, and Stb6, TaWAK5 and TaWAK6 of

wheat. RD and non-RD kinases demonstrate different activation mechanisms, which may affect their signalling pathways. For example, while non-RD receptor kinases FLS2 and EFR require BAK1 (an RD-kinase) for immune signalling (Liebrand *et al*., 2014), the RD receptor kinase CERK1 does not require BAK1.

Recent studies have also identified a guanylyl cyclase (GC) motif embedded within the kinase domain of some WAKs (Bot *et al*., 2019). A web tool GCPred (http://gcpred.com/; Xu *et al*., 2018) predicts several immunity-related WAKs, including Rlm9, AtWAKL10, OsWAK25 and OsWAKL21.2, RFO1 and SlWAK1, as containing the GC functional centre (Figure 1.1). Interestingly, whilst kinase activity of OsWAKL21.2 is required for activation of pathogen resistance in rice, the GC activity is required to activate immune responses when ectopically expressed in Arabidopsis (Malukani *et al.*, 2020). This suggests that these WAKs modulate different signalling pathways, possibly to carry out pleiotropic functions as well as immune responses. For example, AtWAKL10, which contains a GC motif within its kinase domain, has been shown to be involved in responses to both biotic and abiotic stresses, with the *atwakl10* mutant plants showing reduced tolerance to salt stress (Bot *et al*., 2019).

Table 1.1. List of wall-associated kinase (WAK) genes implicated in plant immunity

WAK gene	Plant species	Disease / pathogen species	Differentially regulated genes / pathways	Induced by invasion patterns	Induced by defence signalling molecules	Induced by other signals	Other phenotypes	Protein interactions / associations	Citations
Isolate-specific (gene-for-gene) interactions									
Rlm9	Oilseed rape (*Brassica napus*)	Stem canker / *Leptosphaeria maculans*	Hypersensitive response	AvrLm5-9				AvrLm5-9	Larkan *et al.*, 2019
Stb6 / TaWAKL4	Wheat (*Triticum aestivum*)	Septoria tritici blotch / *Zymoseptoria tritici*	ROS production in substomatal cavity	AvrStb6				AvrStb6	Brading *et al.*, 2002 Saintenac *et al.*, 2018 Shetty *et al.*, 2003
Non gene-for-gene interactions									
AtWAK1	Thale cress (*Arabidopsis thaliana*)	Grey mould / *Botrytis cinerea* Bacterial speck / *Pseudomonas syringae* Bacterial soft rot / *Pectobacterium carotovorum*	JA and ET expression, *MAPK3* expression, Ca^{2+} influx	OGs	SA		Required for cell expansion	AtGRP3 (apoplastic), KAPP (cytoplasmic), defence response requires *NPR1*	Brutus *et al.*, 2010 He *et al.*, 1998 Kohorn, 2006 Moscatiello *et al.*, 2006 Wagner & Kohorn, 2001

AtWAKL10	Thale cress (*A. thaliana*)	Bacterial speck / *Pseudomonas syringae*	Increase in cGMP	Chitin flg22 OGs		Nitric acid	Increases branching and germination under salt stress Negatively regulates drought tolerance		Bot *et al.*, 2019 Meier *et al.*, 2010
GhWAK7A	Cotton (*Gossypium hirsutum*)	Fusarium wilt / *Fusarium oxysporum* Verticillium wilt / *Verticilium longisporum Verticilium dahliae*	Upregulation of *GhMPK3, GhMPK6* and *WRKY30* Production of ROS	Chitin				GhCERK1 (independent of chitin treatment) and GhLYK5	Wang *et al.*, 2020
GhWAKL	Cotton (*G. hirsutum*)	Verticillium wilt / *V. dahliae*			SA			GhDNAJ1 (GhWAKL kinase-dependent)	Feng *et al.*, 2020
OsWAK1	Rice (*Oryza sativa*)	Rice blast / *Magnaporthe oryzae*			SA JA	Wounding		OsRFP	Li *et al.*, 2009
OsWAK14	Rice (*O. sativa*)	Rice blast / *M. oryzae*		Chitin				OsWAK14 and OsWAK92	Cayrol *et al.*, 2016 Delteil *et al.*, 2016
OsWAKL 21.2	Rice (*O. sativa*)	Rice blight / *Xanthamonas oryzae*	Upregulation of JA genes Callose deposition	LipA			Upregulation of SA genes Suppression of JA genes		Malukani *et al.*, 2019

*OsWAK25**	Rice (*O. sativa*)	Rice blight / *X. oryzae* Rice blast / *M. oryzae*	Upregulation of SA-related genes			Wounding	Mimic lesions (OE-lines)	Positive regulator of *Xa21*, XB15	Harkenrider *et al.*, 2016 Jo *et al.*, 2011 Seo *et al.*, 2011
OsWAK91 / OsDEES1	Rice (*O. sativa*)	Rice blast / *M. oryzae* Root rot / *Rhizoctonia solani*	ROS production Upregulation of defence genes Decrease in *M. oryzae* cell-to-cell movement	Chitin			Reduced fertility (KO-lines)	OsWAK92	Cayrol *et al.*, 2016 Delteil *et al.*, 2016
OsWAK92	Rice (*O. sativa*)	Rice blast / *M. oryzae*		Chitin				OsWAK91	Cayrol *et al.*, 2016 Delteil *et al.*, 2016
RFO1 / AtWAKL22	Thale cress (*A. thaliana*)	Fusarium wilt / *F. oxysporum* Verticillium wilt / *V. longisporum* *V. dahliae*		NLPs flg-22	JA Ethylene			RFO2, RFO4, RFO6	Diener & Ausubel, 2005 Johansson *et al.*, 2006 Verica *et al.*, 2002
SlWAK1	Tomato (*Solanum lycopersicum*)	Bacterial speck / *Pseudomonas syringae*		flg22 flg28				FLS2 and FLS3 (required for flg22 PTI response)	Rosli *et al.*, 2013 Zhang *et al.*, 2020
TaWAK2	Durum wheat (*Triticum durum*)	Fusarium head blight / *Fusarium graminearum*	Suppression of PME Reinforcement of cell wall						Gadaleta *et al.*, 2019

TaWAK6	Wheat (*T. aestivum*)	Wheat leaf rust / *Puccinia triticina*			Adult resistance only	Dmochowska-Boguta *et al.*, 2015 Dmochowska-Boguta *et al.*, 2020
Xa4	Rice (*O. sativa*)	Rice blight / *X. oryzae*	Accumulation of JA-Ile Upregulation of CesA genes and phytoalexins Downregulation of expansins	Temperature-dependent resistance	Reduction in height Increase in mechanical strength Higher cellulose content Decrease in lodging	Hu *et al.*, 2017
ZmWAK / qHSR1	Maize (*Zea mays*)	Head smut / *Sporisorium reilianum*	Suppression of auxin, JA, ABA and ethylene Promotion of SA Upregulation of *MEK1*		Promotes cell growth Controls turgor pressure	Zhang *et al.*, 2017 Zuo *et al.*, 2015
ZmHtn1 / ZmWAK-RLK1	Maize (*Z. mays*)	Northern corn leaf blight / *Exserohilum turcicum*	Upregulation of JA and ethylene pathways Lignin biosynthesis		Downregulation of BXs	Hurni *et al.*, 2015 Yang *et al.*, 2019
Susceptibility factors						

*OsWAK25**	Rice (*O. sativa*)	Root rot / *R. solani* Brown spot / *Cochliobolus miyabeanus*	Upregulation of SA-related genes			Wounding	Mimic lesions (OE-lines)	Positive regulator of *Xa21*, XB15	Harkenrider *et al.*, 2016 Jo *et al.*, 2011 Seo *et al.*, 2011
OsWAK112d	Rice (*O. sativa*)	Rice blast / *M. oryzae*		Chitin (down-regulated)				Os02g12450 (related to *Xa21*)	Delteil *et al.*, 2016 Rohila *et al.*, 2006
Snn1 / TaWAK	Wheat (*T. aestivum*)	Septoria nodorum blotch / *Parastagonospora nodorum*	ROS production Upregulation of *PR* genes and a chitinase DNA laddering Upregulation of *TaMAPK3*				Follows circadian expression cycle Light-dependence for susceptibility	SnTox1	Liu *et al.* 2012 Shi *et al.*, 2016
Other WAKs associated with biotic stress									
CsWAKL08	Sweet orange (*Citrus sinensis*)	Bacterial canker / *Xanthomonas citri ssp. citri*	Upregulation of JA biosynthesis and JA-responsive genes ROS production	SA MeJA					Li *et al.*, 2020
GhWAK5A	Cotton (*G. hirsutum*)	Fusarium wilt / *F.oxysporum* Verticillium wilt / *V. longisporum* *V. dahliae*	Silencing induces increased resistance				Negative regulator		Wang *et al.*, 2020

GhWAK26	Cotton (*G. hirsutum*)	Verticillium wilt / *V. longisporum* *V. dahliae*	Silencing leads to reduced resistance Reduced lignin content, nitric oxide and ROS		SA JA		Yang *et al.*, 2021
GhWAK77	Cotton (*G. hirsutum*)	Verticillium wilt / *V. dahliae*	Silencing leads to reduced resistance Reduced lignin content, nitric oxide and ROS		SA		Yang *et al.*, 2021
Rcs5 / Sbs1&2	Barley (*Hordeum vulgare*)	Root rot / *Bipolaris sorokiniana*	ROS production Hypersensitive response	Non-proteinaceous effector		Susceptibility factor	Ameen *et al.*, 2020
TaWAK5	Wheat (*T. aestivum*)	Root rot / *R. solani*	Elevated expression in resistant lines Silencing has no impact on resistance		SA ABA JA		Yang *et al.*, 2014

***OsWAK25 features as both a resistance and susceptibility WAK**

1.4.2 Recognition of pathogen effectors and other invasion molecules by WAKs

Three WAKs have so far been identified as having gene-for-gene interactions with specific pathogen effector proteins (Figure 1.2). Stb6 of wheat and Rlm9 of oilseed rape confer resistance to *Z. tritici* expressing AvrStb6 and *L. maculans* expressing AvrLm5-9, respectively (Brading *et al*., 2002, Larkan *et al*., 2016). However, a direct interaction between these disease resistance proteins and the corresponding fungal effectors has not been observed in either case (Larkan *et al*., 2020, Saintenac *et al*., 2018). The WAK protein STAGONOSPORA NODORUM NECROSIS-1 (Snn1) is a susceptibility factor in the interaction between wheat and *Parastagonospora nodorum*. The effector protein STAGONOSPORA NODORUM TOXIN-1 (SnTox1) induces cell death/necrosis in wheat plants containing *Snn1* leading to disease, in what has been described as effector-induced susceptibility (Friesen *et al*., 2007, Liu *et al.*, 2012). Moreover, Shi et al. (2016) observed a direct interaction between Snn1 and SnTox1. The rice WAK protein Xa4 has been shown to control a race-specific resistance against *Xoo* (Hu *et al.*, 2017), although the invasion molecule recognised by this resistance protein has not yet been identified.

Other WAKs contribute to plant immunity by monitoring for invasion molecules in a non-gene-for-gene manner (Figure 1.2). As discussed above, AtWAK1 is known to bind cell wall pectin and pectin-derived OGs that are recognised as DAMPs (Brutus *et al*., 2010, Verica & He, 2002). This ability to detect DAMPs has led to AtWAK1 and other CSIRs being described as cell wall integrity sensors (Kohorn, 2016). The length of OGs appears to affect the character of the immunity response (Davidsson *et al*., 2017), whilst a decrease in pectin methylation correspondingly increases WAK sensitivity to OGs (Kohorn *et al*., 2014), illustrating a complex interaction between AtWAK1 and its ligands.

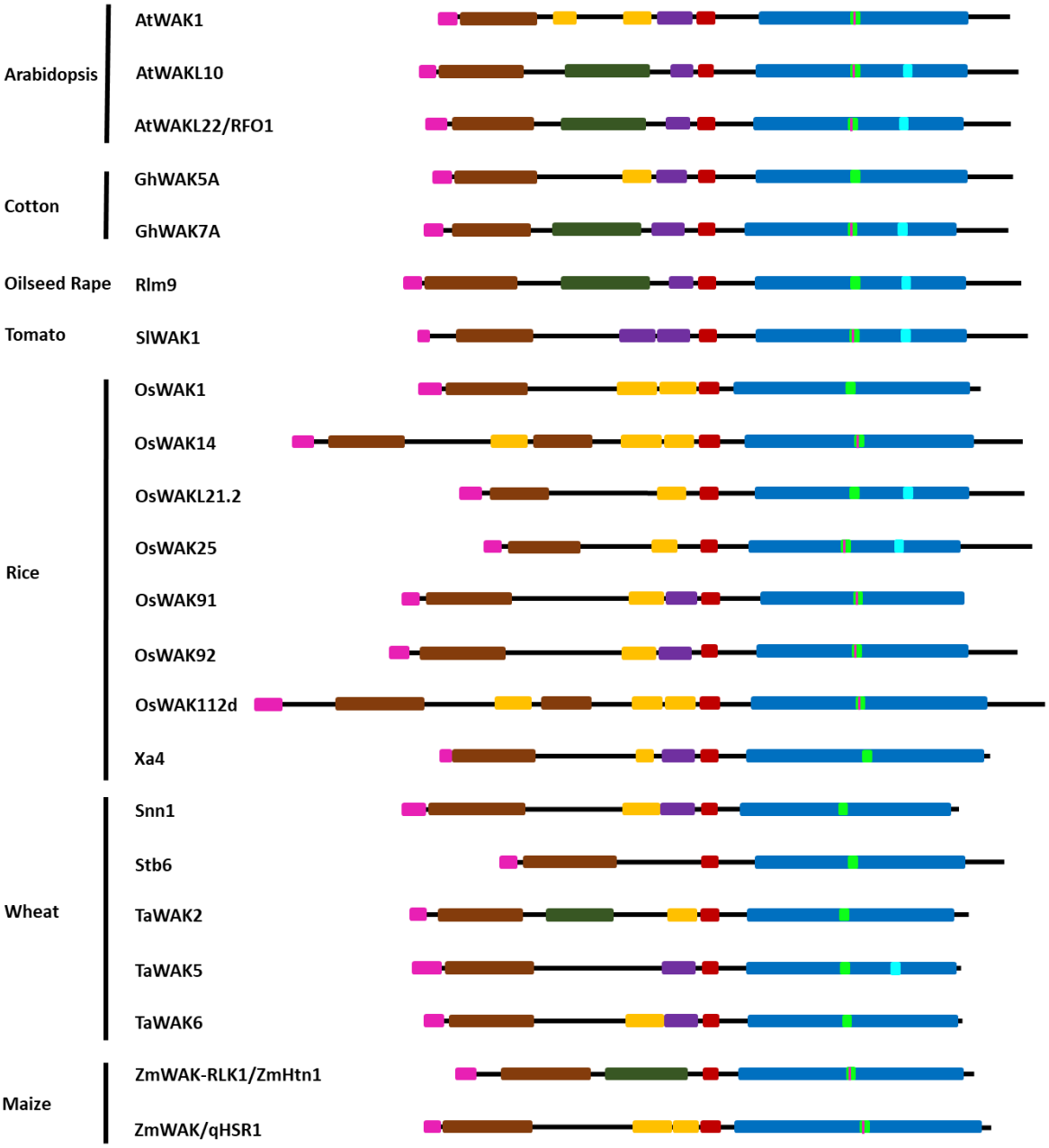

Figure 1.1: Domain architecture of immunity-related WAKs from both dicot and monocot species. The extracellular domains of WAKs show a high degree of diversity, with many possessing galacturonan-binding domains (GUB_WAK_bind; brown), implicated in binding cell wall pectin and epidermal growth factor (EGF)-like (orange) and Ca^{2+}-dependent EGF (purple) that may play a role in protein–protein interactions. The WAK intracellular domains, including a serine/threonine kinase (blue), are more well conserved, with immunity-related WAKs possessing a non-arginine aspartate (RD) motif so far identified exclusively in monocots. Other domains/motifs: signal peptide (pink), WAK_assoc_C (dark green), transmembrane helix (red), serine/threonine kinase (blue), RD motif (pink bar), kinase active site (green), and guanylyl cyclase (cyan).

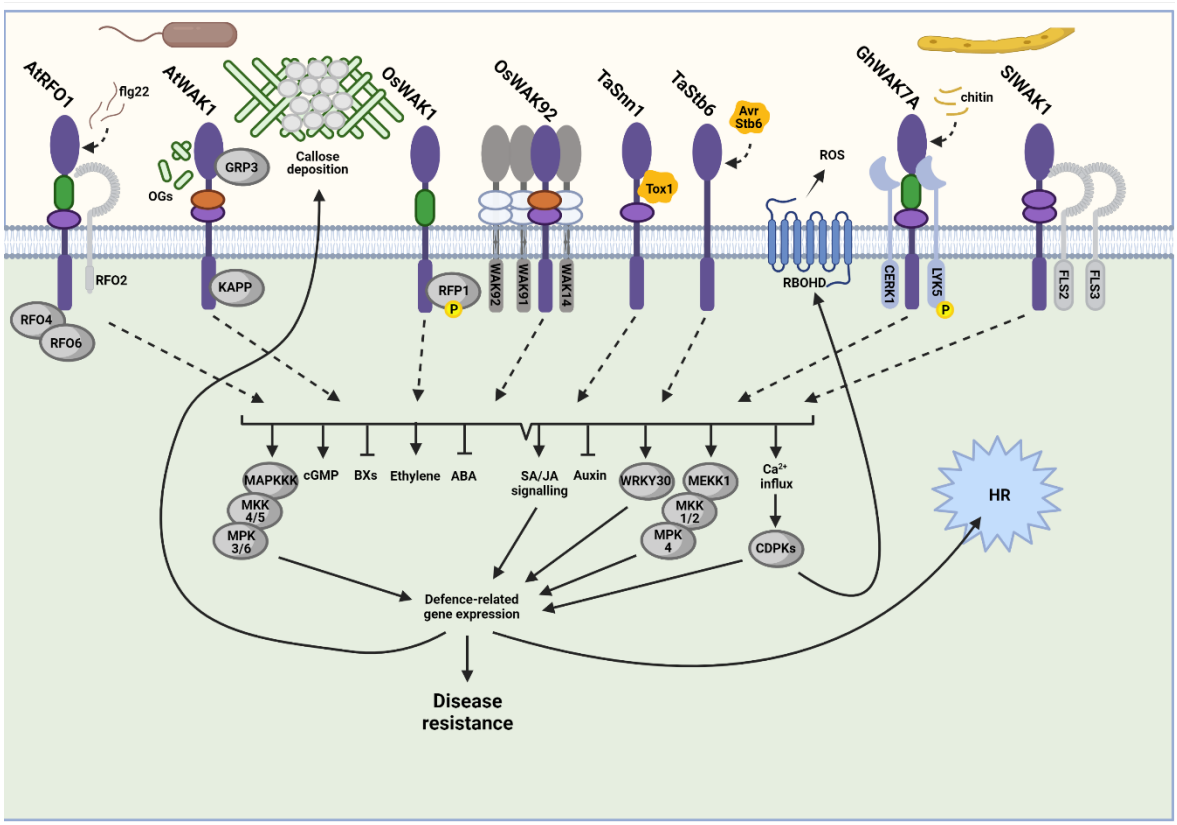

Figure 1.2: Schematic diagram illustrating the downstream pathways employed by some of the better characterized immune-related WAKs, as part of their defence responses. Immune responses directed by different WAKs vary considerably and often involve protein–protein interactions with other membrane-bound proteins or cytoplasmic proteins, which leads to activation of mitogen-activated protein kinase (MAPK) cascades, hormone fluctuations, the production of reactive oxygen species (ROS), and, in some cases, a hypersensitive response (HR). Created with BioRender.com.

Detection of pathogen effectors and other invasion molecules may be utilised by other, as-yet uncharacterised WAKs. Indeed many WAKs have been shown to be upregulated as a result of treatment with PAMPs. *OsWAKL21.2*, an alternative splice variant of rice *OsWAKL21*, is upregulated specifically by enzymatically active forms of the *Xoo* cell-wall degrading enzyme LIPASE A (LipA). Furthermore, suppression of the *OsWAKL21.2* expression reduces the LipA-induced immune responses (Malukani *et al*., 2020). Similarly, expression of *SlWAK1* in tomato is induced by flg22 and flg28 in a FLS2- and FLAGELLIN-SENSING 3 (FLS3)-dependent manner (Zhang *et al*., 2020), with *slwak1* knockout mutant plants showing compromised responsiveness to these invasion molecules. The cotton *GhWAK7A* and rice *OsWAK14*, *OsWAK91* and *OsWAK92* genes were shown to be specifically induced by chitin (Delteil *et al.*,

2016, Wang *et al.*, 2020). Whilst *GhWAK7A* appears to contribute to chitin detection and signal transduction, the induction of *OsWAK14, OsWAK91* and *OsWAK92* is likely to be part of downstream defence responses. Other WAKs induced by invasion molecules include *AtWAKL10*, which is induced by chitin and flg22 (Diener & Ausubel, 2005) and *RFO1*/*AtWAKL22,* which is upregulated in response to flg22 and NECROSIS AND ETHYLENE-INDUCING PEPTIDE 1–LIKE PROTEINS (NLPs) treatment (Meier *et al*., 2010, Qutob *et al*., 2006), both likely as part of downstream defence responses. Combined, the studies discussed above demonstrate the involvement of WAKs in defence responses induced by a wide range of plant- and pathogen-derived invasion molecules.

1.4.3 Exon-intron structure and regulation of WAK genes

The exon-intron structure of WAKs appears to be well conserved. The characterised immunity-related WAK genes comprise either three exons and two introns or four exons and three introns, with most genes typified by the presence of a long first exon and very short second exon (Figure 1.3). This gene structure is conserved across monocot and dicot WAKs. The length of the first intron in the WAK genes is highly variable, ranging from 77-bp (*OsWAK92*) to 8334-bp (*ZmWAK-RLK1/ZmHtn1*), with the increase in length sometimes caused by insertion of transposons (Hurni *et al*., 2015). Interestingly, genes with long (>150-bp) first introns have so far only been identified in monocots. Such long first introns may confer genetic diversity by spanning one or more alternative first exons, leading to splicing variants of the gene. Such is the case for *OsWAKL21* of rice, from which three alternatively spliced transcripts are produced, with only one (*OsWAK21.2*) known to confer resistance to *Xoo* (Malukani *et al.*, 2020). The WAK gene family has been shown to be greatly expanded in monocots (IWGSC, 2018, Tripathi *et al.,* 2020, Zhang *et al*., 2005), and the presence of alternative splicing variants could represent an additional level of diversification of WAKs in monocot species. Despite the large variation in gene size, the size of the resulting WAK proteins is relatively consistent, with the majority comprising between 700-800 amino acids (aa). The smallest characterised is Stb6 (647-aa), whilst the largest is OsWAK112d (1015-aa),

with the majority of length diversity accounted for by variations in the extracellular regions (Figure 1.1).

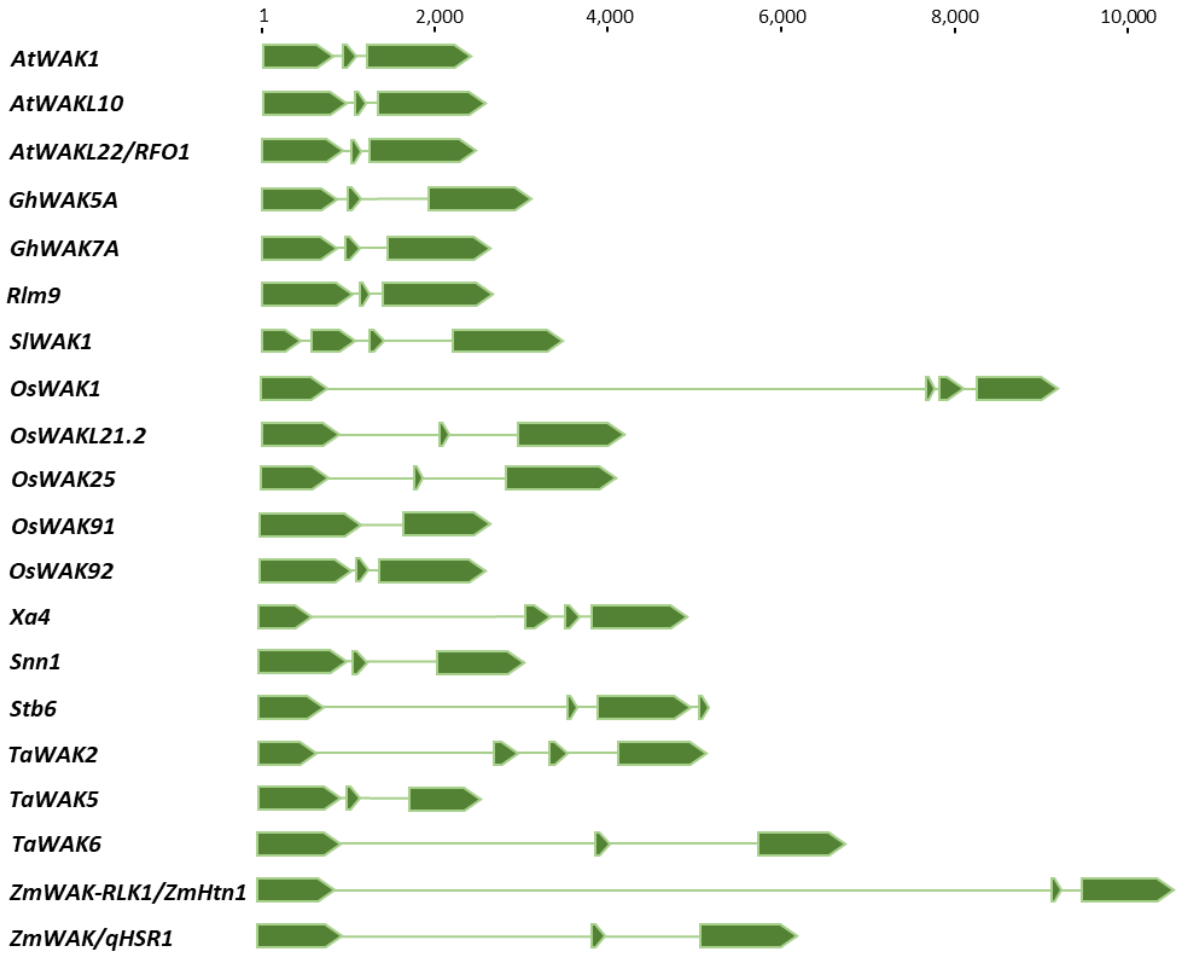

Figure 1.3: Exon–intron structure of immunity-related WAK genes. The majority of WAK genes comprise three or four exons (green boxes), with a short second exon. In monocots, the length of the first intron (green connecting lines) varies considerably and possibly contains alternative exons for splicing variants of WAK genes. Despite the considerable difference in length of different WAK genes, the length of the WAK proteins they encode is more consistent. Gene length in base pairs is shown above.

WAKs often confer or contribute to immunity at different growth stages and in different organs of plants. For example, the head smut resistance gene *ZmWAK/qHSR1* is most highly expressed in the mesocotyl of maize seedlings, which corresponds to the organ and growth stage in which *S. relianum* infection most commonly occurs (Zuo *et al.*, 2015). Similarly, *TaWAK5* was found to be substantially upregulated in roots but not in stems of wheat in response to the

soil-borne pathogen *Rhizoctonia cerealis* (Yang *et al.,* 2014). On a cellular level, the rice protein OsWAK25, whose overexpression enhances resistance to *Magnaporthe oryzae* and *Xoo* (Harkenrider *et al.*, 2016), was found to be localised to plasmodesmata (Jo *et al*., 2011), which the fungus *M. oryzae* uses to spread cell-to-cell (Kankanala *et al*., 2007). Interestingly, *P. nodorum* susceptibility gene *Snn1* was found to have a circadian pattern of expression, with the *Snn1* transcript abundance increasing during darkness and decreasing during daylight and sensitivity to SnTox1 demonstrating light dependence (Liu *et al*., 2012, Shi *et al*., 2016). Overexpression of *TaWAK6* was shown to enhance resistance to the leaf rust fungus *Puccinia triticina* only at the adult plant stage but not at the seedling stage (Dmochowska-Boguta *et al*., 2020). These spatial and temporal differences in expression can give clues to the function of WAKs and their potential molecular interactions, and are correlated with the lifestyles of pathogens against which they confer resistance.

Pathogen challenge induces the upregulation of some WAKs, along with a wide range of other plant immunity-related genes (Dmochowska-Boguta *et al*., 2015). However, the speed, scale and duration of gene upregulation in response to pathogens vary greatly between different WAKs. For some, upregulation occurs only transiently. For example, rice *OsWAK91* and *OsWAK92* that are shown to be CEBiP-dependent, peak in expression at only 4 hours post inoculation (hpi) with *M. oryzae* and 1 h after chitin infiltration. In both cases upregulation of these WAK genes is largely reduced after 24 h (Delteil *et al.*, 2016). By contrast, wheat *TaWAK5* remains upregulated up to 21 days post inoculation with *R. cerealis* (Yang *et al.,* 2014). The fastest increase in expression in response to pathogen inoculation is shown by rice *Xa4*, with a reported 30-fold increase after just 0.5-hpi with the incompatible isolate of *Xoo* (Hu *et al.*, 2017). Some WAK genes show only a very modest upregulation in response to pathogens. For example, a two-fold increase in the expression was observed for *OsWAK25* and *ZmWAK/qHSR1* at 24-hpi (Wei *et al*., 2013, Zuo *et al*., 2015) with *M. oryzae* and *S. reilianum*, respectively. By contrast to WAK genes contributing to disease resistance, the susceptibility gene *Snn1* (Shi *et al.*, 2016) and the negative regulator of immunity *OsWAK112d* (Delteil *et al.*, 2016) have both been shown to be downregulated at 24-hpi with *P. nodorum*

and *M. oryzae*, respectively. However, gene downregulation in response to pathogens appears to not be the universal feature of the WAKs involved in disease susceptibility. For instance, *SUSCEPTIBILITY TO BIPOLARIS SOROKINIANA-1* and *-2* (*Sbs1* and *Sbs2*) genes in barley were found to remain upregulated six-fold at 12-hpi with virulent isolates of *Bipolaris sorokiniana* (Ameen *et al*., 2020).

1.4.4 WAK-mediated defence responses

WAKs have been shown to induce a broad range of host defence responses. *Stb6* and *Rlm9* confer complete gene-for-gene resistance to isolates of *Z. tritici* and *L. maculans* (Brading *et al*., 2002, Larkan *et al*., 2016). While *Rlm9*-mediated resistance is associated with hypersensitive response (HR), *Stb6* confers disease resistance without inducing host cell death. Other WAKs confer quantitative resistance to their respective pathogens. In maize, *ZmWAK-RLK1*/*ZmHtn1* reduces the number of successful penetrations of *Exserohilum turcicum* into the seeding epidermis (Yang *et al*., 2019) while *ZmWAK/qHSR1* induces HR to restrict the growth of *S. relianum* in the mesocotyl (Zhang *et al*., 2017). The disruption of many WAK genes, either through stable gene knockout, virus-induced gene silencing (VIGS), or targeting induced local lesions in genomes (TILLING) approaches, has been shown to result in increased susceptibility, determined by the number and size of lesions or the extent of pathogen proliferation (Delteil *et al*., 2016, Dmochowska-Boguta *et al*., 2020). Correspondingly, overexpression of WAKs in many cases (e.g. *OsWAK1*, *OsWAK25* and *GhWAKL*) results in an enhanced disease resistance (Feng *et al*., 2020, Harkenrider *et al*., 2016, Li *et al*., 2009).

MAP kinase cascades regulate multiple biological processes such as growth and development, and also are implicated in immune responses (Figure 1.2). MPK3 and MPK6 are commonly associated with plant defence and both *AtWAK1*- and *GhWAK7A*-mediated defence involve these pathways, although in Arabidopsis the MPK6 pathway has been proposed to be specifically required for defence (Kohorn & Kohorn, 2012, Wang *et al*., 2020). For susceptibility factors *Snn1* of wheat and *Sbs1* and *Sbs2* of barley, expression of *MPK3* is linked to the susceptibility response (Ameen *et al.*, 2020, Liu *et al*.,

2012). Other MAP kinase pathways could also be utilised by WAKs. For example, the *MEK1* gene encoding a homologue of MAP kinase kinase located upstream of the MPK4 pathway, has been shown to be upregulated as part of the *ZmWAK/qHSR1* mediated defence response (Zhang *et al*., 2017).

Plant defence responses are also commonly orchestrated by hormone fluctuations, with several immunity-related WAKs upregulated by hormone treatments (Figure 1.2). For example, salicylic acid (SA) application induces the upregulation of *AtWAK1*, *OsWAK1*, *OsWAK25*, *GhWAKL* and sweet orange (*Citrus sinensis*) *WALL-ASSOCIATED-KINASE-LIKE-08* (*CsWAKL08*; Feng *et al*., 2020, Harkenrider *et al*., 2016, He *et al.*, 1998, Li *et al.*, 2009, Li *et al*., 2020). Methyl jasmonate (MeJA), a derivative of jasmonic acid, stimulates expression of *RFO1/AtWAKL22*, *OsWAK1* and *CsWAKL08* (Johansson *et al*., 2006, Li *et al*., 2009, Li *et al*., 2020), with *RFO1/AtWAKL22* also known to be induced by treatments with ethylene precursors. In turn, WAKs could induce or suppress hormone biosynthesis as part of their contribution to disease resistance. Some, such as *AtWAK1*, *CsWAKL08*, *Xa4*, *OsWAK21.2* and *ZmWAK-RLK1*/*ZmHtn1*, induce expression of the jasmonic acid (JA)-biosynthesis related genes or JA accumulation (Li *et al*., 2020, Malukani *et al*., 2020, Moscatiello *et al*., 2006, Yang *et al*., 2019, Zuo *et al*., 2015), whilst others, such as *OsWAK25*, induce production of SA (Harkenrider *et al*., 2016). The silencing of cotton WAK genes, *GhWAK26* and *GhWAK77*, was shown to suppress the SA- and JA-related signalling in response to *Verticillium dahliae* infection (Yang *et al*., 2021). Pathways involved in JA, auxin, abscisic acid (ABA) and ethylene biosynthesis were all shown to be suppressed following pathogen challenge in maize overexpressing *ZmWAK/qHSR1*, whilst SA pathways were promoted (Zhang *et al*., 2017, Zuo *et al*., 2015). Interestingly, this trend is reversed in *ZmWAK/qHSR1* maize in the absence of a pathogen challenge. When ectopically overexpressed in Arabidopsis, *OsWAK21.2* induced SA and suppressed JA biosynthesis (Malukani *et al*., 2020). Hormone pathways induced in response to infection vary based on the lifestyle of the infecting pathogen, with SA pathways commonly promoted in response to biotrophic pathogens and JA pathways induced following nectrotrophs infection

(Bari & Jones, 2009). It is likely that WAK-induced hormonal responses correspond to the lifestyles of the pathogens to which they confer resistance.

Other components of the plant immune system often associated with the WAK-induced signalling responses include cytoplasmic RLKs (CRLKs), which relay WAK-induced defence signalling into the cytoplasm and nucleus (Figure 1.2). For example two CRLKs, RESPONSE TO OGs (ROG1 and ROG2), are phosphorylated following OG treatment, with OG responses reduced in transgenic Arabidopsis *rog2* knockout lines (Kohorn *et al*., 2016). Production of ROS, which has antimicrobial properties as well as acting in cell-to-cell signalling, is frequently observed in WAK-mediated defence responses, including those induced by *Stb6* of wheat, *GhWAK7A* of cotton, or *OsWAK91* of rice (Delteil *et al*., 2016, Shetty *et al*., 2003, Wang *et al*., 2020). Accumulation of another biotic stress signalling molecule, cyclic guanosine monophosphate (cGMP), is reported to be induced by *AtWAKL10* in Arabidopsis following inoculation with *P. syringae* (Meier *et al*., 2009, Meier *et al*., 2010). Calcium ion influx, another common feature of plant defence, is observed in the OG-treated Arabidopsis plants (Moscatiello *et al.*, 2006). This is likely to be an AtWAK1-mediated process, which also involves the calcium-dependent kinases CDK5, 6 and 11 (Gravino *et al.*, 2015).

1.4.5 Direct interactions between WAKs and other proteins

CSIRs are frequently identified as forming membrane complexes upon ligand recognition (Hohmann *et al.*, 2017). BAK1 and other SERKs are common co-receptors frequently associated with various CSIRs during immune responses (Liebrand *et al*., 2014), although these co-receptors are yet to be implicated in WAK-associated defence responses. The AtWAK1-mediated defence in response to OGs has been shown to be unaffected by the *P. syringae* effector AvrPto, which targets and inhibits the action of BAK1 and therefore negatively impacts the FLS2- and EFR-mediated immunity (Gravino *et al.*, 2017). Similarly, BAK1 and SOBIR1 appear not to be involved in the *Rlm9*-mediated defence response (Larkan *et al*., 2020). Whether any of the WAKs require interactions with BAK1, SOBIR1, or other co-receptors for induction of immune responses is yet to be elucidated. Non-RD WAKs such as Stb6, Xa4 or

ZmWAK-RLK1/ZmHtn1 are more likely to form a complex with an RD kinase co-receptor to initiate defence signalling (Liebrand *et al.,* 2014).

Interactions with proteins at the plasma membrane have been identified for some WAKs (Figure 1.2). For instance, SlWAK1 have been shown to interact with FLS2 and FLS3 upon recognition of flg22 and flg28, respectively (Zhang *et al*., 2020), with flagellin-induced defence responses shown to be compromised in tomato *slwak1* knockout lines. In rice, OsWAK91 and OsWAK92 were found to form homodimers and heterodimers, as well as heterodimers with OsWAK14, all mediated by their EGF-like domains, thus forming large receptor complexes at the plasma membrane (Cayrol *et al.*, 2016). Cotton GhWAK7A was shown to interact *in vivo* with both GhCERK1 and LYSM RECEPTOR KINASE 5 (GhLYK5), and promote their dimerisation (Wang *et al*., 2020), as well as phosphorylating GhLYK5. Compromised chitin-induced defence responses in *GhWAK7A*-silenced plants suggest an important role for GhWAK7A in chitin detection in cotton. The RFO1-mediated defence response has been demonstrated to be co-dependent on the presence of the receptor-like protein RFO2 (Diener & Ausubel, 2005, Shen & Diener, 2013), suggesting that RFO2 may act as a co-receptor.

Interactions between some WAKs and other proteins within the cytoplasm or in the extracellular space have also been reported (Figure 1.2). In particular, AtWAK1 has been shown to interact in a resting state with the extracellular cell wall- and plasma membrane-localised GLYCINE-RICH PROTEIN-3 (AtGRP3) and the cytoplasmic plasma membrane-localised KINASE-ASSOCIATED PROTEIN PHOSPHATASE (KAPP), forming an approximately 500 kDa complex (Gramegna *et al*., 2016, Park *et al*., 2001). AtGRP3 has been suggested to act as a negative regulator of AtWAK1-mediated cell expansion, whilst a complex allosteric model is proposed for AtGRP3 regulation of AtWAK1–OG interaction (Mangeon *et al*., 2016, Mangeon *et al*., 2017). OsWAK1 phosphorylation of the transcriptional regulator, RING FINGER PROTEIN-1 (OsRFP1; Li *et al.*, 2009), possibly represents a first stage in the OsWAK1-mediated defence response pathway in rice. A direct interaction between GhWAK7A and the heat-shock chaperone protein GhDNAJ1 has also been reported (Feng *et al*., 2020), with GhDNAJ1 shown to be required for

GhWAK7A-mediated immunity. OsWAK25 of rice has been suggested to act as a positive regulator of Xa21-mediated immunity, indicating a possible interaction between these two receptor proteins (Seo *et al*., 2011). Cytoplasmic protein-protein interactions involving the kinase domains of WAKs, may also occur to relay a defence signal to the nucleus or, conversely, to regulate the WAK signalling capacity.

1.4.6 Cell wall modifications induced by WAKs

Many immunity-related WAKs confer the ability to modify the cell wall composition, providing additional strength and preventing pathogen penetration, both constitutively and during pathogen attack. The defence responses directed by *OsWAK21.2* and *SlWAK1* to minimise the pathogen infection include the deposition of callose (Malukani *et al.*, 2020, Zhang *et al*., 2020), while *ZmWAK-RLK1*/*ZmHtn1* induces upregulation of lignin biosynthesis genes (Yang *et al*., 2019). Both callose and lignin are polymers that reinforce the cell wall, strengthening it and limiting the penetration by pathogens. In wheat, *TaWAK2* has been proposed to negatively modulate the expression of *PECTIN METHYLESTERASE-1* (*PME1*) leading to a more rigid cell wall, which limited the penetration and spread of *Fusarium graminearum* (Gadaleta *et al*., 2019). It has also been observed that de-esterified pectin competes with OGs for binding to AtWAK1 in Arabidopsis, with increased concentrations of de-esterified pectin resulting in decreased OG sensitivity (Ferrari *et al*., 2013). It is therefore possible that the downregulation of *PME1* in wheat may lead to the increased OG-sensitivity and consequently to the cell wall reinforcement. Rice *Xa4*-mediated resistance to *Xoo* was associated with the upregulation of genes encoding the CELLULOSE SYNTHASE A (CesA) family enzymes, thus strengthening the cell wall barrier, and the downregulation of cell wall-loosening expansins (Hu *et al*., 2017). Interestingly, the expression of this cell wall strengthening phenotype has thus far only been linked to the action of WAKs involved in defence against non-vascular pathogens (Hu *et al*., 2017, Malukani *et al*., 2020, Yang *et al*., 2019, Zhang *et al*., 2020).

This ability to modulate cell wall characteristics mean some immunity-related WAKs also have additional roles in plant growth, development and/or

responses to abiotic stresses. In rice, *Xa4* expression is highest in the stem, where it strengthens cell walls and reduces cell length, conferring a small reduction in plant height associated with an increased resistance to lodging, thus preventing yield losses from mechanical stresses (Hu *et al*., 2017). Knockout rice lines of *oswak91/osdees1* show not only increased susceptibility to *M. oryzae* but also reduced fertility (Wang *et al*., 2012, Delteil *et al*., 2016), revealing an additional role for this WAK in plant sexual reproduction. *ZmWAK/qHSR1* of maize, which contributes to head smut resistance, promotes cell growth in the absence of pathogen challenge (Zhang *et al*., 2017) and is proposed to be involved in cell turgor regulation and osmotic stress tolerance (Zuo *et al*., 2015). As well as enhancing resistance to *P. syringae* pv. *tomato*, *AtWAKL10* is upregulated in response to treatments with the abiotic stress signalling factor S-nitroso-L-cysteine (a donor of nitric oxide). The *atwakl10* knockout mutant plants demonstrate improved tolerance to drought-stress but reduced salinity stress tolerance (Bot *et al*., 2019), and also show a reduced branching phenotype, suggesting an additional role for *AtWAKL10* in growth and development. These pleiotropic effects often result in additional agronomic benefits for crops possessing these WAK genes.

1.4.7 Trade-offs between disease resistance to different types of plant pathogens

In many aspects of plant immunity, it has been observed that resistance to pathogens with one lifestyle may confer susceptibility to those with others. For example, the *MILDEW RESISTANCE LOCUS O* (*MLO*) genes, characterised in plants including Arabidopsis, tomato, wheat and barley, confer susceptibility to the obligate biotrophic fungi which cause powdery mildew disease, with knockout lines showing enhanced disease resistance (Wang *et al*., 2014). However, barley *mlo* mutants also show increased susceptibility to the necrotrophic pathogen *Ramularia collo-cygni* (McGrann *et al*., 2014), while Arabidopsis *mlo2 mlo6 mlo12* triple mutants show enhanced susceptibility to the hemibiotrophic pathogens *F. oxysporum* and *P. syringae* pv. *maculicola* (Acevedo-Garcia *et al*., 2017). Interestingly, while transgenic rice lines overexpressing *OsWAK25* show enhanced resistance to the hemibiotrophic pathogens *Xoo* and *M. oryzae*, at the same time they display enhanced

susceptibility to the necrotrophic pathogens *Cochliobolus miyabeanus* and *Rhizoctonia solani* (Harkenrider *et al.*, 2016). Disease resistance conferred by other WAKs may also be associated with trade-off between responses to different diseases. For example, although *ZmWAK-RLK1*/*ZmHtn1* of maize confers resistance to Northern corn leaf blight (Hurni *et al*., 2015), it has also been shown to associate with a decrease in the accumulation of benzoxazinoids, indole-derived plant metabolites that function in defense against aphids and other pests (Yang *et al*., 2019).

Other WAKs have been identified as susceptibility factors or negative regulators of immunity. The wheat *Snn1* is the best characterised WAK gene that confers susceptibility to *P. nodorum* (Liu *et al*., 2012), triggered upon recognition of the corresponding fungal effector SnTox1. Under yeast two-hybrid conditions, a direct interaction was observed between SnTox1 and a region of the Snn1 ectodomain between the GUB_WAK_bind and the EGF-like domains (Shi *et al*., 2016). As *Snn1*-mediated susceptibility is associated with the elevated expression of pathogenesis-related genes *PR-1-A1*, *chitinase,* and *thaumatin* and involves activation of host cell death, it has been hypothesised that *P. nodorum* hijacks wheat pathways involved in resistance to biotrophic pathogens, utilising host cell death to gain nutrients and to sporulate (Lorang *et al*., 2012). Rice transgenic lines overexpressing *OsWAK25* often develop disease mimic lesions on their leaves (Harkenrider *et al*., 2016) suggesting constitutive activation of the defensive host cell death pathways, which may explain the observed enhanced resistance to hemibiotrophic pathogens and enhanced susceptibility to necrotrophic pathogens.

Another recently identified susceptibility factor is the barley *Rcs5* locus, which encodes the two WAKs, Sbs1 and Sbs2 (Ameen *et al*., 2020). The Sbs1/Sbs2-mediated susceptibility is thought to be dependent on the recognition of an unknown non-proteinaceous effector secreted by *B. sorokiniana*. Mutants in the rice *OsWAK112d* gene and the transgenic lines overexpressing this WAK gene have been shown to have enhanced resistance and susceptibility, respectively, to *M. oryzae* (Delteil *et al*., 2016). However, unlike Snn1 and Sbs1/Sbs2, OsWAK112d does not appear to be activated by a pathogen effector but rather acts as a negative regulator of defence, interacting with other proteins including

an RLK related to the disease resistance protein Xa21 (Rohila *et al*., 2006). It is conceivable that whilst OsWAK112d negatively regulates immune responses, it may also be involved in other essential processes in a way similar to the Arabidopsis RLK FERONIA, which plays a negative role in defence against *P. syringae* whilst also being a key signalling factor in pollen delivery during fertilisation (Escobar-Restrepo *et al*., 2007).

Despite potential trade-offs, WAKs are increasingly recognised as conferring manifold agronomic benefits to crop species, not only in growth and development, but also in abiotic and biotic stress resistance. Some of these WAKs have already been characterised as broad-spectrum disease resistance genes (Brutus *et al*., 2010) and shown to be durable in the field (Hu *et al*., 2017). WAKs, therefore, represent an important breeding and biotechnology target in the quest to meet future challenges of sustainable food production and feeding the growing world population.

1.5 Wheat and Septoria Tritici Blotch

Wheat species have been cultivated by humans for approximately 10,000 years. It is believed to have begun with the domestication in South-eastern Turkey of the grass species *Triticum monococcum* (Heun *et al*., 1997). Modern hexaploid (AABBDD) bread wheat is the product of several hybridisations between grass species: first between *T. urartu* and *Aegilops speltoides*, the sources of the wheat A and B genomes, respectively. This was followed by a later hybridisation with *A. tauschii*, the progenitor of the D genome (Shewry, 2009). First grown throughout the geographic area known as the Fertile Crescent, cultivation of bread wheat and the tetraploid durum wheat has since spread globally. Wheat is the third most productive cereal crop worldwide, with more than 850 million tonnes of grain harvested in 2018 (www.fao.org/faostat/en/#data).

Zymoseptoria tritici, previously known as *Mycosphaerella graminicola* or *Septoria tritici*, is an ascomycete fungus within the Dothideomycetes class, and

the causal agent of Septoria Tritici Blotch (STB) disease in both bread and durum wheat. This pathogen infects wheat crops globally, especially in temperate regions, with the potential to cause many millions of dollars' worth of losses. It has been described as one of the most devastating foliar diseases of wheat in the European Union, with crop losses of up to 50% reported (Eyal *et al.*, 1985, Fones and Gurr, 2015). Due to its potential impact, up to 70% of all fungicide applications on wheat in Europe are primarily targeted at the control of STB (Torriani *et al*., 2015), representing a cost of more than $1 billion. This persistent exposure to fungicides has resulted in widespread resistance evolving within *Z. tritici* populations. Isolates with resistance to the major fungicide classes quinone outside inhibitors (Torriani *et al.*, 2009), succinate dehydrogenase inhibitors (Scalliet *et al*., 2012) and azoles (Cools and Fraaije, 2008) have all been reported. This loss of chemical control against *Z. tritici* has highlighted the increasing importance of plant genetic resistance as a way of reducing the impact of STB in wheat.

1.5.1 *Zymoseptoria tritici* lifecycle

The infection cycle and cell biology of *Z. tritici* have been described in detail by Kema *et al*. (1996b) and reviewed by Steinberg (2015). Infection begins with spores landing on a wheat leaf, which germinate to form hyphae. Unlike pathogens such as *M. oryzae*, which form specialised penetration structures called appressoria (Howard and Valent, 1996) these hyphae require natural openings such as stomata or wounds to penetrate the leaf surface (Shetty *et al*., 2003). Once within the leaf, hyphae colonise the space between plant cells, remaining exclusively extracellular and forming no feeding structures (Kema *et al*., 1996b). This growth, in which no large scale symptoms are observed, continues for 10-15 days under laboratory conditions (Keon *et al*., 2007) although this can extend to weeks in the field. The exact nature of this initial stage of *Z. tritici* infection has been disputed, being described as either biotrophic or necrotrophic. During this "stealth pathogenesis" phase before the emergence of symptoms the biomass of the fungus does not increase (Keon *et al.*, 2007), with upregulation of lipases suggesting utilisation of internal lipid stores during pre-symptomatic growth. This has led to the characterisation of *Z.*

tritici as a “latent necrotroph” (Sanchez-Vallet *et al.*, 2015), although this debate is yet to be fully decided (Brennan *et al.*, 2019).

The first symptom of disease is the appearance of chlorosis on the leaf surface, followed by rapid host cell collapse and the formation of lesions in the leaf tissue, localised to the areas of fungal penetration. This appears to be a form of programmed cell death (Keon *et al*., 2007), with DNA laddering, MAPK3 accumulation and upregulation of defence-related genes. This is suspected to be initiated by the pathogen exploiting plant defence pathways to stimulate HR (Rudd *et al*., 2008, Rudd *et al*., 2015). Plant cell death and the release of metabolites into the apoplast is accompanied by a rapid increase in fungal biomass. Asexual fruiting bodies known as pycnidia, which begin forming in the substomatal cavities during the asymptomatic phase, now mature. Two different kinds of spores are used by *Z. tritici* to propagate. Large, asexual, multicell pycnidiospores emerge from pycnidia are spread to nearby leaves by a process known as leaf-splash (Steinberg, 2015). Smaller sexual ascospores are also produced when isolates possessing different mating types come into contact on an infected leaf (Kema *et al.*, 1996a). Ascospores are formed within perithecia and once released are capable of travelling long distances on air, initiating broader spread of the disease geographically and between growing seasons (Eyal *et al*., 1985).

1.5.2 *Zymoseptoria tritici* effectors

The coordination of numerous proteins, including effectors, is essential for successful *Z. tritici* infection (Rudd, 2015). Proteins have been identified that are required for changes in *Z. tritici* morphology and those with antimicrobial properties for the clearing of an ecological niche, as well as effectors that disguise the pathogen from the host during asymptomatic growth. Several transcriptomic studies of compatible and incompatible interactions between *Z. tritici* and wheat have unearthed a host of fungal genes with suspected roles in pathogenicity (Kellner *et al*., 2014, Palma-Guerrero *et al*., 2016, Palma-Guerrero *et al*., 2017, Rudd *et al*., 2015). In order to successfully infect host leaves, spores must produce hyphae to penetrate the leaf surface. Under laboratory conditions, growth on nutrient-rich media is characterised by a

prolific budding of blastospores, otherwise known as “yeast-like” growth. Conversely, an increase in temperature or nutrient deprivation trigger growth of hyphal filaments (Mehrabi *et al*., 2006). *Z. tritici* genes such as the MAPK-encoding *MgHog1* and *MgAlg2* have been shown to be essential for hyphae formation and hence pathogenicity (Motteram *et al*., 2006, Mehrabi *et al*., 2011). The elimination of microbial competition is also essential for *Z. tritici* proliferation. Kettles *et al*. (2018) identified the protein Zt6, which demonstrates potent antimicrobial activity and may help clear an ecological niche by eliminating competing microbes.

Numerous putative effectors, small secreted proteins rich in cysteine residues, have been identified in the *Z. tritici* genome (do Amaral *et al*., 2012). However, the functional characterisation of many of these proteins has not yet been possible, often due to functional redundancy (Rudd, 2015). During the asymptomatic infection phase, *Z. tritici* must both evade host detection and protect itself from the adverse conditions of the apoplast. LysM effectors Mg1LysM and Mg3LysM, homologues of Avr4 of *C. fulvum*, are secreted by *Z. tritici* (Marshall *et al*., 2011) and, similarly to their homologue, sequester chitin and prevent chitin-induced immune responses (Lee *et al.*, 2014). Other genes highly expressed during asymptomatic infection encode chloroperoxidases and oxidoreductases, being most highly expressed at 3 and 7 days post infection (dpi) respectively, which are speculated to protect the fungus from apoplastic H_2O_2 (Palma-Guerrero *et al*., 2016). Putative effectors also play a major role in the transition to necrotrophy and subsequent necrotrophic growth. Thirteen putative effectors were among the 50 most highly expressed genes at 9 dpi (Rudd *et al*., 2015). A single necrosis-inducing protein, MgNLP, is expressed immediately prior to the emergence of disease symptoms, although ectopic expression of this protein in wheat does not result in cell death (Motteram *et al*., 2009). Two other *Z. tritici* proteins, ZtNIP1 and ZtNIP2 (M'Barek *et al*., 2015) have been shown to induce cell death on certain wheat cultivars. Expression of the antimicrobial protein Zt6 peaks both prior to fungal penetration and also during the transition to the symptomatic infection phase, suggesting that it could play a secondary role in inducing host cell death (Kettles *et al.*, 2018). Other proteins are expressed during later necrotrophic growth. The putative effector-

encoding gene *Zt80707* was shown to be required for virulence and was most highly expressed at 14 dpi, following symptom development (Poppe *et al*., 2015). Interestingly, the complement of CWDEs in the *Z. tritici* genome appears reduced compared to similar necrotrophic pathogens, with only 22 identified (do Amaral *et al*., 2012), although the protease-encoding gene family is relatively expanded. The characterisation of these, and other proteins secreted by *Z. tritici* during infection could elucidate how this pathogen successfully achieves pathogenicity on wheat leaves.

1.5.3 Wheat STB resistance genes

Twenty-two genetic regions conferring major resistance to STB have been genetically characterised (Brown *et al*., 2015, Yang *et al*., 2018), along with over one hundred resistance quantitative trait loci (QTLs). These major resistance loci are spread across the wheat genome. Some exist in close proximity: *Stb2* and *Stb11* are both located on the short arm of chromosome 1B (Liu *et al*., 2013) and *Stb7* and *Stb12* both on 4AL (Chartrain *et al*., 2005b), although these may in fact be allelic. Commercial wheat cultivars, such as the spring wheat cultivar (cv.) Veranapolis (Chartrain *et al*., 2005a), synthetic hexaploid wheat lines (created by crossing tetraploid durum wheat with a D genome progenitor; Ghaffary *et al*., 2012), and wild wheat relative *T. monococcum* (Jing *et al*., 2008) have all been identified as sources of STB resistance. Immunity conferred by these major resistance genes is narrow, often only to specific isolates. For example, *Stb15*, which confers resistance against the Ethiopian *Z. tritici* isolate IPO88004 (Arraiano *et al*., 2006) is present widely in European wheat cultivars, but is not associated with STB resistance there (Arraiano *et al.*, 2009). This narrow resistance can lead to rapid breakdown, as *Z. tritici* evolves to overcome the individual disease resistance genes. On its introduction to Oregon, USA in 1992, cv. Gene demonstrated broad STB resistance, which is thought to be due to the presence of *Stb4*. However, within three years breakdown of this resistance had led to the widespread abandonment of this cultivar for commercial use (Cowger *et al*., 2000). Similarly, upon discovery the resistance locus *Stb16q* was reported as conferring broad spectrum resistance (Ghaffary *et al*., 2012),

but recent reports suggest that this resistance is being overcome (Kildea *et al.,* 2020, Orellana-Torrejon *et al*., 2021).

Improved technologies are facilitating the discovery of new sources of genetic resistance to STB. Most analysis for STB resistance rests on the visual scoring of disease symptoms on wheat leaves, usually the appearance of pycnidia or the extent of necrotic lesions. Automated imaging technology and high-throughput phenotyping has facilitated an improved quantification of STB resistance, and with it more accurate QTL analysis (Stewart and McDonald, 2014, Stewart *et al*., 2016). The genetic markers used to track STB resistance genes through breeding programs have traditionally been microsatellites (also known as simple-sequence repeats or SSRs; Brown *et al*., 2015). However, these markers cannot be utilised in a high throughput manner. New markers, such as Kompetitive Allele-Specific PCR (KASP), are now more widely used. KASP markers have been used to help track the presence of the most recently identified resistance gene *Stb19*, during marker assisted breeding (Yang *et al*., 2018). These tools promise the more rapid identification and deployment in commercial cultivars of major STB resistance genes and resistance QTLs in future.

1.5.4 *Stb6* and *AvrStb6*

The best characterised STB resistance gene is *Stb6*. First identified by Brading *et al*. (2002) in cvs. Flame and Hereward, it maps to the short arm of chromosome 3A and confers specific resistance to *Z. tritici* isolate IPO323. The crossing of this avirulent isolate with the virulent isolate IPO94269 showed a 1:1 segregation of virulence (Kema *et al*., 2000), demonstrating the existence of a gene-for-gene interaction in this pathosystem. *Stb6* shows a semi-dominant phenotype, with F_2 progeny derived from crosses between cv. Flame (S*tb6*) and cv. Longbow (*stb6*) showing a 1:3 ratio of resistance to intermediate resistance or susceptible phenotype, and F_3 progeny segregating in a 1:2:1 ratio for the respective phenotypes (Brading *et al*., 2002). Incompatible interactions involving *Stb6* usually result in very few disease symptoms – none or very little necrosis and no pycnidia (Kema *et al*., 2000, Rudd *et al*., 2008), although Arraiano and Brown (2006) reported minor disease symptoms for cv. Cadenza

(*Stb6*) inoculated with IPO323. In-depth phenotyping of *Stb6* cv. Flame inoculated with IPO323 also reported the inhibition of hyphal growth following stomatal penetration, accompanied by the accumulation of H_2O_2 in the substomatal cavity (Shetty *et al*., 2003). *Stb6* is thought to have been introduced several times early in wheat cultivation (Chartrain *et al*., 2005a), and is common in modern wheat cultivars: a study of 238 European cultivars found 43 with demonstrated resistance to IPO323 (Arraiano and Brown, 2006).

The *Avr* gene responsible for incompatible interactions on *Stb6* wheat was first cloned by Zhong *et al.* (2017). The *Z. tritici* isolate 1E4, avirulent on wheat cultivars possessing *Stb6*, was crossed with the virulent isolate 1A5, with the resulting progeny showing a 1:1 ratio of virulence/avirulence phenotypes. Fine QTL mapping and GWAS analysis subsequently identified *1A5.g5534*, encoding a small, cysteine-rich secreted protein, found to be identical in 1E4 and IPO323 but possessing 16 SNPs in 1A5. The identity of *1A5.g5534* as the putative *AvrStb6* was confirmed by a subsequent functional analysis, with the transformation of the 1E4 allele of *AvrStb6* into 1A5 resulting in avirulence on *Stb6* wheat. As for many effectors, *AvrStb6* sits in a highly polymorphic, subtelomeric region populated with many transposable elements, which may facilitate duplication or mutation of genes (Sanchez-Vallet *et al*., 2018). *AvrStb6* was found to be expressed throughout the asymptomatic phase of infection, but peaked in both avirulent and virulent strains - being the 3rd and 6th most highly expressed gene, respectively - upon the emergence of disease symptoms. *AvrStb6* is specific to *Z. tritici* and as yet has no known function, with no functional domains identified.

Cloning of the *Stb6* resistance gene has also been achieved (Saintenac *et al*., 2018), by utilising fine mapping to identify two putative gene candidates. Using a variety of functional genomics approaches, including VIGS to silence gene candidates and assess for subsequent loss of *Stb6* resistance, TILLING to identify and test wheat lines lacking candidate genes, and stable wheat transformation to incorporate *Stb6* candidates into otherwise susceptible wheat cvs. Courtot and Bobwhite, *Stb6* was confirmed to be *TaWAKL4*. *Stb6*/*TaWAKL4* encodes a WAK-like protein, possessing a GUB_WAK_bind domain, a transmembrane domain and a cytoplasmic non-RD kinase, but

interestingly no EGF domain, a domain commonly observed in immunity-related WAKs (Figure 1.1). Also, whilst other disease resistance genes involved in gene-for-gene interactions, including many NB-LRRs and the WAK-like gene *Rlm9* of *Brassica napus*, induce HR upon recognition of their respective effectors (Larkan *et al*., 2020), *Stb6*-mediated resistance response lacks HR. Upon inoculation with *Z. tritici*, the expression levels of *Stb6* are upregulated approximately 2-fold above those of mock inoculated plants, until at least 17 dpi (Saintenac *et al.*, 2018). Resequencing of *Stb6* from numerous commercial cultivars and wild wheat relatives identified a strong prevalence of a functional haplotype, identical to that found in cv. Flame, among wheat varieties globally, supporting previous assessments (Chartrain *et al*., 2005a), and implying a historical importance of *Stb6*-mediated resistance in wheat cultivation.

1.6 Understanding the molecular basis of disease resistance against Septoria Tritici Blotch in wheat

Major questions still exist surrounding *Stb6*-mediated defence. No direct interaction has yet been observed between Stb6 and its corresponding fungal effector: yeast two-hybrid analysis identified no direct interaction between AvrStb6 and either the full-length Stb6 protein, the Stb6 kinase domain, or the extracellular portion of Stb6 (Saintenac *et al.*, 2018). Whether Stb6 recognises AvrStb6 directly, or via a decoy or guard mechanism, has yet to be determined. The downstream signalling, and the immediate Stb6 protein-protein interactions which characterise the *Stb6*-mediated defence response are also currently unknown. As for *AvrStb6*, understanding the population dynamics of various *AvrStb6* alleles could determine the breadth of effectiveness of *Stb6*-mediated resistance in modern wheat populations. Two previous studies have carried out sequence diversity analyses of *AvrStb6* in older *Z. tritici* populations, collected in 2010 (Zhong *et al*., 2017) and 1990-2001 (Brunner and McDonald, 2018, Zhan *et al*., 2005). However, the prevalence of *AvrStb6* alleles capable of evading *Stb6*-mediated defence, in either historic or current *Z. tritici* populations, is unknown. The specific polymorphisms that determine virulence or avirulence of the AvrStb6 protein have not yet been determined, although

two amino acid residue changes at positions 41 and 43 have been suggested as being critical for the pathogenicity on wheat cultivars carrying *Stb6* (Kema *et al.*, 2018).

The aims of this PhD project were therefore as follows:

- To analyse the population genetics of *AvrStb6*, including more modern isolates from global wheat growing regions, and to characterise virulence of identified isoforms on *Stb6* wheat, thus elucidating effectiveness of *Stb6* against current field isolates of *Z. tritici*.

- To study the putative function of AvrStb6 in pathogenicity, including identifying whether a direct interaction between Stb6 and AvrStb6 occurs and if this is required for the activation of *Stb6*-mediated defence.

- To identify the downstream components of *Stb6*-mediated defence signalling, thus providing better understanding the function of *Stb6* in plant immunity.

1.7 References

Acevedo-Garcia J, Gruner K, Reinstadler A, Kemen A *et al*. 2017. The powdery mildew-resistant Arabidopsis *mlo2 mlo6 mlo12* triple mutant displays altered infection phenotypes with diverse types of phytopathogens. *Scientific Reports* **7:** 9319.

Albert I, Hua C, Nurnberger T, Pruitt RN, Zhang L. 2020. Surface Sensor Systems in Plant Immunity**.** *Plant Physiol* **182:** 1582-1596.

Ameen G, Solanki S, Drader T, Sager-Bittara L, Steffenson B, Kleinhofs A, Vogiatzis C, Brueggeman RS. 2020. *rcs5*-mediated spot blotch resistance in barley is conferred by wall-associated kinases that resist pathogen manipulation. *bioRxiv*. DOI: 10.1101/2020.04.13.040238.

Anderson CM, Wagner TA, Perret M, He ZH, He DZ, Kohorn BD. 2001. WAKs: cell wall-associated kinases linking the cytoplasm to the extracellular matrix. *Plant Molecular Biology* **47:** 197-206.

Arraiano LS, Balaam N, Fenwick PM, Chapman C, Feuerhelm D, Howell P, Smith SJ, Widdowson JP, Brown JKM. 2009. Contributions of disease resistance and escape to the control of Septoria tritici blotch of wheat. *Plant Pathology* **58:** 910-922.

Arraiano LS, Brown JKM. 2006. Identification of isolate-specific and partial resistance to septoria tritici blotch in 238 European wheat cultivars and breeding lines. *Plant Pathology* **55:** 726-738.

Arraiano LS, Chartrain L, Bossolini E, Slatter HN, Keller B, Brown JKM. 2006. A gene in European wheat cultivars for resistance to an African isolate of *Mycosphaerella graminicola*. *Plant Pathology* **56:** 73-78.

Asai T, Tena G, Plotnikova J, Willmann MR, Chiu WL, Gomez-Gomez L, Boller T, Ausubel FM, Sheen J. 2002. MAP kinase signalling cascade in *Arabidopsis* innate immunity. *Nature* **415:** 977-983.

Bari R, Jones JD. 2009. Role of plant hormones in plant defence responses. *Plant Molecular Biology* **69:** 473-88.

Bot P, Mun BG, Imran QM, Hussain A, Lee SU, Loake G, Yun BW. 2019. Differential expression of *AtWAKL10* in response to nitric oxide suggests a putative role in biotic and abiotic stress responses. *PeerJ* **7**: e7383.

Bouton C, King RC, Chen H, Azhakanandam K, Bieri S, Hammond-Kosack KE, Kanyuka K. 2018. *Foxtail mosaic virus*: A viral vector for protein expression in cereals. *Plant Physiology* **177:** 1352-1367.

Bouwmeester K, Govers F. 2009. Arabidopsis L-type lectin receptor kinases: Phylogeny, classification, and expression profiles. *Journal of Experimental Botany* **60:** 4383-4396.

Brading PA, Verstappen ECP, Kema GHJ, Brown JKM. 2002. A gene-for-gene relationship between wheat and *Mycosphaerella graminicola*, the Septoria tritici blotch pathogen. *Phytopathology* **92:** 439-445.

Brennan CJ, Benbow HR, Mullins E, Doohan FM. 2019. A review of the known unknowns in the early stages of septoria tritici blotch disease of wheat. *Plant Pathology* **68:** 1427-1438.

Brown JKM, Chartrain L, Lasserre-Zuber P, Saintenac C. 2015. Genetics of resistance to *Zymoseptoria tritici* and applications to wheat breeding. *Fungal Genetics and Biology* **79:** 33-41.

Brunner F, Rosahl S, Lee J, Rudd JJ, Geiler C, Kauppinen S, Rasmussen G, Scheel D, Nurnberger T. 2002. Pep-13, a plant defense-inducing pathogen-associated pattern from *Phytophthora* transglutaminases. *EMBO Journal* **21:** 6681-6688.

Brunner PC, McDonald BA. 2018. Evolutionary analyses of the avirulence effector *AvrStb6* in global populations of *Zymoseptoria tritici* identify candidate amino acids involved in recognition. *Molecular Plant Pathology* **19:** 1836-1846.

Brutus A, Sicilia F, Macone A, Cervone F, De Lorenzo G. 2010. A domain swap approach reveals a role of the plant wall-associated kinase 1 (WAK1) as a receptor of oligogalacturonides. *Proceedings of the National Academy of Sciences, USA* **107:** 9452-9457.

Cayrol B, Delteil A, Gobbato E, Kroj T, Morel JB. 2016. Three wall-associated kinases required for rice basal immunity form protein complexes in the plasma membrane. *Plant Signalling & Behavior* **11:** e1149676.

Chartrain L, Brading PA, Brown JKM. 2005a. Presence of the *Stb6* gene for resistance to septoria tritici blotch (*Mycosphaerella graminicola*) in cultivars used in wheat-breeding programmes worldwide. *Plant Pathology* **54:** 134-143.

Chartrain L, Joaquim P, Berry ST, Arraiano LS, Azanza F, Brown JKM. 2005b. Genetics of resistance to septoria tritici blotch in the Portuguese wheat breeding line TE 9111. *Theoretical and Applied Genetics* **110:** 1138-1144.

Cook DE, Mesarich CH, Thomma BPHJ. 2015. Understanding plant immunity as a surveillance system to detect invasion. *Annual Review of Phytopathology* **53:** 541-563.

Cools HJ, Fraaije BA. 2008. Are azole fungicides losing ground against Septoria wheat disease? Resistance mechanisms in *Mycosphaerella graminicola*. *Pest Management Science* **64:** 681-684.

Cowger C, Hoffer ME, Mundt CC. 2000. Specific adaptation by *Mycosphaerella graminicola* to a resistant wheat cultivar. *Plant Pathology* **49:** 445-451.

Dardick C, Schwessinger B, Ronald P. 2012. Non-arginine-aspartate (non-RD) kinases are associated with innate immune receptors that recognize

conserved microbial signatures. *Current Opinion in Plant Biology* **15:** 358-366.

Decreux A, Messiaen J. 2005. Wall-associated kinase WAK1 interacts with cell wall pectins in a calcium-induced conformation. *Plant & Cell Physiology* **46:** 268-278.

Decreux A, Thomas A, Spies B, Brasseur R, Van Cutsem P, Messiaen J. 2006. *In vitro* characterization of the homogalacturonan-binding domain of the wall-associated kinase WAK1 using site-directed mutagenesis. *Phytochemistry* **67:** 1068-1079.

Delteil A, Gobbato E, Cayrol B, Estevan J, Michel-Romiti C, Dievart A, Kroj T, Morel JB. 2016. Several wall-associated kinases participate positively and negatively in basal defense against rice blast fungus. *BMC Plant Biology* **16**: 17.

Diener AC, Ausubel FM. 2005. *RESISTANCE TO FUSARIUM OXYSPORUM 1*, a dominant Arabidopsis disease-resistance gene, is not race specific. *Genetics* **171:** 305-321.

Dmochowska-Boguta M, Alaba S, Yanushevska Y, Piechota U, Lasota E, Nadolska-Orczyk A, Karlowski WM, Orczyk W. 2015. Pathogen-regulated genes in wheat isogenic lines differing in resistance to brown rust *Puccinia triticina*. *BMC Genomics* **16:** 742.

Dmochowska-Boguta M, Kloc Y, Zielezinski A, Werecki P, Nadolska-Orczyk A, Karlowski WM, Orczyk W. 2020. *TaWAK6* encoding wall-associated kinase is involved in wheat resistance to leaf rust similar to adult plant resistance. *PLoS One* **15:** e0227713.

do Amaral AM, Antoniw J, Rudd JJ, Hammond-Kosack KE. 2012. Defining the predicted protein secretome of the fungal wheat leaf pathogen *Mycosphaerella graminicola*. *PLoS One* **7:** e49904 DOI: 10.1371/journal.pone.0049904

Escobar-Restrepo JM, Huck N, Kessler S, Gagliardini V, Gheyselinck J, Yang WC, Grossniklaus U. 2007. The FERONIA receptor-like kinase mediates male-female interactions during pollen tube reception. *Science* **317:** 656-660.

Eyal Z, Scharen AL, Huffman MD, Prescott JM. 1985. Global Insights into virulence frequencies of *Mycosphaerella graminicola*. *Phytopathology* **75:** 1456-1462.

Feng H, Li C, Zhou J, Yuan Y, Feng Z, Shi Y, Zhao L, Zhang Y, Wei F, Zhu H. 2020. A cotton WAKL protein interacted with a DnaJ protein and was involved in defense against *Verticillium dahliae*. *International Journal of Biological Macromolecules* **167:** 633-643.

Ferrari S, Savatin DV, Sicilia F, Gramegna G, Cervone F, De Lorenzo, G. 2013. Oligogalacturonides: Plant damage-associated molecular patterns and regulators of growth and development. *Frontiers in Plant Science* **4**: 49.

Flor HH. 1971. Current status of gene-for-gene concept. *Annual Review of Phytopathology* **9:** 275-296.

Fones H, Gurr S. 2015. The impact of Septoria tritici Blotch disease on wheat: An EU perspective. *Fungal Genetics and Biology* **79: 3-7.**

Friesen TL, Meinhardt SW, Faris JD. 2007. The *Stagonospora nodorum*-wheat pathosystem involves multiple proteinaceous host-selective toxins and corresponding host sensitivity genes that interact in an inverse gene-for-gene manner. *Plant Journal* **51:** 681-692.

Gadaleta A, Colasuonno P, Giove SL, Blanco A, Giancaspro A. 2019. Map-based cloning of *QFhb.mgb-2A* identifies a *WAK2* gene responsible for Fusarium head blight resistance in wheat. *Scientific Reports* **9**: 6929.

Ghaffary SMT, Faris JD, Friesen TL, Visser RGF, van der Lee TAJ, Robert O, KEMA GHJ. 2012. New broad-spectrum resistance to Septoria tritici blotch derived from synthetic hexaploid wheat. *Theoretical and Applied Genetics* **124:** 125-142.

Gomez-Gomez L, Boller T. 2000. FLS2: An LRR receptor-like kinase involved in the perception of the bacterial elicitor flagellin in Arabidopsis. *Molecular Cell* **5:** 1003-1011.

Gramegna G, Modesti V, Savatin DV, Sicilia F, Cervone F, De Lorenzo G. 2016. *GRP-3* and *KAPP*, encoding interactors of WAK1, negatively affect defense responses induced by oligogalacturonides and local response to wounding. *Journal of Experimental Botany* **67**: 1715-1729.

Hahn F, Korolev A, Sanjurjo-Loures L, Nekrasov V. 2020. A modular cloning toolkit for genome editing in plants. *BMC Plant Biology* **20**: 179.

Harkenrider M, Sharma R, De Vleesschauwer D, Tsao L, Zhang XT, Chern M, Canlas P, Zuo SM, Ronald PC. 2016. Overexpression of rice WALL-ASSOCIATED KINASE 25 (OsWAK25) alters resistance to bacterial and fungal pathogens. *PLoS ONE* **11**: e0147310.

He ZH, Cheeseman I, He DZ, Kohorn BD. 1999. A cluster of five cell wall-associated receptor kinase genes, *Wak1-5*, are expressed in specific organs of Arabidopsis. *Plant Molecular Biology* **39:** 1189-1196.

He ZH, Fujiki M, Kohorn BD. 1996. A cell wall-associated, receptor-like protein kinase. *Journal of Biological Chemistry* **271:** 19789-19793.

He ZH, He DZ, Kohorn BD. 1998. Requirement for the induced expression of a cell wall associated receptor kinase for survival during the pathogen response. *Plant Journal* **14:** 55-63.

Heun M, Schäfer-Pregl R, Klawan D, Castagna R, Accerbi M, Borghi B, Salamini F. 1997. Site of einkorn wheat domestication identified by DNA fingerprinting. *Science* **278:** 1312-1314.

Hohmann U, Lau K, Hothorn M. 2017. The structural basis of ligand perception and signal activation by receptor kinases. *Annual Review of Plant Biology* **68:** 109-137.

Holton N, Nekrasov V, Ronald PC, Zipfel C. 2015. The phylogenetically-related pattern recognition receptors EFR and XA21 recruit similar immune signaling components in monocots and dicots. *PLoS Pathogens* **11:** e1004602 DOI: 10.1371/journal.ppat.1004602.

Hou XW, Tong HY, Selby J, Dewitt J, Peng XX, He ZH. 2005. Involvement of a cell wall-associated kinase, WAKL4, in Arabidopsis mineral responses. *Plant Physiology* **139:** 1704-1716.

Howard RJ, Valent B. 1996. Breaking and entering: host penetration by the fungal rice blast pathogen *Magnaporthe grisea*. *Annual Review of Microbiology* **50:** 491-512.

Hu KM, Cao JB, Zhang J *et al*. 2017. Improvement of multiple agronomic traits by a disease resistance gene via cell wall reinforcement. *Nature Plants* **3**: 17009.

Hurni S, Scheuermann D, Krattinger SG *et al*. The maize disease resistance gene *Htn1* against Northern corn leaf blight encodes a wall-associated

receptor-like kinase. *Proceedings of the National Academy of Sciences, USA* **112:** 8780-8785.

International Wheat Genome Sequencing Consortium (IWGSC). 2018. Shifting the limits in wheat research and breeding using a fully annotated reference genome. *Science* **361:** eaar7191.

Jess S, Kildea S, Moody A, Rennick G, Murchie AK, Cooke LR. 2014. European Union policy on pesticides: implications for agriculture in Ireland**.** *Pest Management Science* **70:** 1646-1654**.**

Jing HC, Lovell D, Gutteridge R, Jenk D, Kornyukhin D, Mitrofanova OP, Kema GH, Hammond-Kosack KE. 2008. Phenotypic and genetic analysis of the *Triticum monococcum - Mycosphaerella graminicola* interaction. *New Phytologist* **179, 1121-32.**

Jo Y, Cho WK, Rim Y, Moon J, Chen XY, Chu H, Kim CY, Park ZY, Lucas WJ, Kim JY. 2011. Plasmodesmal receptor-like kinases identified through analysis of rice cell wall extracted proteins. *Protoplasma* **248:** 191-203.

Johal GS, Briggs SP. 1992: Reductase activity encoded by the *HM1* disease resistance gene in maize. *Science* **258:** 985-987.

Johansson A, Staal J, Dixelius C. 2006. Early responses in the Arabidopsis-*Verticillium longisporum* pathosystem are dependent on NDR1, JA- and ET-associated signals via cytosolic NPR1 and RFO1. *Molecular Plant-Microbe Interactions* **19:** 958-969.

Jones JDG, Dangl JL. 2006. The plant immune system. *Nature* **444:** 323-329.

Kadota Y, Sklenar J, Derbyshire P *et al.* 2014. Direct regulation of the NADPH oxidase RBOHD by the PRR-associated kinase BIK1 during plant immunity. *Molecular Cell* **54:** 43-55.

Kaku H, Nishizawa Y, Ishii-Minami N, Akimoto-Tomiyama C, Dohmae N, Takio K, Minami E, Shibuya N. 2006. Plant cells recognize chitin fragments for defense signaling through a plasma membrane receptor. *Proceedings of the National Academy of Sciences, USA* **103:** 11086-11091.

Kankanala P, Czymmek K, Valent B. 2007. Roles for rice membrane dynamics and plasmodesmata during biotrophic invasion by the blast fungus. *Plant Cell* **19:** 706-724.

Kanyuka K, Rudd JJ. 2019. Cell surface immune receptors: the guardians of the plant's extracellular spaces. *Current Opinion in Plant Biology* **50:** 1-8.

Kellner R, Bhattacharyya A, Poppe S, Hsu TY, Brem RB, Stukenbrock EH. 2014. Expression profiling of the wheat pathogen *Zymoseptoria tritici* reveals genomic patterns of transcription and host-specific regulatory programs. *Genome Biology and Evolution* **6:** 1353-1365.

Kema GHJ, Verstappen EC, Todorova M, Waalwijk C. 1996a. Successful crosses and molecular tetrad and progeny analyses demonstrate heterothallism in *Mycosphaerella graminicola*. *Current Genetics* **30:** 251-258.

Kema GHJ, Verstappen EC, Waalwijk C. 2000. Avirulence in the wheat Septoria tritici leaf blotch fungus *Mycosphaerella graminicola* is controlled by a single locus. *Molecular Plant-Microbe Interactions* **13:** 1375-9.

Kema GHJ, Gohari AM, Aouini L *et al.* 2018. Stress and sexual reproduction affect the dynamics of the wheat pathogen effector AvrStb6 and strobilurin resistance. *Nature Genetics* **50:** 375-380.

Kema GHJ, Yu DZ, Rijkenberg FHJ, Shaw MW, Baayen RP. 1996b. Histology of the pathogenesis of *Mycosphaerella graminicola* in wheat. *Phytopathology* **86:** 777-786.

Keon J, Antoniw J, Carzaniga R, Deller S, Ward JL, Baker JM, Beale MH, Hammond-Kosack K, Rudd JJ. 2007. Transcriptional adaptation of *Mycosphaerella graminicola* to programmed cell death (PCD) of its susceptible wheat host. *Molecular Plant-Microbe Interactions* **20:** 178-193.

Kettles GJ, Bayon C, Sparks CA, Canning G, Kanyuka K, Rudd JJ. 2018. Characterization of an antimicrobial and phytotoxic ribonuclease secreted by the fungal wheat pathogen *Zymoseptoria tritici*. *New Phytologist* **217:** 320-331.

Kohorn BD. 2016. Cell wall-associated kinases and pectin perception. *Journal of Experimental Botany* **67**: 489-494.

Kohorn BD, Hoon D, Minkoff BB, Sussman MR, Kohorn SL. 2016. Rapid oligo-galacturonide induced changes in protein phosphorylation in Arabidopsis. *Molecular & Cellular Proteomics* **15:** 1351-1359.

Kohorn BD, Kobayashi M, Johansen S, Friedman HP, Fischer A, Byers N. 2006. Wall-associated kinase 1 (WAK1) is crosslinked in endomembranes, and transport to the cell surface requires correct cell-wall synthesis. *Journal of Cell Science* **119:** 2282-2290.

Kohorn BD, Kohorn SL. 2012. The cell wall-associated kinases, WAKs, as pectin receptors. *Frontiers in Plant Science* **3**: 88.

Kohorn BD, Kohorn SL, Saba NJ, Martinez VM. 2014. Requirement for pectin methyl esterase and preference for fragmented over native pectins for wall-associated kinase-activated, EDS1/PAD4-dependent stress response in Arabidopsis. *The Journal of Biological Chemistry* **289:** 18978-18986.

Krupa A, Preethl G, Srinivasan N. 2004. Structural modes of stabilization of permissive phosphorylation sites in protein kinases: Distinct strategies in Ser/Thr and Tyr kinases. *Journal of Molecular Biology* **339:** 1025-1039.

Lal NK, Nagalakshmi U, Hurlburt NK *et al.* 2018. The receptor-like cytoplasmic kinase BIK1 localizes to the nucleus and regulates defense hormone expression during plant innate immunity. *Cell Host & Microbe* **23:** 485-497.

Lally D, Ingmire P, Tong HY, He ZH. 2001. Antisense expression of a cell wall-associated protein kinase, WAK4, inhibits cell elongation and alters morphology. *Plant Cell* **13:** 1317-1331.

Larkan NJ, Ma L, Haddadi P, Buchwaldt M, Parkin IAP, Djavaheri M, Borhan MH. 2020. The *Brassica napus* wall-associated kinase-like (WAKL) gene *Rlm9* provides race-specific blackleg resistance. *Plant Journal* **104:** 892-900.

Larkan NJ, Yu FQ, Lydiate DJ, Rimmer SR, Borhan MH. 2016. Single *R* gene introgression lines for accurate dissection of the *Brassica* - *Leptosphaeria* pathosystem. *Frontiers in Plant Science* **7**: 1771.

Lauge R, Goodwin PH, De Wit PJ, Joosten MH. 2000. Specific HR-associated recognition of secreted proteins from *Cladosporium fulvum* occurs in both host and non-host plants. *Plant J* **23:** 735-745.

Lee WS, Rudd JJ, Hammond-Kosack KE, Kanyuka K. 2014. *Mycosphaerella graminicola* LysM effector-mediated stealth pathogenesis subverts recognition through both CERK1 and CEBiP homologues in wheat. *Molecular Plant-Microbe Interactions* **27:** 236-243.

Lehti-Shiu MD, Shiu SH. 2012. Diversity, classification and function of the plant protein kinase superfamily. *Philosophical Transactions of the Royal Society of London. Series B, Biological Sciences* **367:** 2619-2639.

Li H, Zhou SY, Zhao WS, Su SC, Peng YL. 2009. A novel wall-associated receptor-like protein kinase gene, OsWAK1, plays important roles in rice blast disease resistance. *Plant Molecular Biology* **69:** 337-346.

Li Q, Hu A, Qi J, Dou W, Qin X, Zou X, Xu L, Chen S, He Y. 2020. CsWAKL08, a pathogen-induced wall-associated receptor-like kinase in sweet orange, confers resistance to citrus bacterial canker via ROS control and JA signalling. *Horticulture Research* **7:** 42.

Liebrand TW, Van Den Burg HA, Joosten MH. 2014. Two for all: receptor-associated kinases SOBIR1 and BAK1. *Trends in Plant Science* **19:** 123-32.

Liu Y, Zhang L, Thompson IA, Goodwin SB, Ohm HW. 2013. Molecular mapping re-locates the *Stb2* gene for resistance to Septoria tritici blotch derived from cultivar Veranopolis on wheat chromosome 1BS. *Euphytica* **190:** 145-156.

Liu ZH, Zhang ZC, Faris JD *et al*. 2012. The cysteine rich necrotrophic effector SnTox1 produced by *Stagonospora nodorum* triggers susceptibility of wheat lines harboring *Snn1*. *PLoS Pathogens* **8:** e1002467.

Lorang J, Kidarsa T, Bradford CS, Gilbert B, Curtis M, Tzeng SC, Maier CS, Wolpert TJ. 2012. Tricking the guard: Exploiting plant defense for disease susceptibility. *Science* **338:** 659-662.

Lu DP, Wu SJ, Gao XQ, Zhang YL, Shan LB, He P. 2010. A receptor-like cytoplasmic kinase, BIK1, associates with a flagellin receptor complex to initiate plant innate immunity. *Proceedings of the National Academy of Sciences, USA* **107:** 496-501.

Malukani KK, Ranjan A, Hota SJ, Patel HK, Sonti RV. 2020. Dual activities of receptor-like kinase OsWAKL21.2 induce immune responses. *Plant Physiology* **183**: 1345-1363.

Mangeon A, Menezes-Salgueiro AD, Sachetto-Martins G. 2017. Start me up: Revision of evidences that AtGRP3 acts as a potential switch for AtWAK1. *Plant Signalling & Behavior* **12**: 2.

Mangeon A, Pardal R, Menezes-Salgueiro AD *et al.* 2016. *AtGRP3* is implicated in root size and aluminum response pathways in *Arabidopsis*. *PLoS One* **11:** e0150583 DOI: 10.1371/journal.pone.0150583

Marshall R, Kombrink A, Motteram J, Loza-Reyes E, Lucas J, Hammond-Kosack KE, Thomma BPHJ, Rudd JJ. 2011. Analysis of two *in planta*

expressed LysM effector homologs from the fungus *Mycosphaerella graminicola* reveals novel functional properties and varying contributions to virulence on wheat. *Plant Physiology* **156:** 756-769.

M'Barek SB, Cordewener JHG, Ghaffary SMT *et al.* 2015. FPLC and liquid-chromatography mass spectrometry identify candidate necrosis-inducing proteins from culture filtrates of the fungal wheat pathogen *Zymoseptoria tritici*. *Fungal Genetics and Biology* **79:** 54-62.

McGrann GR, Stavrinides A, Russell J, Corbitt MM, Booth A, Chartrain L, Thomas WT, Brown JK. 2014. A trade off between *mlo* resistance to powdery mildew and increased susceptibility of barley to a newly important disease, Ramularia leaf spot. *Journal of Experiemntal Botany* **65:** 1025-1037.

Meco V, Egea I, Ortiz-Atienza A *et al*. 2020. The salt sensitivity induced by disruption of cell *Wall-associated kinase 1* (*SlWAK1*) tomato gene is linked to altered osmotic and metabolic homeostasis. *International Journal of Molecular Sciences* **21:** 6308.

Meier S, Madeo L, Ederli L, Donaldson L, Pasqualini S, Gehring C. 2009. Deciphering cGMP signatures and cGMP-dependent pathways in plant defence. *Plant Signaling & Behaviour* **4:** 307-309.

Meier S, Ruzvidzo O, Morse M, Donaldson L, Kwezi L, Gehring C. 2010. The Arabidopsis *Wall associated kinase-like 10* gene encodes a functional guanylyl cyclase and is co-expressed with pathogen defense related genes. *PLoS ONE* **5:** e8904.

Miya A, Albert P, Shinya T *et al.* 2007. CERK1, a LysM receptor kinase, is essential for chitin elicitor signaling in *Arabidopsis*. *Proceedings of the National Academy of Sciences, USA* **104:** 19613-19618.

Moscatiello R, Mariani P, Sanders D, Maathuis FJM. 2006. Transcriptional analysis of calcium-dependent and calcium-independent signalling pathways induced by oligogalacturonides. *Journal of Experimental Botany* **57:** 2847-2865.

Motteram J, Kufner I, Deller S, Brunner F, Hammond-Kosack KE, Nurnberger T, Rudd JJ. 2009. Molecular characterization and functional analysis of MgNLP, the sole NPP1 domain-containing protein, from the

fungal wheat leaf pathogen *Mycosphaerella graminicola*. *Molecular Plant-Microbe Interactions* **22:** 790-799.

Motteram J, Lovegrove A, Pirie E, Marsh J, Devonshire J, van de Meene A, Hammond-Kosack KE, Rudd JJ. 2011. Aberrant protein N-glycosylation impacts upon infection-related growth transitions of the haploid plant-pathogenic fungus *Mycosphaerella graminicola*. *Molecular Microbiology* **81:** 415-433.

Nothnagel EA, McNeil M, Albersheim P, Dell A. 1983. Host-pathogen interactions: XXII. A galacturonic acid oligosaccharide from plant-cell walls elicits phytoalexins. *Plant Physiology* **71:** 916-926.

Oliver RP, Friesen TL, Faris JD, Solomon PS. 2012. *Stagonospora nodorum*: From pathology to genomics and host resistance. *Annual Review of Phytopathology* **50:** 23-43.

Orellana-Torrejon C, Vidal T, Boixel A, Gélisse S, Saint-Jean S, Frédéric S. 2021. Annual dynamics of *Zymoseptoria tritici* populations in wheat cultivar mixtures: a compromise between the efficiency and durability of a recently broken-down resistance gene. *bioRxiv.* DOI: 10.1101/2021.04.23.441180

Palma-Guerrero J, Ma X, Torriani SFF, Zala M, Francisco CS, Hartmann FE, Croll D, McDonald BA. 2017. Comparative transcriptome analyses in *Zymoseptoria tritici* reveal significant differences in gene expression among strains during plant infection. *Molecular Plant-Microbe Interactions* **30:** 231-244.

Palma-Guerrero J, Torriani SFF, Zala M, Carter D, Courbot M, Rudd JJ, McDonald BA, Croll D. 2016. Comparative transcriptomic analyses of *Zymoseptoria tritici* strains show complex lifestyle transitions and intraspecific variability in transcription profiles. *Molecular Plant Pathology* **17:** 845-859.

Park AR, Cho SK, Yun UJ, Jin MY, Lee SH, Sachetto-Martins G, Park OK. 2001. Interaction of the Arabidopsis receptor protein kinase WAK1 with a glycine-rich protein, AtGRP-3. *The Journal of Biological Chemistry* **276:** 26688-26693.

Poppe S, Dorsheimer L, Happel P, Stukenbrock EH. 2015. Rapidly evolving genes are key players in host specialization and virulence of the fungal

wheat pathogen *Zymoseptoria tritici* (*Mycosphaerella graminicola*). *PLoS Pathogens* **11:** e1005055 DOI: 10.1371/journal.ppat.1005055

Qutob D, Kemmerling B, Brunner F *et al*. 2006. Phytotoxicity and innate immune responses induced by Nep1-like proteins. *Plant Cell* **18:** 3721-3744.

Ranf S, Eschen-Lippold L, Frohlich K, Westphal L, Scheel D, Lee J. 2014. Microbe-associated molecular pattern-induced calcium signaling requires the receptor-like cytoplasmic kinases, PBL1 and BIK1. *BMC Plant Biology* **14:** DOI: 10.1186/s12870-014-0374-4

Rohila JS, Chen M, Chen S *et al*. 2006. Protein-protein interactions of tandem affinity purification-tagged protein kinases in rice. *Plant Journal* **46:** 1-13.

Rosli HG, Zheng Y, Pombo MA, Zhong SL, Bombarely A, Fei ZJ, Collmer A, Martin GB. 2013. Transcriptomics-based screen for genes induced by flagellin and repressed by pathogen effectors identifies a cell wall-associated kinase involved in plant immunity. *Genome Biology* **14**: R139.

Roux M, Schwessinger B, Albrecht C *et al.* 2011. The Arabidopsis leucine-rich repeat receptor-like kinases BAK1/SERK3 and BKK1/SERK4 are required for innate immunity to hemibiotrophic and biotrophic pathogens. *Plant Cell* **23:** 2440-2455.

Rudd JJ. 2015. Previous bottlenecks and future solutions to dissecting the *Zymoseptoria tritici*-wheat host-pathogen interaction. *Fungal Genetics and Biology* **79:** 24-28.

Rudd JJ, Kanyuka K, Hassani-Pak K *et al.* 2015. Transcriptome and metabolite profiling of the infection cycle of *Zymoseptoria tritici* on wheat reveals a biphasic interaction with plant immunity involving differential pathogen chromosomal contributions and a variation on the hemibiotrophic lifestyle definition. *Plant Physiology* **167:** 1158-1185.

Rudd JJ, Keon J, Hammond-Kosack KE. 2008. The wheat mitogen-activated protein kinases TaMPK3 and TaMPK6 are differentially regulated at multiple levels during compatible disease interactions with *Mycosphaerella graminicola*. *Plant Physiology* **147:** 802-815.

Saintenac C, Lee W-S, Cambon F *et al*. 2018. Wheat receptor-kinase-like protein Stb6 controls gene-for-gene resistance to fungal pathogen *Zymoseptoria tritici*. *Nature Genetics* **50:** 368-374.

Sampoli Benitez BA, Komives EA. 2000. Disulfide bond plasticity in epidermal growth factor. *Proteins* **40:** 168-74.

Sanchez-Vallet A, Fouche S, Fudal I, Hartmann FE, Soyer JL, Tellier A, Croll D. 2018. The genome biology of effector gene evolution in filamentous plant pathogens. *Annu Rev Phytopathol* **56:** 21-40.

Sanchez-Vallet A, McDonald MC, Solomon PS, McDonald BA. 2015. Is *Zymoseptoria tritici* a hemibiotroph? *Fungal Genetics and Biology* **79:** 29-32.

Scalliet G, Bowler J, Luksch T *et al.* 2012. Mutagenesis and functional studies with succinate dehydrogenase inhibitors in the wheat pathogen *Mycosphaerella graminicola*. *PLoS One* **7:** e35429. DOI: 10.1371/journal.pone.0035429

Schwessinger B, Bart R, Krasileva KV, Coaker G. 2015. Focus issue on plant immunity: from model systems to crop species. *Frontiers in Plant Science* **6:** 195.

Schwessinger B, Ronald PC. 2012. Plant innate immunity: perception of conserved microbial signatures. *Annual Review of Plant Biology* **63:** 451-82.

Selander-Sunnerhagen M, Ullner M, Persson E, Teleman O, Stenflo J, Drakenberg T. 1992. How an epidermal growth factor (EGF)-like domain binds calcium. High resolution NMR structure of the calcium form of the NH2-terminal EGF-like domain in coagulation factor X. *Journal of Biological Chemistry* **267:** 19642-19649.

Seo YS, Chern M, Bartley LE *et al*. 2011. Towards establishment of a rice stress response interactome. *PLoS Genetics* **7**: e1002020.

Shen Y, Diener AC. 2013. *Arabidopsis thaliana RESISTANCE TO FUSARIUM OXYSPORUM2* implicates tyrosine-sulfated peptide signalling in susceptibility and resistance to root infection. *PLoS Genetics* **9:** e1003525.

Shetty NP, Kristensen BK, Newman MA, Moller K, Gregersen PL, Jorgensen HJL. 2003. Association of hydrogen peroxide with restriction of *Septoria tritici* in resistant wheat. *Physiological and Molecular Plant Pathology* **62:** 333-346.

Shewry PR. 2009. Wheat. *Journal of Experimental Botany* **60:** 1537-53.

Shi G, Zhang Z, Friesen TL, Raats D, Fahima T, Brueggeman RS, Lu S, Trick HN, Liu Z, Chao W. 2016. The hijacking of a receptor kinase–driven

pathway by a wheat fungal pathogen leads to disease. *Science Advances* **2:** e1600822.

Sivaguru M, Ezaki B, He ZH, Tong HY, Osawa H, Baluska F, Volkmann D, Matsumoto H. 2003. Aluminum-induced gene expression and protein localization of a cell wall-associated receptor kinase in *Arabidopsis*. *Plant Physiology* **132:** 2256-2266.

Song WY, Wang GL, Chen L *et al*. 1995. A receptor kinase-like protein encoded by the rice disease resistance gene, *Xa21*. *Science* **270:** 1804-1806.

Steinberg G. 2015. Cell biology of *Zymoseptoria tritici*: Pathogen cell organization and wheat infection. *Fungal Genetics and Biology* **79:** 17-23.

Stewart EL, Hagerty CH, Mikaberidze A, Mundt CC, Zhong ZM, McDonald BA. 2016. An improved method for measuring quantitative resistance to the wheat pathogen *Zymoseptoria tritici* using high-throughput automated image analysis. *Phytopathology* **106:** 782-788.

Stewart EL, McDonald BA. 2014. Measuring quantitative virulence in the wheat pathogen *Zymoseptoria tritici* using high-throughput automated image analysis. *Phytopathology* **104:** 985-992.

Sun Z, Song Y, Chen D, Zang Y, Zhang Q, Yi Y, Qu G. 2020. Genome-wide identification, classification, characterization, and expression analysis of the wall-associated kinase family during fruit development and under wound stress in tomato (*Solanum lycopersicum* L.). *Genes* **11**: 1186.

Thomas NC, Oksenberg N, Liu FR, Caddell D, Nalyvayko A, Nguyen Y, Schwessinger B, Ronald PC. 2018. The rice XA21 ectodomain fused to the *Arabidopsis* EFR cytoplasmic domain confers resistance to *Xanthomonas oryzae* pv. *oryzae*. *PeerJ* **6:** e4456 DOI: 10.7717/peerj.4456

Thomma BPHJ, Nurnberger T, Joosten MHAJ. 2011. Of PAMPs and effectors: The blurred PTI-ETI dichotomy. *Plant Cell* **23:** 4-15.

Tocquard K, Lafon-Placette C, Auguin D *et al*. 2014. *In silico* study of wall-associated kinase family reveals large-scale genomic expansion potentially connected with functional diversification in *Populus*. *Tree Genetics and Genomes* **10**: 1135-1147.

Torriani SFF, Brunner PC, McDonald BA, Sierotzki H. 2009. QoI resistance emerged independently at least 4 times in European populations of *Mycosphaerella graminicola*. *Pest Management Science* **65:** 155-162.

Torriani SFF, Melichar JPE, Mills C, Pain N, Sierotzki H, Courbot M. 2015. *Zymoseptoria tritici*: A major threat to wheat production, integrated approaches to control. *Fungal Genetics and Biology* **79:** 8-12.

Tripathi RK, Aguirre JA, Singh J. 2020. Genome-wide analysis of wall associated kinase (WAK) gene family in barley. *Genomics* **113**: 523-530.

Van Der Biezen EA, Jones JDG. 1998. Plant disease-resistance proteins and the gene-for-gene concept. *Trends in Biochemical Sciences* **23:** 454-456.

Verica JA, Chae L, Tong HY, Ingmire P, He ZH. 2003. Tissue-specific and developmentally regulated expression of a cluster of tandemly arrayed cell wall-associated kinase-like kinase genes in Arabidopsis. *Plant Physiology* **133:** 1732-1746.

Verica JA, He ZH. 2002. The cell wall-associated kinase (WAK) and WAK-like kinase gene family. *Plant Physiology* **129:** 455-459.

Wagner TA, Kohorn BD. 2001. Wall-associated kinases are expressed throughout plant development and are required for cell expansion. *Plant Cell* **13:** 303-318.

Wang H, Niu HH, Liang MM, Zhai YF, Huang W, Ding Q, Du Y, Lu MH. 2019. A Wall-associated kinase gene *CaWAKL20* from pepper negatively modulates plant thermotolerance by reducing the expression of ABA-responsive genes. *Frontiers in Plant Science* **10:** 591 DOI: 10.3389/fpls.2019.00591

Wang N, Huang HJ, Ren ST, Li JJ, Sun Y, Sun DY, Zhang SQ. 2012. The rice wall-associated receptor-like kinase gene *OsDEES1* plays a role in female gametophyte development. *Plant Physiology* **160:** 696-707.

Wang P, Zhou L, Jamieson P *et al*. 2020. The cotton wall-associated kinase GhWAK7A mediates responses to fungal wilt pathogens by complexing with the chitin sensory receptors. *Plant Cell* **32:** 3978-4001.

Wang Y, Cheng X, Shan Q, Zhang Y, Liu J, Gao C, Qiu JL. 2014. Simultaneous editing of three homoeoalleles in hexaploid bread wheat confers heritable resistance to powdery mildew. *Nature Biotechnology* **32:** 947-951.

Wei T, Ou B, Li JB *et al*. 2013. Transcriptional profiling of rice early response to *Magnaporthe oryzae* identified OsWRKYs as important regulators in rice blast resistance. *PLoS ONE* **8**: 3.

Wu J, Reca IB, Spinelli F, Lironi D, De Lorenzo G, Poltronieri P, Cervone F, Joosten MH, Ferrari S, Brutus A. 2019. An EFR-Cf-9 chimera confers enhanced resistance to bacterial pathogens by SOBIR1-and BAK1-dependent recognition of elf18. *Molecular Plant Pathology* **20**: 751-764.

Wu X, Bacic A, Johnson KL, Humphries J. 2020. The role of *Brachypodium distachyon* wall-associated kinases (WAKs) in cell expansion and stress responses. *Cells* **9**: 2478.

Xu N, Fu D, Li S, Wang Y, Wong A. 2018. GCPred: a web tool for guanylyl cyclase functional centre prediction from amino acid sequence. *Bioinformatics* **34:** 2134-2135.

Yang J, Xie M, Wang X, Wang G, Zhang Y, Li Z, Ma Z. 2021. Identication of cell wall-associated kinases as important regulators involved in *Gossypium hirsutum* resistance to *Verticillium dahliae*. *BMC Plant Biology* **21**, 220.

Yang K, Qi L, Zhang Z. 2014. Isolation and characterization of a novel wall-associated kinase gene *TaWAK5* in wheat (*Triticum aestivum*). *The Crop Journal* **2:** 255-266.

Yang N, McDonald MC, Solomon PS, Milgate AW. 2018. Genetic mapping of *Stb19*, a new resistance gene to *Zymoseptoria tritici* in wheat. *Theoretical and Applied Genetics* **131:** 2765-2773.

Yang P, Praz C, Li BB *et al*. 2019. Fungal resistance mediated by maize wall-associated kinase ZmWAK-RLK1 correlates with reduced benzoxazinoid content. *New Phytologist* **221:** 976-987.

Yarden Y, Sliwkowski MX. 2001. Untangling the ErbB signalling network. *Nature Reviews Molecular Cell Biology* **2:** 127-137.

Yin XY, Hou XW. 2017. Role of OsWAK124, a rice wall-associated kinase, in response to environmental heavy metal stresses. *Pakistan Journal of Botany* **49:** 1255-1261.

Yuan M, Jiang Z, Bi G et al. 2021. Pattern-recognition receptors are required for NLR-mediated plant immunity. *Nature* **592:** 105–109.

Zhan J, Linde CC, Jurgens T, Merz U, Steinebrunner F, McDonald BA. 2005. Variation for neutral markers is correlated with variation for quantitative

traits in the plant pathogenic fungus *Mycosphaerella graminicola*. *Molecular Ecology* **14:** 2683-2693.

Zhang B, Li P, Su T *et al*. 2019. Comprehensive analysis of wall-associated kinase genes and their expression under abiotic and biotic stress in chinese cabbage (*Brassica rapa* ssp. *pekinensis*). *Journal of Plant Growth Regulation* **39**: 72-86.

Zhang N, Pombo MA, Rosli HG, Martin GB. 2020. Tomato wall-associated kinase SlWak1 depends on Fls2/Fls3 to promote apoplastic immune responses to *Pseudomonas syringae*. *Plant Physiology* **183:** 1869-1882.

Zhang N, Zhang BQ, Zuo WL, Xing YX, Konlasuk S, Tan GQ, Zhang QQ, Ye JR, Xu ML. 2017. Cytological and molecular characterization of ZmWAK-mediated head-smut resistance in maize. *Molecular Plant-Microbe Interactions* **30:** 455-465.

Zhang, SB, Chen C, Li L, Meng L, Singh J, Jiang N, Deng XW, He ZH, Lemaux PG. 2005. Evolutionary expansion, gene structure, and expression of the rice wall-associated kinase gene family. *Plant Physiology* **139:** 1107-1124.

Zhong Z, Marcel TC, Hartmann FE *et al*. 2017. A small secreted protein in *Zymoseptoria tritici* is responsible for avirulence on wheat cultivars carrying the *Stb6* resistance gene. *New Phytologist* **214:** 619-631.

Zipfel C, Kunze G, Chinchilla D, Caniard A, Jones JDG, Boller T, Felix G. 2006. Perception of the bacterial PAMP EF-Tu by the receptor EFR restricts Agrobacterium-mediated transformation. *Cell* **125:** 749-760.

Zuo CW, Liu YL, Guo ZG, Mao J, Chu MY, Chen BH. 2019. Genome-wide annotation and expression responses to biotic stresses of the wall-associated kinase - receptor-like kinase (WAK-RLK) gene family in apple (*Malus domestica*). *European Journal of Plant Pathology* **153:** 771-785.

Zuo WL, Chao Q, Zhang N *et al*. 2015. A maize wall-associated kinase confers quantitative resistance to head smut. *Nature Genetics* **47:** 151-157.

Chapter 2: Materials and Methods

The following chapter describes the origins of materials and organisms used in this study, as well as detailed descriptions of methods used in more than one chapter of this thesis.

2.1 Acknowledgements

Cyril Zipfel (University of Zurich, Switzerland) kindly provided the protocol used for protein extraction from *Nicotiana benthamiana* leaves. Nomad Bioscience GmbH (Halle, Germany) kindly allowed use of their “CryX” strain of *Agrobacterium tumefaciens* for agroinfiltration studies. Thanks also to Steve Thomas (Rothamsted Research) for providing yeast control lines for yeast two-hybrid assays, Govindprasad Bhutada (Rothamsted Research) for providing some restriction enzymes and advice on their use, Peter Buchner (Rothamsted Research) for allowing use of his Odyssey Fc imager and Tsuyoshi Nakagawa (Shimane University, Japan) for providing the pGWB vector series for protein fluorophore tagging.

2.2 Materials and chemicals

2.2.1 Growth media

Bacterial and fungal cultures were grown either on agar media or in liquid broth. Bacterial strains were grown in/on Luria-Bertani (LB) broth/agar, with LB Miller used to culture *Escherichia coli* and LB Lennox for *Agrobacterium tumefaciens*. *Saccharomyces cerevisiae* was cultured on yeast peptone dextrose (YPD), YPD with supplemented adenine (YPAD) or synthetic complete (SC) media, which lacks specific amino acids for yeast transformants selection (Section 2.7). *Zymoseptoria tritici* strains were cultured on YPD for plant inoculation assays (Section 2.6). All growth media was sourced from Formedium (UK).

2.2.2 Bacterial strains

E. coli strains were used to bulk DNA plasmids used within this study. Two strains were used to bulk experimental plasmids: DH5α and DH10B, both from ThermoFisher Scientific, UK. For bulking plasmids containing the toxin-encoding *ccdB* gene, *ccdB* survival cells (derived from DH10B) were used, which possess the anti-toxin *ccdA* gene (ThermoFisher). All *E. coli* strains were incubated at 37˚C. *Agrobacterium tumefaciens* (hereafter referred to as Agrobacterium) was used to transform the tobacco plant *Nicotiana benthamiana* using strains GV3101 (possessing plasmid pMP90) and CryX. The CryX strain was provided by Nomad Bioscience GmbH (Halle, Germany). Incubation of Agrobacterium strains was carried out at 28˚C, unless otherwise stated.

2.2.3 DNA plasmids

Vector plasmids were utilised to create DNA constructs used in this study (Table 2.1). Successful bacterial transformants (Section 2.3.1) were identified by selection for antibiotic resistance. Some plasmids possess secondary selection genes, such as the *ccdB* gene and chloramphenicol resistance (Cm^r) gene, which may be used as counter-selection markers. The *ccdB* gene is lethal to bacterial strains lacking the corresponding *ccdA* gene, thus preventing growth of bacteria transformed with incorrectly assembled constructs. The pDEST32 (“bait”) and pDEST32 (“prey”) plasmids for yeast two-hybrid assays (Section 2.7) possess *Trp1* and *Leu2*, which allow growth of yeast on media lacking tryptophan and leucine, respectively. The pGWB vector series, created by Nakamura *et al*. (2010) also contain the *bar* gene for plant transformant selection, which confers resistance to herbicides such as BASTA. pSOUP, known as a “helper plasmid”, possesses *trfA* which facilitates the replication of co-transformed pGREEN vectors.

2.2.4 Antibiotics

Antibiotics were used for transformation selection, with resistance conferred by the transformed plasmid. See Table 2.2 for antibiotics used and their working concentrations.

Table 2.1. DNA plasmids used in this study

Plasmid name	Cloning site	Antibiotic resistance	Other genes
p19	N/A	Kanamycin	-
pCGEN	Multiple cloning site (MCS)	Kanamycin	-
pDONR207	Gateway BP cloning sites	Gentamicin	ccdB, Cm^r
pDONR221	Gateway BP cloning sites	Kanamycin	ccdB, Cm^r
pSOUP	MCS	Tetracycline	trfA
pDEST22	Gateway LR cloning sites	Ampicillin	ccdB, trp1, Cm^r, ADH1::GAL4 (AD)
pDEST32	Gateway LR cloning sites	Gentamicin	ccdB, leu2, Cm^r, ADH1::GAL4 (DB)
pEN-R2-GSrhinotag-L3	Gateway LR cloning sites	Ampicillin	Gsrhino (C-terminal) tag
pGWB605	Gateway LR cloning sites	Spectinomycin	ccdB, Cm^r, bar, GFP (C-terminal) tag
pGWB654	Gateway LR cloning sites	Spectinomycin	ccdB, Cm^r, bar, mRFP (C-terminal) tag
pGWB655	Gateway LR cloning sites	Spectinomycin	ccdB, Cm^r, bar, mRFP (N-terminal) tag
pEAQ	MCS	Kanamycin	p19
pK7WR2	Gateway LR cloning sites	Spectinomycin	-

Table 2.2. Antibiotics used in this study

Antibiotic	Working concentration (µg/ml)
Ampicillin/Carbenicillin	100
Gentamicin	25
Geneticin (G418)	100
Kanamycin	50
Spectinomycin	100
Tetracycline	10

2.3 Molecular cloning protocols

2.3.1 Bacterial transformation

E. coli and Agrobacterium cells were first made competent for electroporation transformation with plasmids. Bacteria from glycerol stocks were streaked onto LB agar and incubated (24 h for *E. coli*, 48 h for Agrobacterium). Bacterial growth was used to inoculate 2 ml of LB broth, which was incubated overnight (180 rpm rotary shaker). An aliquot (400 µl) of overnight liquid culture was then used to inoculate 450 ml of LB broth and incubated (180 rpm) until optical density at 600 nm wavelength (OD_{600}) reached 0.35-0.4 for *E. coli*, or OD_{500} - 0.5-0.7 for Agrobacterium. Suspensions were transferred to prechilled 250 ml centrifuge tubes (Beckman) and incubated on ice for 30 min. Tubes were then centrifuged (2600 g, 20 min, 4˚C), the supernatant removed and the pellets resuspended in 200 ml ice-cold sterile deionised (D.I.) water. This centrifugation and resuspension of the pellet in D.I. water was repeated at least three times. Following washing, pellets were resuspended in 40 ml ice-cold sterile 10% glycerol and centrifuged as above. The pellet was resuspended in 1-2 ml supernatant, with 50 µl aliquots of this electrocompetent cell suspension snap-frozen on dry ice and stored at -80˚C until use.

Electroporation transformation of *E. coli* and Agrobacterium was carried out using a BioRad Micropulser. Aliquots of electrocompetent cells were thawed on ice and mixed with 0.1-0.5 µg DNA and transferred to a prechilled 1 mm electroporation cuvette (Cell Projects, UK). Following electroporation, bacterial suspension was transferred to a microcentrifuge tube with 1 ml LB broth and incubated (180 rpm; 1 h for *E. coli*, 2 h for Agrobacterium). 50 µl suspension was spread on LB agar plates supplemented with antibiotics for selection. Colonies appeared on selection plates after 24 h (*E. coli*) or 48 h (Agrobacterium) incubation. *E. coli* colonies were assessed for successful transformation by colony PCR (Section 2.3.4).

2.3.2 DNA extraction

Vector constructs, bulked in *E. coli*, were extracted for subsequent use. Successful *E. coli* colonies were picked with a sterile toothpick and transferred to 2 ml LB broth (supplemented with antibiotics) and incubated overnight (180

rpm). Vector extraction from overnight culture was carried out using QIAprep Spin Miniprep Kit (Qiagen). Midipreps were carried out using 50 ml overnight bacterial cultures. In both cases, protocols described in the Qiagen Plasmid Mini, Midi and Maxi Kits Handbook were followed. *S. cerevisiae* DNA extractions were also carried out using EZ Yeast™ Plasmid MiniPrep (G Biosciences). *S. cerevisiae* was grown in 2 ml YPD broth overnight (180 rpm, 30˚C), before following manufacturer's protocol.

Genomic DNA was extracted from *Z. tritici* using the following protocol. *Z. tritici* blastospores from glycerol stocks were streaked onto YPD plates and incubated (7 days, 15˚C) to induce yeast-like growth. A 5 µl loop of yeast-like growth was transferred to a microcentrifuge tube, frozen at -80˚C and freeze-dried overnight. Cells were lysed by adding a small ball bearing and using a Fast Prep-24 homogeniser (4.0 m/sec for 20 sec; MP Biomedicals). 1 ml DNA extraction buffer (Table 2.3) was added to the lysed cells and incubated at 65˚C for 20 min. 350 µl ice-cold ammonium acetate (7.5 M) was added and mixed, before incubation on ice for 20 min. Tubes were centrifuged (16,000 g, 15 min) and the supernatant added to fresh tubes with 900 µl isopropanol. Tubes were incubated (room temperature (RT), 15 min), before centrifugation (16,000 g, 15 min). The DNA pellet was washed with 400 µl 70% ethanol, recentrifuged (16,000 g, 15 min), the pellet air-dried and resuspended in 100 µl nuclease-free water.

Genomic DNA was extracted from wheat leaves for *Stb6* allele analysis. 5 cm sections of leaf were placed in a 2 ml microcentrifuge tube and snap frozen in liquid nitrogen, the leaf material ground with a micro pestle and suspended in 600 µl extraction buffer (Table 2.3), prewarmed to 65˚C. Samples were vortexed and incubated (1 h, 65˚C), with occasional inversion. Tubes were then chilled on ice and 300 µl ice-cold ammonium acetate (6 M) was added. Tubes were vortexed and incubated (30 min, on ice). Tubes were centrifuged (12,000 g, 10 min) and supernatant transferred to a fresh microcentrifuge tube. 0.8 volumes of isopropanol were added, mixed by inversion and incubated (-20˚C, overnight). Tubes were centrifuged (12,000 g, 10 min), the supernatant discarded and the DNA pellet washed with 750 µl 70% ethanol. The above

centrifugation and ethanol washing was repeated. The DNA pellet was air-dried, before resuspension in 50 µl nuclease-free water.

2.3.3 RNA extraction from wheat leaves

For RNA extraction, wheat leaves were snap-frozen in liquid nitrogen, before grinding in a prechilled pestle and mortar under liquid nitrogen. Approximately 50-100 mg of leaf powder was mixed with 1 ml Trizol (ThermoFisher) and vortexed, before incubation for 5 min (RT). 200 µl chloroform was added to each sample and inverted to mix, incubated for 3 min (RT) and centrifuged (12,000 g, 4˚C, 15 min). The upper aqueous phase of the supernatant (~500 µl) was transferred to a fresh tube and mixed 1:1 with isopropanol. RNA extracts were incubated on ice for 10 min to precipitate RNA, before centrifugation (12,000 g, 4˚C, 10 min). The supernatant was removed and the RNA pellet washed with 1 ml 75% ethanol, before re-centrifugation (7500 g, 4˚C, 5 min). The supernatant was removed and the pellet was air-dried, before resuspension in 50 µl nuclease-free water.

RNA extracts were DNase treated and cDNA was synthesised using Turbo DNase treatment kit and SuperScript IV Reverse Transcriptase, respectively (Invitrogen), following manufacturer's protocols. Briefly, for DNase treatment 5-10 µg RNA was mixed with Turbo DNase buffer and enzyme (2 units) in a 50 µl reaction mix and incubated (37˚C, 30 min). Following incubation, DNase inactivation reagent (5 µl) was added, the reaction mix incubated (RT, 5 min) before centrifugation (10,000 g, RT, 90 sec). The supernatant was transferred to fresh microcentrifuge tubes. For cDNA synthesis, 1 µg DNase-treated RNA was mixed with 1 µl dNTPs (10 mM) and 1 µl oligo $d(T)_{20}$ primer (50 µM) in a 13 µl reaction mix and incubated at 65˚C for 5 min, before incubation on ice (2 min). To this was then added 4 µl transcriptase buffer (5x concentrate), 1 µl dithiothreitol (100 mM), 40 units of RNase inhibitor and 200 units Superscript IV reverse transcriptase. This reaction mix was incubated at 55°C (10 min), before inactivation at 80°C (10 min). cDNA was diluted 1:10 in nuclease-free water for subsequent RT-PCR.

Table 2.3. Buffer Components

Buffer name	Components
Extraction buffers	
Z. tritici DNA extraction buffer	250 mM NaCl, 200 mM Tris-HCl, 25 mM EDTA (pH 8.0), 2% sodium dodecyl sulphate (SDS), 5 mM Phenanthroline (PT), 2% Polyvinylpyrrolidone (PVP), 0.5% β-mercaptoethanol[1]
Wheat genomic DNA extraction buffer	0.1 M Tris-HCl (pH 7.5), 0.05 M EDTA (pH 8.0), 1.25% SDS
Nicotiana benthamiana protein extraction buffer	50 mM Tris-HCl (pH 7.5), 150 mM NaCl, 10% glycerol, 2 mM EDTA, 5 mM dithiothreitol (DTT), 0.5% Polyvinylpolypyrrolidone (PVPP), 1% IGEPAL CA-630[1], 1% protease inhibitor cocktail P9599 (Sigma)[1]
Immunoprecipitation buffers	
Agroinfiltration buffer	10 mM $MgCl_2$, 10 mM MES buffer (pH 5.6, filter sterilised), 150 µM acetosyringone[1]
Dilution buffer	10 mM Tris-HCl (pH 7.5), 150 mM NaCl, 0.5 mM EDTA
Washing buffer	10 mM Tris-HCl (pH 7.5), 150 mM NaCl, 0.5 mM EDTA, 0.05% IGEPAL CA-630
2x SDS loading buffer	120 mM Tris-HCl (pH 6.8), 20% glycerol, 4% SDS, 10% β-mercaptoethanol[1], pinch of bromophenol blue
Running & washing buffers	
Western transfer running buffer	25 mM Tris-HCl (pH 8.3), 190 mM glycine, 20% methanol
TBS buffer	2 mM Tris-HCl (pH 7.3), 140 mM NaCl
TBS-TWEEN buffer	2 mM Tris-HCl (pH 7.3), 140 mM NaCl, 0.1% Tween-20
Coomassie staining/destaining solution	~0.3% Coomassie blue R-250, 40% methanol, 10% acetic acid (*destaining solution without Coomassie blue R-250*)
Yeast two-hybrid buffers	
Z-buffer	60 mM Na_2HPO_4, 40 mM NaH_2PO_4, 10 mM KCl, 2 mM $MgSO_4$ (pH 7.0, filter sterilised)
TE/LiOAc buffer	100 mM LiOAc, 10 mM Tris-HCl, 1 mM EDTA (pH 7.5, filter sterilised)
TE/LiOAc/PEG buffer	100 mM LiOAc, 5 mM Tris-HCl, 0.5 mM EDTA, 40% PEG-3350 (pH 7.5, filter sterilised)
Trypan blue staining/destaining	
Trypan blue staining solution	25% lactic acid (v/v); 25% phenol; 25% glycerol; 25% water; trypan blue (50 mg per 100 ml)
Trypan blue destaining solution	15 M chloral hydrate in water

[1]Component added immediately before use.

2.3.4 PCR, DNA quantification and sequencing

Primers for polymerase chain reaction (PCR) amplification were designed using either Geneious version 10.2 (https://www.geneious.com) primer design function, or the NCBI Primer Blast tool (https://www.ncbi.nlm.nih.gov/tools/primer-blast/). Primers for Gibson assembly were designed using the NEBuilder tool (https://nebuilder.neb.com/). See Table 2.4 for a list of primers used in this study. All primers were synthesised by Eurofins Genomics (UK).

Amplification of DNA/cDNA by PCR was carried out for sequence analysis of genomic DNA, amplification of cDNA fragments for subsequent incorporation into vectors, or analysis of vector constructs. PCRs were carried out using a BioRad T100 thermocycler. See Table 2.5 for PCR conditions and reagents used. Primer melting temperature (Tm) was calculated for primer pairs using NEB Tm Calculator (https://tmcalculator.neb.com/). Colony PCR was used to confirm transformation of *E. coli* colonies with correctly assembled vector constructs, following antibiotic selection. A small section of cell material from a colony was picked with a sterile pipette tip and transferred to other PCR components (Table 2.5). PCR products for subsequent analysis by sequencing were purified either using a QIAquick PCR purification kit or QIAquick gel extraction kit (Section 2.3.6), following the manufacturer's protocol. PCRs were carried out using either Phusion High-Fidelity DNA Polymerase (ThermoFisher) or AmpliTaq Gold 360 Master Mix (ThermoFisher), whilst colony PCRs were carried out using RedTaq ReadyMix (Sigma-Aldrich, UK).

Reverse transcriptase-quantitative PCR (RT-qPCR) was carried out to determine wheat or *Z. tritici* gene expression. Total RNA was extracted from wheat leaves using TRIzol. 1 ml of TRIzol was added to 50-100 mg leaf material, ground under liquid N_2. This was incubated (5 min, RT) before addition of 200 µl chloroform, vortexing and incubation (2 min, RT) and centrifugation (15 min, 12,000 g, 4°C). The upper aqueous phase was transferred to a fresh microcentrifuge tube and mixed with 500 µl isopropanol. This was incubated (10 min, RT) and centrifuged (10 min, 12,000 g, 4°C). The RNA pellet was washed with 1 mL of 75% ethanol and recentrifuged (5 min,

7,500 g, 4°C). The pellet was air-dried and resuspended in 50 µl RNase-free water. Any potential traces of genomic DNA were removed using TURBO DNA-free kit (ThermoFisher), following the manufacturer's instructions. cDNA was synthesized from 1 µg of extracted RNA using SuperScript IV Reverse Transcriptase (ThermoFisher) and diluted 1:10 with RNase-free water. RT-qPCR was performed with Powertrack SYBR Green Master Mix (Applied Biosystems), using a QuantStudio6Pro qPCR machine (ThermoFisher).

DNA and RNA solutions were quantified by Nanodrop 2000c (ThermoFisher). Vector constructs were checked before use by Sanger DNA sequencing, carried out using the Eurofins Genomics (UK) Mix2Seq service.

2.3.5 Cloning protocols

Gateway BP and LR reactions were carried out following previously described protocols (http://www.untergasser.de/lab/protocols/index.htm). Insert sequences were first purified by gel extraction (Section 2.3.6). Briefly, for BP reaction 75 ng pDONR vector was mixed with ~1.2X moles of insert sequence in 4 µl reaction volume, to which 1 µl of BP-clonase II was added. This was incubated overnight (RT) before the addition of 0.5 µl proteinase K and subsequent incubation (37˚C, 10 min). The BP reaction construct was then transformed into competent *E. coli* (Section 2.3.1). For LR reaction, 25 ng of BP reaction construct was mixed with 50 ng destination vector in 4 µl reaction volume, with 1 µl of LR-clonase II added. This was incubated for 1 h (RT) before the addition of 0.5 µl proteinase K and subsequent incubation (37˚C, 10 min). The LR reaction was then used for transformation of competent *E. coli* (Section 2.3.1).

Restriction digestion of DNA was carried out in 50 µl reaction volumes using 5 µl CutSmart buffer (NEB), 1 µg DNA and 1 µl (20 units) of each restriction enzyme (NEB). Reaction mix was incubated at 37˚C for 1 h, then inactivated at 80˚C for 20 min. In the case of single restriction enzyme digestion, DNA dephosphorylation using calf intestine alkaline phosphatase (CIAP) was carried out to prevent plasmid re-circularisation. 44 µl restriction digestion solution was mixed with 5 µl 10X alkaline phosphatase buffer and 1 µl CIAP (0.01 units/µl, Promega), with incubation at 37˚C for 30 min. Digestion products were purified

by gel extraction (Section 2.3.6). Ligation of DNA ends was carried out using T4 DNA ligase (Promega). A 4:1 molar ratio of DNA insert to backbone sequence was prepared in a 20 µl reaction volume, with 2 µl 10X T4 DNA ligase buffer and 0.2 µl T4 DNA ligase (1 Weiss unit). The reaction was incubated (RT, 30 min), before inactivation at 65˚C for 10 min.

2.3.6 DNA gel electrophoresis

Agarose gel electrophoresis was used to separate DNA molecules by size. This was used to isolate and purify DNA fragments for use in subsequent protocols, to assess PCR or restriction enzyme digestion reactions or determine the presence/absence of specific DNA sequences (see above). 1% (w/v) agarose gels were prepared by dissolving agarose powder in 1X Tris/Borate/EDTA (TBE) buffer (National Diagnostics) by boiling. Ethidium bromide (5 µg/ml) was added to cooled gel solution prior to casting. Cast gels were transferred to a BioRad Mini-Sub Cell GT chamber filled with 1X TBE buffer. DNA was mixed with 6X loading dye (ThermoFisher) and added to wells in the agarose gel. Gels were run at 75-100 volts (V) for 1 h, or until dye front reached the bottom of the gel. Gels were then imaged using a UVP UVsolo touch imager (Analytik Jena AG, Germany). For gel extraction, gels were observed on a UV transilluminator (Clare Chemical) and DNA bands cut out of the gel using a scalpel blade. DNA bands were then purified using QIAquick gel extraction kit, following manufacturer's protocol.

Table 2.4: DNA Primers Used in this Study

Primer name	DNA sequence (5' > 3')	Use
1186R2	GAGCAAGCTTTCAATTACAGGAG	Amplification and sequencing of *Stb6*[1]
13609F1	CTGAAAAAAAAATACGAGGCCATGA	
8311F16	GCGACATGGTAGCTCAATCAAA	
8311R16	TTCCTTCCATGGTCGGTAACTT	
8311F19	CGCGGTTCCAGTCACATCAC	
8311F3	CCGTTTAGCTCGTGTTGTGC	
8311R5F	CTGGACCGCTGGACTTCGAG	
alpha_T_F	CCCTGAGGTTTGATGGTGCT	qPCR analysis of VIGS wheat lines
alpha_T_R	TGGTGATCTCAGCAACGGAC	
AvrStb6-attB F	GGGGACAAGTTTGTACAAAAAAGCAGGCTTCATGCGCTCCATTCTACAAG	Amplification of *AvrStb6* (I01 & I02) with attB flanks for Gateway cloning
AvrStb6-attB IPO323 R	GGGGACCACTTTGTACAAGAAAGCTGGGTCGACATCCACGCAGCCACAACCAAGAA	
AvrStb6-attB IPO323 STOP	GGGGACCACTTTGTACAAGAAAGCTGGGTCTATCACACGCAGCCACAACCAAGAA	
AvrStb6-attB R	GGGGACCACTTTGTACAAGAAAGCTGGGTCGACATCCACGCAGCCACAACCAGGAA	
AvrStb6-attB R STOP	GGGGACCACTTTGTACAAGAAAGCTGGGTCTATCACACGCAGCCACAACCAGGAA	
avrstb6.f1	CACTTCTTTCCACAACTCCCACTT	Amplification of *AvrStb6* from *Z. tritici* genomic DNA
avrstb6.f3	ATCAACTTCCTCTCAACCAAGACC	
avrstb6.r1	CCTACATTGGCAGCATCAAAATCA	
AvrStb6 F6b	TTCTACAAGGCTTCCTCGC	RT-qPCR analysis of *AvrStb6* expression
AvrStb6 R6b	GCTTTCCGTCGTGGCAGAA	
FTSH_attB1_F1	GGGGACAAGTTTGTACAAAAAAGCAGGCTTCCTTCTGAATGAGGCAGCCATA	Amplification of peptidase region of *FtsH2* Protease (TraesCS7D02G458400.1)
FTSH_attB1_R1	GGGGACCACTTTGTACAAGAAAGCTGGGTCTACAACAGCAAATTCTCCAACCC	
FtsH2 F	TGACAGTTCCTTCCATACCAGC	Amplification of *FtsH2* region for VIGS constructs[1]
FtsH2 R	CATCTTGGATTCCGCTTTGCTT	

FtsH2 F02	TTCCCGCTTATCCTTATCGGC	qPCR analysis of VIGS wheat lines
FtsH2 R02	CTCCATCTGGAACTTGGCCTT	
GFP-attB F1	GGGGACAAGTTTGTACAAAAAAGCAGGCTTCATGGTGAGCAAGGGCGA	Amplification of *GFP* with attB flanks for Gateway cloning
GFP-attB R1	GGGGACCACTTTGTACAAGAAAGCTGGGTTTACTTGTACAGCTCGTCCAT	
Gsrhino R1	GGTTCTCATCGATAGGTCCTTG	Sequencing of Stb6-GSrhino/yellow tag constructs
GSyellow R1	TTCAGGGTCAGCTTGCCGTA	
gwb654F	GCACAATCCCACTATCCTTCGC	Amplification across pGWB654 cloning site[1]
HPH F1	TAAATAGCTGCGCCGATGGT	Amplification of hygromycin gene (*HPH*)
HPH R1	TAAATAGCTGCGCCGATGGT	
JPG BetaT F1	TCATCAGCAAGATCCGTGAG	RT-qPCR analysis of *AvrStb6* expression[2]
JPG BetaT R1	TGTCAATGCAGAAGGTCTCG	
JPG EF1a F1	CAAGAAGGTCGGCTACAACC	
JPG EF1a R1	TGGTCTTGGTCTTGGTCTCC	
JPG G6PDH F1	GCGGCTACTTTGACGAGTTC	
JPG G6PDH R1	GATCCGTCAAGCGACTTCTC	
OE-PCR_R	AGATAAGCTTCTGCAGTTGTTGCAGGATTTTG	Primers for overlap extension PCR for fusing Stb6 and GSrhino tag
OE-PCR_F	CCTGCAACAACTGCAGAAGCTTATCTCCGAGG	
pDONR207 F	TCGCGTTAACGCTAGCATGGATCTC	Amplification across pDONR207 cloning site
pDONR207 R	GTAACATCAGAGATTTTGAGACAC	
pDONR221 F	GCAGTTCCCTACTCTCGCG	Amplification across pDONR221 cloning site
pDONR221 R	GCCAGGAAACAGCTATGACCAT	
pGWB605 F1	GACGTAAGGGATGACGCACA	Amplification across pGWB605 cloning site
pGWB605 R1	GGTCTTGTAGTTGCCGTCGT	
pGWB654 R1	GATCTCGAACTCGTGGCCG	Amplification across pGWB654 cloning site

pK7FWG2 F	GTAGGTCAGGGTGGTCACGAG	Amplification across pK7FGW2 cloning site
pK7FWG2 R	ACGTTCCAACCACGTCTTCA	
Stb6_attB1_F	GGGGACAAGTTTGTACAAAAAAGCAGGCTTCATGTCTCTGAGCTGCTGGT	Amplification of *Stb6* full CDS with attB flanks for Gateway cloning
Stb6_attB2_R	GGGGACCACTTTGTACAAGAAAGCTGGGTCGACATCCAGTTGTTGCAGGATTTTGGAAT	
Stb6_attB1_STOP	GGGGACCACTTTGTACAAGAAAGCTGGGTTCACTACAGTTGTTGCAGGATTTTGG	
Stb6 F2b	GGGGACAAGTTTGTACAAAAAAGCAGGCTTCAACTGCACGGAGAAGGCC	Amplification of *Stb6* ectodomain fragments with attB flanks for Gateway cloning
Stb6 F2c	GGGGACAAGTTTGTACAAAAAAGCAGGCTTCGCACGCCTGGATAAAGA	
Stb6 R2a	GGGGACCACTTTGTACAAGAAAGCTGGGTCGACATCCTTCTTCGCTCTCCTCTCACT	
Stb6 R2b	GGGGACCACTTTGTACAAGAAAGCTGGGTCTATCACAGTTCCCATTTCAGGAGGAA	
Stb6Kin_attB1_F	GGGGACAAGTTTGTACAAAAAAGCAGGCTTCATGTGGCATAGAAATGGGAAAGGAC	Amplification of *Stb6* kinase with attB flank for Gateway cloning
Stb6 R1	CTCCAACCATCTCTAGCAGCA	*Stb6* construct resequencing
Stb6 R2	AGTCCTTTCCCATTTCTATGCCA	
Stb6 R3	GCGAACCACATAATCTTCCTGT	
ToxABP F	CGTCTCCAATCTCTCCTCTCTC	Amplification of *ToxABP* region for VIGS constructs[1]
ToxABP R	CCAGAGATGGGGAAATAGAGTCC	
ToxABP F01	GGACAGGGATGCCATCTTCAA	qPCR analysis of VIGS wheat lines
ToxABP R01	TACCCTGGGCCCTTTCTGATA	

[1]Primers provided by Kostya Kanyuka (Rothamsted Research)

[2]Primers provided by Javier Palma-Guerrero (Rothamsted Research)

2.4 Agroinfiltration of *N. benthamiana* leaves

2.4.1 Preparation of Agrobacterium

Transient expression in *N. benthamiana* was carried out by agroinfiltration. Agrobacterium strains were transformed with binary vector constructs (Section 2.3.1), for subsequent expression of construct genes within tobacco leaves. Transformed Agrobacterium strains were stored as 10% glycerol stocks at -80˚C until use. Transformed Agrobacterium cultures were streaked from glycerol stocks onto LB plates with antibiotic selection and incubated for 4 days. Bacterial growth was used to inoculate 5 ml LB broth with antibiotic selection, which was incubated overnight (180 rpm). Cells were centrifuged (4,260 g, 15˚C, 20 min) and the pellet resuspended in 2 ml infiltration buffer (Table 2.3). The OD_{600} of the Agrobacterium suspension was calculated and mixed with a suspension of Agrobacterium expressing p19 gene silencing suppressor protein of *Tomato bushy stunt virus* prepared in parallel. These suspensions were diluted to a final concentration of OD_{600} 0.5 and 0.1, respectively. This cell suspension was incubated (RT, 3 h) without shaking prior to infiltration.

2.4.2 Infiltration of *N. benthamiana*

N. benthamiana plants were grown from seeds on Levington F2+S soil for two weeks, before transplanting into individual pots. Growth conditions were 16 h light per day, with 23˚C (light)/20˚C (dark) and 65/75% relative humidity. Four to six-week-old plants with fully expanded leaves were used for infiltration (Figure S2.1a). The abaxial side of the leaf was infiltrated with Agrobacterium suspension, using a needleless syringe. For partial leaf infiltrations, the limit of the infiltrated zone was recorded with a marker pen.

2.4.3 Electrolyte leakage assay

Infiltrated leaves were harvested at 1-5 days post infiltration (dpi). Five leaf discs were cut from each infiltrated zone using a cork borer and incubated adaxial side down in 10 ml sterile de-ionised water (3 h, RT). The water electrolyte content was tested using a Eutech COND 6+ probe (Thermofisher Scientific), giving value A. Leaf discs and water were then boiled for 25 min, cooled to RT and electrolyte content retested (value B). Electrolyte leakage was

expressed as the percentage of total ions after boiling ((value A/value B) x 100).

2.4.4 Trypan blue staining

Trypan blue staining was carried out using a protocol adapted from Ma *et al.* (2012). The trypan blue staining solution (Table 2.3) was mixed 50:50 with 96% ethanol. An infiltrated *N. benthamiana* leaf to be stained was harvested and added to a tube with 30 ml of this diluted staining solution. This was boiled until green colouration of the leaf had disappeared. The stained leaf was transferred to a tube containing 10 ml destaining solution and incubated on rollers overnight at RT. Further destaining was carried out in 30 ml 100% ethanol for 1 h (RT) prior to imaging of the leaf.

2.5 Protein analysis

2.5.1 Protein extraction

Protein was extracted from infiltrated *N. benthamiana* leaves at 5 dpi, unless otherwise stated. Full leaves were harvested and snap-frozen in liquid nitrogen. Leaves were ground in a prechilled pestle and mortar and mixed with protein extraction buffer (Table 2.3, 1 ml per gram of leaf tissue). Protein extract slurry was incubated on rollers (30 rpm, 4˚C, 30 min). Tubes were centrifuged (12,100 g, 4˚C, 20 min) and the supernatant filtered through Miracloth (Calbiochem).

Protein extracts were quantified by Pierce BCA protein assay kit (ThermoFisher), following the manufacturer's instructions. Briefly, 25 µl of (1:5 diluted) protein extract, protein extraction buffer or bovine serum albumin (BSA) standard was mixed with 25 µl compatibility reagent and incubated (37˚C, 15 min). 1 ml working reagent was added to the test solution and incubated (37˚C, 30 min), before cooling to RT. Samples were assessed by spectrophotometry at 562 nm and compared to a standard curve of known concentrations of BSA, with the absorbance of the extraction buffer standard subtracted. Protein samples were diluted in extraction buffer to equal concentration prior to SDS-PAGE or immunoprecipitation.

2.5.2 Immunoprecipitation

Immunoprecipitation (IP) to capture GFP, GFP-tagged proteins and their interactors was carried out using Chromotek GFP-Trap agarose beads (Chromotek). 25 µl GFP-Trap beads were washed by suspension in 500 µl ice-cold dilution buffer (Table 2.3), centrifuged (2,500 g, 5 min, 4˚C) and the supernatant discarded. This was repeated three times. 200 µl protein lysate (Section 2.5.1) was mixed with 300 µl dilution buffer and added to the washed beads. This reaction mix was incubated end-over-end at 4˚C for 4 h. The tubes were centrifuged as above, with the supernatant stored as “non-bound fraction”. The beads were resuspended in prechilled wash buffer (Table 2.3), centrifuged as above and the supernatant discarded. This was repeated five times. The beads were resuspended in 50 µl of 2X SDS loading buffer (Table 2.3). For “input” protein samples, 30 µl of protein lysate was mixed with 30 µl 2X SDS loading buffer. Protein and loading buffer mixes were incubated (70˚C, 10 min) prior to SDS-PAGE analysis.

2.5.3 SDS-PAGE

Sodium dodecyl sulphate-polyacrylamide gel electrophoresis (SDS-PAGE) gels were used to separate proteins based on their size. Gels were cast in Mini Protean system using 1 mm spacers and glass plates (BioRad). Resolving gels were prepared at 8% acrylamide. Cast gels were transferred to a Mini Protean Tetra Cell (BioRad), filled with 1X Tris-buffered saline (TBS) running buffer (National Diagnostics). Protein extract (Section 2.5.1) was mixed 5:1 with protein loading buffer (National Diagnostics) and incubated (70˚C, 10 min), or as described previously for IP and “input” samples (Section 2.5.2). Protein marker ladder (8 µl) or protein sample (25 µl) were added to wells of SDS-PAGE gel. Benchmark ladder and MagicMark XP ladder (ThermoFisher) were used for Coomassie staining and western blotting, respectively. Gels were run (80 V) for 90 min or until dye front reached the bottom of the resolving gel. Gels were stained using Coomassie solution (Table 2.3) on a rocker (1 h, RT, 30 rpm), before destaining on a rocker (overnight, RT).

2.5.4 Western blotting

Following electrophoresis, proteins were transferred from SDS-PAGE gel to a nitrocellulose (GE Healthcare, 0.1 µm pore size) or polyvinylidene difluoride (PVDF) membrane (Sigma-Aldrich, 0.45 µm pore size). A wet transfer method was used with a Mini Trans-Blot cell (BioRad), with transfer at 100 V for 40 min (4˚C). Correct transfer to the membrane was assessed by staining with ponceau S solution (0.5% ponceau S, 1% acetic acid) and destained with D.I. water.

The membrane was washed three times (5 min, RT) in TBS buffer (Table 2.3), before blocking in 5% non-fat milk (Cell Signalling) in TBS-Tween buffer (1 h, RT). The membrane was rewashed three times (5 min, RT) in TBS-Tween, before primary antibody blotting (overnight, 4˚C). Anti-GFP blotting was carried out with a 1:1000 dilution of rabbit anti-GFP antibody (Cell Signalling) in 5% BSA TBS-Tween buffer, whilst anti-RFP blotting was carried out with a 1:1000 dilution of rabbit anti-RFP antibody (AbCam) in 5% non-fat milk TBS-Tween buffer. The membrane was rewashed as above in TBS-Tween buffer, before secondary blotting with a 1:10,000 dilution horseradish peroxidase-conjugated goat anti-rabbit antibody (Invitrogen), in 5% non-fat milk TBS-Tween buffer (1 h, RT). The membrane was rewashed as above in TBS-Tween buffer, dried on a paper towel and treated with 1:1 ratio mix of ECL reagents (GE Healthcare). The membrane was incubated in the dark (5 min, RT), before removal of excess ECL reagent and imaging using an Odyssey Fc imager (Li-Cor), with a 10 min exposure time, unless otherwise stated. Images were optimised and saved using Image Studio 5.2.

Table 2.5: PCR Conditions

PCR programme			PCR reaction mix	
Stage	**Temperature (˚C)**	**Time (seconds)**	**Component**	**Volume (µl)**
Colony PCR				
1	95	300	RedTaq ReadyMix	10
2	95	15	F primer (10 µM)	1
3	55[1]	30	R primer (10 µM)	1
4	72	60[2]	Nuclease-free water	8
5	Return to stage 2 (37X repeat)			
6	72	300		
Phusion polymerase PCR				
1	98	30	5X HF PCR buffer	10
2	98	10	10 mM dNTPs	1
3	60[1]	20	F primer (10 µM)	2.5
4	72	30[2]	R primer (10 µM)	2.5
5	Return to stage 2 (37X repeat)		Nuclease-free water	31
6	72	300	Phusion polymerase	0.5
			Genomic DNA (>20 ng/µl)	2.5
AmpliTaq Gold 360 PCR				
1	95	600	AmpliTaq mastermix	10
2	95	30	F primer (10 µM)	1
3	63	30	R primer (10 µM)	1
4	72	45	Nuclease-free water	5.5
5	Return to stage 2 (40X repeat)		Genomic DNA (>20 ng/µl)	2.5
6	72	300		

[1]Temperature changed based on melting temperature (Tm) of primers and polymerase used (calculated using NEB Tm Calculator).

[2]Time changed based on length of PCR product and polymerase speed.

2.6 Wheat leaf inoculation bioassays

Wheat leaf inoculation bioassays were carried out as described by Keon *et al.* (2007). For each wheat cultivar used in inoculation bioassays, 15-20 seeds (pre-soaked in water overnight) were sown in seed trays (220 mm x 170 mm) filled with Levington F2+S compost, approximately 1 cm beneath the surface and 1 cm from the long side wall of the tray. One cultivar was planted in each

seed tray, with two seed trays (one with each cultivar) being placed in a large tray (370 mm x 240 mm) for watering. Plants were grown at 17˚C with 16 h of light per day for 21 days, until at least three leaves have emerged. The second leaf of each plant was then affixed, adaxial side up, onto an inoculation platform using double-sided tape and elastic bands (Figure S2.1b).

Z. tritici strains used in inoculation assays were streaked from 50% glycerol stocks onto YPD plates to encourage conidiospore production ("yeast-like growth") and incubated in the dark (7 days, 15˚C). Fungal growth was transferred to a solution of D.I. water with 0.1% surfactant (either Silwet L-77 (Lehle Seeds) or Tween 20 (Sigma-Aldrich)). These suspensions were filtered through Miracloth to isolate fungal spores. 100X dilutions of the spore suspensions were quantified by spore counting using a hemacytometer and the spore suspensions were diluted to $1x10^7$ spores/ml.

Spore suspensions were spread onto the affixed leaves using a sterile cotton bud soaked in spore suspension, on the leaf area lying between the elastic bands only. The leaf was gently rubbed with the cotton bud until it appeared soaked. Following inoculation, the large trays containing plants were watered and sealed within plastic boxes, to create a 100% humidity environment. Plastic boxes were removed at 3 dpi.

After 21 dpi, the extent of STB infection was assessed by pycnidiospore counting. Inoculated leaf sections were harvested and incubated in a sealed tube at 100% humidity for 72 h (15˚C, continuous dark) to stimulate pycnidia maturation. 2 ml of water and 0.01% Tween 20 was added to each tube, vortexed at full speed for 30 sec and 1 ml of the suspension was measured by spectrophotometry at OD_{600} to quantify pycnidiospore production. This was compared against a dilution series of spore suspensions, obtained from yeast-like growth on YPD plates, which were quantified using both spectrophotometry and by spore counting using a hemacytometer.

2.6.1. Experimental design and data analysis

A split-plot experimental design was used for *Z. tritici* inoculation bioassays carried out in Chapter 3. This design was chosen to minimise variation between treatments, whilst growing wheat genotypes in separate trays. The design was

generated in GenStat (20th Edition), using the “Split-plot design” function. See Table S2.1 for an example of the experimental layout. Five blocks, representing five large trays, were used, with subplots small trays in which each wheat cultivar was planted. There were two levels of treatment factor (wheat genotype). The sub-plot treatment factor was *Z. tritici* isolate – 13 for infection scoring assays (Figure 3.3 and S3.3).

Data collected was analysed graphically using the RStudio ggplot2 package. Statistical analysis to determine any significant differences in disease symptoms between wheat Nearly Isogenic Lines (NILs) treated with *Z. tritici* was determined using least squared difference (LSD). The LSD of the wheat genotype by *Z. tritici* isolate interaction was obtained by ANOVA analysis using GenStat (20th Edition). The difference in LSD between the two wheat genotypes for one *Z. tritici* isolate was then compared to this interaction LSD average, to determine significance.

2.7 Yeast two-hybrid assay

The yeast strain MaV203 was used to carry out yeast two-hybrid studies. This strain possesses leucine synthase (*leu2*) and tryptophan synthase (*trp1*) mutations and thus cannot grow on media lacking these amino acids. MaV203 also possesses three *GAL4* inducible reporter genes, for determination of protein-protein interactions (Section 2.7.4).

2.7.1 Preparation of competent yeast cells

Yeast MaV203 was made competent using the S. c. EasyComp Transformation Kit (ThermoFisher Scientific), following manufacturer’s instructions. Briefly, yeast from glycerol stock was streaked onto a YPD plate and incubated (2 days, 30˚C). A single colony was picked and used to inoculate 10 ml YPD broth overnight (30˚C, 250 rpm). The OD_{600} of the liquid culture was checked, diluted to OD_{600} 0.2 and incubated as above until the diluted culture reached an OD_{600} >0.6. Cells were centrifuged (500 g, 5 min, RT) and the cell pellet resuspended in 10 ml solution I. This suspension was recentrifuged as above and the pellet

resuspended in 1 ml solution II. 50 µl aliquots of this competent cell suspension were transferred to 0.5 ml microcentrifuge tubes and stored at -80˚C until use.

2.7.2 Control yeast transformants

Two positive interaction controls were utilised in the yeast two-hybrid tests performed in this study. The strong interaction control was between the Arabidopsis GAI (GIBBERELLIN-INSENSITIVE) and ARF19 (AUXIN RESPONSE FACTOR 19) proteins (Oh *et al*., 2014). The weak interaction between was between GAI and ARR1 (ARABIDOPSIS RESPONSE REGULATOR 1) proteins (Marin-de la Rosa *et al.,* 2015). A negative control yeast transformant was generated, containing empty bait and prey vectors. Additional negative controls were also generated, in which each test hybrid construct was tested alongside an empty plasmid, to assess the possibility of unwanted autoactivation of reporter genes.

2.7.3 Yeast transformation and plating

Yeast transformation was carried out following manufacturer's instructions using the S. c. EasyComp Transformation Kit (Thermofisher). Competent yeast cell aliquots were mixed with 1 µg each of pDEST32 (bait) and pDEST22 (prey) plasmid constructs for transformation. Also added to the reaction tube was 500 µl solution III from the S. c. EasyComp kit. Tubes were vortexed thoroughly and then incubated at 30˚C for 1 h, with repeated vortexing of the tubes every 15 min. 100 µl of each transformant suspension was then plated onto SC agar plates lacking leucine and tryptophan (SC-LT), to select for yeast transformants possessing both bait and prey plasmids.

Subsequent analysis for protein-protein interactions in transformed yeast was adapted from the protocol described in the ProQuest Two-Hybrid System manual (Thermofisher). Following identification of successful transformants, these were transferred to a master SC-LT plate for subsequent transfer to test plates (see below). This was carried out by picking colonies using a sterile toothpick and restreaking onto a SC-LT master plate, or by picking the colony and resuspending in 100 µl 0.9% NaCl solution. 5µl of this suspension was then spotted onto the master plate.

Transfer from master plates to test plates was carried out by restreaking, as described above, or by replica plating. After incubation of the master plate (18 h, 30°C), sterile velvets were mounted on a platform and the master plate inverted and pressed onto the velvet, to transfer cells. The test plates were then pressed onto this velvet, to transfer cells to the test plates.

2.7.3.1 Library-scale yeast transformation

Library-scale transformation of yeast cells was performed as described in the ProQuest Two-Hybrid System manual (Thermofisher). Yeast cells transformed with bait plasmid only (Section 2.7.3) were made competent by inoculating 20 ml SC broth lacking leucine (SC-Leu) and incubating overnight (30˚C, 250 rpm). This was diluted to OD_{600} 0.1 in 300 ml SC-Leu and allowed to grow to OD_{600} 0.5. Cells were pelleted by centrifugation (1,500 g, 5 min, RT) and resuspended in 30 ml sterile water. This suspension was recentrifuged as above and cells resuspended in 1.5 ml TE/LiOAc buffer (Table 2.3).

The cDNA prey library, generated by ThermoFisher, was derived from a mixture of total RNA extracts of two susceptible and one resistant wheat lines inoculated with *Z. tritici* isolate IPO323 (as well as mock inoculated) with timepoints taken at 1 to 14 dpi.

The competent cells were aliquoted into 30 microcentrifuge tubes (50 µl each). To each tube was added 1 µg library DNA, 50 µg salmon sperm carrier DNA (ThermoFisher) and 300 µl TE/LiOAc/PEG buffer (Table 2.3). Tubes were incubated (30˚C, 30 min), before addition of 40 µl dimethyl sulfoxide (DMSO) and incubation at 42˚C for 7 min. Test SC-LT plates were inoculated with 100 µl of a 1:100 or 1:1,000 dilution from a single transformation tube, to check transformation efficiency. The full volume of each other transformation tube was then plated onto a separate large SC-LTH (15 cm diameter) selection plate, containing sufficient 3-aminotriazole (3-AT) to suppress yeast growth due to autoactivation (Section 2.7.4.1). Following 3 days incubation (30˚C), the large selection plates were replica cleaned and incubated for 3 more days.

2.7.4 Direct interaction assay protocol

Two reporter gene systems were used to test for protein-protein interactions. Expression of the histidine biosynthesis gene *HIS3* is evidenced by growth on media lacking histidine. The strength of *HIS3* expression is determined by adding the HIS3 enzyme inhibitor 3-AT to the growth media at a range of concentrations. Growth under high 3-AT concentrations indicates a strong protein-protein interaction. The second reporter gene is *LacZ*, encoding β-galactosidase, which metabolises X-gal (5-bromo-4-chloro-3-indolyl-β-D-galactopyranoside) to create an intense blue stain for blue-white selection.

For testing *HIS3* reporter gene expression, cells transferred from a master plate by replica plating (Section 2.7.3) to SC agar plates lacking leucine, tryptophan and histidine (SC-LTH) and supplemented with 3-AT to a concentration of 10-75 mM. Test plates were replica cleaned following transfer of cells to the plate to remove excess cell material, by pressing the test plate against a sterile velvet. Plates were incubated at 30˚C for 24 h, replica cleaned once again and incubated for a further 2 days before assessing yeast growth. His^+ transformants were those found to be capable of growth on media lacking histidine.

For X-gal blue-white selection assay, yeast transformants were transferred by replica plating (Section 2.7.3) to YPAD agar plates covered with a nylon membrane (Roche) and incubated (37˚C, 24 h). X-gal test solution was prepared by making a 10% (w/v) X-gal solution in dimethylformamide (DMF), with 100 µl of this added to 10 ml of Z-buffer (Table 2.3) and 60 µl β-mercaptoethanol. Two 125 mm diameter filter papers (Whatman) were placed in a 150 mm petri dish and soaked with X-gal test solution. Nylon membranes with yeast growth were submerged in liquid nitrogen (30 sec) before being transferred (yeast side up) to the soaked filter papers. Excess buffer was removed, plates were sealed and incubated (37˚C). Blue colouration was continually analysed up to 48 h, with images taken at 24 h.

2.7.4.1 Yeast two-hybrid library screening

Prior to library-scale yeast two-hybrid screening, yeast transformants possessing bait construct and empty pDEST22 plasmid were inoculated onto SC-LTH agar plates supplemented with a range of 3-AT concentrations (as described in Section 2.7.4). This was used to determine the minimum concentration of 3-AT required to suppress unwanted autoactivation of the *HIS3* reporter gene by the bait hybrid construct.

For selection of library-scale transformants, selection plates consisted of SC-LTH supplemented with the required concentration of 3-AT to suppress unwanted autoactivation. Induction of the *HIS3* reporter gene was determined by growth of yeast transformants on this selective media. Yeast colonies found to grow on selection media were restreaked onto SC-LT plates for direct interaction assay testing (Section 2.7.4).

2.8 Confocal microscopy

Confocal microscopy was carried out using a Zeiss LSM 780 microscope, to visualise the localisation of fluorophores and fluorophore-tagged proteins transiently expressed in *N. benthamiana* leaf cells (Section 2.4). Leaf sections (approximately 5 x 5 mm) were mounted on a glass slide and abaxial sides were observed at 40X objective (1.20 numerical aperture). Fluorophores were excited at 561 nm (GFP) and 488 nm (mRFP). Wavelength filters of 493-556 nm and 582-658 nm were used to observe GFP and mRFP fluorescence, respectively. To plasmolyse leaf cells, leaf sections were imbibed in 0.8 M mannitol solution, by removing water under glass slide and replacing it with the mannitol solution, incubating samples for 30 min (RT) before imaging. Once captured, images were processed using ZEN 2010 software.

2.9 References

Keon J, Antoniw J, Carzaniga R, Deller S, Ward JL, Baker JM, Beale MH, Hammond-Kosack KE, Rudd JJ. 2007. Transcriptional adaptation of *Mycosphaerella graminicola* to programmed cell death (PCD) of its susceptible wheat host. *Molecular Plant-Microbe Interactions* **20:** 178-193.

Ma L, Lukasik E, Gawehns F, Takken FL. 2012. The use of agroinfiltration for transient expression of plant resistance and fungal effector proteins in *Nicotiana benthamiana* leaves. *Methods in Molecular Biology* **835:** 61-74. DOI: 10.1007/978-1-61779-501-5_4

Marin-de la Rosa N, Pfeiffer A, Hill K *et al*. 2015. Genome wide binding site analysis reveals transcriptional coactivation of cytokinin-responsive genes by DELLA proteins. *PLoS Genetics* **11:** e1005337. DOI: 10.1371/journal.pgen.1005337

Nakamura S, Mano S, Tanaka Y *et al.* 2010. Gateway binary vectors with the bialaphos resistance gene, *bar*, as a selection marker for plant transformation. *Bioscience Biotechnology and Biochemistry* **74:** 1315-1319.

Oh E, Zhu JY, Bai MY, Arenhart RA, Sun Y, Wang ZY. 2014. Cell elongation is regulated through a central circuit of interacting transcription factors in the *Arabidopsis* hypocotyl. *eLife* **3:** e03031. DOI: 10.7554/eLife.03031.001

Chapter 3: Global Population Analysis of the *Zymoseptoria tritici* Effector *AvrStb6*

3.1 Summary

Zymoseptoria tritici, the causal agent of Septoria tritici blotch (STB), is an economically important pathogen of wheat, causing crop losses globally in temperate regions. To date, only two STB resistance genes, *Stb6* and *Stb16q*, have been successfully cloned in wheat. The *Z. tritici* avirulence gene *AvrStb6* with which *Stb6* interacts in a gene-for-gene manner, has also recently been identified. Previous analyses of *AvrStb6* in *Z. tritici* populations have revealed a high diversity of *AvrStb6* haplotypes. In addition, many isolates were found to possess the avirulence isoform of AvrStb6, originally identified in the reference isolate IPO323. In this chapter, we report on a targeted re-sequencing of *AvrStb6* from *Z. tritici* isolates collected from major wheat-growing regions of the world between 2013–2017. We found that, contrary to previous studies, the AvrStb6 avirulence isoform was completely absent from our collection. Furthermore, we discovered that a single isoform of AvrStb6, conferring virulence on *Stb6* wheat, was predominant in almost all regions throughout the global population. Interestingly, this isoform was completely absent from isolates collected in Turkey, which possessed a far higher diversity of isolates than found in other regions. These data present a very different view of modern *Z. tritici* populations in contrast to previous studies, one in which *Stb6*-mediated resistance has been completely overcome.

3.2 Acknowledgment of Contributions

This chapter is adapted from the manuscript “Remarkable recent changes in genetic diversity of the avirulence gene *AvrStb6* in global populations of the wheat pathogen *Zymoseptoria tritici*”, published by Molecular Plant Pathology in July 2021 (https://doi.org/10.1111/mpp.13101). This work could not have been completed without the contributions of many other researchers locally, nationally, and

internationally. Hannah Blyth (Rothamsted Research) contributed to the *AvrStb6* resequencing for many *Z. tritici* isolates. From Bart Fraaije's group at Rothamsted Research, Guilherme Rossato-Augusti and Pilar Diez (Rothamsted Research) provided genomic DNA preparations of *Z. tritici* isolates from the UK, Europe, USA, and South America. Fatih Ölmez (Sivas Science and Technology University, Turkey) and Emine Burcu Turgay (Field Crops Central Research Institute, Ankara, Turkey) provided *AvrStb6* sequences from Turkish *Z. tritici* isolates, whilst Peter Solomon and Megan McDonald (Australian National University, Canberra, Australia) and Andrew Milgate (NSW Department of Primary Industries, Wagga Wagga, Australia) provided Australian isolates of *Z. tritici* for pathoassays as well as sequences of *AvrStb6* from the Australian *Z. tritici* population. For *Stb6* resequencing, Mike Hammond-Kosack (Rothamsted Research) provided genomic DNA preparations for several wheat cultivars, whilst Martin Quinke (Instituto Nacional de Investigación Agropecuaria, Colonia, Uruguay) and Christina Hagerty (Oregon State University, USA), provided seeds of South American and USA wheat cultivars, respectively. Vladimir Nekrasov and Florian Hahn (Rothamsted Research) provided the gene-edited Cadenza lines that were used in *Z. tritici* pathoassays. The development of a near-isogenic Chinese Spring wheat line carrying a susceptibility haplotype at the *Stb6* locus was carried out previously and aided by Cyrille Saintenac (INRAE, GDEC, Clermont- Ferrand, France). Thanks also to Daniel Croll (University of Neuchâtel, Switzerland) for the *AvrStb6* haplotype data from the *Z. tritici* population previously analysed by Zhong *et al.* (2017), Suzanne Clarke, Maider Abadie, Anuradha Bansal and Ana Machado-Wood (Rothamsted Research) for helping with experimental design and data analysis of plant inoculation bioassays and *AvrStb6* expression analysis, Javier Palma-Guerrero (Rothamsted Research) for the *Z. tritici G6PDH*-specific RT-qPCR primer sequences and Hongxin Chen (Rothamsted Research) for the pycnidiospore estimation methodology and for whole-genome sequences of various European *Z. tritici* isolates.

3.3 Introduction

The interactions between plant pathogens and their hosts during infection are highly complex and evolutionarily dynamic. Pathogens secrete proteins known as effectors during infection. These proteins are often essential to successful infection of plant hosts (Lo Presti *et al.*, 2015), acting to disguise the presence of the pathogen, suppress plant immune responses or otherwise alter the metabolism of the host plant to facilitate infection (Djamei *et al.*, 2011, Marshall *et al.*, 2011, Kleemann *et al.*, 2012). However, plants also possess a sophisticated innate immune system comprised of cell surface immune receptors (CSIRs) and intracellular immune receptors (IIRs), known collectively as resistance (*R*) genes, which can recognise pathogen effectors and initiate an immune response (Jones and Dangl, 2006, Cook *et al.*, 2015, Kanyuka and Rudd, 2019).

Once an effector (otherwise known as an avirulence or Avr factor) is recognised by the host plant, this creates an evolutionary pressure on the pathogen to mutate the effector to evade detection, or even eliminate it entirely from its genome. Effectors are often located in highly plastic genomic regions rich in transposon activity which drives effector diversity (Dong *et al.*, 2015), and Avr factors are frequently lost through the introduction of frameshift or nonsense mutations (Luderer *et al.*, 2002), transposon insertion (Zhang *et al.*, 2015), or repeat-induced point mutations (RIPs; Rouxel *et al.*, 2011). Pathogen virulence may also be restored through the suppression of Avr factor expression, possibly by promoter region mutations, histone modification (Wang *et al.*, 2020) or post-transcriptional silencing (Qutob *et al.*, 2013). For some Avr effectors, especially those playing an important role in infection, the introduction of point mutations in the coding gene sequence may allow evasion of recognition whilst maintaining protein function (Blondeau *et al.*, 2015, Plissonneau *et al.*, 2017). In geographic regions where the corresponding *R* gene is widely prevalent, once these *Avr* gene mutations emerge they often spread rapidly through the pathogen population (Cowger *et al.*, 2000, Hovmøller and Justesen, 2007).

Septoria tritici blotch (STB), caused by the fungal pathogen *Zymoseptoria tritici*, is one of the most economically important fungal diseases of wheat (*Triticum aestivum*) worldwide, with fungicide control costs exceeding €1 billion per year in Europe alone

(Torriani *et al.*, 2015). A battery of effector proteins are secreted by *Z. tritici* during wheat infection. This includes AvrStb6 (Zhong *et al.*, 2017, Kema *et al.*, 2018), which is recognised in a gene-for-gene manner by the wheat CSIR Stb6 (Brading *et al.*, 2002, Saintenac *et al.*, 2018). The Dutch *Z. tritici* isolate IPO323, collected in 1981 and avirulent on *Stb6* wheat, was first identified as possessing the *AvrStb6* gene and was later used to clone this *Avr* gene (Zhong *et al.*, 2017, Kema *et al.*, 2018). *AvrStb6* encodes a small, cysteine-rich secreted protein with no recognised protein domains/motifs, characteristic of a fungal effector. The corresponding wheat STB disease resistance gene *Stb6* has also been cloned and found to encode a wall-associated kinase (WAK)-like protein (Saintenac *et al.*, 2018). Functional, disease resistance-conferring haplotypes of *Stb6* were found to be present in over half of current commercial cultivars across Europe. In addition, *Stb6* may have been present in wheat populations since early in agricultural history (Chartrain *et al.*, 2005, Dutta *et al.,* 2021), creating considerable pressure on *Z. tritici* to eliminate or evolve *AvrStb6* variants capable of evading *Stb6*-mediated defence.

Two previous studies have re-sequenced *AvrStb6* from *Z. tritici* populations, with one study analysing a global population collected between 1990–2001 (Zhan *et al.*, 2005, Brunner and McDonald, 2018), whilst the second analysed a predominantly French population collected in 2009–2010 (Zhong *et al.*, 2017). In both studies a high diversity of *AvrStb6* haplotypes, and evidence of positive selection driven by point mutations and recombination was identified. This is supported by analysis of the region of *Z. tritici* chromosome 5 in which *AvrStb6* is located, which was found to be highly dynamic, with extensive transposon activity (Sánchez-Vallet *et al.*, 2018). Whilst these studies provide a detailed analysis of *AvrStb6* haplotype diversity in past *Z. tritici* populations, an understanding of *AvrStb6* status in more contemporary populations is unknown. This includes not only *AvrStb6* diversity, but also the prevalence of *AvrStb6* haplotypes conditioning virulence on *Stb6* wheat. The specific polymorphisms that drive the change from avirulence to virulence phenotype in the AvrStb6 protein have not yet been determined, although changes at the two amino acid residues (positions 41 and 43) in the AvrStb6 protein have been suggested as being critical for the pathogenicity on wheat cultivars carrying *Stb6* (Kema *et al.*, 2018).

In this chapter, I report on the re-sequencing of *AvrStb6* from recent field populations of *Z. tritici* isolates collected between 2013–2017 around the world. This global snapshot of *AvrStb6* haplotype diversity revealed dramatic changes across the global *Z. tritici* population: not only a marked decrease in *AvrStb6* diversity compared to previous studies, but also a worldwide shift towards haplotypes encoding *Stb6* resistance-breaking isoforms. One resistance-breaking isoform, named here as I02, was found to be the most abundant in several of the global regions of the world examined. Interestingly isolates collected in Turkey appeared to buck this global trend, with a high diversity of *AvrStb6* and the complete absence of I02 from the population. Further experiments described in this chapter also demonstrated that *AvrStb6* is expressed in all isolates tested, and that *Stb6* resistance-breaking isoforms predominate both on wheat cultivars possessing *Stb6* and where the resistance gene is absent.

3.4 Methods

3.4.1 *Zymoseptoria tritici* isolates collection

A collection of 381 *Z. tritici* isolates were analysed in this study (Table S3.1). These were collected from naturally infected wheat fields in the UK (*n* = 150), Ireland (*n* = 8), France (*n* = 12), Germany (*n* = 12), Australia (*n* = 58) and Turkey (*n* = 57), and from single fields in Chile (*n* = 10), Argentina (*n* = 10), Uruguay (*n* = 10) and the USA (*n* = 52). Most of these isolates were collected between 2015–2017, with the exception of isolates collected in Australia (2014) and Turkey (2013–2016). Control isolates were also included: IPO323 (avirulent on *Stb6* wheat), collected in the Netherlands in 1981 and IPO88004 (virulent on *Stb6* wheat) sampled in Ethiopia in 1988 (Kema and Van Silfhout, 1997, Goodwin *et al.*, 2011). Stocks of *Z. tritici* isolates were stored as blastospore water suspensions in 50% (v/v) glycerol at -80°C.

3.4.2 Sequencing and phylogenetic analysis of *AvrStb6*

Genomic DNA extraction was carried out from *Z. tritici* isolates using a previously published procedure (Rudd *et al.*, 2010), which is fully described in Section 2.3.2.

Briefly, *Z. tritici* cells were lysed and incubated in DNA extraction buffer (Table 2.3) and ammonium acetate, before centrifugation to separate cell material from solubilised genomic DNA in the supernatant. DNA was precipitated using isopropanol and centrifuged, the pellet washed and resuspended in nuclease-free water.

Primers for PCR amplification and sequencing of the *AvrStb6* gene were designed in conserved regions of the 5' and 3' UTRs of the gene, using both publicly available genome sequences and others, unpublished that were kindly provided by Hongxin Chen. Primers avrstb6.f1 and avrstb6.r1 were selected for amplification of *AvrStb6* from European isolates, and primers avrstb6.f3 and avrstb6.r1 were used to amplify *AvrStb6* from North and South American isolates (Table 2.4). All amplifications were performed using Phusion High-Fidelity DNA Polymerase, and PCR products purified using a QIAquick PCR Purification Kit. AvrStb6 sequences were obtained using Sanger sequencing service, provided by Eurofins Genomics UK Ltd., Wolverhampton, UK. Otherwise, *AvrStb6* sequences were provided by other groups for analysis (Section 3.2), with sequences from Australian *Z. tritici* isolates extracted from the whole-genome sequencing data (NCBI BioProject accession number PRJNA480739; McDonald *et al.*, 2019).

AvrStb6 haplotype and the corresponding protein isoform sequences were aligned using MAFFT v.7.388 (Multiple Alignment using Fast Fourier Transform; Katoh and Standley, 2013) with the phylogenetic tree assembled using PhyML (Phylogenetic inferences using Maximum Likelihood; Guindon and Gascuel, 2003). The *AvrStb6* sequence from the *Z. tritici* isolate IPO323 was used as a reference for MAFFT alignments, whilst a paralogue of *AvrStb6* present on chromosome 10 (gene *Mycgr3G82331*; Brunner and McDonald, 2018) was used to root the phylogenetic tree. A TCS haplotype network (Clement *et al.*, 2000) was created to visualise the diversity of *AvrStb6* haplotypes identified in the population using PopArt 1. 7 (Leigh and Bryant, 2015). Coding regions were annotated and translated to amino acid sequence using Geneious 10.2.3 (Biomatters Ltd., Auckland, New Zealand). Repeat-induced point mutation (RIP) analysis of the region of *Z. tritici* chromosome 5 containing *AvrStb6* was carried out using RIPper software (Van Wyk *et al.,* 2019).

The *AvrStb6* sequence diversity data obtained here was compared to the similar previously published datasets for the historic *Z. tritici* collections. The *AvrStb6* haplotype sequences obtained in Zhong *et al.* (2017) was kindly provided by Daniel Croll (University of Neuchâtel, Switzerland) and those obtained in Brunner and McDonald (2018) were downloaded from the NCBI PopSet Database (accession number 1337388362).

3.4.3 *Z. tritici* inoculation bioassays

Leaves of three-week-old wheat seedlings were inoculated with *Z. tritici* blastospore suspensions at 1 x 10^7 spores/mL as previously described (Keon *et al.*, 2007; Section 2.6). In this chapter the wheat cultivar (cv.) Cadenza, which carries *Stb6*, was used as a resistant control, whilst a CRISPR/Cas9-induced Cadenza*ΔStb6* mutant (kindly provided by Vladimir Nekrasov and Florian Hahn) was used as a susceptible control. Inoculation bioassays using these wheat cultivars was carried out in three independent experiments. A final inoculation assay was also carried out using the cv. Chinese Spring, which also possesses *Stb6*, and a near-isogenic line (NIL) of Chinese Spring background that carries a susceptibility haplotype at *Stb6* locus, from the cv. Courtot. A split plot randomised experimental design was used when carrying out the bioassays. For each bioassay, candidate *Z. tritici* isolates were inoculated onto five individual leaves of each wheat cultivar, with each leaf assessed for disease symptoms independently.

A full description of the inoculation bioassay is provided in Section 2.6. STB disease symptoms on each inoculated leaf were visually assessed at 21 days post inoculation (dpi) as previously described (Lee *et al.*, 2015), and this was complemented by pycnidiospores counting.

3.4.4 Wheat *Stb6* haplotype analysis

Information of the *Stb6* status of ten wheat cultivars from which *Z. tritici* isolates used in this study were collected, was available from a recently published study (Saintenac *et al.*, 2018). For ten other cultivars with unknown *Stb6* status, genomic DNA was extracted from 3-week-old wheat plants and *Stb6* re-sequenced following the previously published methodology of Saintenac *et al.*, (2018), and fully described

previously (Section 2.3.2). For *Z. tritici* isolates collected from Australia, Turkey and a few from Western Europe no cultivar data was available, so this analysis was not possible.

3.4.5 Analysis of *AvrStb6* expression during wheat infection

Three-week-old seedlings of wheat cv. Taichung 29, which is highly susceptible to *Z. tritici* and contains no known genes/QTLs for resistance to STB (Ghaffary *et al.*, 2012), were inoculated with spore suspensions of candidate *Z. tritici* isolates, as previously described (Section 2.6; Keon *et al.*, 2007). Visible disease symptoms emerged on infected leaves between 12-16-dpi, and at this timepoint symptomatic leaves were harvested and snap-frozen in liquid nitrogen. See Section 2.3.4 for reverse transcriptase-quantitative PCR (RT-qPCR). Primers used are specified in Table 2.4. Three biological and three technical replicates were carried out for each sample, with expression of *AvrStb6* measured as relative to the *Z. tritici* housekeeping gene *glucose-6-phosphate 1-dehydrogenase* (*G6PDH*; gene ID Mycgr3G100879), as calculated using the $2^{\Delta\Delta CT}$ method (Livak and Schmittgen, 2001).

3.5 Results

3.5.1 *AvrStb6* haplotype analysis

Primers flanking the *AvrStb6* gene were designed and used to amplify *AvrStb6* by PCR from a global collection of 383 *Z. tritici* isolates. These isolates were sampled from bread wheat grown in fields in ten countries across five continents. Subsequent sequencing of PCR products revealed a total of 52 *AvrStb6* haplotypes (named H01 to H52; Table S3.1) encoding 44 protein isoforms (named I01 to I44; Figure 3.1). Two well-characterised isolates, for which *AvrStb6* had already been sequenced, were also included in this population: the AvrStb6 haplotypes/isoforms of the avirulent isolate IPO323 and the virulent isolate IPO88004, were named as H01/I01 (IPO323) and H52/I44 (IPO88004). Whilst PCR amplification of the *AvrStb6* genomic region was successful for all isolates, three haplotypes - all identified in the Turkish population - were found to encode non-functional AvrStb6 isoforms. This included H17, present in

four isolates from Turkey and containing a nonsense mutation in the exon 1. H24 and H46, each represented by a single isolate, both contained single nucleotide deletions that led to frameshift mutations, in exon 3 for H24 and exon 2 for H46. However, the vast majority of *Z. tritici* isolates were found to possess functional *AvrStb6* alleles. All functional *AvrStb6* sequences possessed three exons and two introns, with the majority of coding sequences (361 of 381) being 365-bp in length, and others ranging from 362-bp to 366-bp. Exon 1, particularly the N-terminal signal peptide region, showed relatively high conservation, with many more polymorphisms found in exons 2 and 3 (Figure 3.1). Eight haplotypes (H09, H10, H12, H21, H22, H23, H37 and H51), encoding seven protein isoforms (I08, I09, I10, I11, I17, I40 and I43) and represented by 18 isolates, contained in-frame 3-bp deletions, all in exon 3. With the exception of two isolates from Western Europe possessing I17, these isolates were exclusively found within the Turkish population. The AvrStb6 isoforms identified here ranged in length from 80–82 amino acid residues. Amino acids at 52 positions within AvrStb6, including all 12 cysteines, were invariant across the collection (excluding the I42 frameshift mutant) (Figure 3.1). All other residues in AvrStb6 were polymorphic, with the highest variation identified at positions 41, 61 and 77. The amino acid sequence alignment (Figure 3.1) and a haplotype network analysis (Figure 3.2a) suggested that AvrStb6 isoforms fall into three broad groups, denoted in figures as I, II and III. A further phylogenetic analysis (Figure 3.2b) also broadly supported this observation, with *AvrStb6* haplotypes from group III, largely represented by isolates of Turkish origin, being distant from those in groups I and II in this phylogeny.

3.5.2 One AvrStb6 isoform predominates among current *Z. tritici* isolates globally

The majority of isolates analysed in this study (280 of 381, 73.5%) possessed the AvrStb6 isoform I02, making it by far the predominant isoform globally (Figure 3.1). Most isolates possessed I02 in almost every geographic region studied including Australia (96.6%), Western Europe (91.8%), USA (82.7%) and Chile (80%) (Table 3.1). Exceptions to this were Argentina and Uruguay, where isoform I03 was most prevalent and interestingly in Turkey isoform I02 was not identified at all. Several haplotypes, H02 (239 isolates), H03 (34 isolates), H06 (6 isolates), H15 (2 isolates), and H33 (1 isolate) all encoded isoform I02. Whilst multiple of these haplotypes were

each identified in most regions where I02 predominated, in the USA collection only a single I02-encoding haplotype (H02) was identified.

The next most common isoform globally was I03, incidentally the only other isoform to be found in multiple regions. I03 was identified in 23 isolates (6% of isolate collection), originating in Western Europe, South America and Turkey. All other identified AvrStb6 isoforms were represented by between 1 to 8 isolates in the collection. Twenty-nine haplotypes and twenty-five AvrStb6 protein isoforms, representing more than half of the identified isoforms, were unique to single isolates in the collection (Figure 3.1 and S3.1). Remarkably, the avirulence isoform I01, found at a high frequency in previous studies (Zhong *et al.*,2017), was completely absent in our population.

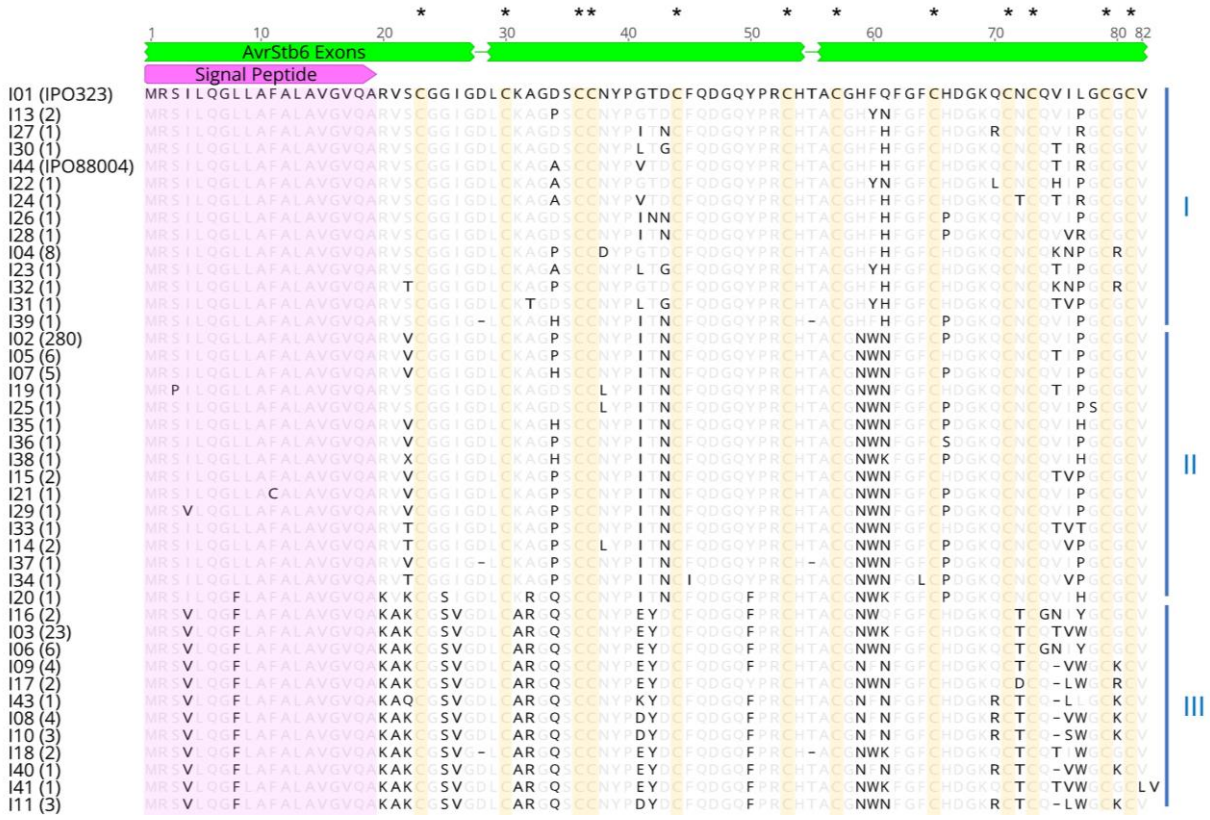

Figure 3.1: Alignment of the AvrStb6 isoform sequences identified in this study. Protein sequences were aligned using MAFFT v7.388. Numbers in brackets represent the number of isolates identified possessing each isoform. Amino acids synonymous to the I01 sequence are greyed. Missing residues relative to I01 are represented as dashes. The pink arrow annotates the secretion signal peptide, whilst the green bars represent the exons of the coding gene sequence. The three alignment groupings (I, II and III) of the isoforms are indicated by vertical blue lines to the right of the sequences, and invariant cysteine residues are highlighted in yellow and by asterisks above the alignment.

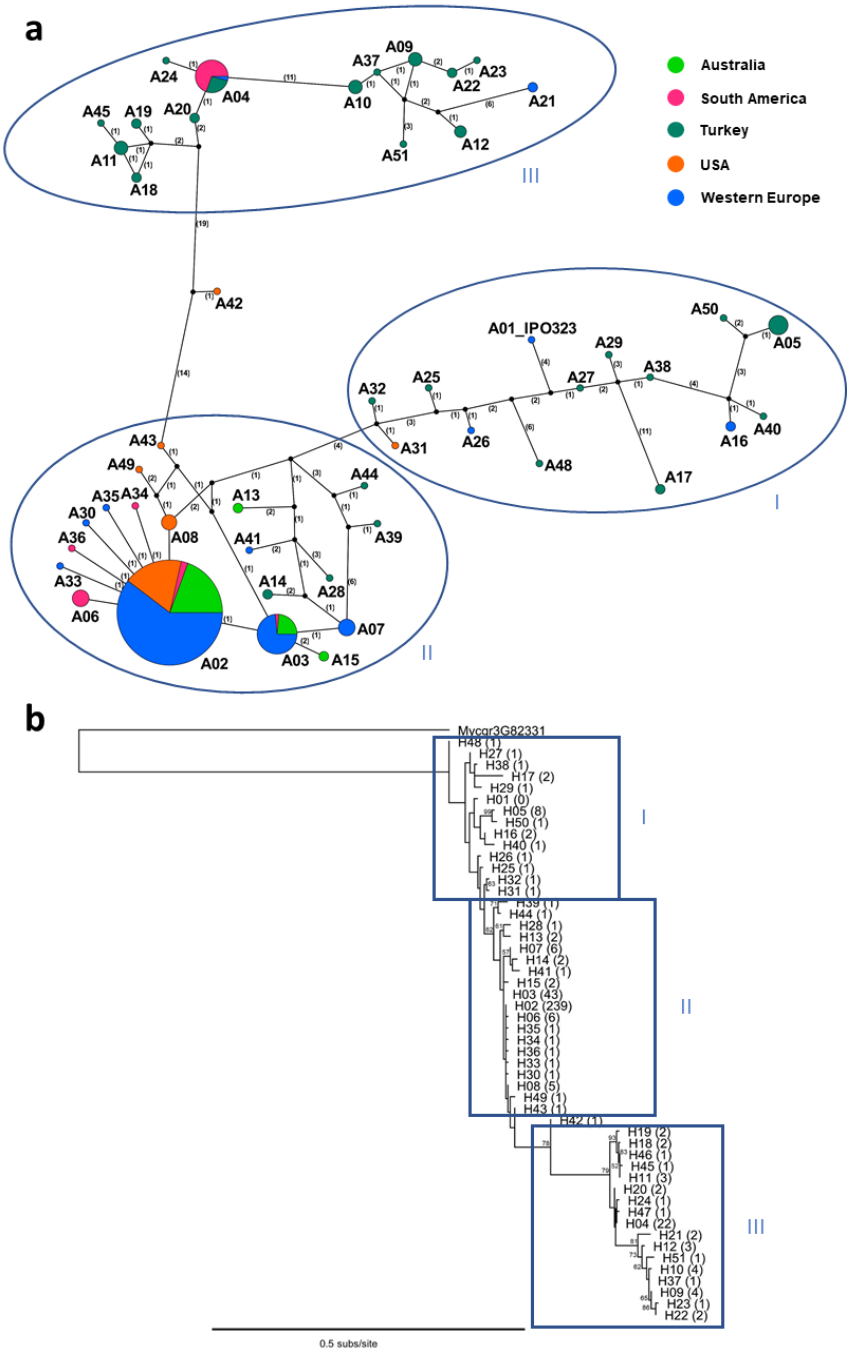

Figure 3.2: Analysis of *AvrStb6* haplotype distribution in the global *Zymoseptoria tritici* population. a) Haplotype network for global *AvrStb6* sequences obtained from the TCS analysis. Each node represents a separate haplotype identified in this study. The node size represents the number of isolates identified possessing this haplotype. The nodes are coloured depending on the geographic region(s) from which the isolates of the same node were identified. Connecting lines between nodes denote closely related haplotypes. Numbers in brackets correspond to the number of mutations between adjoined haplotypes, with line lengths *not* proportional to genetic distances. Black unlabelled nodes represent hypothetical common ancestors of related haplotypes. The three groupings of haplotypes I, II and III are highlighted by blue ellipses. **b)** Phylogenetic tree of the AvrStb6 haplotypes constructed using PhyML. The tree was rooted using a *Z. tritici* paralogue of *AvrStb6*; *Mycgr3G82331* located on chromosome 10. Numbers on branches indicate bootstrap scores for each branch, whilst numbers in brackets indicate the number of isolates identified possessing each haplotype.

3.5.3 Turkey is a hotspot of *AvrStb6* diversity

Z. tritici isolates from Turkey were analysed as part of this study, with a total of fifty-seven sourced from smallholder farmers' wheat fields. From this isolate collection, 29 *AvrStb6* haplotypes encoding 26 isoforms were identified. The finding that more than half of all identified AvrStb6 isoforms being found in Turkey and 25 being unique to this region, demonstrate a substantially higher rate of diversity in this population than any other in this study. This high diversity is visualised by the *AvrStb6* haplotype network (Figure 3.2a), which identifies two major branches of variant haplotypes. These branches mostly consist of haplotypes exclusive to the Turkish *Z. tritici* population. As mentioned above isoform I02, the most prevalent isoform globally (Section 3.5.2), was not observed in the Turkish population. This population therefore represents a notable break in the trend toward the predominance of a single isoform described for other global regions.

3.5.4 *Stb6* resistance-breaking isoforms are widespread in the current population

The frequency of AvrStb6 isoforms in our collection capable of evading *Stb6*-mediated defence of wheat was unknown. To determine this, one *Z. tritici* isolate was randomly selected for each of the nine AvrStb6 isoforms identified in more than one isolate in the collection (Figure S3.2). The exception to this was isoform I02, for which two representative isolates "2NIAB" and "R16.1" (collected from different commercial fields in the UK) were selected. The previously characterised avirulent and virulent *Z. tritici* isolates IPO323 (Brading *et al.*, 2002) and IPO88004 (Saintenac *et al.*, 2018) possessing isoforms I01 and I44, respectively, were used as controls. Using these isolates inoculation bioassays were carried out, involving inoculation of fungal spore solutions onto wheat leaves at the seedling stage. Two genotypes were tested: the wheat cv. Cadenza which possesses *Stb6*, and a CRISPR/Cas9 gene-edited line of cv. Cadenza lacking a functional *Stb6*, due to a large frameshift deletion in the first exon of this gene. The genotypes were thus genetically identical except for the presence/absence of *Stb6*.

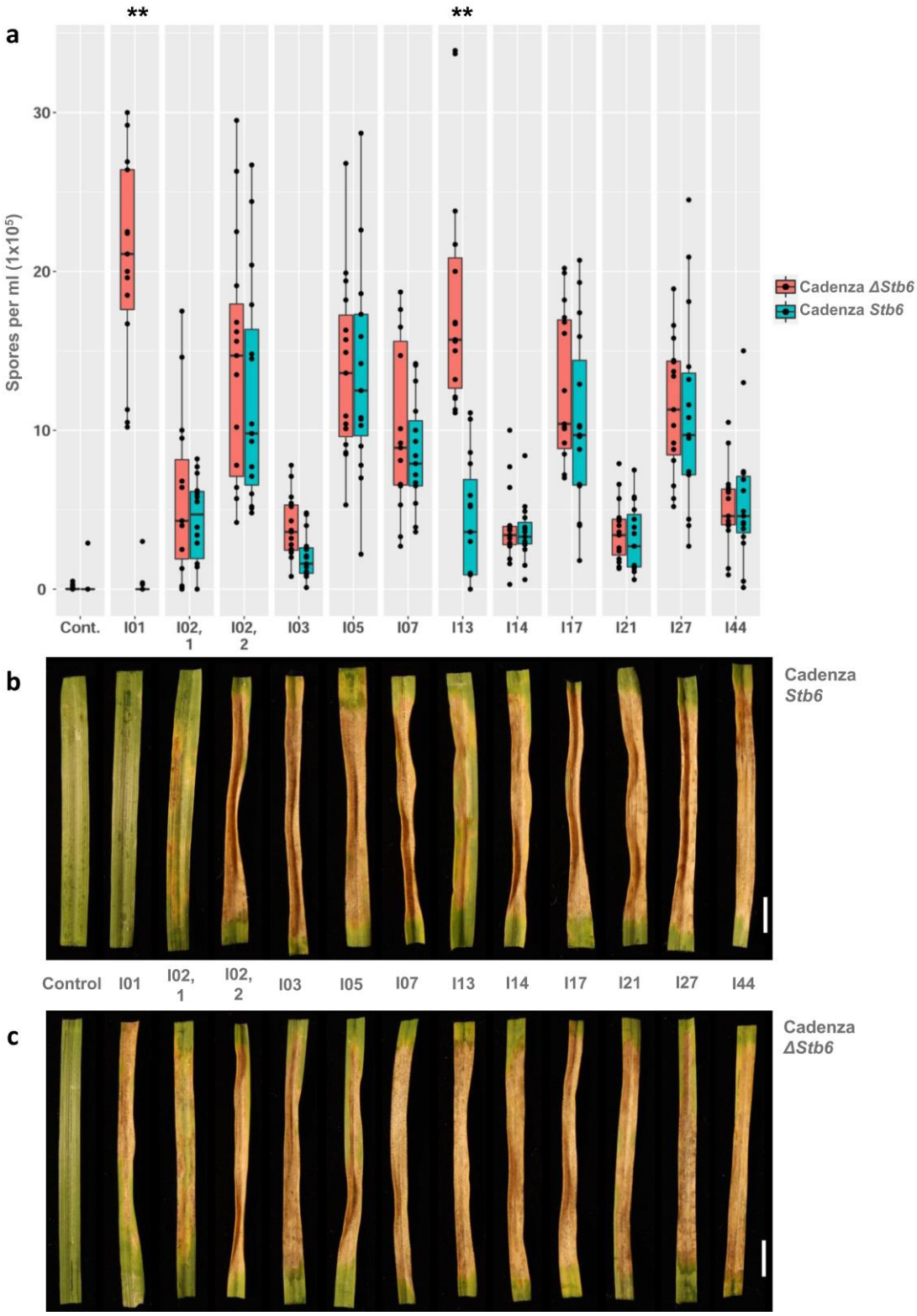

Figure 3.3: Wheat leaf inoculation bioassay results. Leaves of wild-type cultivar Cadenza (possessing *Stb6*) and a CRISPR/Cas9-induced *Stb6* deletion mutant (Cadenza*ΔStb6*) were inoculated with candidate *Z. tritici* isolates possessing different AvrStb6 isoforms. **a)** Pycnidiospore counts from inoculated wheat leaves at 21 days post inoculation (dpi). Asterisks represent isolates with highly significant (**, p <0.005) differences in pycnidiospore counts between the resistant and susceptible genotypes. The most common isoform, I02, was represented by the two isolates (labelled 1 and 2) originating from two different geographic regions. **b)** and **c)** Images of inoculated wheat leaves harvested at 21 dpi and incubated for two days under ~100% humidity to induce pycnidia formation. Scale bar, 10 mm.

Of the ten test isolates (representing 9 different AvrStb6 isoforms) inoculated, nine consistently induced STB disease symptoms on wheat genotypes irrespective of the presence/absence of *Stb6*; inducing host cell death and forming black asexual fruiting bodies known as pycnidia on all tested wheat genotypes (Figure 3.3). This included both isolates representing I02, the most prevalent AvrStb6 isoform in our collection. This inoculation assay was repeated in three independent experiments with similar results. In addition, this assay was carried out using a wheat cultivar pair comprising the wheat landrace Chinese Spring (also possessing *Stb6*) and a NIL that contains the *Stb6* susceptibility haplotype, developed from a cross between Chinese Spring and a susceptible cv. Courtot (Saintenac *et al.*, 2018). Again, this assay yielded similar results to previous assays (Figure S3.3). As AvrStb6 isoforms found in the vast majority of isolates in our collection were represented in these inoculation assays, these results suggest a prevalence for *Stb6* resistance-breaking isoforms in the global *Z. tritici* population.

Other than the avirulent reference isolate IPO323 (I01), only one other isolate was identified as having consistently reduced virulence on *Stb6* wheat. This isolate, possessing the isoform I13, induced leaf chlorosis but no necrosis nor any pycnidia, in one experiment carried out on Cadenza cultivars and the experiment on Chinese Spring NILs (Figures 3.3b and S3.3). Whilst subsequent assays using the Cadenza cultivars revealed that *Z. tritici* possessing I13 was in fact capable of inducing necrosis and forming pycnidia on *Stb6* wheat, the extent of disease symptoms was still significantly reduced compared to gene-edited line lacking the resistance gene. Interestingly, AvrStb6 isoform I13 shares the highest percent amino-acid identity with the known avirulence isoform I01 (Figure S3.2). Another isolate, representative of isoform I03, also showed reduced virulence on *Stb6* wheat across the three Cadenza inoculation assays (Figure 3.3a), whilst the isolate possessing I14 showed reduced virulence on Chinese Spring wild-type wheat relative to the susceptible NIL. However, the reduction in virulence on *Stb6* wheat of the isolate possessing I14 was not observed for Cadenza genotypes, and differences in pycnidiospores count data for the isolate possessing I03 were not significant (at $p < 0.01$). Only the *Z. tritici* isolate representing isoform I13 and the control avirulent isolate IPO323 showed consistent, significant reductions in virulence on *Stb6* wheat.

3.5.5 Virulent AvrStb6 isoforms are common on wheat genotypes both with and without *Stb6*

The AvrStb6 haplotype diversity reported in this study represents a notable break from previous studies. In particular, Zhong *et al.* (2017) reported that ~18% of isolates collected in France in 2009-2010 possess the avirulence isoform identical to IPO323, whilst this was completely absent in our collection (Section 3.5.2). It was hypothesised that sampling from *Stb6*-containing wheat cultivars may lead to over-representation of isolates possessing AvrStb6 virulence isoforms. The identity of the wheat cultivars from which 254 of the 381 *Z. tritici* isolates in our collection was available. Of these, ten cultivars had already been characterised for their *Stb6* status (Saintenac *et al.*, 2018). A further ten cultivars were sourced for genotyping, with *Stb6* re-sequenced from cvs. Consort, Dickens, Gallant, Genesis INIA 2375, Kaseberg, KWS Cashel, KWS Lumos, Marston, Solace, and Zulu (Table S3.1). It was determined that 9/20 of these characterised cultivars possess haplotype 1 of *Stb6*, which confers disease resistance, and were the source of 73 (34.8%) *Z. tritici* isolates in our collection. The other eleven cultivars contained non-functional susceptibility *Stb6* haplotypes 3 or 7 – named following nomenclature used by Saintenac *et al.* (2018) and represented sources of 137 (65.2%) isolates (Table 3.2). I therefore concluded that no overall bias existed in the wheat cultivars used in this study towards *Stb6* susceptibility or resistance, and indeed that a large proportion of *Z. tritici* isolates were sampled from cultivars containing non-functional *Stb6*.

3.5.6 *AvrStb6* expression is highly variable between *Z. tritici* isolates

The numerous polymorphisms between the avirulent AvrStb6 isoform I01 and the virulent isoforms described in this study suggests that changes in protein sequence has led to evasion of *Stb6*-mediated resistance by the current *Z. tritici* isolates (Figures 1 and 3.3). However, it may also be possible that the suppression of *AvrStb6* expression during infection may also contribute to the *Stb6* resistance breakdown. The expression of *AvrStb6* in ten *Z. tritici* isolates each carrying a different isoform of AvrStb6 and IPO323 (Section 3.5.4) was therefore analysed by RT-qPCR. A fully susceptible wheat cv. Taichung 29, that does not possess *Stb6* (Ghaffary *et al.*, 2012), was chosen for infection assays. With the aim to collect samples at a similar phase of

infection, infected leaf tissues for RT-qPCR analysis were harvested when the first symptoms of the disease become visible. This infection phase was chosen as many *Z. tritici* effector genes, including *AvrStb6*, display maximal expression during this transition to necrotrophy phase (Rudd *et al.*, 2015, Zhong *et al.*, 2017). RT-qPCR analysis revealed that *AvrStb6* was expressed in each tested isolate (Figure S3.4). This analysis revealed *AvrStb6* expression levels to be highly variable between different isolates. All isolates, with the exception of the isolate representing I21, showed reduced expression relative to IPO323 (avirulence isoform I01), although statistical differences were not calculated. Importantly, however, in all virulent isolates AvrStb6 expression was detected, although it was markedly reduced in the isolate possessing isoform I14 (Figure S3.4). Whilst it is not possible to rule out that variations in *AvrStb6* expression affect the evasion of *Stb6*-mediated defence, these data suggest that the mechanism of *Stb6* resistance breakdown is more likely due to protein sequence polymorphism, rather than the suppression of *AvrStb6* expression.

3.6 Discussion

Few studies have analysed the temporal changes in Avr factor prevalence driven by selection pressure from host species in pathogen populations. Often, these have a fairly narrow geographical area coverage. For example, studies into the changes in *Avr* gene prevalence in the fungal pathogen *Leptosphaeria maculans* of *Brassica* crops over time have focussed on single countries such as Canada (Fernando *et al.*, 2018) or Australia (Van de Wouw *et al.*, 2018). On the other hand, studies with a global geographical scope often do not consider the possibility of temporal changes in Avr factor prevalence. This chapter reports on the diversity analysis of the avirulence factor *AvrStb6* in recent global *Z. tritici* populations. Moreover, the recent publication of two similar studies which analysed the *AvrStb6* population diversity in *Z. tritici* populations collected before our own - in 1990–2001 and 2009–2010, respectively (Zhong *et al.*, 2017, Brunner and McDonald, 2018) – provided an opportunity for comparisons of AvrStb6 diversity changes over time. This comparison suggests that large shifts in *AvrStb6* haplotype prevalence have taken place in multiple global regions over a relatively short period. These include the possible extinction of the

avirulence isoform of AvrStb6 originally described from the reference isolate IPO323 (collected in the Netherlands in 1981). In its place have emerged multiple virulence isoforms, one of which now predominates globally. It is possible that these changes in *Z. tritici* populations are imposed by a worldwide increase in the deployment of commercial wheat cultivars carrying *Stb6* (Chartrain *et al.*, 2005, Saintenac *et al.*, 2018), although evidence for this hypothesis is currently unavailable.

The high proportion of AvrStb6 isoforms to haplotypes illustrates the high frequency of non-synonymous mutations within the effector gene, which in turn suggests a strong selection pressure for the evolution of novel AvrStb6 protein isoforms that cannot be recognised by the corresponding wheat immune receptor Stb6. This phenomenon is well documented for other pathogen effectors, for instance with diversifying selection observed for ToxA, Tox1 and Tox3 of *Parastagonospora nodorum* (Stukenbrock and McDonald, 2007, McDonald *et al.*, 2013), NIP1 of *Rhynchosporium commune* (Schürch *et al.*, 2004), and AvrP123 and AvrP4 of the flax rust pathogen *Melampsora lini* (Barrett *et al.*, 2009). In several fungal pathogens, repeat-induced point (RIP) mutations have been shown to facilitate the evolution of virulence due to the diversification of effector gene sequences, including the introduction of multiple premature stop codons (Fudal *et al.*, 2009). Given the transposon rich, highly dynamic region of the genome in which *AvrStb6* is located (Sánchez-Vallet *et al.*, 2018) it seemed possible that a similar mechanism has contributed to the diversification of this *Z. tritici* effector. However, an *in-silico* analysis suggests a low frequency of RIP-associated mutations in the *AvrStb6* genomic region (Figure S3.5). The AvrStb6 secretion signal peptide region and all cysteine residues in AvrStb6 were highly conserved (Figure 3.1). The signal peptide of effectors is required for protein secretion and cysteine residues are believed to form disulphide bonds to help to stabilise the protein in the harsh alkaline pH apoplastic environment. Additionally, premature stop codon mutations within the gene were extremely rare, building a picture of an effector that is retained with extraordinarily high frequency across the *Z. tritici* population. RT-qPCR analysis also showed that *AvrStb6* was expressed in all tested *Z. tritici* isolates, during the infection transition from biotrophy to necrotrophy (Figure S3.4). These findings combined suggest an evolutionary pressure to maintain a functional effector, implying potential contribution of AvrStb6 to fungal virulence or fitness. Intriguingly,

however, the elimination of *AvrStb6* from the *Z. tritici* genome appeared to have no impact on its virulence, under laboratory conditions (Kema *et al.*, 2018), perhaps suggesting that any fitness advantage conferred by *AvrStb6* occurs under as-yet-unknown environmental conditions.

Table 3.1. List of all regions from which *Z. tritici* isolates were sourced as part of this study

Collection	Country / state of collection	Year of collection	Number of isolates	Prevalence (%) of AvrStb6 I02[1]
Western Europe				
Current study	England	2015-2017	135	94.8
	Scotland	2015-2017	14	92.9
	Ireland	2015-2017	8	87.5
	France	2015-2017	12	91.7
	Germany	2015-2017	12	66.7
Brunner & McDonald, 2018[2]	Switzerland	1999	29	51.7
Zhong et al., 2017[2]	France	2009-2010	102	49
USA				
Current Study	Oregon	2016	48	89.6
Brunner & McDonald, 2018[2]	Oregon	1990	56	0
Australia				
Current Study	Tasmania	2014	58	96.6
Brunner & McDonald, 2018[2]	New South Wales	2001	27	74.1
South America				
Current Study	Chile	2016	10	90
	Argentina	2016	10	20
	Uruguay	2016	10	30
Turkey				
Current Study	Turkey	2013-2016	46	0

[1]The prevalence of AvrStb6 I02 is given as a proportion of the collected isolates which possessed the AvrStb6 I02 isoform.

[2]For the purposes of comparison, also listed are the *Z. tritici* isolate numbers and source locations for the studies carried out by Zhong et al. (2017) and Brunner & McDonald (2018).

This analysis of a global population of *Z. tritici* isolates also revealed the abundance of a single AvrStb6 isoform, I02 (Section 3.5.2). This isoform was predominant in all countries of Western Europe from which the isolates were sourced, as well as Australia, USA and Chile. A comparison of isoform I02 frequency between the *Z. tritici* population collected in Western Europe between 2015–2017 and reported on here, and those of other previously published studies comprising isolates sampled in 1999 (Brunner and McDonald, 2018) and 2009–2010 (Zhong *et al.*, 2017) suggested a profound increase in I02 prevalence (Table 3.1). This was also true of *Z. tritici* isolates collected in Oregon, USA, with sequencing of *AvrStb6* from *Z. tritici* isolates sourced from Oregon, USA in 1990 notably failing to identify a single occurrence of I02 (Table 3.1). This stands in sharp contrast to the analysis of isolates collected in 2016 and reported here, which identified I02 in 82.7% of tested isolates. This result suggests a population shift and, combined with the fact that in all cases I02 was coded by a single haplotype H02, may suggest the introduction and rapid proliferation of this virulence *AvrStb6* haplotype throughout the population of *Z. tritici* in Oregon. This has occurred in other pathogens, such as with the recent accidental importation of *Pyricularia oryzae*, a wheat blast pathogen, from Brazil to Bangladesh (Islam *et al.*, 2016). Interestingly, in Australia a high prevalence of AvrStb6 I02 was already evident in the local *Z. tritici* population sampled in 2001 (Table 3.1; Zhan *et al.*, 2005).

In addition to the increasing dominance of a single isoform I02, the overall diversity of AvrStb6 isoforms seem to have decreased over time. Thus, for example, the previous population studies by Brunner and McDonald (2018) and Zhong *et al.* (2017) identified thirty and eighteen AvrStb6 isoforms in the populations comprising 142 or 103 isolates, respectively. These numbers are substantially higher than the 42 isoforms identified from 381 isolates analysed here. It is unknown why isoform I02 specifically may have become so prevalent in multiple regions around the world recently, given that other isoforms are also capable of evading *Stb6*-mediated resistance (Figure 3.3). However, the limited diversity of *Stb6* haplotypes (n = 3) in the host wheat plants sampled (Table 3.2) may reflect the narrow *Stb6* diversity of commercial wheat cultivars more broadly (Fu and Somers, 2009). AvrStb6 isoform I02 may be specifically adapted for successful infection of wheat possessing these *Stb6* haplotypes. The virulence isoform I02 may also be the best-adapted for carrying out

its as-yet-unknown effector function. Other studies have shown changes in the Avr factor prevalence, such as an increased incidence of *AvrLm4-7* in *Leptosphaeria maculans* from 47.2% in 2005–2006 (Dilmaghani *et al.*, 2009) to 89.7% in 2010–2011 (Liban *et al.*, 2016) in Western Canada, demonstrating the ability of pathogens to adapt rapidly to changing conditions in host populations. However, to our knowledge this is the first time that a shift of such significance has been shown to occur across a global population of a plant pathogen.

Table 3.2. *Stb6* genotyping of wheat cultivars from which *Z. tritici* isolates were sourced

Wheat cultivar	*Stb6* haplotype[1]	No. of *Z. tritici* isolates collected from cultivar[2]
Alchemy	7	1
Consort	7	17
Cordiale	7	13
Cougar	1	22
Crusoe	7	1
Dickens	1	22
Evolution	1	6
Gallant	7	7
Genesis	3	10
JB Diego	7	2
Kaseburg	7	52
KWS Cashel	3	21
KWS Santiago	1	4
KWS Siskin	1	13
Lumos	7	8
Marston	1	1
Reflection	7	5
Solace	1	1
Trapez	1	2
Zulu	1	2
Haplotype totals	1	73
	3	31
	7	106

[1]*Stb6* haplotype 1 encodes a functional kinase and confers resistance; haplotypes 3 and 7 possess a non-functional kinase and confer no resistance.

[2]Wheat cultivars were *Stb6* genotyped for 209 of the 381 isolates collected as part of this study.

The analysis of *AvrStb6* haplotypes did not identify I02 as the predominant isoform in Argentina and Uruguay, and this isoform was completely absent from the Turkish *Z.*

tritici population (Section 3.5.3). It is possible that the local wheat cultivars used for sampling *Z. tritici* isolates in these countries and analysed here may have unique genetic makeups, varying from the genetically narrow commercial cultivars of other analysed regions. However, it is not currently possible to test this hypothesis. The Turkish population is of particular interest, given its substantially higher *AvrStb6* haplotype diversity compared to those in other wheat growing regions. The exact reasons for this difference are unknown, although local and genetically diverse landraces of wheat are frequently grown in Turkey, and this may be a driver for matching diversification of *Z. tritici* genomes. In addition, the location of Turkey near or at the hypothesised geographic region of origin of both wheat (Shewry, 2009) and *Z. tritici* (Stukenbrock *et al.*, 2006) may also be a cause for the high diversity of *AvrStb6* haplotypes observed here, as origins of species often also correspond to the centres of their genetic diversity.

A recent study (Kema *et al.*, 2018) suggested that the *Z. tritici* virulence on wheat cultivars carrying *Stb6* was associated with changes at the amino acid positions 41 and 43 in the AvrStb6 protein. Other than the avirulence I01, the only other isolate demonstrating consistently reduced virulence on *Stb6* wheat possessed isoform I13 (Figure 3.3). Whilst the isolate possessing I14 also showed a significant reduction in virulence on Chinese Spring wild-type when compared to the susceptible NIL, this result was not observed on Cadenza wild-type and the gene-edited Cadenza line lacking *Stb6*, for which similar levels of pycnidiospore counts and disease symptoms were observed on both genotypes. Both I01 and I13 possess identical residues, glycine and aspartic acid, at positions 41 and 43, respectively (Figure S3.2). However, other AvrStb6 isoforms, including I03, I17, and I44, also possess an aspartic acid at position 43, but showed virulence on *Stb6* wheat (Figure S3.2, Figure 3.3). Whilst expression data for isolates possessing I03, I17 and I44 showed reduced *AvrStb6* expression compared to the avirulence isolate possessing I01, expression is not fully suppressed in any of these isolates (Figure S3.4). This suggests that amino acid changes in AvrStb6 at position 41 alone may be sufficient for the *Stb6* resistance-breaking ability of *Z. tritici* isolates. Further experiments, such as testing the virulence on *Stb6* wheat of transgenic *Z. tritici* lines expressing each of these AvrStb6 isoforms under the control of an ectopic promoter, could confirm this hypothesis.

The number of *Z. tritici* isolates analysed in this study and the failure to identify AvrStb6 isoform I01 in the collection suggest that this isoform has been eliminated from the modern *Z. tritici* population. However, the *AvrStb6* haplotype network analysis indicates that the true diversity of *AvrStb6* may be higher than identified, as in some cases multiple mutations were found to separate the neighbouring haplotypes in the network (Figure 3.2a). A significant amount of undiscovered sequence variation in *AvrStb6* may still be present in the global *Z. tritici* population. However, what is clear from our analysis is that wheat disease resistance gene *Stb6* has currently been almost completely overcome due to predominance of isolates carrying resistance-breaking AvrStb6 isoforms in the modern *Z. tritici* populations around the world. This suggests, that despite the ability of *Z. tritici* to sexually reproduce on resistant hosts (Kema *et al.,* 2018), Avr factors tend to be eliminated in subsequent populations.

In the following chapter we describe experimentation aimed to identify the function of AvrStb6, through the study of its localisation *in planta* and analysis of its interactions with plant proteins. Furthermore, we also aimed to determine whether a direct interaction takes place between the avirulence isoform of AvrStb6 and Stb6, an interaction not unequivocally ruled out in the previous study (Saintenac *et al*, 2018).

3.7 References

Barrett LG, Thrall PH, Dodds PN, Van der Merwe M, Linde CC, Lawrence GJ, Burdon JJ. 2009. Diversity and evolution of effector loci in natural populations of the plant pathogen *Melampsora lini*. *Molecular Biology & Evolution* **26**: 2499–2513.

Blondeau K, Blaise F, Graille M, *et al*. 2015. Crystal structure of the effector AvrLm4-7 of *Leptosphaeria maculans* reveals insights into its translocation into plant cells and recognition by resistance proteins. *Plant Journal* **83**: 610–624.

Brading PA, Verstappen ECP, Kema GHJ, Brown JKM. 2002. A gene-for-gene relationship between wheat and *Mycosphaerella graminicola*, the Septoria tritici blotch pathogen. *Phytopathology* **92**: 439–445.

Brunner PC, McDonald BA. 2018. Evolutionary analyses of the avirulence effector AvrStb6 in global populations of *Zymoseptoria tritici* identify candidate amino acids

involved in recognition. *Molecular Plant Pathology* **19**: 1836–1846.

Chartrain L, Brading PA, Brown JKM. 2005. Presence of the *Stb6* gene for resistance to septoria tritici blotch (*Mycosphaerella graminicola*) in cultivars used in wheat-breeding programmes worldwide. *Plant Pathology* **54**: 134–143.

Clement M, Posada D, Crandall KA. 2000. TCS: a computer program to estimate gene genealogies. *Molecular Ecolology* **9**: 1657–1659.

Cook DE, Mesarich CH, Thomma BPHJ. 2015. Understanding plant immunity as a surveillance system to detect invasion. *Annual Review Phytopathology* **53**: 541–563.

Cowger C, Hoffer ME, Mundt CC. 2000. Specific adaptation by *Mycosphaerella graminicola* to a resistant wheat cultivar. *Plant Pathology* **49**: 445–451.

Dilmaghani A, Balesdent MH, Didier JP *et al*. 2009. The *Leptosphaeria maculans* - *Leptosphaeria biglobosa* species complex in the American continent. *Plant Pathology* **58**: 1044–1058.

Djamei A, Schipper K, Rabe F *et al*. 2011. Metabolic priming by a secreted fungal effector. *Nature* **478**: 395–398.

Dong S, Raffaele S, Kamoun S. 2015. The two-speed genomes of filamentous pathogens: waltz with plants. *Current Opinion in Genetics & Development* **35**: 57–65.

Dutta A, Croll D, McDonald BA, Krattinger SG. 2021. Genome-wide association study for septoria tritici blotch resistance reveals the occurrence and distribution of *Stb6* in a historic Swiss landrace collection. *Euphytica* **217**: 108. DOI: 10.1007/s10681-021-02843-7

Fernando, W.G.D., Zhang, X., Selin, C., *et al*. 2018. A six-year investigation of the dynamics of avirulence allele profiles, blackleg incidence, and mating type alleles of *Leptosphaeria maculans* populations associated with canola crops in Manitoba, Canada. *Plant Disease* **102**: 790–798.

Fu YB, Somers DJ. 2009. Genome-wide reduction of genetic diversity in wheat breeding. *Crop Science* **49**: 161–168.

Fudal I, Ross S, Brun H, Besnard AL, Ermel M, Kuhn ML, Balesdent MH, Rouxel T. 2009. Repeat-induced point mutation (RIP) as an alternative mechanism of evolution toward virulence in *Leptosphaeria maculans. Molecular Plant-Microbe Interactions* **22**: 932–941.

Ghaffary SMT, Faris JD, Friesen TL, Visser RGF, Van der Lee TAJ, Robert O, Kema GHJ. 2012. New broad-spectrum resistance to Septoria tritici blotch derived from synthetic hexaploid wheat. *Theoretical & Applied Genetics* **124**: 125–142.

Goodwin SB, M'barek SB, Dhillon B *et al*. 2011. Finished genome of the fungal wheat pathogen *Mycosphaerella graminicola* reveals dispensome structure, chromosome plasticity, and stealth pathogenesis. *PLoS Genetics* **7**: e1002070.

Guindon S, Gascuel O. 2003. A simple, fast, and accurate algorithm to estimate large phylogenies by maximum likelihood. *Systematic Biology* **52**: 696–704.

Hovmøller MS, Justesen AF. 2007. Rates of evolution of avirulence phenotypes and DNA markers in a northwest European population of *Puccinia striiformis* f. sp. *tritici*. *Molecular Ecology* **16**: 4637–4647.

Islam MT, Croll D, Gladieux P *et al*. 2016. Emergence of wheat blast in Bangladesh was caused by a South American lineage of *Magnaporthe oryzae*. *BMC Biology* **14**: 84.

Jones JDG, Dangl JL. 2006. The plant immune system. *Nature* **444**: 323–329.

Kanyuka K, Rudd JJ. 2019. Cell surface immune receptors: the guardians of the plant's extracellular spaces. *Current Opinion in Plant Biology.* **50**: 1–8.

Katoh K, Standley DM. 2013. MAFFT multiple sequence alignment software version 7: improvements in performance and usability. *Molecular Biology & Evolution* **30**: 772–780.

Kema GH, van Silfhout CH. 1997. Genetic variation for virulence and resistance in the wheat - *Mycosphaerella graminicola* pathosystem III. Comparative seedling and adult plant experiments. *Phytopathology* **87**: 266–272.

Kema GHJ, Mirzadi Gohari A, Aouini L *et al*. 2018. Stress and sexual reproduction affect the dynamics of the wheat pathogen effector AvrStb6 and strobilurin resistance. *Nature Genetics* **50**: 375–380.

Keon J, Antoniw J, Carzaniga R, Deller S, Ward JL, Baker JM, Beale MH, Hammond-Kosack K, Rudd JJ. 2007. Transcriptional adaptation of *Mycosphaerella graminicola* to programmed cell death (PCD) of its susceptible wheat host. *Molecular Plant-Microbe Interactions* **20**: 178–193.

Kleemann J, Rincon-Rivera LJ, Takahara H *et al*. 2012. Sequential delivery of host-induced virulence effectors by appressoria and intracellular hyphae of the phytopathogen *Colletotrichum higginsianum*. *PLoS Pathogens* **8**: e1002643.

Lee WS, Rudd JJ, Kanyuka K. 2015. Virus induced gene silencing (VIGS) for functional analysis of wheat genes involved in *Zymoseptoria tritici* susceptibility and resistance. *Fungal Genetics Biology* **79**: 84–88.

Leigh JW, Bryant D. 2015. POPART: full-feature software for haplotype network construction. *Methods in Ecology & Evolution* **6**: 1110–1116.

Liban SH, Cross DJ, Kutcher HR, Peng G, Fernando WGD. 2016. Race structure and frequency of avirulence genes in the western Canadian *Leptosphaeria maculans* pathogen population, the causal agent of blackleg in brassica species. *Plant Pathology* **65**: 1161–1169.

Livak KJ, Schmittgen TD. 2001. Analysis of relative gene expression data using real-time quantitative PCR and the $2^{-\Delta\Delta CT}$ method. *Methods* **25**: 402–408.

Lo Presti L, Lanver D, Schweizer G, Tanaka S, Liang L, Tollot M, Zuccaro A, Reissmann S, Kahmann R. 2015. Fungal effectors and plant susceptibility. *Annual Review of Plant Biology* **66**: 513–545.

Luderer R, Takken FLW, de Wit PJGM, Joosten MHAJ. 2002. *Cladosporium fulvum* overcomes *Cf-2*-mediated resistance by producing truncated AVR2 elicitor proteins. *Molecular Microbiology* **45**: 875–884.

Marshall R, Kombrink A, Motteram J, Loza-Reyes E, Lucas J, Hammond-Kosack KE, Thomma BPHJ, Rudd JJ. 2011. Analysis of two *in planta* expressed LysM effector homologs from the fungus *Mycosphaerella graminicola* reveals novel functional properties and varying contributions to virulence on wheat. *Plant Physiology* **156**: 756–769.

McDonald MC, Oliver RP, Friesen TL, Brunner PC, McDonald BA. 2013. Global diversity and distribution of three necrotrophic effectors in *Phaeosphaeria nodorum* and related species. *New Phytologist* **199**: 241–251.

McDonald MC, Renkin M, Spackman M, Orchard B, Croll D, Solomon PS, Milgate A. 2019. Rapid parallel evolution of azole fungicide resistance in Australian populations of the wheat pathogen *Zymoseptoria tritici*. *Applied & Environmental Microbiology* **85**: e01908-18.

Plissonneau C, Blaise F, Ollivier B, Leflon M, Carpezat J, Rouxel T, Balesdent MH. 2017. Unusual evolutionary mechanisms to escape effector-triggered immunity in the fungal phytopathogen *Leptosphaeria maculans*. *Molecular Ecology* **26**: 2183–2198.

Qutob D, Patrick Chapman B, Gijzen M. 2013. Transgenerational gene silencing causes gain of virulence in a plant pathogen. *Nature Communications* **4**: 1349.

Rouxel T, Grandaubert J, Hane JK *et al*. 2011. Effector diversification within compartments of the *Leptosphaeria maculans* genome affected by repeat-induced point mutations. *Nature Communications* **2**: 202.

Rudd JJ, Antoniw J, Marshall R, Motteram J, Fraaije B, Hammond-Kosack K. 2010. Identification and characterisation of *Mycosphaerella graminicola* secreted or surface-associated proteins with variable intragenic coding repeats. *Fungal Genetics & Biology* **47**: 19–32.

Rudd JJ, Kanyuka K, Hassani-Pak K *et al*. 2015. Transcriptome and metabolite profiling of the infection cycle of *Zymoseptoria tritici* on wheat reveals a biphasic interaction with plant immunity involving differential pathogen chromosomal contributions and a variation on the hemibiotrophic lifestyle definition. *Plant Physiology* **167**: 1158–1185.

Saintenac C, Lee WS, Cambon F *et al*. 2018. Wheat receptor-kinase-like protein Stb6 controls gene-for-gene resistance to fungal pathogen *Zymoseptoria tritici*. *Nature Genetics* **50**: 368–374.

Sánchez-Vallet A, Fouché S, Fudal I, Hartmann FE, Soyer JL, Tellier A, Croll D. 2018. The genome biology of effector gene evolution in filamentous plant pathogens. *Annual Review Phytopathology* **56**: 21–40.

Schürch S, Linde CC, Knogge W, Jackson LF, McDonald BA. 2004. Molecular population genetic analysis differentiates two virulence mechanisms of the fungal avirulence gene *NIP1*. *Molecular Plant-Microbe Interactions* **17**: 1114–1125.

Shewry PR. 2009. Concomitant increases of the developing seed phosphoenolpyruvate carboxylase activity and the seed protein content of field-grown wheat with nitrogen supply. *Agricultural Sciences* **60**: 1537–1553.

Stukenbrock EH, Banke S, Javan-Nikkhah M, McDonald BA. 2006. Origin and domestication of the fungal wheat pathogen *Mycosphaerella graminicola* via sympatric speciation. *Molecular Biology & Evolution* **24**: 398–411.

Stukenbrock EH, McDonald BA. 2007. Geographical variation and positive diversifying selection in the host-specific toxin SnToxA. *Molecular Plant Pathology* **8**: 321–332.

Torriani SFF, Melichar JPE, Mills C, Pain N, Sierotzki H, Courbot M. 2015.

Zymoseptoria tritici: a major threat to wheat production, integrated approaches to control. *Fungal Genetics & Biology* **79**: 8–12.

Van Wyk S, Harrison CH, Wingfield BD, De Vos L, Van der Merwe NA, Steenkamp ET. 2019. The RIPper, a web-based tool for genome-wide quantification of Repeat-Induced Point (RIP) mutations. *PeerJ* **7**: e7447.

Van de Wouw AP, Howlett BJ, Idnurm A. 2018. Changes in allele frequencies of avirulence genes in the blackleg fungus, *Leptosphaeria maculans*, over two decades in Australia. *Crop & Pasture Science* **69**: 20-29.

Wang L, Chen H, Li J, Shu H, Zhang X, Wang Y, Tyler BM, Dong S. 2020. Effector gene silencing mediated by histone methylation underpins host adaptation in an oomycete plant pathogen. *Nucleic Acids Research* **48**: 1790-1799

Zhan J, Linde CC, Jürgens T, Merz U, Steinebrunner F, McDonald BA. 2005. Variation for neutral markers is correlated with variation for quantitative traits in the plant pathogenic fungus *Mycosphaerella graminicola*. *Molecular Ecology* **14**: 2683–2693.

Zhang S, Wang L, Wu W, He L, Yang X, Pan Q. 2015. Function and evolution of *Magnaporthe oryzae* avirulence gene *AvrPib* responding to the rice blast resistance gene *Pib*. *Scientific Reports* **5**: 11642.

Zhong Z, Marcel TC, Hartmann FE *et al*. 2017. A small secreted protein in *Zymoseptoria tritici* is responsible for avirulence on wheat cultivars carrying the *Stb6* resistance gene. *New Phytologist* **214**: 619–631.

Chapter 4: Understanding the functions of AvrStb6 and its interaction with Stb6

4.1 Summary

Plant pathogens secrete batteries of proteins known as effectors during infection, which can disguise the presence of the pathogen, suppress host immunity and promote disease. Some of these effectors may be directly or indirectly detected by corresponding resistance proteins in the host plant, which initiate a defence response and pathogen resistance. The fungal pathogen *Zymoseptoria tritici*, the causal agent of Septoria tritici blotch (STB) disease of wheat, secretes the effector AvrStb6 during infection. Some wheat cultivars carry the corresponding disease resistance gene *Stb6*, which recognises AvrStb6 and specifies resistance against *Z. tritici* isolates possessing this effector. The function of AvrStb6 during wheat colonisation, as well as whether the AvrStb6 interacts with Stb6 directly or indirectly is currently unknown. Here, I investigated whether AvrStb6 plays a role in facilitating infection of its host wheat and whether Stb6 recognises AvrStb6 through a direct protein-protein interaction. This study revealed that *AvrStb6* does not induce cell death or other defence responses when transiently expressed in the non-host plant *Nicotiana benthamiana* and I demonstrated that AvrStb6 accumulates in the apoplastic space in this model plant species. Using the yeast two-hybrid (Y2H) screen I identified several wheat proteins potentially interacting with AvrStb6. Further functional analysis of these candidate interactors will help to reveal the cellular processes in wheat targeted by AvrStb6. Although no direct interaction has been observed between AvrStb6 and Stb6 using Y2H and co-immunoprecipitation assays, this is yet to be fully explored as absence of evidence is not evidence of absence. Deciphering the role of *AvrStb6*, a gene retained throughout the global population of *Z. tritici*, may provide new breeding targets for development of enhanced Septoria resistance in future.

4.2 Acknowledgement of Contributions

Kostya Kanyuka (Rothamsted Research) developed the AvrStb6 expression constructs for use in Y2H assays and designed the AvrStb6 Y2H library screen from which the putative wheat protein interactors were identified. Steve Thomas (Rothamsted Research) provided the positive control yeast transformants used in Y2H assays and described previously (Section 2.6.2.). *Agrobacterium tumefaciens* strain CryX was provided by Anatoli Giritch and Yuri Gleba (NOMAD Biosciences GmbH, Halle, Germany). Protein extraction from *Nicotiana benthamiana* was adapted from a protocol shared by Cyril Zipfel (University of Zurich, Switzerland; see Section 2.4.1), who also provided the FLS2:GFP expression vector. Thanks also to Kirstie Halsey, Hannah Walpole, Eudri Venter and Smita Kurup (Rothamsted Research) for help with confocal microscopy and image interpretation, Guillaume Menard (Rothamsted Research) for providing a control construct for expression of mRFP used in the transient expression assays in *N. benthamiana* and Hannah Blyth (Rothamsted Research) for assistance with Y2H assays.

4.3 Introduction

Plants possess a sophisticated array of extracellular sensors to detect the presence of potentially pathogenic microorganisms, responding to their detection with a conserved basal resistance response that prevents infection by non-adapted pathogens. Adapted pathogens overcome basal resistance and successfully colonise host plants by secreting proteins known as effectors during infection. Effectors act to suppress the immune response of the host plant, evade host detection, or to modify host plant metabolism to the advantage of the pathogen. Effectors secreted by pathogens such as the rice blast pathogen *Magnaporthe oryzae* during biotrophic growth can be directly translocated into the host plant cells via a biotrophic interfacial complex (BIC). Recent studies have also identified that some effectors of extracellular pathogens could also be translocated into host plant cells (Jiang *et al*., 2020). Intracellularly targeted effectors employ a plethora of functions to suppress host

immunity (Irieda *et al*., 2019, Han *et al*., 2021) or modify the host cellular processes to their advantage (Wang *et al*., 2016b).

Many effectors of filamentous fungal pathogens are not translocated into host cells, but instead localise to the intercellular space known as the apoplast. Apoplastic effectors adopt numerous virulence functions to facilitate infection (Rocafort *et al*., 2020). For example, effectors may disguise the presence of the pathogen from the host by sequestering PAMPs, which are frequently monitored by host cell-surface immune receptors (CSIRs). One of the better characterised is Ecp6 of the tomato pathogen *Cladosporium fulvum.* It contains three LysM domains through which it binds to chitin oligomers more efficiently than the corresponding plant immune receptor protein CERK1, thus preventing detection of the pathogen by the host early during infection (de Jonge *et al*., 2010, Sanchez-Vallet *et al*., 2013). Other effectors, such as Avr4 and Avr2 of *C. fulvum*, protect the pathogen from host defences and the harsh apoplastic environment. Avr4 protects fungal chitin against hydrolysis by host chitinases, whilst Avr2 physically interacts with and inhibits the antimicrobial activity of tomato Rcr3 protease (Van Esse *et al*., 2008, Van den Burg *et al*., 2006). Many phytopathogens also gain access to host cells by degrading host cell walls with cell wall-degrading enzymes (CWDEs). Both necrotrophs which kill host cells and biotrophs which colonise live host cells secrete diverse batteries of CWDEs, specialised to degrade the different components of the cell wall such as cellulose, pectin and xylan (Kubicek *et al*., 2014). Some necrotrophic pathogens have been shown to exploit the host immune system by secreting necrotrophic effectors, which target/highjack the different immune receptors to induce host cell death and gain access to the nutrients required for the pathogen growth (Section 1.3.6; Friesen *et al*., 2008). Finally, recent studies have identified effectors possessing anti-microbial activity, suggesting an additional category of proteins secreted to clear an ecological niche for the pathogen during infection (Kettles *et al*., 2018, Snelders *et al*., 2018, Snelders *et al*., 2020).

Whilst bioinformatic effector prediction pipelines are increasingly effective at identifying candidate effectors (Kanja and Hammond-Kosack, 2020), the role of the majority of these proteins during infection remains elusive. Fungal effectors

frequently have no identifiable domains and no or low sequence identity with other proteins, although apoplastic effectors are often small (<300 amino acids) and rich in cysteine residues (Sperschneider *et al*., 2018). In addition, the multiplicity of effectors and their propensity for duplication also often results in functional redundancy. This makes effectors difficult subjects to study, as they can rarely be characterised based on protein sequence, and their elimination often has no discernible change on the pathogen phenotype (Kvitko *et al*., 2009, Lawrence *et al*., 2010, Motteram *et al*., 2009). The transient expression of effectors in model plants such as *Nicotiana benthamiana* can provide clues to their function. For example, expression of *Puccinia striiformis* effector *Pst_8713* in *N. benthamiana* suppressed cell death otherwise induced by *Phytophthora infestans* PAMP INF1 (Zhao *et al*., 2018). Virus-mediated overexpression (VOX) may also be used to determine the roles of effector proteins in host plants (Bouton *et al*., 2018). For example, the stem rust effectors AvrSr50 and AvrSr27 were found to be recognised by the intracellular immune receptors Sr50 and Sr27, respectively, using *Barley stripe mosaic virus* (BSMV) as a vector for VOX in wheat (*Triticum aestivum*). BSMV expressing these rust effectors were unable to infect wheat plants carrying the corresponding disease resistance genes, but were virulent on susceptible wheat (Chen *et al*., 2017, Upadhyaya *et al*., 2021).

Many apoplastic effectors have been shown to be involved in gene-for-gene relationships with corresponding host CSIRs (Boutrot and Zipfel, 2017). It has been proposed that the complexing of the fungal Avr2 with the plant Rcr3 in the tomato apoplast is detected by the immune leucine-rich repeat receptor-like protein (LRR-RLP) Cf-2, inducing an immune response (Rooney *et al*., 2005, Van't Klooster *et al*., 2011). The rice LRR receptor-like kinase XA21 specifically detects the *Xanthomonas oryzae* pv. *oryzae* protein RaxX, with a 21-amino acid fragment sufficient to trigger defence responses (Pruitt *et al*., 2015, Thomas *et al*., 2018). The tomato LRR-RLK Cold Shock Protein Receptor (CORE) recognises the csp22 peptide, a fragment of the bacterial cold shock protein, *in vitro* (Wang *et al*., 2016a). Similarly, nlp20, a conserved fragment of necrosis and ethylene-inducing peptide 1-like proteins (NLPs) produced by many pathogens, was shown to be recognised by tomato LRR RLP23 both *in*

vitro and *in planta* (Albert *et al*., 2015). However, in relatively few cases have the direct interactions between effectors and their corresponding CSIRs been observed. The interaction between the CSIR and fungal effector protein most pertinent to this study was documented by Shi *et al*. (2016). They described the direct interaction under yeast two-hybrid conditions between the necrotrophic effector SnTox1 of *P. nodorum* and an extracellular domain fragment of the wheat WAK protein Snn1.

Several effectors of the fungal pathogen *Zymoseptoria tritici* have been previously characterised. Three homologues of the LysM-motif containing group of effectors, similar to Ecp6 of *C. fulvum*, have been identified in *Z. tritici* (Marshall *et al*., 2011, Tian *et al*., 2021). Whilst these effectors were found to show functional redundancy, Mg3LysM was found to have the greatest contribution to *Z. tritici* virulence on wheat, with the other two effectors Mg1LysM and MgxLysM demonstrating smaller effects. Another *Z. tritici* effector, MgNLP, which contains an NPP1 domain conserved among other NLPs, induced cell death when transiently expressed in *N. benthamiana* (Motteram *et al*., 2009) although interestingly not in wheat. An avirulence effector Avr3D1, has been hypothesised to induce a quantitative resistance response in wheat lines carrying the *Stb7* gene (Meile *et al*., 2018). Homologues of Avr3D1 were identified in related species *Z. pseudotritici* and *Z. ardabiliae*, suggesting Avr3D1 originated before speciation. Other *Z. tritici* effectors appear to be translocated into host cells. For example, Zt6 induces cell death when expressed in *N. benthamiana* even when its native signal peptide is removed (Kettles *et al*., 2018). This protein shows structural homology to secreted ribotoxic ribonucleases (RNases) and demonstrates strong anti-microbial activity as well as toxicity to wheat cells. ZtSSP2, expressed early in *Z. tritici* infection, was found to interact with a wheat E3 ubiquitin ligase (Karki *et al*., 2020). It is unknown what role this E3 ubiquitin ligase plays, although its suppression increased wheat susceptibility to STB.

AvrStb6 shares several features with the other known *Z. tritici* avirulence factor *Avr3D1*. Expression of both during *Z. tritici* infection follows a similar profile, increasing throughout the asymptomatic phase and peaking at the switch to necrotrophy (Zhong *et al*., 2017, Meile *et al*., 2018). Despite being located in

genomic regions rich in transposable elements (TEs), which frequently disrupt nearby genes by TE insertion or repeat-induced point mutations (RIPs), both effectors are retained throughout the global population of *Z. tritici*, suggesting important functions in the fungal lifecycle (Section 3.5.1; Meile *et al*., 2018). However, unlike *Avr3D1*, *AvrStb6* appears to have no homologues in related *Zymoseptoria* species. Interestingly, an *avrstb6* knockout mutant of the *Z. tritici* strain IPO323 was shown to be equally virulent on susceptible wheat as the wild type (Kema *et al*., 2018), suggesting functional redundancy, or that this gene is not required for infection of wheat under laboratory conditions. Previous attempts have been made to determine if AvrStb6 interacts with Stb6. Saintenac *et al*. (2018) used a Y2H assay to test for interactions between the effector and the full-length Stb6 protein, its ectodomain and its kinase domain. However, no interaction was observed in any case. The function of AvrStb6 during infection of susceptible wheat, and whether it interacts directly or indirectly with the disease resistance protein Stb6 therefore remain elusive.

In this chapter, I report on studies that aimed to determine the function of the AvrStb6 effector protein in host infection, through bioinformatic analysis, transient expression in *N. benthamiana* and Y2H library screening. Using Y2H library screening, several putative interactors of AvrStb6 in wheat were identified. I also confirmed, using transient expression of an AvrStb6:mRFP fusion construct in *N. benthamiana*, that AvrStb6 localises to the apoplast. The transient expression of AvrStb6 in *N. benthamiana* did not induce host cell death, unlike some of the previously characterised *Z. tritici* effectors. Finally, the interaction between AvrStb6 and Stb6 was tested, both using the Y2H assays and *in planta* using co-immunoprecipitation.

4.4 Methods

4.4.1 Yeast two-hybrid assays

Transformation competent *Saccharomyces cerevisiae* strain MaV203 (hereafter referred to as “yeast”) cells were transformed with bait and prey constructs, as described in Chapter 2 (Section 2.7). Briefly, 50 µl yeast cell aliquots were mixed with 1 µg of each plasmid, incubated for 1 h at 30˚C, spread on complete

supplement agar plates lacking leucine and tryptophan (SC-LT) for transformants selection, and then incubated for 4 days at 30˚C. For testing AvrStb6 dimerisation, successful transformants were restreaked onto SC-Leu-Trp master plates and from these they were restreaked to the test plates. For testing AvrStb6 and Stb6 interactions, transformants were first suspended in sterile saline (0.9% NaCl) and 5 µl aliquots spotted onto a master plate, followed by replica plating the transformants from the master plates to the test plates using velvet (Section 2.7.3). Activation of the reporter genes, *His3* and *LacZ,* evidenced by the yeast growth on media supplemented with 3-aminotriazol (3-AT) and appearance of blue coloration in the yeast patch in the X-gal assay, was used as an indicator of protein-protein interaction (Section 2.7.4).

4.4.2 Bioinformatic analysis of AvrStb6 sequences

The structure and stability of AvrStb6 was assessed using the following online tools. The Protein Homology/analogY Recognition Engine V 2.0 (Phyre 2.0, http://www.sbg.bio.ic.ac.uk/phyre2, Kelley *et al*., 2015) was used to model the predicted 3D structure of proteins, including any ligand binding sites or common motifs, as well as identifying candidate proteins of similar sequence or structure from its protein database. The DiAminoacid Neural Network Application (DiANNA) server (http://clavius.bc.edu/~clotelab/DiANNA/, Ferrè and Clote, 2005) was used to predict the disulphide bonding of proteins. Finally, the UIPred3 tool (short disorder, https://iupred.elte.hu/, Meszaros *et al*., 2018) and the PONDR VL-XT tool (http://www.pondr.com/, Xue *et al*., 2010) were both used to predict a relative disorder of AvrStb6 protein isoforms.

4.4.3 Expression of C-terminal tagged AvrStb6 in *N. benthamiana*

AvrStb6 expression constructs (Figure 4.2a) were generated using the Gateway-compatible pGWB vector series (Nakamura *et al*., 2010). pGWB654 vector provides a C-terminal monomeric red fluorescent protein (mRFP) tag, whilst pGWB605 provides a C-terminal green fluorescent protein (GFP) tag. See Section 5.5.2 for details on Stb6 C-terminal GFP tag constructs, used in co-expression with AvrStb6. These constructs were transformed into *Agrobacterium tumefaciens* (hereafter referred to as Agrobacterium) strains

GV3101 and CryX and agroinfiltration was used to transiently express the proteins in *N. benthamiana* (see Section 2.4). Briefly, transformed Agrobacterium cultures were incubated in growth media overnight, diluted to optical density at 600 nm (OD_{600}) of 0.5 in agroinfiltration buffer and infiltrated into the abaxial side of fully expanded leaves of 4- to 6-week-old *N. benthamiana* plants using a needleless syringe.

Electrolyte leakage testing and trypan blue staining of *N. benthamiana* leaves transiently expressing proteins was carried out as described in Sections 2.4.3 and 2.4.4, respectively.

4.4.4 Confocal microscopy

Confocal microscopy was carried out as described in Section 2.8. All images shown are from leaves harvested at 5 days post infiltration (dpi), with fluorophores expressed within *N. benthamiana* pavement cells excited and fluorescence imaged to determine the localisation of fluorophores. Plasmolysis of leaf cells was performed by imbibing leaf sections in 0.8 M mannitol solution for 30 min at room temperature before imaging.

4.4.5 Protein extraction from *N. benthamiana* leaves and immunoprecipitation

N. benthamiana leaves fully infiltrated with Agrobacterium were harvested at 5 dpi and snap frozen in liquid nitrogen. Protein extraction from leaves was carried out as described in Section 2.5.1. See Section 2.5.2 for detailed GFP-trap immunoprecipitation (IP) protocol. Briefly, 200 µl protein extract was mixed with 25 µl pre-washed GFP-trap beads and incubated end-over-end at 4˚C for 4 h. Beads were washed by centrifugation and resuspension of pellet in wash buffer, prior to release of the proteins into 2X SDS loading buffer by incubation at 70˚C for 10 min.

4.4.6 SDS-PAGE and western blotting

See Sections 2.4.3 and 2.4.4 for detailed SDS-PAGE and western blotting protocols, respectively. SDS-PAGE of 25 µl protein extract (approx. 40 µg protein) or IP fraction was carried out using 8% acrylamide gels, run at 80 V. Western blotting transfer was carried out onto PVDF membranes, using a Bio-

Rad Mini Trans-Blot Cell system, at 100 V for 40 min. Membranes were blocked using 5% milk in TRIS-buffered saline (TBS) containing 0.1% Tween 20, at room temperature for 1 h. Co-immunoprecipitation studies (Co-IP) were carried out using anti-GFP and anti-RFP antibodies. For probing with anti-GFP primary antibody, the membrane was incubated in a 1:1000 antibody dilution in 1X TBS-Tween buffer supplemented with 5% bovine serum albumin (BSA). For anti-RFP probing, a 1:1000 antibody dilution in 1X TBS-Tween buffer supplemented with 5% milk was used. For probing with either primary antibody, membranes were incubated at 4˚C overnight. Secondary antibody probing was carried out using a 1:10,000 antibody dilution in 1X TBS-Tween buffer plus 5% milk, for 1 h at room temperature. Following incubation with ECL reagent (GE healthcare), membranes were imaged using an Odyssey imager (Li-Cor).

4.5 Results

4.5.1 AvrStb6 does not form dimers under yeast two-hybrid assay conditions

A preliminary study in which the AvrStb6 protein was expressed in the fungus *Pichia pastoris* suggested that the effector protein may form dimers (Bayon C & Kanyuka K, *personal comm.*). Dimerisation has been observed previously for some pathogen effectors and was suggested to be functionally important (Gurlebeck *et al*., 2005). We hypothesised that dimerisation may also be important to the functioning of AvrStb6 *in planta*. A Y2H assay was therefore carried out to determine whether AvrStb6 can interact with itself. Bait and prey constructs containing the avirulence allele of *AvrStb6* (encoding isoform I01) and the virulence allele (encoding isoform I44) were transformed into the yeast strain MaV203. AvrStb6 interaction was tested by assessing the activation of both the *HIS3* and *LacZ* reporter genes. Very little growth of test transformants expressing AvrStb6 bait and prey pairs was observed on media lacking histidine and no blue colouration was observed following X-gal assay, whilst the expected results for both positive and negative controls were observed (Figure S4.1). This suggests that no dimerization occurs for either tested isoform of AvrStb6, at least under Y2H assay conditions.

4.5.2 Diverse plant proteins identified as candidate AvrStb6 interactors

To identify a potential *in planta* function for AvrStb6, a Y2H library screen (see Section 2.7.3.1) was carried out previously by Kostya Kanyuka, with AvrStb6 I01 used as the bait. This screen yielded twelve His^+ colonies which grew on selection media lacking histidine. I first tested the sensitivity of these His^+ colonies to increasing concentrations of 3-AT (25, 50, 75, and 100 mM), and in parallel assessed *LacZ* reporter gene activation using the X-gal assay. Three out of twelve tested colonies demonstrated no or very limited growth in the presence of 25 mM 3-AT and remained white in the X-gal assay, and thus were not investigated further. The remaining nine His^+ colonies were able to grow in the presence of at least 25 mM of 3-AT and turned blue in one replication of the X-gal assay but not in the other, indicating a weak interaction. Prey vector inserts from these colonies were amplified by colony PCR and Sanger sequenced to identify the nature of different candidate interactors. Whilst all insert sequences were in frame with the GAL4 activation domain, five of the sequences were predicted to encode long poly-cysteine tracks and were therefore considered to be false positive interactors. Analysis of the remaining four sequences through BLAST against the Ensembl Plants database for wheat (https://plants.ensembl.org/Triticum_aestivum/Info/Index) revealed that two corresponded to the gene TraesCS1D02G404800 predicted to encode a monothiol glutaredoxin-S9-like protein (Table S4.1). The glutaredoxin-like/thioredoxin-like superfamily (GRX/TRX) proteins are known to play a role in defence against oxidative stress. Another putative interactor corresponded to the gene TraesCS2B02G233300 predicted to encode a chloroplast-localised PtrToxA-binding protein 1 (ToxABP; also known as Thf1, Thylakoid formation 1; and as Psb29, Photosystem b protein 29) which is hypothesised to be involved in the biosynthesis of photosystem II (PSII) complexes in the thylakoid membrane. Interestingly, ToxABP has also been shown to interact with PtrToxA necrotrophic effector of *Pyrenophora tritici-repentis* (Manning *et al*., 2007). The third candidate interactor corresponded to the gene TraesCS5A02G524800, predicted to encode another chloroplast-localised protein, dihydrodipicolinate reductase, which likely functions in biogenesis or stabilisation of the chloroplast NAD(P)H dehydrogenase complex involved in electron transfer between PSII

and photosystem I (PSI). Similar BLAST searches utilising the *Z. tritici* Ensembl database (https://fungi.ensembl.org/Zymoseptoria_tritici/Info/Index) yielded no high confidence hits.

As ToxABP was an intriguing putative interactor of AvrStb6, the Y2H assay was repeated utilising AvrStb6 isoforms I01 and I02 along with the ToxABP fragment identified from the library screen, to confirm this interaction. The test yeast transformants grew on selection media lacking histidine and supplemented with 3-AT up to a concentration of 50 mM (Figure S4.2) - a growth phenotype similar to that of the positive control ARR1. However, the parallel X-gal assay identified no blue colouration of these test transformants, whilst both positive and negative controls performed as expected. Whilst this contradicts the previous results, the good growth on media lacking histidine even in the absence of blue coloration in the X-gal assays does still support a putative weak interaction between ToxABP and AvrStb6.

4.5.3 Structure modelling analysis reveals high predicted 3D structure diversity amongst AvrStb6 isoforms and no conserved protein folds

Further dissection of the putative role of AvrStb6 was carried out through modelling of the effector protein 3D structure. Three AvrStb6 isoforms were selected for analysis using Phyre 2.0 (http://www.sbg.bio.ic.ac.uk/phyre2, Kelley *et al*., 2015), which uses advanced computational remote homology detection methods to predict 3D protein models. The two control AvrStb6 isoforms, I01 and I44, which are avirulent and virulent on *Stb6* wheat, respectively (Section 3.5.1) and the isoform I02 that is most prevalent in modern *Z. tritici* populations (Section 3.5.2), were selected for this analysis. The Phyre 2.0 analysis results for these three mature AvrStb6 isoforms (lacking the signal peptide) were compared, with a focus on structural homology or shared alignment with other known proteins/protein domains. However, this analysis revealed that the predicted 3D structure for each of the three AvrStb6 isoform varied considerably (Figure S4.3), whilst very few high confidence alignments with other known proteins were identified (Table S4.2). The most frequent were with the zinc finger transcriptional domains, hydrolase enzymes and toxins, although in all cases both the confidence and alignment length (ID) were low.

A further analysis of the AvrStb6 protein isoforms was carried out using the DiANNA 1.1 artificial neural network and web server (http://clavius.bc.edu/~clotelab/DiANNA/, Ferrè and Clote, 2005), which allows prediction of cysteine residues within a protein sequence likely to form a disulphide bond, based on the predicted secondary structure of the protein and the cysteine oxidation state. It was anticipated that this analysis would identify some conservation in the disulphide connectivity amongst the AvrStb6 isoforms. However, as for the Phyre 2.0 analysis, very few disulphide bridges were consistently predicted for all investigated AvrStb6 isoforms (Table S4.3). This analysis, therefore, also contributed little to our understanding of the AvrStb6 effector structure and function.

Protein disorder has previously been shown to play a role in the ability of effectors to be translocated into host cells, evade plant host resistance proteins and function to facilitate infection (Yang *et al*., 2020, Marin *et al*., 2013). The mature versions of all AvrStb6 isoforms previously assessed for their pathogenicity (Section 3.5.1) were analysed for their intrinsic disorder using the UIPred3 tool (https://iupred.elte.hu/, Meszaros *et al*., 2018) and the PONDR VL-XT tool (http://www.pondr.com/, Xue *et al*., 2010). This analysis showed that all isoforms of AvrStb6 possess higher levels of disorder at the N-terminus of the amino acid sequence (UIPred3 and PONDR) and at the C-terminus (PONDR only, Figure S4.4). However, compared to the effector Avr2 of the oomycete pathogen *Phytophthora infestans*, previously shown to have high levels of intrinsic disorder (Yang *et al*., 2020), all AvrStb6 isoforms showed consistently low levels of disorder. This suggests that AvrStb6 virulence/avirulence phenotype is not driven by increased intrinsic disorder in virulence isoforms, as has been suggested for Avr2 of *P. infestans* (Yang *et al*., 2020).

4.5.4 No direct AvrStb6-Stb6 interaction observed using the yeast two-hybrid assay

The avirulent isoforms of AvrStb6 are hypothesised to interact either directly or indirectly with the WAK protein Stb6, to initiate a resistance response. Although a previous study utilising a Y2H assay found no direct interaction between

AvrStb6 and the full-length Stb6 ectodomain (Saintenac *et al*., 2018), another study that employed a similar approach reported an interaction between the *Parastagonospora nodorum* effector SnTox1 and a specific region of the ectodomain of the corresponding wheat WAK protein Snn1. Specifically, interaction was observed between SnTox1 and a region in Snn1 located between the GUB_WAK_bind and the EGF-like domains, characterised by the absence of any known protein domains or motifs (Shi *et al*., 2016). It was therefore hypothesised that a region of the Stb6 ectodomain outside of the known domains may be involved in binding AvrStb6, with this region being potentially buried and inaccessible to this interaction due to the 3D fold of the full-length ectodomain in the yeast nucleus (the cellular compartment where interaction between tested proteins takes place under the Y2H assay conditions). Y2H assays were therefore performed to test the above hypothesis.

Four fragments of the Stb6 ectodomain of different lengths, located between the GUB_WAK_bind domain and the transmembrane helix, were tested for interaction with the avirulent (I01) and the virulent (I02) isoforms of AvrStb6 (Figure 4.1a). However, no interaction was observed between AvrStb6 and any of the Stb6 fragments tested, as no growth of yeasts containing both Stb6 bait and AvrStb6 prey constructs was observed on the selective media lacking histidine. Similarly, these yeast double transformants developed no blue colouration in an X-gal assay (Figure 4.1). All positive and negative control colonies performed as expected. These results suggest that no direct interaction occurs between AvrStb6 and these regions of the Stb6 ectodomain, under yeast nucleus conditions.

4.5.5 Transient expression of *AvrStb6* in *N. benthamiana* induces no visible cell death

To further assess the role of AvrStb6 during wheat colonisation, and to investigate its potential interaction with Stb6 *in planta*, a series of AvrStb6 expression constructs were created using the pGWB vector series (Nakamura *et al*., 2010). These constructs allow for the expression of the AvrStb6 effector, with or without a C-terminal mRFP or GFP fluorophore tag (Figure 4.2a).

Following their generation, these constructs were expressed in the tobacco plant *N. benthamiana* using agroinfiltration.

Expression of *AvrStb6* in *N. benthamiana* resulted in no visible phenotype, with no cell death-like symptoms such as the accumulation of phenolic compounds, visible under UV light or following trypan blue staining, or electrolyte leakage, a hallmark of stress response in plant cells (Demidchik *et al*., 2014; Figure 4.2b, c). This contrasts with the phenotype induced by the positive controls, such as the necrosis-inducing *Z. tritici* effector MgNLP. Therefore, neither of the AvrStb6 isoforms, I01 or I02, appear to play a role in inducing cell death in plants, or at least in this model plant species (Figure S4.5a). Furthermore, co-expression of *AvrStb6* with the *Stb6* resistance haplotype 1 (such as that found in wheat cultivar Cadenza) in *N. benthamiana* leaves did not appear to either reduce or accelerate the *Stb6*-induced cell death phenotype (Section 5.5.2; Figure S4.5b).

4.5.6 AvrStb6 localises to the apoplast in *N. benthamiana*

Fluorophore tagging was used to identify the subcellular localisation of AvrStb6 *in planta*. AvrStb6 I01 and I02 C-terminally tagged with mRFP (AvrStb6:mRFP) were co-expressed in *N. benthamiana* along with a C-terminal GFP-tagged kinase-dead version of Stb6 (Stb6:GFP, see Section 5.5.3). Confocal microscopy revealed that the AvrStb6:mRFP and Stb6:GFP fusion proteins both localised to the cell periphery. By contrast, free mRFP expressed in *N. benthamiana* was found to accumulate in the cytoplasm and cell nucleus (Figure 4.3a). Following plasmolysis of *N. benthamiana* cells by immersion of leaf sections in 0.8M mannitol, the differences in localisation between free mRFP and AvrStb6:mRFP were even more marked. Whilst the free mRFP protein clearly accumulated within the cells, being present in both the nucleus and the cytoplasm, the AvrStb6:mRFP accumulated specifically in the apoplastic space between plasmolysed cells (Figure 4.3b). A similar result was also observed for AvrStb6 I02:mRFP (Figure S4.6). This demonstrates that the AvrStb6 effector is a secreted protein that accumulates outside of host cells, when expressed in *N. benthamiana*.

4.5.7 Co-Immunoprecipitation (Co-IP) analysis to study protein-protein interactions between AvrStb6 and Stb6

As previously (Section 4.5.6), AvrStb6:mRFP isoforms I01 and I02 were co-expressed with the kinase-dead version of Stb6:GFP in *N. benthamiana* leaves using agroinfiltration. At 5 dpi, the total leaf proteins were extracted and then subjected to immunoprecipitation (IP) using GFP-trap beads (Chromotek). Proteins eluted from the beads were analysed using western blotting with anti-GFP or anti-RFP antibodies. In preliminary western blotting experiments, bands corresponding to Stb6:GFP were observed following IP of protein extracts, although free GFP was also observed in these extracts (Figure S4.7). In initial Co-IP experiments, in which Stb6:GFP and AvrStb6:mRFP were co-expressed, no bands corresponding to Stb6:GFP were observed either before or after IP (Figure S4.8). However, anti-RFP blotting revealed a band in the IP fraction of AvrStb6 I01:mRFP and Stb6:GFP co-expression extract. Although the predicted size of this protein band is somewhat smaller than would be expected for AvrStb6:mRFP, it is observed only following co-expression of AvrStb6 I01:mRFP and Stb6:GFP, and not in control lanes or following co-expression of Stb6 with the virulence AvrStb6 isoform. However, repeated Co-IP experiments could not recreate this initial finding (Figure 4.4), suggesting that it may have been a false positive. These blots also reveal extensive cleavage of Stb6 and AvrStb6 from their fluorophore tags, potentially reducing the sensitivity of the Co-IP experiments.

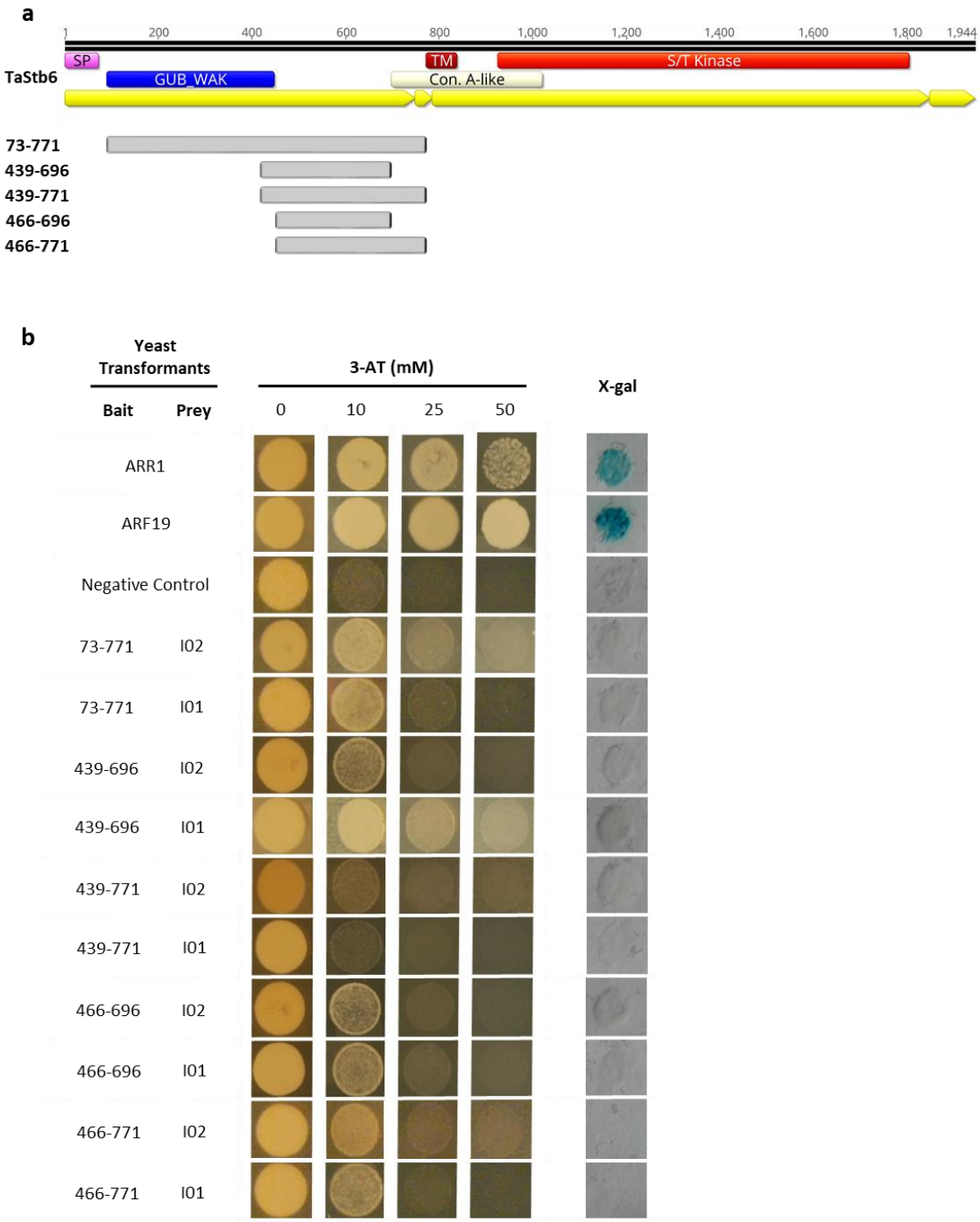

Figure 4.1: AvrStb6 does not interact with Stb6 ectodomain under yeast two-hybrid assay conditions. **a)** Schematic illustration of the Stb6 fragments generated and utilised for testing interaction with AvrStb6. Identified domains are signal peptide (SP), galacturonan-binding (GUB_WAK), concanavalin A-like lectin/glucanase (Con. A-like), transmembrane helix (TM) and serine/threonine kinase (S/T Kinase). *Stb6* gene exons are represented by yellow bars. Gray bars indicate the extent of each fragment construct. *Stb6* fragment names indicate the starting and end base pair of the fragment. **b)** Yeast two-hybrid interaction results. "ARR1" and "ARF19" are positive interaction controls. Negative control transformant contains empty bait and prey vectors. Stb6 fragments were used as baits against prey containing AvrStb6 isoforms I01 (IPO323, avirulent) and I02 (virulent). Images on the left illustrate yeast growth on complete supplement media lacking leucine, histidine and tryptophan and supplemented with a range of 3-aminotriazole (3-AT) concentrations. Images on the right illustrate results from X-gal assay.

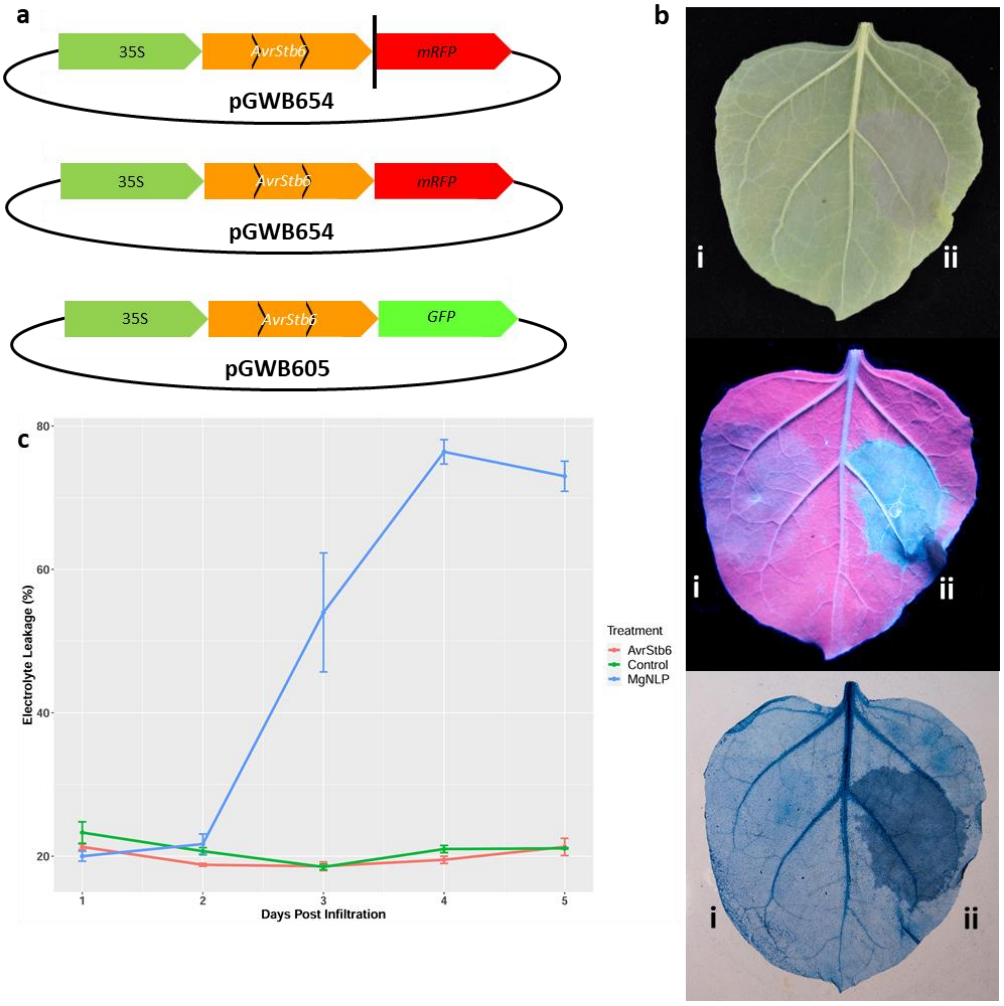

Figure 4.2: *AvrStb6* does not induce cell death when expressed in *N. benthamiana*. a) Schematic illustration of the *AvrStb6* constructs generated and utilised for expression in *N. benthamiana*. The *AvrStb6* gene was under control of a 35S promoter (from Cauliflower Mosaic Virus, CaMV). Black bar represents a stop codon (TGA) introduced between the *AvrStb6* gene and the fluorescent tag. pGWB654 (mRFP, C-terminal tag) and pGWB605 (GFP, C-terminal tag) were used from the construct series developed by Nakamura et al. (2010). *AvrStb6* cDNA sequence was used within each construct. Two AvrStb6 isoforms, I01 and I02, were expressed from the constructs generated. **b)** Images of *N. benthamiana* leaf transiently expressing AvrStb6 I01 (i) or MgNLP (ii), under normal light (top), UV light (centre) or following trypan blue staining (bottom). Images taken at 5 dpi. **c)** Electrolyte leakage of leaves during transient expression of AvrStb6 I01, MgNLP or following infiltration with untransformed *Agrobacterium* (control).

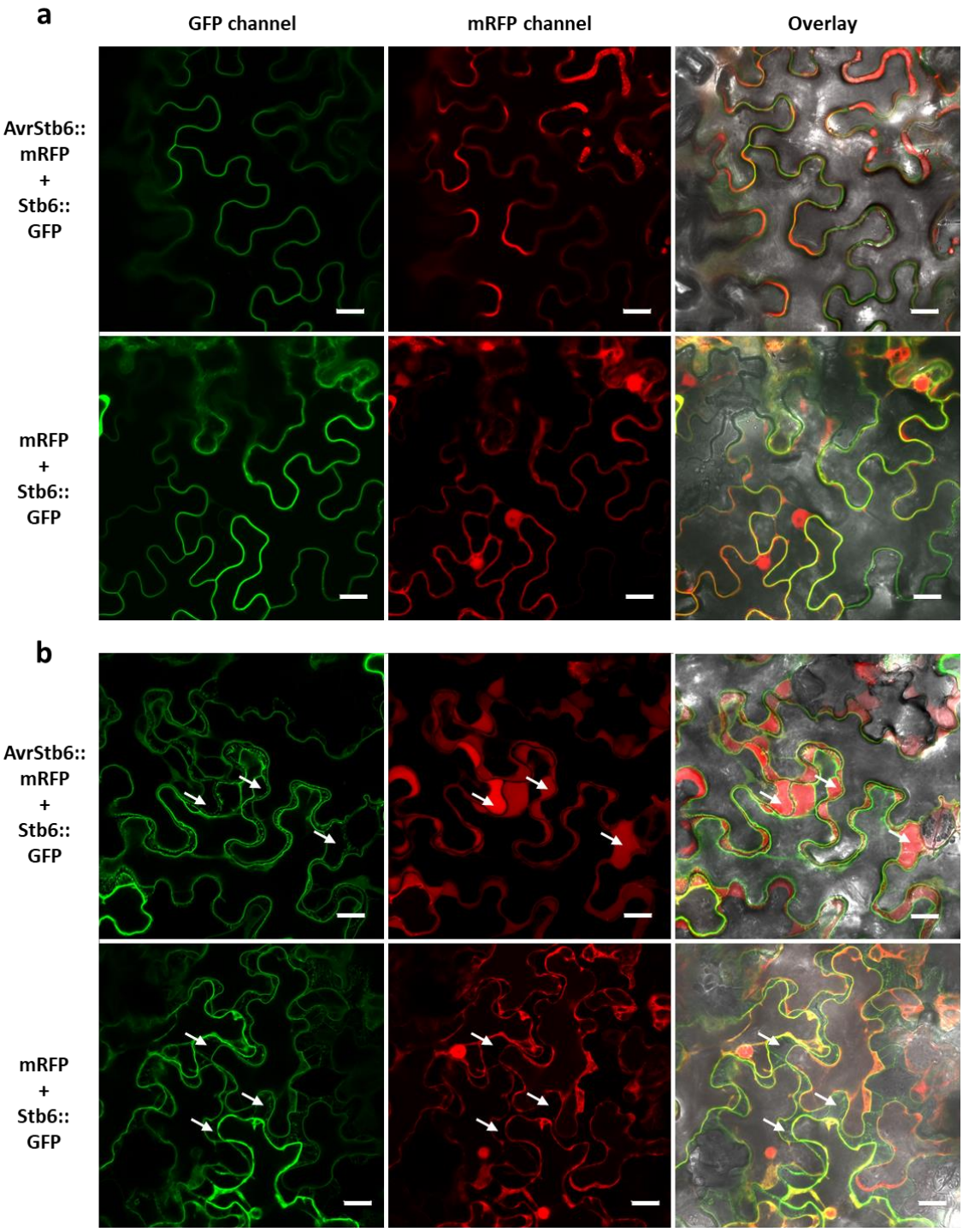

Figure 4.3: AvrStb6 localises to the apoplast when expressed in *N. benthamiana*. Confocal microscope images were taken of *N. benthamiana* cells transiently co-expressing AvrStb6 I01 with a C-terminal mRFP tag and Stb6 from cultivar Courtot with a C-terminal GFP tag (AvrStb6:mRFP + Stb6:GFP), or free mRFP and *Stb6* from cultivar Courtot with a C-terminal GFP tag (mRFP + Stb6:GFP). Leaves were harvested at 5 days post infiltration (dpi). **a)** Leaf cells prior to plasmolysis using 0.8 M mannitol solution **b)** Leaf cells after 30 minutes incubation with mannitol solution. White arrows indicate example locations of the apoplastic space, following plasmolysis. White bars represent 20µm.

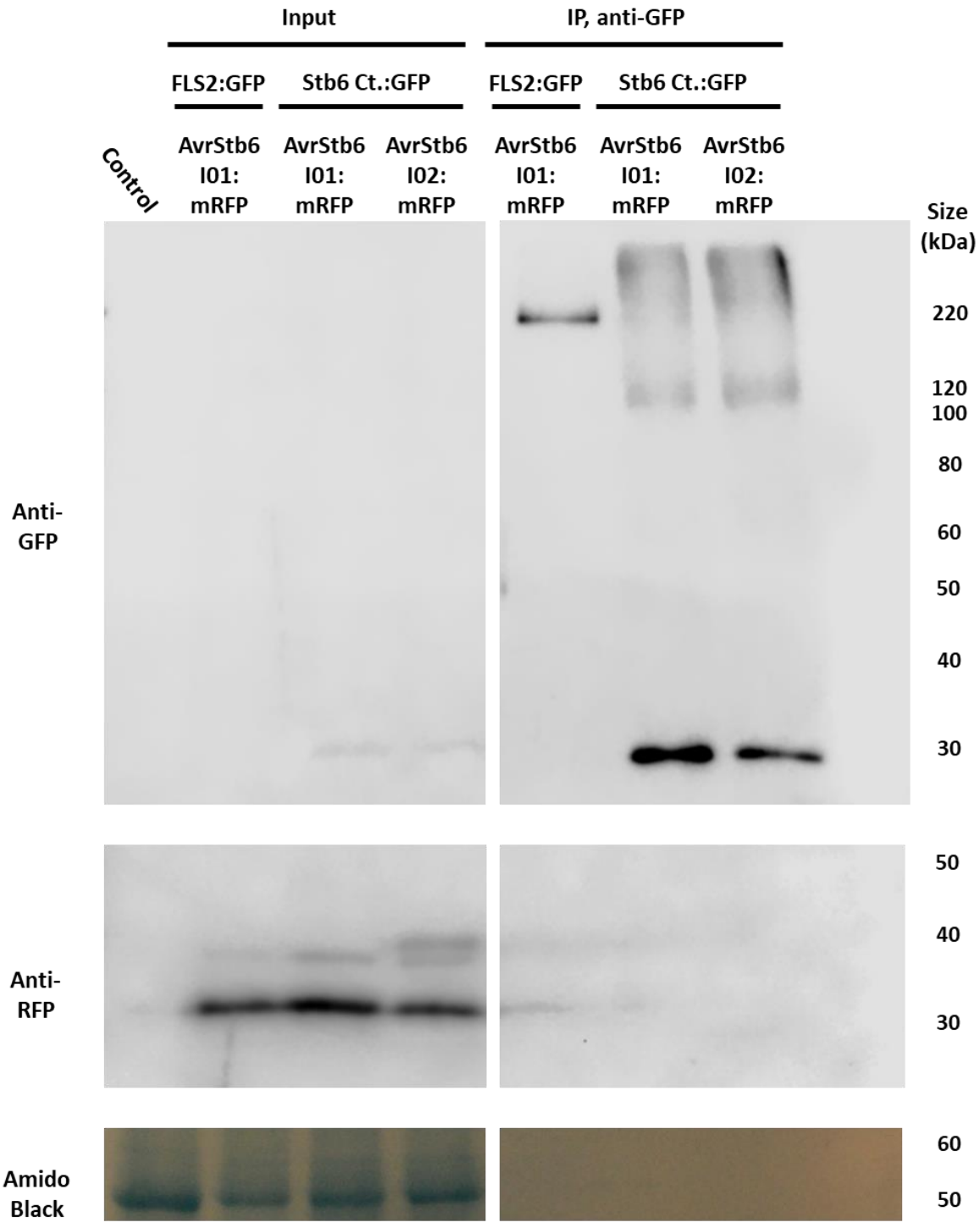

Figure 4.4: No interaction between Stb6 and AvrStb6 observed *in planta*. Co-IP experiment using protein extracts from *N. benthamiana* transiently expressing Stb6 cv. Courtot:GFP as bait and AvrStb6 (I01 or I02):mRFP as prey. FLS2:GFP co-expressed with AvrStb6 I01:mRFP was used as a negative control. Top panel: western blotting with anti-GFP antibodies, to identify GFP constructs in input protein and IP fractions. Middle panels: western blotting with anti-RFP antibodies, to identify RFP constructs in input protein and any mRFP constructs pulled down following anti-GFP IP. Bottom panel: amido black staining of exemplary membrane (anti-GFP).

4.6 Discussion

Yeast two-hybrid analysis indicates that AvrStb6 isoforms I01 and I44 do not form dimers under yeast nucleus conditions (Figure S4.1). Effector dimerisation has been observed previously, for example the *Xanthomonas campestris* effector AvrBs3 was shown to self-interact both in a Y2H assay as well as *in planta* (Gurlebeck *et al*., 2005). Dimerisation has also been shown to play a role in effector action: the *Z. tritici* chitin-sequestering effector Mg1LysM forms both chitin-dependent and independent dimers, which contribute to the binding of chitin by the effector pair (Sanchez-Vallet *et al*., 2020). Effectors of oomycetes such as PsCRN63 of *Phytophthora sojae* and CRN8 of *P. infestans* are also shown to form dimers, with dimerisation of PsCRN63 found to be crucial to its virulence function (Van Damme *et al*., 2012, Li *et al*., 2016). Li *et al*. (2016) identified that PsCRN63 dimerisation was dependent on N- and C-terminal motifs conserved across many CRN (CRinkling and Necrosis) effectors, suggesting that dimerisation of CRNs may be common.

The Y2H library screen using AvrStb6 as a bait identified three putative interactors, all of which were found to be host plant proteins (Table S4.1). These putative interactors are yet to be followed up to verify their interaction with AvrStb6 *in planta*. Interestingly, two of the identified interactors, ToxABP/Thf1/Psb29 and a dihydrodipicolinate reductase, were characterised as chloroplastic proteins. A dihydrodipicolinate reductase homologue, CRR1, of Arabidopsis has been found to be coregulated with photosynthetic genes (Avin-Wittenberg *et al*., 2012) and is required for biogenesis or stabilisation of NAD(P)H dehydrogenase. The Arabidopsis *crr1* mutants showed a lack of NAD(P)H dehydrogenase activity (Shimizu and Shikanai, 2007) which is known to be required for photosystem activity, transferring electrons between photosystems I and II. Similarly, ToxABP is thought to be required for photosystem functions, being implicated in PSII complex biogenesis (Keren *et al*., 2005) and Δ*toxabp* mutants of the photosynthetic bacterium *Synechococcus* sp. PCC7942 showed reduced PSI activity and stability (Zhan *et al*., 2016). The third putative interactor is predicted to encode a glutaredoxin-S9-like protein, part of a larger superfamily of GRX/TRX redox proteins. This superfamily is implicated in a wide array of functions, including resistance to

oxidative stress (Vieira Dos Santos and Rey, 2006). These putative interactions suggest a role for AvrStb6 in interfering with normal host photosynthetic functions. Indeed, previous experiments in which AvrStb6 has been overexpressed in wheat using the plant virus-mediated overexpression (VOX) system, wheat leaves were shown to develop severe chlorosis/photobleaching-like symptoms (Figure S4.9; Bouton C & Kanyuka K, *unpublished*). It is possible, given this phenotype, that AvrStb6 is interfering with chloroplastic activity or resistance to oxidative stress, by interacting with one or more of these proteins.

The observation that AvrStb6 localises to the apoplast, when expressed in *N. benthamiana* (Figure 4.3), would appear to contradict the above hypothesis. However, it seems possible that AvrStb6 may be translocated into cells using a wheat-specific mechanism, or that the fused fluorophore tag, which is relatively large, impeded intracellular translocation in our studies. Further experiments to determine AvrStb6 interactions *in planta*, such as bimolecular fluorescence (BiFC) or Co-IP of AvrStb6 with ToxABP/Thf1/Psb29, the GRX/TRX homologue and the dihydrodipicolinate reductase homologue, could strengthen the hypothesis of AvrStb6 accumulation and action within the chloroplast. The ToxABP-AvrStb6 interaction may also occur in the cytoplasm: a study investigating the *in planta* interaction between the tomato resistance protein N' and ToxABP found this interaction to occur in the cytosol (Hamel *et al.*, 2016). Although no other pathogen effectors have yet been shown to possess dual roles in the apoplast and the host cell, effectors with such properties are anticipated (Rocafort *et al*., 2020). Further studies are required to verify AvrStb6 interactions with one or more of these chloroplastic wheat proteins.

Potential functions for some pathogen effectors have previously been inferred based on their homology to known protein 3D structures. For example, analysis of *Colletotrichum graminicola* effector Cgfl using the Phyre 2.0 protein fold recognition tool identified that 95% residues of this effector could be modelled with high degree of confidence using the 3D structure of *Aspergillus fumigatus* fungalysin protein known to degrade host chitinases. Cgfl was also predicted to have structural similarities with chitinase-degrading proteases from other fungI such as *Fusarium verticillioides* (Sanz-Martin *et al*., 2016). However, in the

case of AvrStb6 isoforms, no consistent structural motifs or homology with other known proteins was predicted. Indeed, the three AvrStb6 isoforms analysed using Phyre 2.0 appeared to form radically different structures (Figure S4.2), and very few disulphide bridges were consistently predicted between isoforms (Table S4.3). Effectors frequently have no characterised protein domains, and AvrStb6 is no exception. It is therefore not possible to predict AvrStb6 function, based on bioinformatic analyses.

A previous study of effector protein disorder observed a positive correlation between the virulence of the *Phytophthora infestans* effector AVR2 and its predicted intrinsic disorder (Yang *et al*., 2020). This study suggests that increased protein disorder may contribute to the ability of effectors to evade detection by host disease resistance proteins. In our analysis, all tested AvrStb6 isoforms showed increased levels of disorder at the N- and C-termini, but no notable differences between those capable of evading Stb6 detection and those conferring avirulence on *Stb6* wheat (Figure S4.3). In addition, all isoforms showed low levels of disorder compared to *P. infestans* Avr2. It is therefore unlikely that differences in protein disorder contribute to the ability of some AvrStb6 isoforms to evade Stb6-mediated detection.

No interaction was observed between either avirulence or virulence AvrStb6 isoforms and the ectodomain fragments of Stb6 in a Y2H interaction assay (Figure 4.2). However, it has been observed previously that many membrane-bound plant proteins, including other CSIRs, undergo post-translational modifications such as glycosylation during the export pathway (Haweker *et al*., 2010, Liebrand *et al*., 2012). An analysis of putative glycosylation sites in the ectodomain of Stb6 revealed six high probability sites, suggesting considerable potential posttranslational modification of the protein during secretion (Figure S4.10). Similarly, AvrStb6 may undergo specific folding upon secretion from *Z. tritici*. Moreover, the low pH conditions of the apoplast may also influence the conformation of Stb6 and AvrStb6, thus impacting any potential protein-protein interactions. If posttranslational modification or secretion-specific folding is required for the interaction between Stb6 and AvrStb6, then the Y2H assays may not be appropriate for identifying such interactions, as the lack of such modifications within the yeast nucleus may prevent correct protein folding and

thus also the interactions between these proteins. *In planta* protein-protein interaction assays, such as Co-IP, may therefore be more suitable.

AvrStb6 expression in *N. benthamiana* was found to induce no cell death in this plant species, which a non-host for *Z. tritici*. This is in contrast to the twelve other characterised *Z. tritici* apoplastic effectors (Kettles *et al*., 2017), which all induced a BAK1-dependent cell death indicative of these effectors being detected by *N. benthamiana* CSIRs. Interestingly, no chlorosis occurred in *N. benthamiana* leaves overexpressing *AvrStb6*, as was previously reported when this effector was overexpressed in wheat leaves using VOX (Figure S4.9; Bouton C & Kanyuka K, *unpublished*). This could imply that AvrStb6 targets a wheat-specific protein, such as one or more of those chloroplastic putative interactors identified in the Y2H library screen, thus inducing the chlorotic phenotype observed following expression in wheat.

A possible interaction between Stb6 and AvrStb6 is yet to be confirmed using Co-IP (Figure 4.4), despite earlier results suggesting that this may be the case (Figure S4.8). It is notable that extensive cleavage of the fluorophore tags was observed for both the Stb6 and AvrStb6 constructs (Figure S4.7) and this would certainly reduce the sensitivity of the assay to detect any interaction. Other CSIR-ligand interactions have been identified using Co-IP in previous published studies, supporting the use of this method in detecting the AvrStb6-Stb6 interaction. For example, the interaction between the LRR-RLK CORE (cold shock protein receptor) of tomato and a peptide fragment of cold shock protein csp22 was identified using Co-IP. CORE:GFP fusion proteins were immunoprecipitated with anti-GFP beads and incubated with csp22 tagged with a chemiluminescent acridinium ester label, with the observed chemiluminescence from the acridinium ester label suggesting protein-ligand interaction (Wang *et al*., 2016a). An interaction between RLP23 of *Arabidopsis thaliana* and a fragment of the necrosis-inducing protein NLP has also been demonstrated using a similar approach (Albert *et al*., 2015). A biotinylated fragment of NLP, nlp24, was infiltrated into *N. benthamiana* transiently expressing RLP23:GFP fusion or into stably transformed *A. thaliana* expressing the same fusion protein. In that study, this was followed by the infiltration of ethylene glycol bis(succinimidyl succinate), which allowed crosslinking the

nlp24 epitope with RLP23. The Stb6-AvrStb6 interaction may also occur only transiently, as has been shown for many important receptor-ligand interactions, so the use of techniques such as crosslinking in combination with Co-IP may aid in the observation of a direct interaction. Alternatively, proximity labelling systems such as the biotin ligase TurboID system (Branon *et al*., 2018) could be used to detect transient interactions between the two proteins.

In this chapter, I have reported on the putative characterisation of the function of AvrStb6. The obtained data suggest that AvrStb6 may be engaged in interactions with one or more proteins involved in oxidative stress or in the function and maintenance of host plant photosystems. This fits well with previous data suggesting that overexpression of AvrStb6 in wheat induces strong chlorosis. I therefore hypothesise that AvrStb6 interferes with the host photosynthetic machinery to facilitate *Z. tritici* infection. Interestingly, no chlorosis is observed following AvrStb6 transient expression in *N. benthamiana.* The possibility of a direct interaction between AvrStb6 and the disease resistance protein Stb6 was also assessed both *in vitro* and *in planta*. Although no direct interaction has so far been observed between these two proteins, it would be worth investigating this further using alternative approaches, such as those that allow detection of transient protein-protein interactions.

4.7 References

Albert I, Böhm H, Albert M, Feiler CE, Imkampe J, Wallmeroth N, Brancato C, Raaymakers TM, Oome S, Zhang H. 2015. An RLP23–SOBIR1–BAK1 complex mediates NLP-triggered immunity. *Nature Plants* **1**: 15140.

Avin-Wittenberg T, Tzin V, Angelovici R, Less H, Galili G 2012. Deciphering energy-associated gene networks operating in the response of Arabidopsis plants to stress and nutritional cues. *Plant Journal* **70**: 954-966.

Bouton C, King RC, Chen H, Azhakanandam K, Bieri S, Hammond-Kosack KE, Kanyuka K. 2018. Foxtail mosaic virus: A viral vector for protein expression in cereals. *Plant Physiology* **177**: 1352-1367.

Boutrot F, Zipfel C. 2017. Function, discovery, and exploitation of plant pattern recognition receptors for broad-spectrum disease resistance. *Annual Review Phytopathology* **55**: 257-286.

Branon TC, Bosch JA, Sanchez AD, Udeshi ND, Svinkina T, Carr SA, Feldman JL, Perrimon N, Ting AY. 2018. Efficient proximity labeling in living cells and organisms with TurboID. *Nature Biotechnology* **36**: 880-887.

Chen JP, Upadhyaya NM, Ortiz *et al.* 2017. Loss of *AvrSr50* by somatic exchange in stem rust leads to virulence for *Sr50* resistance in wheat. *Science* **358**: 1607-1610.

De Jonge R, Van Esse HP, Kombrink A, Shinya T, Desaki Y, Bours R, Van der Krol S, Shibuya N, Joosten MHAJ, Thomma BPHJ. 2010. Conserved fungal LysM effector Ecp6 prevents chitin-triggered immunity in plants. *Science* **329**: 953-955.

Demidchik V, Straltsova D, Medvedev SS, Pozhvanov GA, Sokolik A, Yurin V. 2014. Stress-induced electrolyte leakage: the role of K-permeable channels and involvement in programmed cell death and metabolic adjustment. *Journal of Experimental Botany* **65**: 1259-1270.

Ferrè F, Clote P. 2005. DiANNA: a web server for disulfide connectivity prediction. *Nucleic Acids Research* **33**: W230-232.

Friesen TL, Stukenbrock EH, Liu ZH, Meinhardt S, Ling H, Faris JD, Rasmussen JB, Solomon PS, McDonald BA, Oliver RP. 2006. Emergence of a new disease as a result of interspecific virulence gene transfer. *Nature Genetics* **38**: 953-956.

Friesen TL, Zhang Z, Solomon PS, Oliver RP, Faris JD. 2008. Characterization of the interaction of a novel *Stagonospora nodorum* host-selective toxin with a wheat susceptibility gene. *Plant Physiology* **146**: 682-693.

Gurlebeck D, Szurek B, Bonas U. 2005. Dimerization of the bacterial effector protein AvrBs3 in the plant cell cytoplasm prior to nuclear import. *Plant Journal* **42**: 175-187.

Hamel LP, Sekine KT, Wallon T, Sugiwaka Y, Kobayashi K, Moffett P. 2016. The chloroplastic protein THF1 interacts with the coiled-coil domain of the disease resistance protein N' and regulates light-dependent cell death. *Plant Physiology* **171**: 658-674.

Han J, Wang X, Wang F, Zhao Z, Li G, Zhu X, Su J, Chen L. 2021. The fungal effector Avr-Pita suppresses innate immunity by increasing COX activity in rice mitochondria. *Rice* **14**: 12. DOI: https://doi.org/10.1186/s12284-021-00453-4

Haweker H, Rips S, Koiwa H, Salomon S, Saijo Y, Chinchilla D, Robatzek S, Von Schaewen A. 2010. Pattern recognition receptors require N-glycosylation to mediate plant immunity. *Journal of Biological Chemistry* **285**: 4629-4636.

Irieda H, Inoue Y, Mori M *et al.* 2019. Conserved fungal effector suppresses PAMP-triggered immunity by targeting plant immune kinases. *Proceedings of the National Academy of Sciences, USA* **116**: 496-505.

Jiang C, Hei R, Yang Y *et al.* 2020. An orphan protein of *Fusarium graminearum* modulates host immunity by mediating proteasomal degradation of TaSnRK1alpha. *Nature Communications* **11**: 4382.

Kanja C, Hammond-Kosack KE. 2020. Proteinaceous effector discovery and characterization in filamentous plant pathogens. *Molecular Plant Pathology* **21**: 1353-1376.

Karki SJ, Reilly A, Zhou B, Mascarello M, Burke J, Doohan F, Douchkov D, Schweizer P, Feechan A. 2020. A small secreted protein from *Zymoseptoria tritici* interacts with a wheat E3 ubiquitin to promote disease. *Journal of Experimental Botany* **72**: 733–746.

Kelley LA, Mezulis S, Yates CM, Wass MN, Sternberg MJ. 2015. The Phyre2 web portal for protein modeling, prediction and analysis. *Nature Protocols* **10**: 845-858.

Kema GHJ, Gohari AM, Aouini L *et al.* 2018. Stress and sexual reproduction affect the dynamics of the wheat pathogen effector AvrStb6 and strobilurin resistance. *Nature Genetics*. **50**: 375-380.

Keren N, Ohkawa H, Welsh EA, Liberton M, Pakrasi HB. 2005. Psb29, a conserved 22-kD protein, functions in the biogenesis of Photosystem II complexes in *Synechocystis* and Arabidopsis. *Plant Cell* **17**: 2768-2781.

Kettles GJ, Bayon C, Canning G, Rudd JJ, Kanyuka K. 2017. Apoplastic recognition of multiple candidate effectors from the wheat pathogen *Zymoseptoria tritici* in the nonhost plant *Nicotiana benthamiana*. *New Phytologist* **213**: 338-350.

Kettles GJ, Bayon C, Sparks CA, Canning G, Kanyuka K, Rudd JJ. 2018. Characterization of an antimicrobial and phytotoxic ribonuclease secreted by the fungal wheat pathogen *Zymoseptoria tritici*. *New Phytologist* **217**: 320-331.

Kubicek CP, Starr TL, Glass NL. 2014. Plant cell wall-degrading enzymes and their secretion in plant-pathogenic fungi. *Annual Review Phytopathology* **52**: 427-451.

Kvitko BH, Park DH, Velasquez AC, Wei CF, Russell AB, Martin GB, Schneider DJ, Collmer A. 2009. Deletions in the repertoire of *Pseudomonas syringae* pv. tomato DC3000 type III secretion effector genes reveal functional overlap among effectors. *PLoS Pathogens* **5**: e1000388. DOI: https://doi.org/10.1371/journal.ppat.1000388

Lawrence GJ, Dodds PN, Ellis JG. 2010. Transformation of the flax rust fungus, *Melampsora lini*: selection via silencing of an avirulence gene. *Plant Journal* **61**: 364-369.

Li Q, Zhang M, Shen D, Liu T, Chen Y, Zhou JM, Dou D. 2016. A *Phytophthora sojae* effector PsCRN63 forms homo-/hetero-dimers to suppress plant immunity via an inverted association manner. *Scientific Reports* **6**: 26951. DOI: https://doi.org/10.1038/srep26951

Liebrand TWH, Smit P, Abd-El-Haliem A *et al.* 2012. Endoplasmic reticulum-quality control chaperones facilitate the biogenesis of Cf receptor-like proteins involved in pathogen resistance of tomato. *Plant Physiology* **159**: 1819-1833.

Manning VA, Hardison LK, Ciuffetti LM. 2007. Ptr ToxA interacts with a chloroplast-localized protein. *Molecular Plant-Microbe Interactions* **20**: 168-177.

Marin M, Uversky VN, Ott T. 2013. Intrinsic disorder in pathogen effectors: protein flexibility as an evolutionary hallmark in a molecular arms race. *Plant Cell*. **25**: 3153-3157.

Marshall R, Kombrink A, Motteram J, Loza-Reyes E, Lucas J, Hammond-Kosack KE, Thomma BPHJ, Rudd JJ. 2011. Analysis of two *in planta* expressed LysM effector homologs from the fungus *Mycosphaerella graminicola* reveals novel functional properties and varying contributions to virulence on wheat. *Plant Physiology* **156**: 756-769.

Meile L, Croll D, Brunner PC, Plissonneau C, Hartmann FE, McDonald BA, Sanchez-Vallet A. 2018. A fungal avirulence factor encoded in a highly plastic genomic region triggers partial resistance to Septoria tritici blotch. *New Phytologist* **219**: 1048-1061.

Meszaros B, Erdos G, Dosztanyi Z. 2018. IUPred2A: context-dependent prediction of protein disorder as a function of redox state and protein binding. *Nucleic Acids Research* **46:** W329-W337.

Motteram J, Kufner I, Deller S, Brunner F, Hammond-Kosack KE, Nurnberger T, Rudd JJ. 2009. Molecular characterization and functional analysis of MgNLP, the sole NPP1 domain-containing protein, from the fungal wheat leaf pathogen *Mycosphaerella graminicola*. *Molecular Plant-Microbe Interactions* **22**: 790-799.

Nakamura S, Mano S, Tanaka Y, Ohnishi M, Nakamori C, Araki M, Niwa T, Nishimura M, Kaminaka H, Nakagawa T, Sato Y, Ishiguro S. 2010. Gateway binary vectors with the bialaphos resistance gene, bar, as a selection marker for plant transformation. *Bioscience Biotechnology and Biochemistry* **74**: 1315-1319.

Pruitt RN, Schwessinger B, Joe A *et al.* 2015. The rice immune receptor XA21 recognizes a tyrosine-sulfated protein from a Gram-negative bacterium. *Science Advances* **1**: e1500245. DOI: https://doi.org/10.1126/sciadv.1500245

Rocafort M, Fudal I, Mesarich CH. 2020. Apoplastic effector proteins of plant-associated fungi and oomycetes. *Current Opinion Plant Biology* **56**: 9-19.

Rooney HCE, Van't Klooster JW, Van der Hoorn RAL, Joosten MHAJ, Jones JDG, De Wit PJGM. 2005. *Cladosporium* Avr2 inhibits tomato Rcr3 protease required for Cf-2-dependent disease resistance. *Science* **308:** 1783-1786.

Saintenac C, Lee WS, Cambon F *et al.* 2018. Wheat receptor-kinase-like protein Stb6 controls gene-for-gene resistance to fungal pathogen *Zymoseptoria tritici*. *Nature Genetics* **50**: 368-374.

Sanchez-Vallet A, Saleem-Batcha R, Kombrink A, Hansen G, Valkenburg DJ, Thomma BPHJ, Mesters JR. 2013. Fungal effector Ecp6 outcompetes host immune receptor for chitin binding through intrachain LysM dimerization. *eLife* **2**: e00790. DOI: https://doi.org/10.7554/eLife.00790

Sanchez-Vallet A, Tian H, Rodriguez-Moreno L *et al.* 2020. A secreted LysM effector protects fungal hyphae through chitin-dependent homodimer polymerization. *PLoS Pathogens* **16**: e1008652. DOI: https://doi.org/10.1371/journal.ppat.1008652

Sanz-Martin JM, Pacheco-Arjona JR, Bello-Rico V, Vargas WA, Monod M, Diaz-Minguez JM, Thon MR, Sukno SA. 2016. A highly conserved metalloprotease effector enhances virulence in the maize anthracnose fungus *Colletotrichum graminicola*. *Molecular Plant Pathology* **17**: 1048-1062.

Shi G, Zhang Z, Friesen TL, Raats D, Fahima T, Brueggeman RS, Lu S, Trick HN, Liu Z, Chao W. 2016. The hijacking of a receptor kinase–driven pathway by a wheat fungal pathogen leads to disease. *Science advances* **2**: e1600822. DOI: https://doi.org/10.1126/sciadv.1600822

Shimizu H, Shikanai T. 2007. Dihydrodipicolinate reductase-like protein, CRR1, is essential for chloroplast NAD(P)H dehydrogenase in Arabidopsis. *Plant Journal* **52**: 539-547.

Snelders NC, Kettles GJ, Rudd JJ, Thomma B. 2018. Plant pathogen effector proteins as manipulators of host microbiomes? *Molecular Plant Pathology* **19**: 257-259.

Snelders NC, Rovenich H, Petti GC, Rocafort M, Van den Berg GCM, Vorholt JA, Mesters JR, Seidl MF, Nijland R, Thomma B. 2020. Microbiome manipulation by a soil-borne fungal plant pathogen using effector proteins. *Nature Plants* **6**: 1365-1374.

Sperschneider J, Dodds PN, Singh KB, Taylor JM. 2018. ApoplastP: prediction of effectors and plant proteins in the apoplast using machine learning. *New Phytologist* **217**: 1764-1778.

Thomas NC, Oksenberg N, Liu FR, Caddell D, Nalyvayko A, Nguyen Y, Schwessinger B, Ronald PC. 2018. The rice XA21 ectodomain fused to the Arabidopsis EFR cytoplasmic domain confers resistance to *Xanthomonas oryzae* pv. *oryzae*. *Peerj* **6**: e4456 DOI: https://doi.org/10.7717/peerj.4456

Tian H, Mackenzie CI, Rodriguez-Moreno L, Van den Berg GCM, Chen H, Rudd JJ, Mesters JR, Thomma B. 2021. Three LysM effectors of *Zymoseptoria tritici* collectively disarm chitin-triggered plant immunity. *Molecular Plant Pathology* **22**: 683-693.

Upadhyaya NM, Mago R, Panwar V *et al.* 2021. Genomics accelerated isolation of a new stem rust avirulence gene-wheat resistance gene pair. *Nature Plants* **7**: 1220-1228.

Van't Klooster JW, Van der Kamp MW, Vervoort J, Beekwilder J, Boeren, S, Joosten MH, Thomma BP, De Wit PJ. 2011. Affinity of Avr2 for tomato cysteine protease Rcr3 correlates with the Avr2-triggered Cf-2-mediated hypersensitive response. *Molecular Plant Pathology* **12**: 21-30.

Van Damme M, Bozkurt TO, Cakir C, Schornack S, Sklenar J, Jones AM, Kamoun S. 2012. The Irish potato famine pathogen *Phytophthora infestans* translocates the CRN8 kinase into host plant cells. *PLoS Pathogens* **8**: e1002875 DOI: https://doi.org/10.1371/journal.ppat.1002875

Van den Burg HA, Harrison SJ, Joosten MHAJ, Vervoort J, De Wit PJGM. 2006. *Cladosporium fulvum* Avr4 protects fungal cell walls against hydrolysis by plant chitinases accumulating during infection. *Molecular Plant-Microbe Interactions* **19**: 1420-1430.

Van Esse HP, Van't Klooster JW, Bolton MD, Yadeta KA, Van Baarlen P, Boeren S, Vervoort J, De Wit PJGM, Thomma BPHJ. 2008. The *Cladosporium fulvum* virulence protein Avr2 inhibits host proteases required for basal defense. *Plant Cell* **20**: 1948-1963.

Vieira Dos Santos C, Rey P. 2006. Plant thioredoxins are key actors in the oxidative stress response. *Trends in Plant Science* **11**: 329-334.

Wang L, Albert M, Einig E, Furst U, Krust D, Felix G. 2016a. The pattern-recognition receptor CORE of Solanaceae detects bacterial cold-shock protein. *Nature Plants* **2**: 16185 DOI: https://doi.org/10.1038/nplants.2016.185

Wang R, Ning Y, Shi X *et al.* 2016b. Immunity to rice blast disease by suppression of effector-triggered necrosis. *Current Biology* **26**: 2399-2411.

Xue B, Dunbrack RL, Williams RW, Dunker AK, Uversky VN. 2010. PONDR-FIT: a meta-predictor of intrinsically disordered amino acids. *Biochimica et Biophysica Acta* **1804**: 996-1010.

Yang LN, Liu H, Duan GH, Huang YM, Liu S, Fang ZG, Wu EJ, Shang L, Zhan J. 2020. The *Phytophthora infestans* AVR2 effector escapes R2 recognition through effector disordering. *Molecular Plant-Microbe Interactions* **33**: 921-931.

Zhan J, Zhu X, Zhou W, Chen H, He C, Wang Q. 2016 Thf1 interacts with PS I and stabilizes the PS I complex in *Synechococcus* sp. PCC7942. *Molecular Microbiology* **102**: 738-751.

Zhao M, Wang J, Ji S, Chen Z, Xu J, Tang C, Chen S, Kang Z, Wang X. 2018. Candidate effector Pst_8713 impairs the plant immunity and contributes to virulence of *Puccinia striiformis* f. sp. *tritici*. *Frontiers in Plant Science* **9**: 1294. DOI: https://doi.org/10.3389/fpls.2018.01294

Zhong Z, Marcel TC, Hartmann FE *et al.* 2017. A small secreted protein in *Zymoseptoria tritici* is responsible for avirulence on wheat cultivars carrying the *Stb6* resistance gene. *New Phytologist* **214**: 619-631.

Chapter 5: Identifying the downstream components of *Stb6*-mediated defence signalling

5.1 Summary

Cell surface immune receptors (CSIRs) are increasingly well understood as playing a key role in plant pathogen resistance. The wheat CSIR *Stb6* confers resistance to certain isolates of the fungal pathogen *Zymoseptoria tritici* possessing the corresponding *AvrStb6* effector gene. The cell-surface interactions and downstream signalling pathways of many CSIRs have been characterised, with many aspects widely conserved. Many CSIRs possess an intracellular kinase domain, which is required for downstream signalling. The *Stb6*-mediated downstream defence response and mechanism of resistance to *Z. tritici* infection is currently unknown. In this chapter, I report on the identification of a strong candidate interactor of Stb6, based on a yeast two-hybrid library screen for interacting wheat proteins using the Stb6 kinase domain. This interactor is the chloroplast-localised ATP-dependent zinc metalloprotease FtsH2. A kinase-dependent cell death phenotype was also observed following the expression of *Stb6* in the wild tobacco plant *Nicotiana benthamiana*, with the *Stb6*-meditated induction of cell death shown to be independent of the common CSIR co-receptor BAK1. Whilst the observed Stb6 kinase-mediated cell death prevented the verification of the Stb6 kinase-FtsH2 interaction *in planta*, the identification of this interactor could represent a novel downstream signalling mechanism for CSIRs. A better understanding of CSIR downstream signalling and the role played by chloroplasts in plant immunity could improve the development of resistant crop plants in future.

5.2 Acknowledgment of contributions

Thanks to Gert de Jaeger (VIB, Gent, Belguim) for providing GSrhino and GSyellow tag constructs and Cyrille Saintenac (INRAE, Clermont-Ferrand, France) for providing the vector for expression of the susceptibility haplotype 3 of *Stb6* originating from the wheat cultivar Courtot. Thanks also to Mike

Grimwade-Mann and Ana Machado-Wood (Rothamsted Research) for advice and assistance with trypan blue staining and electrolyte leakage assays and Kirstie Halsey, Hannah Walpole, Eudri Ventner and Smita Kurup (Rothamsted Research) for their help with confocal microscopy and interpretation of microscopy images. Steve Thomas (Rothamsted Research) kindly provided positive control transformants for yeast two-hybrid assays. *Agrobacterium tumefaciens* strain CryX was kindly provided by Anatoli Giritch and Yuri Gleba (NOMAD Biosciences GmbH, Halle, Germany). Thanks also to Johannes Stuttmann (Martin Luther University of Halle-Wittenberg, Halle, Germany) for providing the *Nicotiana benthamiana* gene-edited *bak1* mutant and to Cyril Zipfel (University of Zurich, Switzerland), who provided the FLS2:GFP expression vector.

5.3 Introduction

Cell surface immune receptors (CSIRs) have been increasingly shown to play an important role in plant immunity and as such represent an important breeding target for future crops (Chapter 1). Some CSIRs have been shown to induce defence following detection of both widely conserved pathogen associated molecular patterns (PAMPs) including fungal chitin (Kaku *et al.*, 2006), whilst others confer resistance following detection of pathogen-specific effector proteins such as I-3 of tomato, which detects the *Fusarium oxysporum* f. sp. *lycopersici* effector SECRETED-IN-XYLEM-1 (SIX1; Rep *et al*., 2004). CSIRs have been characterised in model plants such as *Arabidopsis thaliana* (hereafter Arabidopsis), including the receptor-like kinases (RLKs) FLAGELLIN-SENSITIVE-2 (FLS2; Gomez-Gomez & Boller, 2000), ELONGATION FACTOR THERMO UNSTABLE RECEPTOR (EFR; Zipfel *et al*., 2006) and CHITIN ELICITOR RECEPTOR KINASE 1 (CERK1; Miya *et al.*, 2007), which detect bacterial flagellin fragment flg22, elongation factor thermo-unstable (EF-Tu) and fungal chitin, respectively. Many other CSIRs have also been identified in major crop species, including FLS3 of tomato (*Solanum lycopersicum*) which confers resistance to *Pseudomonas cannabina* pv. *alisalensis*, the *Xanthomonas oryzae* pv. *oryzae* resistance gene *Xa21* in rice (*Oryza sativa*) and LEPR3 of

oilseed rape (*Brassica napus*), which confers resistance to *Leptosphaeria maculans* (Song *et al.*, 1995, Larkan *et al*., 2013, Hind *et al*., 2016). The major role which CSIRs play in defence against pathogens is now coming into focus. The genetic transformation of crop plants with CSIR genes from other plant species (Schwessinger *et al*., 2015) or the generation of chimeric CSIRs (Thomas *et al*., 2018) demonstrates their potential utility in agriculture for pathogen control.

CSIRs require an array of other proteins to relay immune signalling into the cell and to induce defence responses (Couto and Zipfel, 2016). Recognition of pathogen elicitors by FLS2 and EFR induces interaction of these CSIRs with the co-receptor BRI1-ASSOCIATED RECEPTOR KINASE 1/SOMATIC EMBRYOGENESIS RECEPTOR KINASE 3 (BAK1/SERK3), which is required for downstream signalling (Roux *et al*., 2011, Schwessinger *et al*., 2011). Ligand-induced Interaction between FLS2 or EFR and BAK1 leads to the transphosphorylation of the kinase domains of both proteins (Sun *et al.*, 2013). Many CSIRs are non-RD kinases, which lack the arginine-aspartic acid motif common in the kinase domain of RLKs. It has been suggested that, since the activation loop of non-RD kinases does not auto-phosphorylate, non-RD kinase CSIRs require an RD kinase co-receptor such as BAK1 for phosphorylation and signal transduction (Dardick *et al*., 2012), and that in some cases non-RD kinase catalytic activity is not required for signal transduction (Bender *et al.,* 2021). Cytoplasmic proteins also interact with CSIR receptor complexes to relay the defence signal intracellularly. BOTRYTIS-INDUCED KINASE-1 (BIK1), a receptor-like cytoplasmic kinase (RLCK) was shown to interact with both FLS2 and BAK1 *in planta* and was phosphorylated following flg22 perception in an FLS2/BAK1-dependent manner (Lu *et al*., 2010). In turn, BIK1 has been demonstrated to phosphorylate RbohD and thereby enhance the production of reactive oxygen species (ROS; Li *et al.*, 2014), as well as interacting with WRKY transcription factors in the nucleus to regulate jasmonic acid and salicylic acid pathways (Lal *et al.*, 2018).

Wall-associated kinase (WAK) family proteins implicated in plant immunity have also been found to form protein complexes, as part of downstream signalling to induce immune responses (Section 1.4.5). SlWAK1 of tomato complexes with

FLS2 and FLS3, with tomato Δ*slwak1* mutant plants showing compromised flagellin-induced defence responses (Zhang *et al*., 2020). Another WAK, GhWAK7A of cotton (*Gossypium hirsutum*), was implicated in cotton immune responses to fungal chitin and was found to form complexes with GhCERK1 and LYSIN-MOTIF-CONTAINING RLK-5 (GhLYK5), another protein involved in chitin detection and signalling (Wang *et al.*, 2020).

Chloroplasts also play a central function in plant immune responses. They are the source for the biosynthesis of several important hormones required for immune signalling, such as salicylic acid (Rekhter *et al*., 2019), jasmonic acid (Wasternack and Song, 2017) and abscisic acid (Nambara and Marion-Poll, 2005). It has also been observed that extensions from the chloroplast known as stromules are engaged in the transfer of ROS to the nucleus, a process associated with defence responses such as programmed cell death (Caplan *et al*., 2015). These stromules are also observed to extend out to the plasma membrane, suggesting that chloroplasts may be involved in relaying defence signals from the cell surface to the nucleus (Hanson and Sattarzadeh, 2011). Proteins which play important roles in chloroplast function are subsequently common targets of pathogen effectors (Littlejohn *et al*., 2021). The chloroplastic protein Thylakoid formation 1 (Thf1) is also known as Photosystem B protein 29 (Psb29) and ToxA binding protein (ToxABP) due to its reported interaction with the necrotrophic effector PtrToxA of *Pyrenophora tritici-repentis* (Manning *et al*., 2007). As described in Section 4.5.2, ToxABP may also be a target of the *Zymoseptoria tritici* effector AvrStb6. The overexpression of AvrStb6 in wheat leaves has been observed to result in a photobleaching phenotype (Figure S4.9; Bouton C & Kanyuka K, *unpublished*), further supporting a function of AvrStb6 in impeding chloroplast function and suggesting that this may contribute to successful *Z. tritici* infection.

Previous investigations into the protein-protein interactions of immune-related WAKs have utilised different technologies. Li *et al.* (2009) employed yeast two-hybrid (Y2H) assay to demonstrate an interaction between OsWAK1 and OsRFP1. Y2H assay has also been used to identify epidermal growth factor (EGF)-like domain-mediated interactions between rice WAKs OsWAK14, OsWAK91 and OsWAK92 (Delteil *et al.*, 2016), as well as an interaction

between Arabidopsis AtWAK1 and an extracellular glycine-rich protein AtGRP3 (Park *et al*., 2001). Other studies have utilised co-immunoprecipitation (Co-IP) to study protein-protein interactions, including those involving SlWAK1 and GhWAK7A (Wang *et al*., 2020, Zhang *et al*., 2020). Indeed, Co-IP is considered the “gold standard” for studying protein-protein interactions (Lampugnani *et al*., 2018). Once identified, reverse genetics approaches may be used to determine whether these interacting proteins are essential for the function of resistance proteins in immunity. *Barley stripe mosaic virus* mediated virus-induced gene silencing (BSMV-VIGS) has been used to silence genes of interest in monocots (Holzberg *et al.*, 2002), and represents a powerful tool for the investigation of wheat proteins involved in disease resistance to *Z. tritici* (Lee *et al*., 2015).

The wheat disease resistance gene *Stb6* is a member of the WAK gene family and confers immunity against isolates of *Z. tritici* expressing specific isoforms of the secreted effector protein AvrStb6 (Section 3.5.4; Brading *et al*., 2002). *Stb6* is expressed only in wheat leaves and wheat *stb6*-knockout lines are reported to show no phenotypic differences from wild-type (Saintenac *et al*., 2018), other than susceptibility to *Z. tritici* expressing AvrStb6. This suggests that *Stb6* plays no major role in plant growth and development. Saintenac *et al*. (2018) demonstrated not only that *Stb6* is involved in a gene-for-gene interaction with *AvrStb6*, but also that Stb6 kinase activity is required for the *Stb6*-mediated immune response. *Stb6* from wheat cultivar (cv.) Courtot (*Stb6* haplotype 3), encodes a protein with a single mutation in the kinase active site relative to *Stb6* (haplotype 1) from cv. Cadenza (Figure S5.1), which abolishes kinase activity. Two other *Stb6* mutant lines, carrying missense mutations G387E and E522K, also showed reduced kinase activity compared to Stb6 encoded by haplotype 1. Wheat cv. Cadenza lines carrying G387E, E522K mutations in Stb6 and cv. Courtot all demonstrate compromised resistance to *Z. tritici* isolate IPO323, which is avirulent towards *Stb6* wheat.

In the following chapter, I report on studies aiming to identify the wheat proteins interacting with Stb6 using different *in planta* and *in vitro* biochemical approaches. Interestingly, expression of *Stb6* in the wild tobacco species *Nicotiana benthamiana* induced kinase activity-dependent cell death. Screening of a wheat Y2H library using the Stb6 kinase protein fragment as a bait

identified a strong candidate interacting protein: a chloroplastic ATP-dependent zinc metalloprotease FtsH2. Interaction between these proteins was subsequently further tested using the Y2H assay and *in planta* by Co-IP, although these experiments could not confirm the interaction. When expressed in *N. benthamiana* a fusion with a fluorescent protein tag, Stb6 displayed an unusual cellular localisation pattern, being present predominantly in the plasma membrane following plasmolysis but also observed in the cell wall and filaments adjoining the cell wall and membrane as well as in the cell wall. Interestingly, a CRISPR/Cas9 induced *Stb6* knock-out mutant was found to have a small but statistically significant increase in the first true leaf length, compared to the corresponding parental cv. Cadenza line and a tissue cultured control cv. Cadenza line.

5.4 Methods

5.4.1 Wheat Y2H library screen

Library-scale transformation of competent *Saccharomyces cerevisiae* strain MaV203 (hereafter referred to as yeast) cells was carried out as described previously (Section 2.7.3.1). Briefly, a 50 µl competent yeast cell aliquot was mixed with 1 µg of pDEST32-Stb6_kinase bait plasmid and incubated for 1 h at 30˚C. The transformation mixture was then spread on complete supplement agar plates lacking leucine (SC-Leu) for transformants selection, and the plates incubated for 4 days at 30˚C. Resulting recombinant yeast colonies were picked and made competent for library transformation (Section 2.7.3.1). Prior to library-scale transformation, the minimal concentration of 3-amino-1,2,4-triazole (3-AT) required to prevent unwanted autoactivation of the *HIS3* reporter gene by the Stb6 kinase bait in yeast transformants was determined (Section 2.7.4.1; Figure S5.2).

Library-scale transformation was carried out using 30 µg cDNA prey library (Section 2.7.3.1), with cells transformed using salmon sperm carrier DNA and LiAc/PEG/TE buffer (Table 2.5). Following incubation at 30˚C, addition of dimethyl sulfoxide (DMSO) and heat shock treatment, transformants were spread on complete supplement agar plates lacking leucine, tryptophan and

histidine (SC-LTH) and supplemented with 30 mM 3-AT for identification of yeast transformants expressing the *HIS3* reporter gene. Approximately 6.9x10^6 transformants were tested. Yeast colonies demonstrating growth on selection media were restreaked and tested again for induction of *HIS3* by growth on SC-LTH media supplemented with 3-AT (0-100 mM), as well as for induction of the *LacZ* reporter gene, as evidenced by the appearance of blue coloration in the yeast patch in the X-gal assay (Section 2.7.4).

5.4.2 Development of constructs for expression of Stb6 and FtsH2 proteins tagged with fluorescent reporter proteins

Stb6 expression constructs (Figure 5.2a) were generated using the Gateway-compatible pGWB vector series (Nakamura *et al*., 2010). The pGWB654 vector provides a C-terminal monomeric red fluorescent protein (mRFP) tag, whilst pGWB605 provides a C-terminal green fluorescent protein (GFP) tag. The pGWB655 vector was used for the development of the expression construct of the peptidase fragment of FtsH2, with an N-terminally fused mRFP protein. Expression of genes of interest in the pGWB vector series is under the control of the *Cauliflower mosaic virus* (CaMV) 35S promoter.

A second set of constructs were generated in the pGWB605 vector for expression of Stb6 with a C-terminal “GSRhino” tag. This tag consists of two protein G immunoglobulin-binding domains, two human rhinovirus 3C protease cleavage sites and a streptavidin-binding peptide (SBP). The *Stb6* gene haplotypes 1 and 3 fused in frame with the GSrhino tag were first cloned into the Gateway donor vector pDONR221 to generate entry clones (Figure S5.3), and then recombined into pGWB605 for *in planta* expression.

5.4.3 Transient expression of *Stb6* in *N. benthamiana*

Vector constructs were transformed into *Agrobacterium tumefaciens* (hereafter Agrobacterium) strains GV3101 and CryX, and agroinfiltration was used to transiently express the proteins in *N. benthamiana* (Section 2.4). Briefly, transformed Agrobacterium strains were incubated in growth media overnight, cells were pelleted and diluted to optical density at 600 nm (OD_{600}) of 0.5 in agroinfiltration buffer, and infiltrated into the abaxial side of fully expanded leaves of 4- to 6-week-old *N. benthamiana* plants using a needleless syringe.

Electrolyte leakage testing and trypan blue staining of agroinfiltrated zones of *N. benthamiana* leaves transiently expressing proteins was carried out as described in Sections 2.4.3 and 2.4.4, respectively.

5.4.4 Immunoprecipitation, SDS-PAGE, and western blotting

See Section 2.5.2 for immunoprecipitation (IP) protocol. See Sections 2.5.3 and 2.5.4 for SDS-PAGE and western blotting protocols, respectively. SDS-PAGE of 25 µl protein extract aliquots or IP fractions was carried out in 8% acrylamide gels, run at 80 V. Proteins were transferred from gels onto PVDF membranes, using a Bio-Rad Mini Trans-Blot Cell system, at 100 V for 40 min. Membranes were blocked using 5% milk in TRIS-buffered saline (TBS) containing 0.1% Tween 20, at room temperature for 1 h. Immunoblotting was carried out using anti-GFP or anti-RFP antibodies, both overnight at 4°C. Anti-GFP antibodies were diluted 1:2,000 in TBS-Tween 20 supplemented with 5% bovine serum albumin (BSA), whilst anti-RFP antibodies were diluted 1:1,000 in TBS-Tween 20 with 5% fat-free milk. Secondary antibody probing was carried out using a 1:10,000 dilution in TBS-Tween 20 with 5% milk, for 1 h at room temperature. Following incubation with ECL reagent (GE healthcare), membranes were imaged using an Odyssey imager (Li-Cor).

5.4.5 Confocal microscopy of *N. benthamiana* leaves

Confocal microscopy was carried out as described in Section 2.8. All images shown are from leaves harvested at 5 days post infiltration (dpi), with fluorophores expressed within *N. benthamiana* pavement cells excited and fluorescence imaged to determine the localisation of fluorophores. Plasmolysis of leaf cells was performed by imbibing leaf sections in 0.8 M mannitol solution for 30 min at room temperature before imaging.

5.4.6 Y2H assays

Y2H assays to validate the interaction between Stb6 kinase and FtsH2 were carried out as described in Section 2.7. Briefly, 50 µl yeast cell aliquots were mixed with 1 µg each of bait and prey plasmid, incubated for 1 h at 30˚C, spread on complete supplement agar plates lacking leucine and tryptophan (SC-LT) for transformants selection, and then incubated for 4 days at 30˚C.

Successful transformants were first suspended in sterile saline (0.9% NaCl) and 5 µl aliquots spotted onto a SC-LT master plate. Following incubation transformants were replica plated from the master plates to the test plates using velvet transfer (Section 2.7.3). Activation of the reporter genes *HIS3* and *LacZ* was evidenced by yeast growth on SC-LTH media supplemented with 3-AT and the blue coloration of the yeast patch in the X-gal assay, respectively (Section 2.7.4).

5.4.7 BSMV-mediated virus induced gene silencing of wheat genes encoding candidate Stb6 interactors

See Lee *et al*. (2015) for detailed BSMV-VIGS methodology. BSMV vectors were developed by Kostya Kanyuka for silencing *FtsH2* and *ToxABP* in wheat cv. Cadenza (WT and *Δstb6* gene edited) plants. The BSMV:*FtsH2* construct targeted the *FtsH2* mRNA region encoding the ATP-binding domain of the protein, whilst the BSMV:*asToxABP* construct targeted the 5' terminal portion of the coding region of *ToxABP* mRNA. In both cases, VIGS constructs were designed to silence all 3 homeologues of each target gene, by targeting conserved regions in the coding gene sequences (CDS). Targeted regions were amplified by PCR from total wheat cDNA (Section 2.3.4) and incorporated into pCassRZ-BSMVγ-LIC vector using ligation-independent cloning. As controls, a mock inoculation of wheat seedlings with buffer only and no BSMV, a negative control BSMV:mcs4d construct for expression of a non-plant sequence, and a BSMV:*asTaChlH* construct as a positive control for VIGS directing silencing of the wheat *MAGNESIUM CHELATASE SUBUNIT H* (*TaChlH*) gene were used.

VIGS vectors were transformed into Agrobacterium strain GV3101 and the resulting Agrobacterium transformants were infiltrated into *N. benthamiana* plants (Section 2.4). At 6 dpi, agroinfiltrated leaves were harvested and ground in a chilled pestle and mortar with 10 mM potassium phosphate buffer at pH 7.0 (2 ml per 1 g of leaf material). To this virus-containing leaf sap was added 1-2% w/v Celite 545 AW (Sigma). This slurry was used for rub-inoculation of the two first true leaves of 14-days-old wheat seedlings. Following inoculation, plants were left at low light intensity for 18 h to recover before being returned to

regular growth conditions (Section 2.6). Viral symptoms began to emerge on third and fourth leaves of inoculated wheat at 12-14 dpi. At 23 dpi inoculation of BSMV-infected leaves with *Z. tritici* isolate IPO323 was carried out, as described previously (Section 2.6).

The efficiency of VIGS of target genes in upper uninoculated leaves showing virus-induced symptoms was assessed by reverse transcriptase-quantitative PCR (RT-qPCR). See Section 2.3.3 for RNA extraction, cDNA preparation and Section 2.3.4 for RT-qPCR protocol. Primers used are specified in Table 2.4. Three technical replicates of four biological replicates were analysed for BSMV:*asFtsH2* and Mock treatments with two biological replicates for BSMV:*asToxABP*, due to lack of leaf material. Expression of *ToxABP* or *FtsH2* measured as relative to the wheat housekeeping gene *alpha tubulin* (*TUB*; gene ID U76558), as calculated using the Pfaffl method (Pfaffl, 2001).

5.4.8 First leaf length analysis of Δ*stb6* vs wild-type wheat

A pilot study was carried out to determine the length of first fully expanded true leaves of different wheat cv. Cadenza lines. Wild-type cv. Cadenza parent and the gene-edited Δ*stb6* mutant in the same genetic background were analysed, along with three control cv. Cadenza lines recovered after particle bombardment and subsequent tissue culture. The line B3694 R7P1 was generated in parallel and from identical progeny to wheat used to generate Δ*stb6* gene-edited cv. Cadenza mutant, whilst the lines B3692 R1P1 and R3P3 were generated in a separate experiment. For control line B3692 R1P1, no DNA was introduced during the particle bombardment and tissue culture process, whilst wheat lines B3692 R3P3 and B3694 R7P1 were both transformed with the *Bar* gene, which confers resistance to the herbicide BASTA (Hahn *et al*., 2021). Seeds were sown in pots placed in larger trays for watering, in a randomised complete block design, with fully expanded first (L1) and second (L2) leaves measured at two and three weeks after sowing.

5.5 Results

5.5.1 Generation of Stb6:GSrhino constructs

A series of constructs were generated to study the protein-protein interactions involving Stb6. *Stb6* haplotypes 1 and 3 were both used to generate constructs, using cDNA from wheat cvs. Cadenza and Courtot, respectively. *Stb6* was first cloned with a C-terminal tandem affinity purification (TAP) tag known as GSrhino, which contained two protein G tags and a streptavidin-binding peptide, separated by rhinovirus 3C protease cleavage sites. The generation of a second set of TAP tag constructs utilising the GSyellow tag (Besbrugge *et al*., 2018) was attempted, but was not successful. TAP tags allow for two rounds of affinity purification, thus increasing the sensitivity for detection of protein-protein interactions (Puig *et al*., 2001). The GSrhino tag has already been used to identify protein-protein interactions in the model plant Arabidopsis (Van Leene *et al*., 2015), as well as cereal plants such as rice (Dedecker *et al*., 2016). Using a combination of overlap-extension PCR (Table S5.1) and Gateway cloning, the Stb6:GSrhino construct was generated in the Gateway donor vector pDONR221 (Figure S5.3) and subsequently recombined into pGWB605, under the control of a CaMV 35S promoter. However, financial restraints prevented the subsequent use of this construct for affinity purification and mass spectrometry for identification of proteins interacting with Stb6 in *N. benthamiana*.

5.5.2 Transient expression of *Stb6* in *N. benthamiana* induces cell death

Another series of constructs were generated with *Stb6* (haplotypes 1 and 3) in the pGWB vector series, which provides either a C-terminal GFP tag (pGWB605) or a C-terminal mRFP tag (pGWB654, Nakamura *et al*., 2010). These constructs were transformed into Agrobacterium and the resulting Agrobacterium transformants were subsequently infiltrated into *N. benthamiana*. See Figure 5.1a for *Stb6* constructs used in this study.

From 3 days post infiltration (dpi), leaf patches expressing resistance version of Stb6 (hapotype 1) which possesses a functional kinase, began to show a marked cell death phenotype. This phenotype was observed following expression of Stb6 with or without a C-terminal fluorophore tag. However,

expression of the susceptibility version of Stb6 (haplotype 3), which possesses a single mutation abolishing kinase activity, resulted in no cell death. This observation was confirmed by trypan blue staining and electrolyte leakage analysis (Figure 5.1b, c). These results show that the protein kinase activity of Stb6 is required for inducing cell death in *N. benthamiana*.

RLKs such as Stb6, which do not possess an arginine-aspartate (RD) motif in the catalytic loop of their kinase domains, often require a co-receptor RD kinase to transmit defence signals. Frequently the role of co-receptor is played by BAK1 (Liebrand *et al*., 2014). The transient expression of both variants of Stb6 was repeated in wild-type *N. benthamiana* and in a gene-edited *Δbak1* mutant. At 5 dpi leaves were assessed for appearance of cell death. Expression of the kinase-active, resistance version of Stb6 was found to induce cell death in *N. benthamiana Δbak1* leaves that was similar in intensity and the timing to the wild type (Figure S5.4). This result suggests that *Stb6* defence signaling does not require *BAK1*.

5.5.3 Stb6 localises primarily to the plasma membrane in *N. benthamiana*

Due to the kinase-dependent cell death induced by the kinase-active, resistance version of Stb6 following its transient expression in *N. benthamiana*, subsequent cellular localisation studies were performed using the kinase-dead, susceptibility version of Stb6. Confocal microscopy was used to image *N. benthamiana* epidermal cells transiently expressing an Stb6:mRFP fusion protein. This revealed Stb6 localisation to the cell periphery (Figure 5.2a). Subsequent plasmolysis of *N. benthamiana* leaf sections (Figure 5.2b) using 0.8 M mannitol solution revealed that most of the fluorescence signal retreated with the plasma membrane. However, even at 30 min following plasmolysis some fluorescence foci were detected in the cell wall, as well as in thread-like structures connecting the plasma membrane and cell wall. The latter are most likely Hechtian strands. It is also possible that the points of contact between the putative Hechtian strands and the cell wall are associated with specific cell wall structures such as plasmodesmata (Cheng *et al.*, 2017), although this is yet to be determined experimentally.

5.5.4 In-house wheat Y2H library screening using Stb6 kinase as a bait yielded no interactors

A screen for candidate interactors with the kinase domain of the Stb6 protein was carried out using the Y2H system. In this screen, the kinase domain encoded by *Stb6* haplotype 1 was used as a bait (Figure S5.1) and tested for interactions against a cDNA prey library, developed in-house and derived from wheat infected with *Z. tritici* (Section 2.7.3.1). Bait-only yeast transformants were assessed for autoactivation on selective media, with 30 mM 3-amino-1,2,4,-triazole (3-AT) shown to be sufficient to suppress growth (Figure S5.2). This 3-AT concentration in SC-LTH media was subsequently used for the library screen. Approximately 6.9 x 10^6 transformants were tested, with 91 His^+ colonies showing growth on selective media isolated for retesting.

Subsequent analysis of these 91 His^+ transformants (Figures 5.3 and S5.5) found that although many showed growth on SC-LTH media supplemented with 3-AT at all concentrations, none showed any blue colouration when analysed using the X-gal blue-white screening assay. It is therefore unlikely that any of these transformants possessed positive interactors and were likely false positives. Insufficient replica cleaning, to remove excess cell material following replica plating from the master plate to test plates, is likely the reason for the growth observed on SC-LTH test plates supplemented with a high 3-AT concentration.

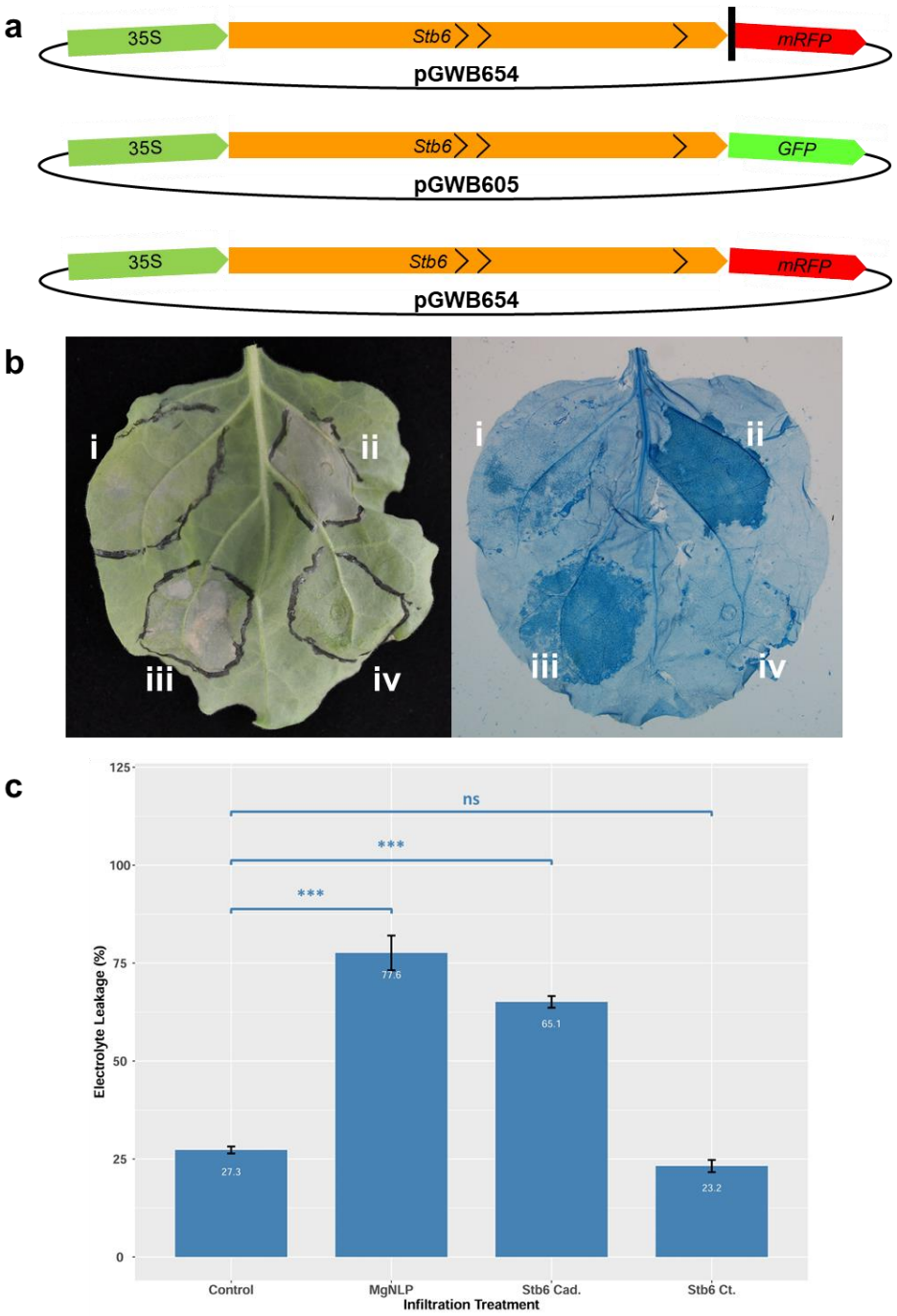

Figure 5.1: *Stb6* expression in *Nicotiana benthamiana* induces kinase-dependent cell death. Agroinfiltration was used to transiently express *Stb6* in tobacco leaves. a) Schematic illustration of *Stb6* constructs generated and utilised for expression in *N. benthamiana*. *Stb6* genes were under control of a *Cauliflower mosaic virus* 35S promoter. Black bar represents a STOP codon introduced between *Stb6* and the tag. pGWB654 (mRFP, C-terminal tag) and pGWB605 (GFP, C-terminal tag) were used from the construct series developed by Nakamura et al. (2010). *Stb6* full cDNA sequence was cloned into each construct. Two *Stb6* haplotypes, from cultivar Cadenza (Stb6 Cad., encoding a functional kinase) and cv. Courtot (Stb6 Ct., encoding a non-functional kinase), were used to generate constructs. b) *N. benthamiana* leaves imaged at 5 days post agroinfiltration (dpi), under visible light (left) and after trypan blue staining (right). i = untransformed *Agrobacterium* (control); ii = *Mycosphaerella graminicola* necrosis- and ethylene-inducing peptide 1 (Nep1)-like protein family (MgNLP); iii = Stb6 Cad.; iv = Stb6 Ct. c) Electrolyte leakage assay results for *N. benthamiana* leaves at 5 dpi. *** represents significant difference with $p < 0.001$. “ns” represents no significant difference. Error bars represent standard error for three biological replicates.

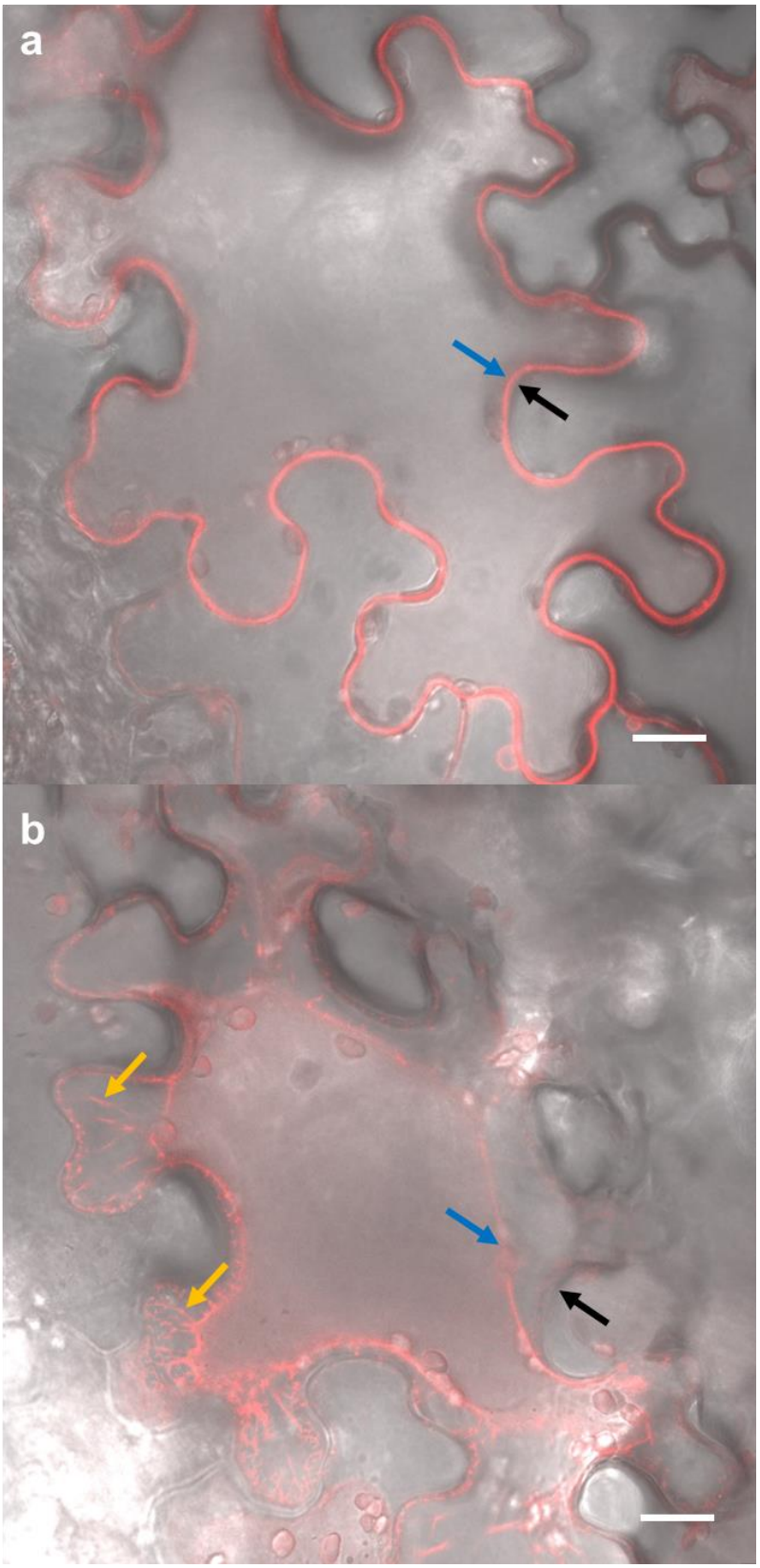

Figure 5.2: Stb6 localises to the cell membrane when expressed in *Nicotiana benthamiana*. Confocal microscope images were taken of *N. benthamiana* leaf cells transiently expressing *Stb6* (haplotype 3) with a C-terminal mRFP tag. Leaves were harvested at 5 days post agroinfiltration. **a)** *N. benthamiana* leaf pavement cell expressing *Stb6::mRFP* construct, prior to plasmolysis using 0.8M mannitol solution. **b)** *N. benthamiana* leaf pavements cell, following plasmolysis induced by 30 minute incubation in mannitol solution. Black arrows indicate location of cell wall, blue arrows location of plasma membrane and orange arrows indicate Hechtian strands. White bars represent 20 µm. Experiment was repeated three times with similar results.

5.5.5 Commercial wheat Y2H library screening using Stb6 kinase as a bait identified FtsH2 as a high confidence candidate interactor

A second attempt was made to identify wheat proteins interacting with the Stb6 kinase domain with the help of Hybridgenics, a protein interaction service provider. This screen utilised a commercial prey library developed from *Z. tritici*-infected wheat, which had previously been used to identify proteins interacting with the fungal effector ZtSSP2 (Karki *et al*., 2020). Whilst an initial screen using the LexA DNA binding domain-Stb6 kinase fusion as a bait recovered no interactors, a subsequent screen using the the Gal4 DNA binding domain-Stb6 kinase fusion identified 49 independent positive clones for 66.3 million interactions tested. Inserts in the prey plasmids recovered from these positive clones were sequenced, and all sequences aligned to the same *Triticum aestivum* gene encoding the chloroplast-localised ATP-dependent zinc metalloprotease FtsH2. Sequences corresponding to the gene region encoding the C-terminal portion of FtsH2 downstream of transmembrane helix were identified, comprising either the P-loop NTPase or peptidase domains. All three homeologues of *FtsH2* (in wheat A, B and D genomes) were represented in the positive clones (Table S5.2).

The interaction between Stb6 kinase and the FtsH2 peptidase domain was further assessed using the Y2H system. Yeast transformants possessing Stb6 kinase in the bait vector pDEST32 and FtsH2 peptidase in the prey vector pDEST22 were tested for expression of *HIS3* and *LacZ* reporter genes. However, no reporter gene expression was identified in this assay, suggesting no interaction between the two proteins (Figure S5.5). The experiment was repeated with Stb6 kinase in the prey vector and FtsH2 peptidase in the bait, with similar results. We were therefore unable to recapitulate the high confidence interaction reported by Hybridgenics in their screen, using our own targeted Y2H assays.

5.5.6 No interaction between FtsH2 and Stb6 detected *in planta*

The peptidase fragment of FtsH2 with an N-terminal mRFP tag was co-expressed *in planta* along with the C-terminal GFP-tagged Stb6 protein. No Stb6 (resistance version) was detected after either 2 (*data not shown*) or 3 days

(Figure 5.4) post infiltration in the input or anti-GFP immunoprecipitated fractions. This is likely due to the induction of *Stb6*-mediated cell death following its expression in *N. benthamiana* cells. Therefore, interactions were assessed between Stb6 encoded by the susceptibility haplotype 3 and FtsH2 peptidase. This analysis identified no interaction between these two proteins (Figure 5.4). The interaction between Stb6 kinase and FtsH2 identified in the Y2H library screen could therefore not be replicated *in planta*.

5.5.7 BSMV-mediated virus-induced gene silencing of *FtsH2*

Constructs for the targeted silencing of the three *FtsH2* homeologues in wheat, using the BSMV-VIGS system, were generated. These constructs were expressed in *N. benthamiana* before rub-inoculation of wheat plants. From 12 dpi, *FtsH2*-silenced wheat plants demonstrated a bleaching and variegation phenotype on emerging leaves (Figure 5.5a). This phenotype was similar to that observed on *MAGNESIUM CHELATASE SUBUNIT H*-silenced control plants (Lee *et al.*, 2015) and resembles the phenotype reported for the *ftsh2* (syn. *var2*) mutant of Arabidopsis (Sakamoto *et al*., 2002). Silencing of the wheat gene encoding the AvrStb6 candidate interactor protein ToxABP (Section 4.5.2) was also carried out. Whilst viral infection symptoms were visible on ToxABP silenced leaves, no bleaching phenotype was observed. RT-qPCR analysis of RNA extracted from symptomatic wheat leaves confirmed that in BSMV:*asFtsH2*-treated plants, the expression of *FtsH2* was significantly reduced compared to mock inoculated or BSMV:mcs4d-treated plants (Figure 5.5b). However, gene expression following BSMV:*asToxABP* treatment was not reduced, suggesting that gene silencing was not efficient in this case.

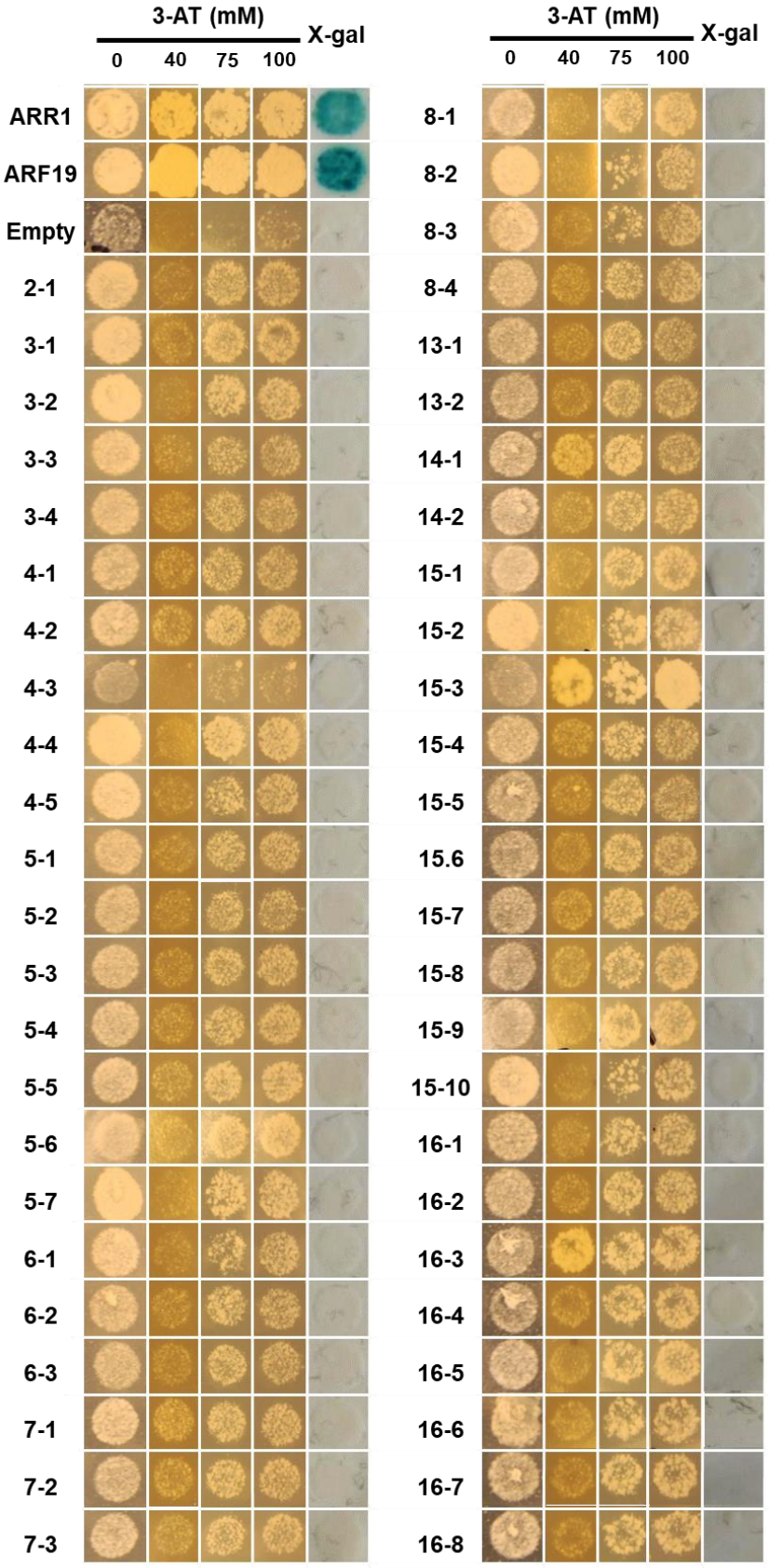

Figure 5.3: No candidate Stb6 kinase interactors were identified from a yeast two-hybrid library screen. HIS^+ colonies found to grow on complete supplement plates lacking leucine, tryptophan and histidine (SC-LTH) plates with 30 mM 3-amino-1,2,4,-triazole (3-AT) were isolated and retested. HIS^+ colonies were spotted onto SC-LTH plates with 3-AT (0-100 mM) to test *HIS3* expression and tested by treatment with X-gal (5-Bromo-4-chloro-3-indolyl-β-D-galactopyranoside) for *LacZ* expression. This figure shows results for colonies 2-1 to 16-8; see Figure S5.5 for retesting of HIS^+ colonies 17-1 to 30-5.

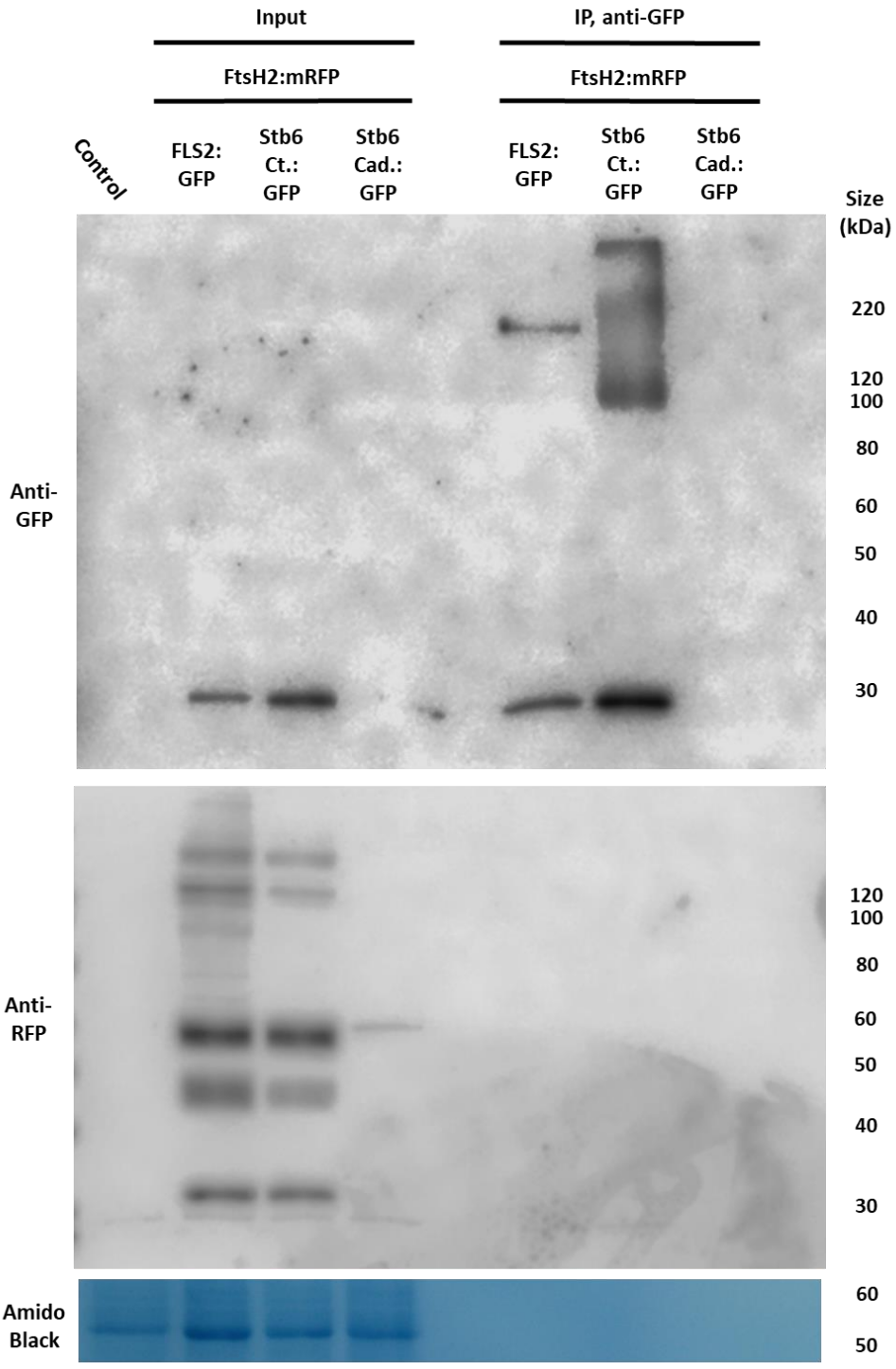

Figure 5.4: No *in planta* interaction between Stb6 and FtsH2 observed.
Coimmunoprecipitation (Co-IP) experiment using protein extracts from *N. benthamiana* transiently expressing *Stb6:GFP* constructs from cultivar Courtot (Stb6 Ct., non-functional kinase) or cv. Cadenza (Stb6 Cad., functional kinase) as bait and FtsH2 peptidase:mRFP as prey. FLS2:GFP co-expressed with FtsH2 peptidase:mRFP was used as a negative interaction control. Control lane is protein harvested from *N. benthamiana* agroinfiltrated with untransformed *Agrobacterium*. Stb6 Cad. proteins were harvested at 3 days post agroinfiltration (dpi), all other protein extracts were harvested at 5 dpi. Top panel: blotting with anti-GFP antibodies, to identify GFP constructs in input protein and anti-GFP immunoprecipitated (IP) fractions. Middle panel: blotting with anti-RFP antibodies, to identify RFP constructs in input protein and any RFP constructs pulled down following anti-GFP IP. Bottom panel: amido black staining of exemplary membrane (anti-GFP).

At 23 days post viral infection, the third or fourth leaves of VIGS inoculated plants, both those displaying viral symptoms as well as non-symptomatic controls, were inoculated with *Z. tritici* isolate IPO323 spore suspensions, as previously described (Section 2.6). Unfortunately, an error in the experimental set-up led to many of these inoculated leaves dying due to stress before *Z. tritici* infection could be established. The inoculation assay could therefore not be completed, and no data was obtained to determine whether the silencing of *FtsH2* or *ToxABP* compromised *Stb6*-mediated resistance to IPO323.

5.5.8 *Stb6* may confer a small but significant reduction in first true leaf length

Although no morphological differences between wild-type wheat cv. Cadenza and cv. Cadenza ethyl methanesulfonate (EMS)-induced mutants carrying missense mutations in the *Stb6* gene were previously reported (Saintenac *et al*., 2018), it was observed in my initial experiments that wild-type wheat cv. Cadenza plants appeared to have shorter first leaves than gene-edited Δ*stb6* wheat cv. Cadenza plants. This was investigated further by growing wild-type cv. Cadenza, Δ*stb6* gene-edited Cadenza and control Cadenza lines, recovered from tissue culture following particle bombardment, a technique used to stably transform wheat lines (Sparks and Doherty, 2020) and previously used to generate Δ*stb6* Cadenza. Analysis of first leaf length three weeks after sowing revealed a dramatic difference in the development of the wild-type cv. Cadenza plants from all other tested Cadenza lines, with the first leaves of the wild-type plants being significantly shorter than in all other lines (Figure S5.7). A small but significant increase in first leaf length was also observed for the Cadenza ***Δstb6*** mutant plants compared to the control Cadenza line B3694 R7P1, although analysis using Dunnett's multiple comparison test found non-significant differences between Cadenza ***Δstb6*** and the two other control Cadenza lines (Figure S5.7). Differences may not be the result of the presence or absence of *Stb6*, but may rather reflect variations between cv. Cadenza wheat lines, or differences in the speed of growth.

5.6 Discussion

Stb6 confers resistance to *Z. tritici* in wheat without inducing an HR response (Brading *et al*., 2002). However, following expression in *N. benthamiana*, Stb6 triggers rapid cell death (Figure 5.1). This cell death was found to be dependent on the Stb6 kinase activity, with the expression of a kinase-dead Stb6 variant inducing no visible cell death. The *Brachypodium distachyon* WAK *BdWAK2*, implicated in plant defence due to its upregulation following salicylic acid treatment, also induced cell death when transiently expressed in *N. benthamiana*, with this phenotype also found to be requiring BdWAK2 kinase activity (Wu *et al*., 2020). The exact mechanism by which *Stb6* or *BdWAK2* induce cell death remains unknown. It is also not known why this phenotype occurs in *N. benthamiana* but not in the respective monocots. The cell death phenotype induced by the kinase active Stb6 was also not affected by the presence of GFP or mRFP tags. This suggests that the tagging of Stb6 does not impede its function. This is encouraging for future interaction studies, as the tagging of CSIRs such as FLS2 has been previously shown to impede their function *in planta* (Hurst *et al*., 2018).

Interestingly, the cell death phenotype induced by the expression of *Stb6* in *N. benthamiana* was observed to be independent of *BAK1* (Figure S5.4). This observation corresponds to previous studies, in which IPO323 was found to be avirulent on both wild-type wheat cv. Cadenza (*Stb6*) and on cv. Cadenza *bak1* gene-edited mutant lines (Hahn *et al*., 2021). BAK1 is a co-receptor for many non-RD RLK-class CSIRs, being required for their downstream signalling (Couto and Zipfel, 2016). This result suggests that Stb6 utilises another co-receptor, possibly another SERK, for signal transduction in *N. benthamiana*, or that no co-receptor is required to induce *Stb6*-mediated cell death in this plant species. Another WAK, Rlm9 of *Brassica napus*, has also been shown to induce immune responses independently of BAK1 (Larkan *et al.*, 2020). It should be noted, however, that the *N. benthamiana* CRISPR/Cas9-induced *Δbak1* mutant used here displayed no visible phenotypic differencies compared to the wild-type, whereas the Arabidopsis *bak1* mutants were found to display a semi-dwarf phenotype (Li *et al*., 2002). In other studies, *N. benthamiana* displayed a slight stunting and weak distortion of leaves three weeks after

silencing of *BAK1* using *Tobacco ratlle virus* mediated VIGS (Heese *et al*., 2007). Further investigation of the *N. benthamiana Δbak1* mutant line is currently underway to verify the CRISPR/Cas9-induced mutation is stable.

Stb6 was found to localise to the cell periphery when transiently expressed in *N. benthamiana* (Figure 5.2). Plasmolysis of *N. benthamiana* cells expressing *Stb6* revealed that much of the protein remained bound to the plasma membrane, but fluorescence was also observed in the cell wall and filaments which may be Hechtian strands connecting the two. This localisation to both the cell wall and plasma membrane is unusual for WAKs (Section 1.4.1). One other WAK, OsWAK91 of rice, was reported to display a similar localisation pattern when expressed in rice cells, being observed within both the cell wall, membrane and Hechtian strands following plasmolysis (Wang *et al*., 2012). However, the cellular localisation pattern for Stb6 observed in *N. benthamiana* may not necessarily occur in wheat. A commelinoid monocot, wheat possesses a type II cell wall which contains glucuronoarabinoxylan as its primary non-cellulosic polysaccharide. Dicots such as *N. benthamiana* possess type I cell walls that are, by contrast, generally rich in xyloglucan and pectin (Kubicek *et al*., 2014). AtWAK1 was previously reported to bind specifically to pectin (Anderson *et al*., 2001) and other WAKs such as Stb6 may also interact with pectin in the cell wall. The differing quantities of cell wall pectin may therefore lead to different cell wall-binding phenotypes for WAKs expressed in monocot or dicot cells. Expression of Stb6 with a fluorophore tag in wheat cells, induced using a biolistics method (Sparks and Doherty, 2020), will be carried out to determine if this phenotype is consistent for different cell wall types.

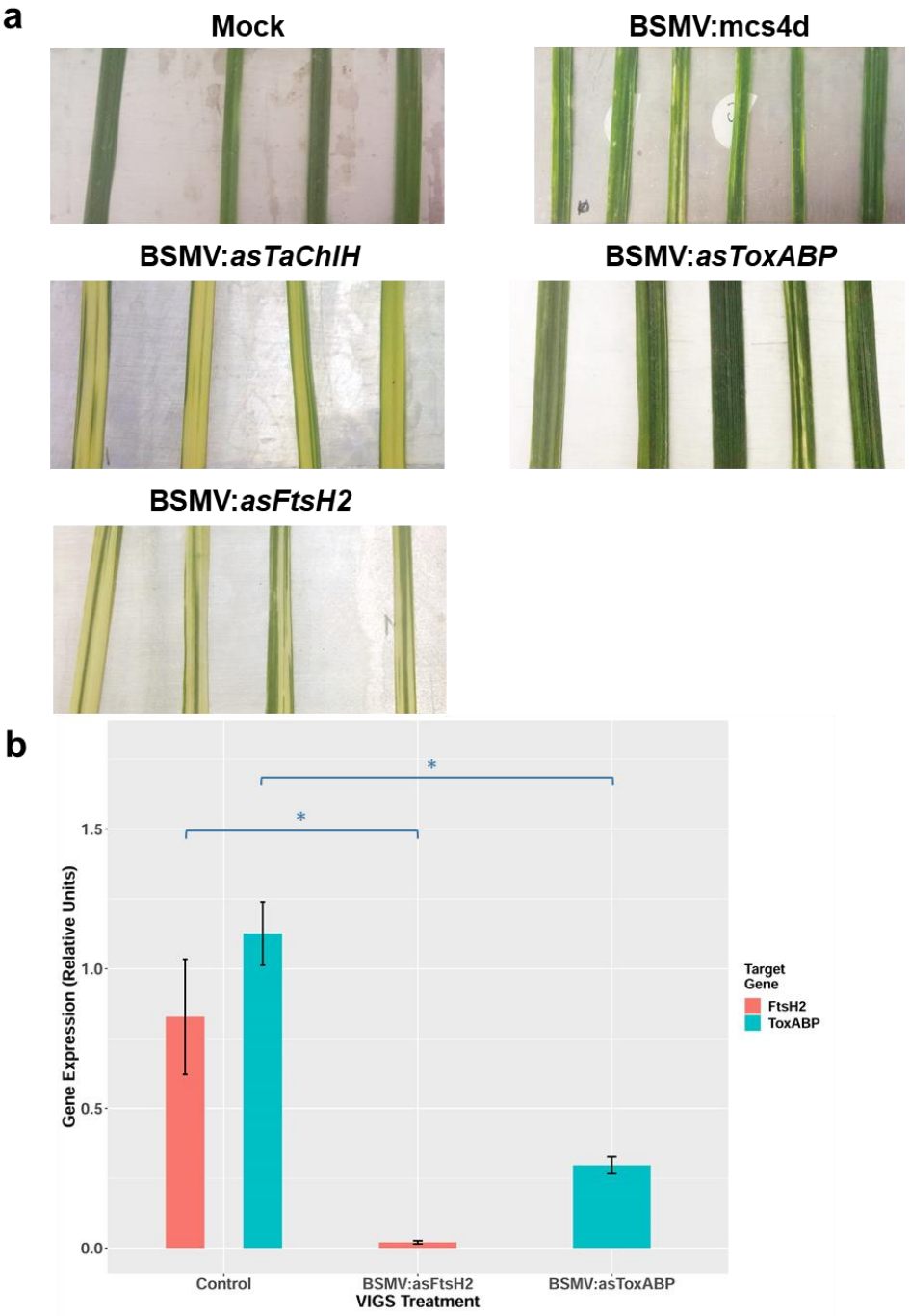

Figure 5.5: Virus-induced gene silencing of *FtsH2* in wheat leaves induces bleaching phenotype. Wheat plants were treated with *Barley stripe mosaic virus* (BSMV) to induce silencing of target genes. **a)** Images were taken of newly emerged, symptomatic wheat leaves 22 days following inoculation with BSMV-VIGS constructs. Mock plants were treated with inoculation buffer only; BSMV:mcs4d construct possesses an empty multiple cloning site (mcs); BSMV:*asTaChlH*, BSMV:*asToxABP* and BSMV:*asFtsH2* target wheat *MAGNESIUM CHELATASE SUBUNIT H* (*ChlH*), *TOXA-BINDING PROTEIN* (*ToxABP*) and *FtsH2* for silencing, respectively. **b)** *FtsH2* and *ToxABP* gene expression in BSMV:*asFtsH2* lines and BSMV:*asToxABP* line vs control lines (mock and BSMV:mcs4d). * represents significant difference with $p < 0.05$. Error bars represent standard error for two biological replicates (BSMV:*asToxABP*) or four biological replicates (BSMV:*asFtsH2* and control).

Small but significant differences in first leaf length between wild-type Cadenza and Cadenza *Δstb6* lines, and between Cadenza *Δstb6* and the control Cadenza line R3694 R7P1 were observed in a pilot study. As previously stated, these differences could be the result of random variation between cv. Cadenza lines. However, this reduction in first leaf length displayed by wild-type Cadenza lines, which possess *Stb6*, relative to the gene-edited *Δstb6* lines, may also reflect subsequent morphological differences between Stb6 and non-Stb6 wheat cultivars. Very few agronomic traits have been linked to first leaf length. Those that have show a positive correlation between beneficial traits and longer first leaves (Zhao *et al*., 2019), as they reflect increased plant vigour and establishment speed. However, in rice the WAK *Xa4* has been shown to confer a small reduction in plant height, which in turn provides resistance to lodging (Hu *et al.*, 2017). It is possible that *Stb6* affects cell wall composition similarly to *Xa4* and provides similar morphological benefits. Such benefits would explain the retention of *Stb6* within commercial wheat lines, despite the widespread break-down of *Stb6*-mediated resistance to *Z. tritici* (Section 3.5.5, Chartrain *et al.*, 2005).

FtsH2 was found to be a high-confidence candidate interactor with the kinase domain of Stb6, based on a Y2H library screen. FtsH2 was first characterised in photosynthetic cyanobacteria, where it was shown to form a hetero-hexameric complex with a homologous protein FtsH3 (Boehm *et al*., 2012). In plants, FtsH2 is localised to the chloroplast, where it forms a similar hexameric complex with a homologuous FtsH5 protein in the thylakoid membrane (Sakamoto *et al*., 2003). There, this complex acts to digest and remove the photodamaged proteins associated with the photosystem II complex. The FtsH hexameric complex forms a single central pore, and it is hypothesised that the ATP-binding domains facilitate the extraction of target proteins from the lipid bilayer, their unfolding and transportation through the central pore for digestion by the protease domains (Niwa *et al*., 2002, Figure S5.8). The FtsH complex specifically degrades the D1 protein, which plays an essential role in the photosystem reaction centre and is prone to damage by light or oxidation (Kato *et al.*, 2009) and thus requires frequent recycling (Aro *et al*., 1993). FtsH complexes are also hypothesised to be involved in the maintenance of the

chloroplast thylakoid membrane (Kato *et al*., 2012, Zaltsman *et al*., 2005). The role of FtsH complexes in chloroplast stability and photosystem maintenance is supported by variegation phenotypes and photosensitivity observed in both Arabidopsis and *N. benthamiana*, following the silencing of *FtsH2* (Sakamoto *et al*., 2002). We have observed a similar phenotype in wheat (Figure 5.5), which supports a hypothesis for a conserved role for the FtsH complex in this species. Although at this time we were unable to complete a *Z. tritici* inoculation bioassay on *FtsH2*-silenced wheat leaves, we hypothesise that the downregulation of this gene, which plays an important role in chloroplast function, would compromise *Stb6*-mediated immunity in wheat to the otherwise avirulent *Z. tritici* isolate IPO323.

The virus-induced overexpression (VOX) of AvrStb6 in wheat has previously been reported to induce a bleaching phenotype in infected wheat leaves (Figure S4.9; Bouton C & Kanyuka K, *unpublished*). AvrStb6 putatively interacts with the wheat chloroplastic protein ToxABP (Section 4.5.2), possibly interfering with ToxABP function. Previous studies in which ToxABP has been silenced in wheat using BSMV-VIGS report phenotypes including necrosis, photobleaching and stunting of emerging leaves (Manning *et al*., 2010), whilst Arabidopsis *Thf1/ToxABP* mutant lines display a variegarion phenotype (Wang *et al.*, 2004). However, a similar photobleaching phenotype was not observed following BSMV:*asToxABP* treatment (Figure 5.5) and subsequent RT-qPCR analysis suggests that in this case *ToxABP* silencing was not efficient. It remains to be tested whether the successful silencing of *ToxABP* could induce a similar phenotype to that seen following overexpression of AvrStb6 in wheat. A similar phenotype would support the hypothesis that AvrStb6 inhibits ToxABP *in planta*.

We were not able to confirm the interaction between FtsH2 and Stb6 kinase, either in yeast or *in planta* (Figure 5.4 and S5.6). It is unclear why the Y2H assays failed to recreate the interaction observed in the commercial library screen, although it should be noted that the vectors used in the commercial screen were high copy number, whilst the vectors used in-house were low copy number. The higher copy number of the vectors used in the commercial screen could increase the assay sensitivity and thus identify interactions not detected

using the in-house assay. The *in planta* interaction between FtsH2 and Stb6 kinase may require Stb6 kinase activity. It has been observed in previous studies that RLK kinase activity is required for some protein-protein interactions. For example, Halter *et al*. (2014) observed that interactions both in yeast nucleus and *in planta* between Arabidopsis BAK1 and BAK1-INTERACTING RLK 2 (BIR2) were dependent on the kinase activity of BAK1. Unfortunately, the *in planta* interaction between the functional Stb6 kinase and FtsH2 cannot be tested following co-expression in *N. benthamiana*, due to Stb6 kinase-induced cell death observed in *N. benthamiana* (Section 5.5.2).

Although at this time the Stb6:GSrhino constructs could not be used to assess Stb6 protein interactions, this may be a possibility in the future. The increased specificity of the TAP tags would provide stronger candidates for putative interactors, and those interactions identified *in planta* would be more likely to be biologically relevant to *Stb6*-mediated immune signalling in wheat. The development of the Stb6:GSrhino tag series could therefore provide a useful tool for the future study of Stb6 protein-protein interactions, including the validation of interactions between Stb6 and FtsH2 *in planta*.

5.7 References

Anderson CM, Wagner TA, Perret M, He ZH, He DZ, Kohorn BD. 2001. WAKs: cell wall-associated kinases linking the cytoplasm to the extracellular matrix. *Plant Molecular Biology* **47**: 197-206.

Aro EM, McCaffery S, Anderson JM. 1993. Photoinhibition and D1 protein degradation in peas acclimated to different growth irradiances. *Plant Physiol*ogy **103**: 835-843.

Bender KW, Couto D, Kadota Y *et al.* 2021. Activation loop phosphorylaton of a non-RD receptor kinase initiates plant innate immune signaling. *Proceedings of the National Academy of Sciences, USA*, **118**: e2108242118.

Besbrugge N, Van Leene J, Eeckhout D *et al.* 2018. GS(yellow), a multifaceted tag for functional protein analysis in monocot and dicot plants. *Plant Physiology* **177**: 447-464.

Boehm M, Yu J, Krynicka V, Barker M, Tichy M, Komenda J, Nixon PJ, Nield J. 2012. Subunit organization of a *Synechocystis* hetero-oligomeric thylakoid FtsH complex involved in photosystem II repair. *Plant Cell* **24**: 3669-3683.

Brading PA, Verstappen ECP, Kema GHJ, Brown JKM. 2002. A gene-for-gene relationship between wheat and *Mycosphaerella graminicola*, the Septoria tritici blotch pathogen. *Phytopathology* **92**: 439-445.

Caplan JL, Kumar AS, Park E, Padmanabhan MS, Hoban K, Modla S, Czymmek K, Dinesh-Kumar SP. 2015. Chloroplast stromules function during innate immunity. *Developmental Cell* **34**: 45-57.

Chartrain, L., Brading, P.A. and Brown, J.K.M. (2005) Presence of the *Stb6* gene for resistance to Septoria tritici blotch (*Mycosphaerella graminicola*) in cultivars used in wheat-breeding programmes worldwide. *Plant Pathology* **54**, 134–143.

Cheng X, Lang I, Adeniji OS, Griffing L. 2017. Plasmolysis-deplasmolysis causes changes in endoplasmic reticulum form, movement, flow, and cytoskeletal association. *Journal of Experimental Botany* **68**: 4075-4087.

Couto D, Zipfel C. 2016. Regulation of pattern recognition receptor signalling in plants. *Nature Reviews Immunology* **16**: 537-552.

Dardick C, Schwessinger B, Ronald P. 2012. Non-arginine-aspartate (non-RD) kinases are associated with innate immune receptors that recognize conserved microbial signatures. *Current Opinion in Plant Biology* **15**: 358-366.

Dedecker M, Van Leene J, De Winne N *et al.* 2016. Transferring an optimized TAP-toolbox for the isolation of protein complexes to a portfolio of rice tissues. *Plant Molecular Biology* **91**: 341-354.

Delteil A, Gobbato E, Cayrol B, Estevan J, Michel-Romiti C, Dievart A, Kroj T, Morel JB. 2016. Several wall-associated kinases participate positively and negatively in basal defense against rice blast fungus. *BMC Plant Biology* **16**: 17.

Gomez-Gomez L, Boller T. 2000. FLS2: An LRR receptor-like kinase involved in the perception of the bacterial elicitor flagellin in Arabidopsis. *Molecular Cell* **5**: 1003-1011.

Gravino M, Locci F, Tundo S, Cervone F, Savatin DV, De Lorenzo G. 2017. Immune responses induced by oligogalacturonides are differentially affected by AvrPto and loss of BAK1/BKK1 and PEPR1/PEPR2. *Molecular Plant Pathology* **18**: 582-595.

Hahn F, Sanjurjo Loures L, Sparks CA, Kanyuka K, Nekrasov V. 2021. Efficient CRISPR/Cas-mediated targeted mutagenesis in spring and winter wheat varieties. *Plants* **10**: 1481.

Halter T, Imkampe J, Mazzotta S *et al.* 2014. The leucine-rich repeat receptor kinase BIR2 is a negative regulator of BAK1 in plant immunity. *Current Biology* **24**: 134-143.

Hanson MR, Sattarzadeh A. 2011. Stromules: recent insights into a long neglected feature of plastid morphology and function. *Plant Physiology* **155**: 1486-1492.

Heese A, Hann DR, Gimenez-Ibanez S, Jones AM, He K, Li, J., Schroeder JI, Peck SC, Rathjen JP. 2007. The receptor-like kinase SERK3/BAK1 is a central regulator of innate immunity in plants. *Proceedings of the National Academy of Sciences, USA* **104**: 12217-12222.

Hind SR, Strickler SR, Boyle PC *et al.* 2016. Tomato receptor FLAGELLIN-SENSING 3 binds flgII-28 and activates the plant immune system. *Nature Plants* **2**: 16128.

Holzberg S, Brosio P, Gross C, Pogue GP. 2002. *Barley stripe mosaic virus*-induced gene silencing in a monocot plant. *Plant Journal* **30**: 315-327.

Hu KM, Cao JB, Zhang J *et al.* 2017. Improvement of multiple agronomic traits by a disease resistance gene via cell wall reinforcement. *Nature Plants* **3**: 17009.

Hurst CH, Turnbull D, Myles SM, Leslie K, Keinath NF, Hemsley PA. 2018. Variable effects of C-terminal tags on FLS2 function - not all epitope tags are created equal. *Plant Physiology* **177**: 522-531.

Kaku H, Nishizawa Y, Ishii-Minami N, Akimoto-Tomiyama C, Dohmae N, Takio K, Minami E, Shibuya N. 2006. Plant cells recognize chitin fragments for defense signaling through a plasma membrane receptor. *Proceedings of the National Academy of Sciences, USA* **103**: 11086-11091.

Karki SJ, Reilly A, Zhou B, Mascarello M, Burke J, Doohan F, Douchkov D, Schweizer P, Feechan A. 2020. A small secreted protein from

Zymoseptoria tritici interacts with a wheat E3 ubiquitin to promote disease. *Journal of Experimental Botany* **72**: 733-746.

Kato Y, Kouso T, Sakamoto W. 2012. Variegated tobacco leaves generated by chloroplast FtsH suppression: implication of FtsH function in the maintenance of thylakoid membranes. *Plant Cell Physiology* **53**:, 391-404.

Kato Y, Miura E, Ido K, Ifuku K, Sakamoto W. 2009. The variegated mutants lacking chloroplastic FtsHs are defective in D1 degradation and accumulate reactive oxygen species. *Plant Physiology* **151**: 1790-1801.

Kubicek CP, Starr TL, Glass NL. 2014. Plant cell wall-degrading enzymes and their secretion in plant-pathogenic fungi. *Annual Review Phytopathology* **52**: 427-451.

Lal NK, Nagalakshmi U, Hurlburt NK *et al.* 2018. The receptor-like cytoplasmic kinase BIK1 localizes to the nucleus and regulates defense hormone expression during plant innate immunity. *Cell Host & Microbe* **23**: 485-497.

Lampugnani ER, Wink RH, Persson S, Somssich M. 2018. The toolbox to study protein-protein interactions in plants. *Critical Reviews in Plant Sciences* **37**: 308-334.

Larkan NJ, Lydiate DJ, Parkin IA, Nelson MN, Epp DJ, Cowling WA, Rimmer SR, Borhan MH. 2013. The *Brassica napus* blackleg resistance gene *LepR3* encodes a receptor-like protein triggered by the *Leptosphaeria maculans* effector AVRLM1. *New Phytologist* **197**: 595-605.

Larkan NJ, Ma L, Haddadi P, Buchwaldt M, Parkin IAP, Djavaheri M, Borhan MH. 2020. The *Brassica napus* wall-associated kinase-like (WAKL) gene *Rlm9* provides race-specific blackleg resistance. *Plant Journal* **104**: 892-900.

Lee WS, Rudd JJ, Kanyuka K. 2015. Virus induced gene silencing (VIGS) for functional analysis of wheat genes involved in *Zymoseptoria tritici* susceptibility and resistance. *Fungal Genetics and Biology* **79**: 84-88.

Li H, Zhou SY, Zhao WS, Su SC, Peng YL. 2009. A novel wall-associated receptor-like protein kinase gene, *OsWAK1*, plays important roles in rice blast disease resistance. *Plant Molecular Biology* **69**: 337-346.

Li J, Wen J, Lease KA, Doke JT, Tax FE, Walker JC. 2002. BAK1, an Arabidopsis LRR receptor-like protein kinase, interacts with BRI1 and modulates brassinosteroid signaling. *Cell* **110**: 213-222.

Li L, Li M, Yu LP *et al.* 2014. The FLS2-associated kinase BIK1 directly phosphorylates the NADPH oxidase RbohD to control plant immunity. *Cell Host & Microbe* **15**: 329-338.

Liebrand TW, Van den Burg HA, Joosten MH. 2014. Two for all: receptor-associated kinases SOBIR1 and BAK1. *Trends in Plant Science* **19**: 123-132.

Littlejohn GR, Breen S, Smirnoff N, Grant M. 2021. Chloroplast immunity illuminated. *New Phytologist*, **229**: 3088-3107.

Lu DP, Wu SJ, Gao XQ, Zhang YL, Shan LB, He P. 2010. A receptor-like cytoplasmic kinase, BIK1, associates with a flagellin receptor complex to initiate plant innate immunity. *Proceedings of the National Academy of Sciences, USA* **107**: 496-501.

Manning VA, Chu AL, Scofield SR, Ciuffetti LM. 2010. Intracellular expression of a host-selective toxin, ToxA, in diverse plants phenocopies silencing of a ToxA-interacting protein, ToxABP1. *New Phytologist* **187**: 1034-1047.

Manning VA, Hardison LK, Ciuffetti LM. 2007. Ptr ToxA interacts with a chloroplast-localized protein. *Molecular Plant-Microbe Interactions* **20**: 168-177.

Miya A, Albert P, Shinya T, Desaki Y, Ichimura K, Shirasu K, Narusaka Y, Kawakami N, Kaku H, Shibuya N. 2007. CERK1, a LysM receptor kinase, is essential for chitin elicitor signaling in Arabidopsis. *Proceedings of the National Academy of Sciences, USA* **104**: 19613-19618.

Nakamura S, Mano S, Tanaka Y *et al.* 2010. Gateway binary vectors with the bialaphos resistance gene, *bar*, as a selection marker for plant transformation. *Bioscience Biotechnology and Biochemistry* **74**: 1315-1319.

Nambara E, Marion-Poll A. 2005. Abscisic acid biosynthesis and catabolism. *Annual Review Plant Biology* **56**: 165-185.

Niwa H, Tsuchiya D, Makyio H, Yoshida M, Morikawa K. 2002. Hexameric ring structure of the ATPase domain of the membrane-integrated

metalloprotease FtsH from *Thermus thermophilus* HB8. *Structure* **10**: 1415-1423.

Park AR, Cho SK, Yun UJ, Jin MY, Lee SH, Sachetto-Martins G, Park OK. 2001. Interaction of the Arabidopsis receptor protein kinase WAK1 with a glycine-rich protein, AtGRP-3. *Journal of Biological Chemistry* **276**: 26688-26693.

Pfaffl MW. 2001. A new mathematical model for relative quantification in real-time RT-PCR. *Nucleic Acids Research* **29**: e45. DOI: 10.1093/nar/29.9.e45

Puig O, Caspary F, Rigaut G, Rutz B, Bouveret E, Bragado-Nilsson E, Wilm M, Seraphin B. 2001. The tandem affinity purification (TAP) method: A general procedure of protein complex purification. *Methods* **24**: 218-229.

Rekhter D, Ludke D, Ding Y, Feussner K, Zienkiewicz K, Lipka V, Wiermer M, Zhang Y, Feussner I. 2019. Isochorismate-derived biosynthesis of the plant stress hormone salicylic acid. *Science* **365**: 498-502.

Rep M, Van der Does HC, Meijer M, Van Wijk R, Houterman PM, Dekker HL, De Koster CG, Cornelissen BJC. 2004. A small, cysteine-rich protein secreted by *Fusarium oxysporum* during colonization of xylem vessels is required for *I-3*-mediated resistance in tomato. *Molecular Microbiology* **53**: 1373-1383.

Roux M, Schwessinger B, Albrecht C, Chinchilla D, Jones A, Holton N, Malinovsky FG, Tor M, De Vries S, Zipfel C. 2011. The Arabidopsis leucine-rich repeat receptor-like kinases BAK1/SERK3 and BKK1/SERK4 are required for innate immunity to hemibiotrophic and biotrophic pathogens. *Plant Cell* **23**: 2440-2455.

Saintenac C, Lee WS, Cambon F *et al.* 2018. Wheat receptor-kinase-like protein Stb6 controls gene-for-gene resistance to fungal pathogen *Zymoseptoria tritici*. *Nature Genetics* **50**: 368-374.

Sakamoto W, Tamura T, Hanba-Tomita Y, Murata M, Sodmergen. 2002. The VAR1 locus of Arabidopsis encodes a chloroplastic FtsH and is responsible for leaf variegation in the mutant alleles. *Genes Cells* **7**: 769-780.

Sakamoto W, Zaltsman A, Adam Z, Takahashi Y. 2003. Coordinated regulation and complex formation of YELLOW VARIEGATED1 and YELLOW VARIEGATED2, chloroplastic FtsH metalloproteases involved in the repair

cycle of photosystem II in Arabidopsis thylakoid membranes. *Plant Cell* **15**: 2843-2855.

Schwessinger B, Bahar O, THOMAS N *et al.* 2015. Transgenic expression of the dicotyledonous pattern recognition receptor EFR in rice leads to ligand-dependent activation of defense responses. *PLoS Pathogens* **11**: e1004872.

Schwessinger B, Roux M, Kadota Y, Ntoukakis V, Sklenar J, Jones A, Zipfel C. 2011. Phosphorylation-dependent differential regulation of plant growth, cell death, and innate immunity by the regulatory receptor-like kinase BAK1. *PLoS Genet*ics **7**: e1002046.

Song WY, Wang GL, Chen LL *et al.* 1995. A receptor kinase-like protein encoded by the rice disease resistance gene, *Xa21*. *Science* **270**: 1804-1806.

Sparks CA, Doherty A. 2020. Genetic transformation of common wheat (*Triticum aestivum L.*) using biolistics. *Methods in Molecular Biology* **2124**: 229-250.

Sun YD, Li L, Macho AP, Han ZF, Hu ZH, Zipfel C, Zhou JM, Chai JJ. 2013. Structural basis for flg22-induced activation of the Arabidopsis FLS2-BAK1 immune complex. *Science* **342**: 624-628.

Thomas NC, Oksenberg N, Liu FR, Caddell D, Nalyvayko A, Nguyen Y, Schwessinger B, Ronald PC. 2018. The rice XA21 ectodomain fused to the Arabidopsis EFR cytoplasmic domain confers resistance to *Xanthomonas oryzae* pv. *oryzae*. *PeerJ*, **6**: e4456.

Van Leene J, Eeckhout D, Cannoot B *et al.* 2015. An improved toolbox to unravel the plant cellular machinery by tandem affinity purification of Arabidopsis protein complexes. *Nature Protocols* **10**: 169-187.

Wang N, Huang HJ, Ren ST, Li JJ, Sun Y, Sun DY, Zhang SQ. 2012. The rice wall-associated receptor-like kinase gene *OsDEES1* plays a role in female gametophyte development. *Plant Physiology* **160**: 696-707.

Wang P, Zhou L, Jamieson P *et al*. 2020. The cotton wall-associated kinase GhWAK7A mediates responses to fungal wilt pathogens by complexing with the chitin sensory receptors. *Plant Cell* **32**: 3978-4001.

Wang Q, Sullivan RW, Kight A, Henry RL, Huang J, Jones AM, Korth KL. 2004. Deletion of the chloroplast-localized *Thylakoid formation1* gene

product in Arabidopsis leads to deficient thylakoid formation and variegated leaves. *Plant Physiology* **136**: 3594-3604.

Wasternack C, Song S. 2017. Jasmonates: biosynthesis, metabolism, and signaling by proteins activating and repressing transcription. *Journal of Experimental Botany* **68**: 1303-1321.

Wu X, Bacic A, Johnson KL, Humphries J. 2020. The role of *Brachypodium distachyon* wall-associated kinases (WAKs) in cell expansion and stress responses. *Cells* **9**: 2478.

Zaltsman A, Feder A, Adam Z. 2005. Developmental and light effects on the accumulation of FtsH protease in Arabidopsis chloroplasts--implications for thylakoid formation and photosystem II maintenance. *Plant Journal* **42**: 609-617.

Zhang N, Pombo MA, Rosli HG, Martin GB. 2020. Tomato wall-associated kinase SlWak1 depends on Fls2/Fls3 to promote apoplastic immune responses to *Pseudomonas syringae*. *Plant Physiology* **183**: 1869-1882.

Zhao Z, Rebetzke GJ, Zheng B, Chapman SC, Wang E. 2019. Modelling impact of early vigour on wheat yield in dryland regions. *Journal of Experimental Botany* **70**: 2535-2548.

Chapter 6: General Discussion and Outlook

The understanding of how genetic resistance in crop plants functions to suppress potential pathogens is essential for breeding more resilient and productive crops for future food consumption. In this study, I have investigated the function of the Septoria tritici blotch (STB) resistance protein Stb6, as well as its putative interaction with the corresponding *Zymoseptoria tritici* effector AvrStb6. *Z. tritici*, the causal agent of STB, is a global pathogen of wheat with a dramatic impact on potential yields. The *Stb6* resistance gene is one of only two Septoria resistance genes currently cloned (Upadhyaya *et al.*, 2021) and thus presents a promising insight into the mechanism of STB resistance in wheat. Here, I will discuss the findings from this study, their context within wider research and possible approaches for further studies.

6.1 Dramatic shifts in AvrStb6 isoform prevalence were observed in the global *Z. tritici* population

I have reported a dramatic shift in the global diversity of AvrStb6 isoforms relative to previous studies (Section 3.5.2; Brunner and McDonald, 2018, Zhong *et al.*, 2017). This appears to be part of a breakdown in the ability of *Stb6* to confer resistance against *Z. tritici*, in several regions globally. The appearance and spread of effector variants capable of evading widely deployed crop resistance genes has been observed previously. Resistance conferred by the *Rlm1* and *Rlm3* genes of oilseed rape (*Brassica napus*) to the stem canker pathogen *Leptosphaeria maculans* has been widely overcome, following the widespread use of these resistance genes in France and Canada, respectively (Rouxel *et al.*, 2003, Zhang *et al.*, 2016). More recently the breakdown of the *Stb16q* gene conferring broad spectrum STB resistance, has been reported in Ireland (Kildea *et al.*, 2020). The previously reported AvrStb6 avirulence isoform I01 was not identified in this *Z. tritici* population study. Only one other isoform, I13, was associated with reduced virulence on *Stb6* wheat compared to gene-edited *stb6*-knockout wheat lines (Section 3.5.4). These avirulence

isoforms have only a single consistent amino acid difference relative to virulence isoforms, at position 41. A previous study has utilised site-directed mutagenesis to demonstrate the importance of single mutations in the effector for recognition by the corresponding plant resistance gene. The detection of the *L. maculans* effector AvrLm4-7 by the Rlm4 resistance protein was shown to be dependent on a single amino acid change in the effector (Parlange *et al.*, 2009). In future, an avirulence *AvrStb6* gene construct possessing a point mutation corresponding to aa position 41 could be generated and transformed into the *Z. tritici* IPO323 Δ*avrstb6* mutant strain (Kema *et al.*, 2018). The virulence of the resulting *Z. tritici* transformants on *Stb6* wheat versus wild-type *Z. tritici* isolate IPO323 could determine the extent to which this amino acid polymorphism determines the *AvrStb6* virulence/avirulence phenotype.

The global prevalence of AvrStb6 isoform I02 (Section 3.5.2) may reflect its enhanced ability to evade detection by the Stb6 isoforms most commonly deployed in modern wheat. In this study I identified only a single resistance *Stb6* haplotype in elite wheat lines, with a low diversity of *Stb6* haplotypes observed in this study and in a larger survey of wheat varieties (Section 3.5.5; Saintenac *et al.*, 2018). This low diversity of *Stb6* haplotypes in commercial wheat varieties may drive a correspondingly low diversity of *AvrStb6* virulence alleles in *Z. tritici*. The absence of AvrStb6 I02 and increased *AvrStb6* genetic diversity in Turkey (Section 3.5.3) may reflect a corresponding increased diversity of *Stb6* haplotypes in the local wheat landraces grown in this region, following the so-called trench warfare model (Sanchez-Vallet *et al.*, 2018). It is possible that in Turkey *Stb6* may still offer a defence against local *Z. tritici* isolates. Future studies could focus on the ability of *Z. tritici* isolates identified in Turkey to infect *Stb6* wheat, as well as the diversity of *Stb6* haplotypes in Turkish wheat varieties. Analysis of *AvrStb6* diversity in *Z. tritici* isolates collected from other wheat-growing regions where STB is prevalent, such as Tunisia, Algeria and Israel, could also give a more complete picture of the current state of *Stb6* resistance breakdown globally, and determine the utility of deploying *Stb6* wheat in these regions to control STB.

6.2 AvrStb6 may disrupt host chloroplast functions

Chloroplasts are emerging as a central player in plant immunity (Yang *et al.*, 2021, Littlejohn *et al.*, 2021), being involved in the production of defence signalling hormones salicylic acid and jasmonic acid, as well as reactive oxygen species (ROS) (Serrano *et al.*, 2016, Wasternack and Song, 2017, Rekhter *et al.*, 2019). Chloroplast-derived ROS is thought to be involved in retrograde signalling from the chloroplast to the nucleus, inducing immune gene expression and in some cases a hypersensitive response (HR; Nomura *et al.*, 2012, Zurbriggen *et al.*, 2009). Calcium Sensing Receptor (CAS) is also localised to the chloroplasts and is involved in Ca^{2+} ion generation (Nomura *et al.*, 2008). CAS and calcium ion bursts are necessary for PAMP-triggered immunity (PTI)-related gene expression and other defence responses such as stomatal closure (Nomura *et al.*, 2012). These functions make chloroplasts an important intersection in immune signalling from the apoplast to the nucleus (Padmanabhan and Dinesh-Kumar, 2010), and consequently a major target of pathogen effectors to facilitate pathogenicity. Many examples of chloroplast localised effectors have been reported in previous studies (reviewed by Kretschmer *et al.*, 2019), although few have been identified for filamentous fungi. The effector Pst_12806 of the stripe rust fungus *Puccinia striiformis* f. sp. *tritici* (Pst) is translocated into host wheat cells and accumulates in chloroplasts. There, it interacts with the putative cytochrome b6-f complex component protein TaISP. Expression of Pst_12806 in *N. benthamiana* reduces callose deposition and immune-related gene expression as well as reducing aspects of photosynthesis such as the electron transport chain rate (Xu *et al.*, 2019).

The wheat chloroplastic protein Thylakoid formation 1/PtrToxA-binding protein 1 (Thf1/ToxABP) has been reported to interact with the *Pyrenophora tritici-repentis* necrotrophic effector PtrToxA (Manning *et al.*, 2007). ToxA homologues have also been identified in *Parastagonospora nodorum* and *Bipolaris sorokiniana* (McDonald *et al.*, 2018), suggesting that these effector homologues play an important conserved role in pathogen virulence. In this study, ToxABP was also found to be a putative interactor of AvrStb6 in Y2H studies (Section 4.5.2), although this is still to be validated *in planta*. ToxABP has been identified as a frequent target of pathogens and is also targeted by *P.*

syringae pv. *tomato* and *Tobamovirus* effectors (Littlejohn *et al.*, 2021), and the *P. syringae* phytotoxin COR1 (Wangdi *et al.*, 2010). ToxABP is also suggested to be involved in thylakoid membrane formation and photosystem maintenance, with Arabidopsis *ToxABP*-mutant lines showing severe stunting and leaf variegation (Wang *et al.*, 2004). Silencing of *ToxABP* in wheat resulted in chlorosis and necrosis of affected wheat leaves, with a similar phenotype observed following virus-induced overexpression (VOX) of ToxA in wheat leaves (Manning *et al.*, 2010). Although in the current study similar bleaching or necrosis phenotypes were not observed following VIGS of *ToxABP*, this is likely due to inefficient silencing (Section 5.5.7). I also observed no bleaching of *N. benthamiana* leaves, following the transient expression of AvrStb6 by Agroinfiltration (Section 4.5.5). Chlorosis was observed following ToxA expression in *N. benthamiana*, but only at 12 days post agroinfiltration (dpi; Manning *et al.*, 2010). Further studies to assess the phenotypes of *N. benthamiana* leaves at later timepoints following AvrStb6 transient expression would determine if this effector induces a similar phenotype to ToxA in this plant species.

ToxA expression within toxin-sensitive wheat cells results in cell death, reportedly accompanied by a ROS burst (Manning *et al.*, 2007, Manning and Ciuffetti, 2005). The death of host wheat cells benefits the necrotrophic fungi which express this effector. It is possible that AvrStb6, which induces a chlorosis phenotype when overexpressed in wheat leaves (Bouton C & Kanyuka K, *personal comm.*), also targets wheat ToxABP to induce disease susceptibility during *Z. tritici* infection of wheat. The peak in AvrStb6 expression corresponds to the appearance of necrosis in infected wheat leaves (Zhong *et al.*, 2017). The observation in this study that almost all *Z. tritici* isolates possessed virulence *AvrStb6* isoforms (Section 3.5.1) suggests an important function for the effector, as the retention of effector genes is unusual in *Z. tritici* (Hartmann and Croll, 2017). However, it should be noted that the IPO323 *Δavrstb6* mutant strain shows no reduction in virulence compared to wild-type IPO323 on wheat lines (Kema *et al.*, 2018). There are two homologues of AvrStb6 located on chromosome 10 in the *Z. tritici* genome (Brunner and McDonald, 2018), which present possible candidates for functional redundancy

of AvrStb6. In future studies, a yeast two-hybrid library screen using ToxABP as a bait, against a cDNA library of proteins secreted by *Z. tritici* during wheat infection, could be carried out. This might identify other putative *Z. tritici* ToxABP-interacting effectors, which may share the hypothesised AvrStb6 function.

In *N. benthamiana* AvrStb6 appears to localise to the apoplast, not to chloroplasts (Section 4.5.6). However, as discussed previously, this could be due to AvrStb6 translocation requiring a wheat-specific mechanism. In oomycetes, some effectors include an N-terminal RxLR motif which is thought to be necessary for internalisation into host cells (Whisson *et al.*, 2007). However, in ascomycete fungi no such conserved translocation motif has yet been recognised (Petre and Kamoun, 2014). The PtrToxA effector has been shown to contain an RGD motif required for translocation (Manning *et al.*, 2008), but this is not conserved across fungal effectors. The relatively large mRFP tag may also be responsible for inhibiting AvrStb6 translocation, or may be cleaved from the effector prior to translocation. However, other effectors fused to the yellow fluorescent protein (YFP), such as CSEP0139 and CSEP0182 of *Blumeria graminis* f. sp. *tritici* (Li *et al.*, 2021), were found to localise to the cytoplasm and nucleus when expressed in *N. benthamiana* cells. This suggests that, for some effectors, the relative size of the fluorophore tag does not inhibit the correct translocation and localisation of effectors within plant cells, although translocation to chloroplasts specifically may be inhibited by large tags. AvrStb6 localisation could be re-examined in future experiments following expression of effector-fluorophore fusion protein in wheat. This could be carried out by VOX of the AvrStb6-fluorophore construct in wheat (Bouton *et al.*, 2018), or by particle bombardment of wheat tissue (Sparks and Doherty, 2020). Alternatively, the AvrStb6-fluorophore fusion protein could be generated in an organism such *Pichia pastoris*, purified and infiltrated into wheat leaves. These experiments could determine the localisation of AvrStb6 in a more biologically relevant setting.

6.3 How could Stb6 interact with FtsH2 *in planta*?

In this study, a high-confidence interaction in yeast was identified between the kinase domain of Stb6 and the chloroplastic protein FtsH2 (Section 5.5.5). FtsH2 and the FtsH complex localises to the thylakoid membrane (Sakamoto *et al.*, 2002), an internal membrane within chloroplasts, whilst Stb6 localises to the plasma membrane (Section 5.5.3). Therefore, it is not immediately obvious how these two proteins could interact *in planta* without trafficking of one or both proteins outside of their regular localisation sites. Whilst no evidence yet exists for the movement of either protein between cell compartments *in planta*, changes in cell physiology during plant infection could provide clues to a possible mechanism for Stb6-FtsH2 interaction. Chloroplasts are highly motile, utilising membrane extensions known as stromules to move along actin filaments within cells (Kumar *et al.*, 2018). Chloroplasts move in response to light levels, migrating upwards to the periclinal plasma membrane under low light conditions to optimise photosynthetic efficiency and moving down away from the periclinal membrane under high light to avoid photodamage (Wada, 2016). Chloroplasts also often move in response to infection. Some studies observe chloroplast accumulation around the nucleus during defence responses, driven by ROS production (Ding *et al.*, 2019). Other studies suggest that chloroplasts can localise around sites of infection. Toufexi *et al.* (2021) identified that chloroplasts of *N. benthamiana* cells surround and interact with haustoria formed by the potato blight pathogen *Phytophthora infestans* during infection. This study also suggested that chloroplast localisation in response to infection is mediated by plasma membrane proteins, with VIGS-induced silencing of *BAK1* in potato cells reducing the formation of stromules and relocalisation of chloroplasts to haustoria. In Arabidopsis, the movement of chloroplasts within epidermal cells towards the site of infection has also been shown to contribute to non-host resistance against fungal pathogens (Irieda and Takano, 2021). As well as facilitating movement, chloroplast stromules have been shown to be involved in ROS signalling from chloroplasts to the nucleus (Caplan *et al.*, 2015) and in protein exchange between plastids (Hanson and Sattarzadeh, 2011).

PRRs have previously been shown to be internalised following ligand detection (Robatzek *et al.*, 2006). Endocytosis of receptors frequently occurs for protein recycling, but is also at least partially required for inducing immune responses (Robatzek, 2014). Both plant and viral proteins have been shown to shift localisation between the plasma membrane and the chloroplast. Medina-Puche *et al.* (2020) carried out analyses for proteins expressed in Arabidopsis, tomato (*Solanum lycopersicum*) and rice (*Oryza sativa*) which possessed an N-myristoylation motif and a chloroplast transit peptide (cTP) and were involved in immune signalling, identifying a large number of protein kinases fitting these characteristics in each plant species. One of these proteins, CPK16 of Arabidopsis, was found to localise to the plasma membrane but relocalised to chloroplasts following treatment of the plants with elicitors such as flg22 (Medina-Puche *et al.*, 2020, Stael *et al.*, 2011). Similarly, the C4 protein of the *Tomato yellow leaf curl virus* localises to the host plasma membrane under basal conditions, where it plays a role in disrupting host plant miRNA transfer through plasmodesmata. However, following the activation of plant defence signalling, C4 is relocalised to the chloroplast where it interacts with CAS to suppress downstream defence responses (Medina-Puche *et al.*, 2020). It is possible that this mechanism or one similar is utilised by Stb6, to relocalise to the chloroplast following detection of AvrStb6. However, chloroplast relocalising proteins have previously been shown to contain a cTP and analysis of Stb6, carried out using ChloroP 1.1 (Emanuelsson *et al.*, 1999; http://www.cbs.dtu.dk/services/ChloroP/) and LOCALIZER (Sperschneider *et al.*, 2017; http://localizer.csiro.au/) identified no cTP in Stb6. As previously discussed for AvrStb6 (Section 4.6), the Stb6-FtsH2 interaction could also occur in the cytoplasm. The *in planta* interaction between the tomato resistance protein N' and ToxABP, which is required for a defence response, was found to occur in the cytosol (Hamel *et al.*, 2016). Future studies could assess the localisation of Stb6 in transgenic wheat cells expressing an Stb6-fluorophore construct, before and after *Z. tritici* infection.

6.4 A possible model for *Stb6*-mediated defence

As discussed above, ToxABP was identified as a putative interactor of AvrStb6 in this study, whilst a yeast two-hybrid library screen using Stb6 kinase as a bait identified FtsH2 as a high-confidence interaction candidate. Intriguingly, previous studies have identified that, in the photosynthetic cyanobacterium *Synechocystis* sp. PCC6803 a homologue of ToxABP, Psb29, interacts with FtsH2 and is required for its normal accumulation (Bečková *et al.*, 2017). This supports other observations that Thf1 is required for normal FtsH2 accumulation in Arabidopsis (Wu *et al.*, 2013). A variegation phenotype is observed following the silencing or mutation of *FtsH2* in Arabidopsis (Sakamoto *et al.*, 2003), *N. benthamiana* (Kato *et al.*, 2012) and in wheat, as shown in this study (Section 5.5.7). Indeed, accompanying suppression of *FtsH2* in ToxABP-silenced plants may also contribute to the observed variegation phenotype following VIGS of ToxABP. The interaction between ToxABP and FtsH2 is hypothesised to be conserved in higher plants (Bečková *et al.*, 2017, Lu, 2016). This, together with the observations made in this study, suggest a connection between the hypothesised interactions of AvrStb6, ToxABP, FtsH2 and Stb6 that could affect the disease outcome of wheat infection by *Z. tritici* (Figure 6.1).

It is currently unclear how a putative Stb6-FtsH2 interaction would affect the activity and stability of the FtsH protein complex, and how this interaction might lead to the resistance observed following the inoculation of avirulent *Z. tritici* isolates such as IPO323 onto *Stb6* wheat. Increased stabilisation of the FtsH complex enhances the PSII repair cycle (Silva *et al.*, 2003, Kato and Sakamoto, 2019). Stael *et al.* (2012) found that both FtsH2 and FtsH5, with which FtsH2 forms a complex in Arabidopsis, are phosphorylated in a calcium-dependent manner. FtsH proteins have been shown to have high rates of turnover (Li *et al.*, 2017, Kato *et al.*, 2018) and FtsH protein level were shown to decrease following phosphatase treatment, suggesting that dephosphorylated FtsH complexes have decreased stability (Kato and Sakamoto, 2019). Stb6 kinase activity, which is required for *Stb6*-mediated resistance (Saintenac *et al.*, 2018), could mediate phosphorylation of proteins in the FtsH complex, increasing their activity or stability. This hypothesised Stb6 function would counter the proposed

function of AvrStb6 (above), in which AvrStb6 suppresses the activity of ToxABP and hence decreases FtsH complex formation.

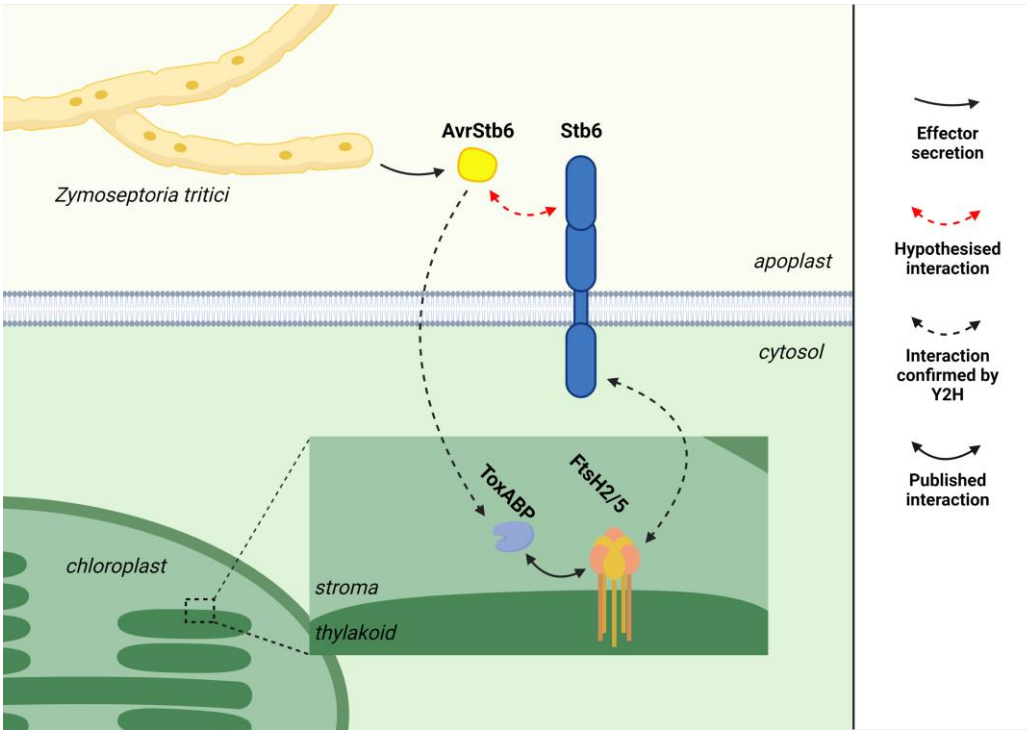

Figure 6.1: Schematic representation of the putative interactions of Stb6 and AvrStb6 with chloroplastic proteins. Yeast two hybrid (Y2H) studies identified Ptr ToxA Binding Protein (ToxABP) as an interactor of AvrStb6 and FtsH2 as a strong candidate interactor for the functional Stb6 kinase domain. Bečková *et al.* (2017) identified a putative interaction between ToxABP and FtsH2 in the cyanobacterium *Synechocystis* sp. PCC6803, which is hypothesised to be conserved in higher plants. Both ToxABP and FtsH2 are involved in photosystem function and maintenance. A direct interaction between AvrStb6 and Stb6 is hypothesised.

Histological studies of compatible and incompatible wheat-*Z. tritici* interactions suggest that *Stb6*-mediated defence is associated with an accumulation of H_2O_2 in the substomatal cavity, corresponding to the initial penetration of avirulent *Z. tritici* hyphae through the stomata (Shetty *et al.*, 2003). Hyphal growth is subsequently restricted to the substomatal cavity, preventing successful infection. At similar timepoints during compatible interactions, very little H_2O_2 accumulation was observed. Arabidopsis *FtsH2* mutant lines appear to accumulate significantly higher levels of ROS, compared to the wild type

(Kato *et al.*, 2009). In tobacco, a decrease in *FtsH* expression corresponds to the induction of HR, providing resistance to infection by *Tobacco mosaic virus* (TMV; Seo *et al.*, 2000). Whilst *Stb6*-mediated defence is not accompanied by HR, it has been hypothesised that, in some cases plants may deliberately downregulate chloroplast FtsH activity to produce ROS in response to stress. It could therefore be hypothesised that Stb6 may downregulate FtsH2, inducing the production of ROS upon pathogen infection to suppress hyphal growth.

In contrast to early timepoints of compatible wheat-*Z. tritici* interactions, where little ROS production is observed, the onset of necrosis at 11-15 dpi is associated with a ROS burst, along with other symptoms of programmed cell death (PCD; Shetty *et al.*, 2003, Keon *et al.*, 2007). As has been discussed above (Section 1.4.7), trade-offs in resistance to pathogens of different lifestyles are common. In this case it is possible that Stb6 and AvrStb6, hypothesised interact with proteins in the same chloroplastic complex, induce similar defence responses, but at different timepoints of infection. The Stb6-mediated induction of this response at early timepoints may benefit the plant, restricting hyphal growth immediately following stomatal penetration, whilst AvrStb6-mediated induction later in the infection cycle benefits the pathogen, inducing host cell death and the release of nutrients once the fungus is established within the host plant. Currently, there is little evidence for this “temporal trade-off” hypothesis. Further investigations into the characteristics of *Stb6*-mediated incompatible and compatible interactions could identify if there is any change in accumulation of FtsH complexes over the course of infection, and whether differences in FtsH accumulation contribute to disease outcomes.

6.5 Is there a direct Stb6-AvrStb6 interaction?

In this study we identified no evidence for a direct interaction between Stb6 and AvrStb6. However, as stated previously (Section 4.1), absence of evidence is not evidence of absence. As discussed (Section 4.6), the Y2H system is not ideal for studying interactions between secreted proteins. The size or orientation of fluorophore tags and their observed cleavage from the proteins of interest (Section 4.5.7) may also have inhibited detection of Stb6-AvrStb6

interactions during *in planta* studies. The hypothesised model for the mechanism of *Stb6*-mediated immunity (above), in which both proteins interact with chloroplastic proteins, does not preclude a direct Stb6-AvrStb6 interaction in the apoplast.

As has been previously discussed (Section 4.6), other studies have identified CSIR-elicitor interactions using Co-IP. Flg22, the flagellin epitope responsible for FLS2-mediated immune responses (Chinchilla *et al.*, 2006) was bound to glutathione-S-transferase (GST) tags, which were in turn bound to Glutathione Sepharose 4B (GS4B) agarose beads. With these beads it was possible to pull down FLS2 in immunoprecipitation studies (Sun *et al.*, 2013), demonstrating FLS2-flg22 interaction. The study also demonstrated that FLS2-flg22 interaction triggered the formation of FLS2-BAK1 heterodimers, and also identified specific residues in the FLS2 ectodomain required for flg22 binding. Other studies have utilised cross-linking or tag transfer between ligand and receptor to increase interaction assay sensitivity, and to detect potentially transient interactions. Hind *et al.* (2016) demonstrated the specific binding of flgII-28 to FLS3 of tomato. FlgII-28 probes (flgII-28*) were generated, tagged with both a UV irradiation-triggered crosslinking moiety and an alkyne handle, which allows for transfer of a biotin tag to interacting proteins. The use of crosslinking or biotin labelling may present a more fruitful approach to detecting the Stb6-AvrStb6 interaction, which may be transient. Importantly, as demonstrated in other studies using flgII-28* (Hind *et al.*, 2016) and in a study investigating the interaction between csp22, a peptide derivative of bacterial cold-shock proteins (CSPs; Wang *et al.*, 2016) and the tomato COLD SHOCK PROTEIN RECEPTOR (CORE), the correct biological activity of ligands following tagging must be demonstrated, to validate the biological relevance of the interaction. In future, the correct function of AvrStb6, and its gene-for-gene interaction with *Stb6*, when fused to mRFP could be validated by the transformation of *Z. tritici* isolates otherwise virulent on *Stb6* wheat with AvrStb6:mRFP constructs. Avirulence of these transformants on *Stb6* wheat would demonstrate that the mRFP tag doesn't impede AvrStb6 function.

More recently developed technologies, such as Turbo ID and miniTurbo (Branon *et al.*, 2018) could also be used to investigate AvrStb6-Stb6

interactions. The TurboID system has been adapted for use in plant model systems (Arora *et al.*, 2020), including in *N. benthamiana* to detect interactions of intracellular immune receptors (Zhang *et al.*, 2019). Further developments in the TurboID system, such as the use of split-Turbo ID (Cho *et al.*, 2020) could also be used to validate putative interactions. The miniTurbo biotin ligase is only 28kDa in size (Branon *et al.*, 2018), making it more likely to not impede the regular function of AvrStb6 when expressed as a protein fusion *in planta*. An AvrStb6-miniTurbo tag fusion protein is also within the size limit for virus-induced overexpression (VOX) of protein constructs in wheat using the recently developed *Foxtail mosaic virus* system (Bouton *et al.*, 2018). This makes VOX of AvrStb6 with a proximity tag a possibility for future studies to investigate AvrStb6 interactions in wheat.

CRISPR/Cas9 technology has also been used in generating tagged proteins for protein interaction studies. The in-locus addition of epitope tags to transcription factors (TFs) in mouse cells has been carried out using CRISPR/Cas9-mediated homologous recombination (Savic *et al.*, 2015), followed by Chip-seq to identify TF binding sites across the genome. This system reduces the possibility of false positive interactions resulting from the overexpression of tagged protein constructs, as constructs remain under their endogenous promoters. As CRISPR-Cas9 has already been developed in wheat (Hahn *et al.*, 2020) and in filamentous fungi (Munoz *et al.*, 2019, Schuster and Kahmann, 2019), this approach could also provide a future avenue for protein-protein interaction research in wheat or *Z. tritici*. The development of C-terminally tagged Stb6 with GSrhino (Section 5.5.1) also offers a strategy for future investigations of Stb6 protein-protein interactions, be that with AvrStb6 or other proteins. Affinity purification/mass spectrometry (AP/MS) is incrasingly used to understand protein complexes *in planta*, and tandem affinity purification tags such as GSrhino increase the specificity with which interactions can be detected (Bontinck *et al.*, 2018). These systems could be used to identify protein interactors with Stb6:GSrhino following its transient expression in *N. benthamiana*, or possibly in wheat lines stably transformed with the fusion construct (Sparks and Doherty, 2020). There therefore remain many avenues

for the future investigation of Stb6 and AvrStb6 interactions, utilisng the array of technologies discussed.

6.6 Main findings from this study

In this study, I have reported on a number of findings pertinent to our understanding of *Stb6*-mediated immunity in wheat, the putative virulence function of AvrStb6 and the possible protein-protein interactions of both:

- In the global *Z. tritici* population, *AvrStb6* has apparently adapted to evade recognition by the wheat Stb6 protein. The nature of this pathogen evolution, in which non-synonymous mutations were introduced rather than the widespread elimination of the effector from the fungal genome, suggests an important function for AvrStb6.

- AvrStb6 putatively interacts with ToxABP, under yeast nucleus conditions. This suggests that AvrStb6 plays a role in pathogenicity in which it interferes with chloroplast function.

- FtsH2 is a strong candidate interactor of Stb6. If the interaction between Stb6 and FtsH2 can be validated *in planta* this would, as far as I am aware, represent an entirely novel mechanism of immunity mediated by CSIRs.

- No direct interaction has yet been identified between Stb6 and AvrStb6. However, I have highlighted new approaches that could be taken both to further test for this interaction, as well as other interactions that Stb6 and AvrStb6 may be involved in.

It is hoped that these findings and the others reported in this thesis can contribute to advancing the understanding of plant immunity mechanisms, which may in future be utilised to breed more resilient crops.

6.7 References

Arora D, Abel NB, Liu C *et al.* 2020. Establishment of proximity-dependent biotinylation approaches in different plant model systems. *Plant Cell* **32**: 3388-3407.

Bečková M, Yu J, Krynicka V, Kozlo A, Shao S, Konik P, Komenda J, Murray JW, Nixon PJ. 2017. Structure of Psb29/Thf1 and its association with the FtsH protease complex involved in photosystem II repair in cyanobacteria. *Philosophical Transactions of the Royal Society B: Biological Sciences* **372**: 20160394.

Bontinck M, Van Leene J, Gadeyne A, De Rybel B, Eeckhout D, Nelissen H, De Jaeger G. 2018. Recent trends in plant protein complex analysis in a developmental context. *Frontiers in Plant Science* **9**: 640.

Bouton C, King RC, Chen H, Azhakanandam K, Bieri S, Hammond-Kosack KE, Kanyuka K. 2018. *Foxtail mosaic virus*: A viral vector for protein expression in cereals. *Plant Physiology* **177**: 1352-1367.

Branon TC, Bosch JA, Sanchez AD, Udeshi ND, Svinkina T, Carr SA, Feldman JL, Perrimon N, Ting AY. 2018. Efficient proximity labeling in living cells and organisms with TurboID. *Nature Biotechnology* **36**: 880-887.

Brunner PC, McDonald BA. 2018. Evolutionary analyses of the avirulence effector AvrStb6 in global populations of *Zymoseptoria tritici* identify candidate amino acids involved in recognition. *Molecular Plant Pathology* **19**: 1836-1846.

Caplan JL, Kumar AS, Park E, Padmanabhan MS, Hoban K, Modla S, Czymmek K, Dinesh-Kumar SP. 2015. Chloroplast stromules function during innate immunity. *Developmental Cell* **34**: 45-57.

Chinchilla D, Bauer Z, Regenass M, Boller T, Felix G. 2006. The *Arabidopsis* receptor kinase FLS2 binds flg22 and determines the specificity of flagellin perception. *Plant Cell* **18**: 465-476.

Cho KF, Branon TC, Udeshi ND, Myers SA, Carr SA, Ting AY. 2020. Proximity labeling in mammalian cells with TurboID and split-TurboID. *Nature Protocols* **15**: 3971-3999.

Emanuelsson O, Nielsen H, Von Heijne G. 1999. ChloroP, a neural network-based method for predicting chloroplast transit peptides and their cleavage sites. *Protein Science* **8**: 978-984.

Hahn F, Korolev A, Sanjurjo Loures L, Nekrasov V. 2020. A modular cloning toolkit for genome editing in plants. *BMC Plant Biology* **20**: 179.

Hamel LP, Sekine KT, Wallon T, Sugiwaka Y, Kobayashi K, Moffett P. 2016. The chloroplastic protein THF1 interacts with the coiled-coil domain of the disease resistance protein N' and regulates light-dependent cell death. *Plant Physiology* **171**: 658-674.

Hanson MR, Sattarzadeh A. 2011. Stromules: recent insights into a long neglected feature of plastid morphology and function. *Plant Physiol*ogy **155**: 1486-1492.

Hartmann FE, Croll D. 2017. Distinct trajectories of massive recent gene gains and losses in populations of a microbial eukaryotic pathogen. *Molecular Biology and Evolution* **34**: 2808-2822.

Hind SR, Strickler SR, Boyle PC *et al.* 2016. Tomato receptor FLAGELLIN-SENSING 3 binds flgII-28 and activates the plant immune system. *Nature Plants* **2**: 16128.

Irieda H, Takano Y. 2021. Epidermal chloroplasts are defense-related motile organelles equipped with plant immune components. *Nature Communications* **12**: 2739.

Kato Y, Hyodo K, Sakamoto W. 2018. The Photosystem II repair cycle requires FtsH turnover through the EngA GTPase. *Plant Physiology* **178**: 596-611.

Kato Y, Kouso T, Sakamoto W. 2012. Variegated tobacco leaves generated by chloroplast FtsH suppression: implication of FtsH function in the maintenance of thylakoid membranes. *Plant Cell Physiology* **53**: 391-404.

Kato Y, Miura E, Ido K, Ifuku K, Sakamoto W. 2009. The variegated mutants lacking chloroplastic FtsHs are defective in D1 degradation and accumulate reactive oxygen species. *Plant Physiology* **151**: 1790-1801.

Kato Y, Sakamoto W. 2019. Phosphorylation of the chloroplastic metalloprotease FtsH in *Arabidopsis* characterized by Phos-Tag SDS-PAGE. *Frontiers in Plant Science* **10**: 1080.

Kema GHJ, Gohari AM, Aouini L *et al.* 2018. Stress and sexual reproduction affect the dynamics of the wheat pathogen effector AvrStb6 and strobilurin resistance. *Nature Genetics* **50**: 375-380.

Keon J, Antoniw J, Carzaniga R, Deller S, Ward JL, Baker JM, Beale MH, Hammond-Kosack K, Rudd JJ. 2007. Transcriptional adaptation of *Mycosphaerella graminicola* to programmed cell death (PCD) of its susceptible wheat host. *Molecular Plant-Microbe Interactions* **20**: 178-193.

Kildea S, Byrne JJ, Cucak M, Hutton F. 2020. First report of virulence to the septoria tritici blotch resistance gene *Stb16q* in the Irish *Zymoseptoria tritici* population. *New Disease Reports* **41**: 13-13.

Kretschmer M, Damoo D, Djamei A, Kronstad J. 2019. Chloroplasts and plant immunity: where are the fungal effectors? *Pathogens* **9**: 19.

Kumar AS, Park E, Nedo A *et al.* 2018. Stromule extension along microtubules coordinated with actin-mediated anchoring guides perinuclear chloroplast movement during innate immunity. *Elife* **7**. DOI: 10.7554/eLife.23625.001

Li L, Nelson CJ, Trosch J, Castleden I, Huang S, Millar AH. 2017. Protein degradation rate in *Arabidopsis thaliana* leaf growth and development. *Plant Cell* **29**: 207-228.

Li X, Jin C, Yuan H, Huang W, Liu F, Fan R, Xie J, Shen Q. 2021. The barley powdery mildew effectors CSEP0139 and CSEP0182 suppress cell death and promote *B. graminis* fungal virulence in plants. *Phytopathology Research* **3**: 7.

Littlejohn GR, Breen S, Smirnoff N, Grant M. 2021. Chloroplast immunity illuminated. *New Phytologist* **229**: 3088-3107.

Lu Y. 2016. Identification and roles of photosystem II assembly, stability, and repair factors in *Arabidopsis*. *Frontiers in Plant Science* **7**: 168.

Manning VA, Chu AL, Scofield SR, Ciuffetti LM. 2010. Intracellular expression of a host-selective toxin, ToxA, in diverse plants phenocopies silencing of a ToxA-interacting protein, ToxABP1. *New Phytologist* **187**: 1034-1047.

Manning VA, Ciuffetti LM. 2005. Localization of Ptr ToxA produced by *Pyrenophora tritici-repentis* reveals protein import into wheat mesophyll cells. *Plant Cell* **17**: 3203-3212.

Manning VA, Hamilton SM, Karplus PA, Ciuffetti LM. 2008. The Arg-Gly-Asp-containing, solvent-exposed loop of Ptr ToxA is required for internalization. *Molecular Plant Microbe Interactions* **21**: 315-325.

Manning VA, Hardison LK, Ciuffetti LM. 2007. Ptr ToxA interacts with a chloroplast-localized protein. *Molecular Plant Microbe Interactions* **20**: 168-177.

McDonald MC, Ahren D, Simpfendorfer S, Milgate A, Solomon PS. 2018. The discovery of the virulence gene *ToxA* in the wheat and barley pathogen *Bipolaris sorokiniana*. *Molecular Plant Pathology* **19**: 432-439.

Medina-Puche L, Tan, H, Dogra V *et al.* 2020. A defense pathway linking plasma membrane and chloroplasts and co-opted by pathogens. *Cell* **182**: 1109-1124 e25.

Munoz IV, Sarrocco S, Malfatti L, Baroncelli R, Vannacci G. 2019. CRISPR-Cas for fungal genome editing: a new tool for the management of plant diseases. *Frontiers in Plant Science* **10**: 135. DOI: 10.3389/fpls.2019.00135.

Nomura H, Komori T, Kobori M, Nakahira Y, Shiina T. 2008. Evidence for chloroplast control of external Ca^{2+}-induced cytosolic Ca^{2+} transients and stomatal closure. *Plant Journal* **53**: 988-998.

Nomura H, Komori T, Uemura S *et al.* 2012. Chloroplast-mediated activation of plant immune signalling in *Arabidopsis*. *Nature Communications* **3**: 926.

Padmanabhan MS, Dinesh-Kumar SP. 2010. All hands on deck-the role of chloroplasts, endoplasmic reticulum, and the nucleus in driving plant innate immunity. *Molecular Plant Microbe Interactions* **23**: 1368-1380.

Parlange F, Daverdin G, Fudal I, Kuhn ML, Balesdent MH, Blaise F, Grezes-Besset B, Rouxel T. 2009. *Leptosphaeria maculans* avirulence gene *AvrLm4-7* confers a dual recognition specificity by the *Rlm4* and *Rlm7* resistance genes of oilseed rape, and circumvents *Rlm4*-mediated recognition through a single amino acid change. *Molecular Microbiology* **71**: 851-863.

Petre B, Kamoun S. 2014. How do filamentous pathogens deliver effector proteins into plant cells? *PloS Biology* **12**: e1001801.

Rekhter D, Ludke D, Ding Y, Feussner K, Zienkiewicz K., Lipka V, Wiermer M, Zhang Y, Feussner I. 2019. Isochorismate-derived biosynthesis of the plant stress hormone salicylic acid. *Science* **365**: 498-502.

Robatzek S. 2014. Endocytosis: at the crossroads of pattern recognition immune receptors and pathogen effectors. *Applied Plant Cell Biology* **22**: 273-297.

Robatzek S, Chinchilla D, Boller T. 2006. Ligand-induced endocytosis of the pattern recognition receptor FLS2 in *Arabidopsis*. *Genes & Development* **20**: 537-542.

Rouxel T, Penaud A, Pinochet X, Brun H, Gout L, Delourme R, Schmit J, Balesdent MH. 2003. A 10-year survey of populations of *Leptosphaeria maculans* in France indicates a rapid adaptation towards the *Rlm1* resistance gene of oilseed rape. *European Journal of Plant Pathology* **109**: 871-881.

Saintenac C, Lee WS, Cambon F *et al.* 2018. Wheat receptor-kinase-like protein Stb6 controls gene-for-gene resistance to fungal pathogen *Zymoseptoria tritici*. *Nature Genetics* **50**: 368-374.

Sakamoto W, Tamura T, Hanba-Tomita Y, Murata M, Sodmergen. 2002. The *VAR1* locus of *Arabidopsis* encodes a chloroplastic FtsH and is responsible for leaf variegation in the mutant alleles. *Genes to Cells* **7**: 769-780.

Sakamoto W, Zaltsman A, Adam Z, Takahashi Y. 2003. Coordinated regulation and complex formation of YELLOW VARIEGATED1 and YELLOW VARIEGATED2, chloroplastic FtsH metalloproteases involved in the repair cycle of photosystem II in *Arabidopsis* thylakoid membranes. *Plant Cell* **15**: 2843-2855.

Sanchez-Vallet A, Fouche S, Fudal I, Hartmann FE, Soyer JL, Tellier A, Croll D. 2018. The genome biology of effector gene evolution in filamentous plant pathogens. *Annual Review of Phytopathology* **56**: 21-40.

Savic D, Partridge EC, Newberry KM, Smith SB, Meadows SK, Roberts BS, Mackiewicz M, Mendenhall EM, Myers R. M. 2015. CETCh-seq: CRISPR epitope tagging ChIP-seq of DNA-binding proteins. *Genome Research* **25**: 1581-1589.

Schuster M, Kahmann R. 2019. CRISPR-Cas9 genome editing approaches in filamentous fungi and oomycetes. *Fungal Genetics and Biology* **130**: 43-53.

Seo S, Okamoto M, Iwai T, Iwano M, Fukui K, Isogai A, Nakajima N, Ohashi Y. 2000. Reduced levels of chloroplast FtsH protein in *tobacco mosaic virus*-

infected tobacco leaves accelerate the hypersensitive reaction. *Plant Cell* **12**: 917-932.

Serrano I, Audran C, Rivas S. 2016. Chloroplasts at work during plant innate immunity. *Journal of Experimental Botany* **67**: 3845-3854.

Shetty NP, Kristensen BK, Newman MA, Moller K, Gregersen PL, Jorgensen HJL. 2003. Association of hydrogen peroxide with restriction of *Septoria tritici* in resistant wheat. *Physiological and Molecular Plant Pathology* **62**: 333-346.

Silva P, Thompson E, Bailey S, Kruse O, Mullineaux CW, Robinson C, Mann NH, Nixon PJ. 2003. FtsH is involved in the early stages of repair of photosystem II in *Synechocystis* sp PCC 6803. *Plant Cell* **15**: 2152-2164.

Sparks CA, Doherty A. 2020. Genetic transformation of common wheat (*Triticum aestivum* L.) using biolistics. *Methods in Molecular Biology* **2124**: 229-250.

Sperschneider J, Catanzariti AM, DeBoer K, Petre B, Gardiner DM, Singh KB, Dodds PN, Taylor JM. 2017. LOCALIZER: subcellular localization prediction of both plant and effector proteins in the plant cell. *Scientific Reports* **7**: 44598.

Stael S, Bayer RG, Mehlmer N, Teige M. 2011. Protein N-acylation overrides differing targeting signals. *FEBS Letters* **585**: 517-522.

Stael S, Rocha AG, Wimberger T, Anrather D, Vothknecht UC, Teige M. 2012. Cross-talk between calcium signalling and protein phosphorylation at the thylakoid. *Journal of Experimental Botany* **63**: 1725-1733.

Sun YD, Li L, Macho AP, Han ZF, Hu ZH, Zipfel C, Zhou JM, Chai JJ 2013. Structural basis for flg22-induced activation of the *Arabidopsis* FLS2-BAK1 immune complex. *Science* **342**: 624-628.

Toufexi A, Duggan C, Pandey P *et al*. 2021. Chloroplasts navigate towards the pathogen interface to counteract infection by the Irish potato famine pathogen. *bioRxiv.* DOI: 10.1101/516443

Upadhyaya NM, Mago R, Panwar V *et al*. 2021. Genomics accelerated isolation of a new stem rust avirulence gene-wheat resistance gene pair. *Nature Plants* **7**: 1220-1228.

Wada M. 2016. Chloroplast and nuclear photorelocation movements. *Proceedings of the Japan Academy, Series B* **92**: 387-411.

Wang Q, Sullivan RW, Kight A, Henry RL, Huang J, Jones AM, Korth KL. 2004. Deletion of the chloroplast-localized *Thylakoid formation1* gene product in *Arabidopsis* leads to deficient thylakoid formation and variegated leaves. *Plant Physiology* **136**: 3594-3604.

Wangdi T, Uppalapati SR, Nagaraj S, Ryu CM, Bender CL, Mysore KS. 2010. A virus-induced gene silencing screen identifies a role for *Thylakoid Formation1* in *Pseudomonas syringae* pv *tomato* symptom development in tomato and *Arabidopsis*. *Plant Physiology* **152**: 281-292.

Wasternack C, Song S. 2017. Jasmonates: biosynthesis, metabolism, and signaling by proteins activating and repressing transcription. *Journal of Experimental Botany* **68**: 1303-1321.

Wu W, Zhu Y, Ma Z, Sun Y, Quan Q, Li P, Hu P, Shi T, Lo C, Chu IK, Huang J. 2013. Proteomic evidence for genetic epistasis: *ClpR4* mutations switch leaf variegation to virescence in *Arabidopsis*. *Plant Journal* **76**: 943-956.

Xu Q, Tang CL, Wang XD, Sun ST, Zhao JR, Kang ZS, Wang XJ. 2019. An effector protein of the wheat stripe rust fungus targets chloroplasts and suppresses chloroplast function. *Nature Communications* **10**: 5571.

Yang F, Xiao K, Pan H, Liu J. 2021. Chloroplast: the emerging battlefield in plant-microbe interactions. *Frontiers in Plant Science* **12**: 637853.

Zhang X, Peng G, Kutcher HR, Balesdent M, Delourme R, Fernando WG. 2016. Breakdown of *Rlm3* resistance in the *Brassica napus–Leptosphaeria maculans* pathosystem in western Canada. *European Journal of Plant Pathology* **957**: 659-674.

Zhang YL, Song GY, Lai NK *et al.* 2019. TurboID-based proximity labeling reveals that UBR7 is a regulator of N NLR immune receptor-mediated immunity. *Nature Communications* **10**: 3252.

Zhong Z, Marcel TC, Hartmann FE *et al*. 2017. A small secreted protein in *Zymoseptoria tritici* is responsible for avirulence on wheat cultivars carrying the *Stb6* resistance gene. *New Phytologist* **214**: 619-631.

Zurbriggen MD, Carrillo N, Tognetti VB, Melzer M, Peisker M, Hause B, Hajirezaei MR. 2009. Chloroplast-generated reactive oxygen species play a major role in localized cell death during the non-host interaction between tobacco and *Xanthomonas campestris* pv. *vesicatoria*. *Plant Journal* **60**: 962-973.

Professional Internships for PhD Students reflection form

At the start of the year 2020, I had finalised an agreement with the German biotech company Nomad Biosciences, based in Halle, Germany, to carry out my PIPS working on a project at their laboratories between March and June. However, as the Covid-19 pandemic swept across the globe, it became increasingly apparent that I would be unable to even visit Germany, let alone carry out any work on my arrival. However, following advertisement from the University of Nottingham and learned societies such as the Genetics society, I instead volunteered to work at the UK Biocentre Lighthouse Lab. This newly constructed laboratory had been tasked with processing diagnostic tests, carried out by the NHS, for the presence of SARS-CoV-2, from individuals with suspected Covid-19. The test itself involves a multiplex reverse transcriptase-quantitative polymerase chain reaction (RT-qPCR) assay, with the lab having to process tens of thousands of such tests every single day as part of efforts to prevent the further spread of Covid-19.

The UK Biocentre Lighthouse Lab is ordinarily a diagnostic testing facility, which had been transformed into a large-scale production line for carrying out Covid-19 testing. Almost all other projects carried out previously had been suspended, and almost 200 new staff and volunteers had been assembled to help in the coronavirus testing effort. The scale of the change was awe-inspiring: from receiving the call to set up the testing facility on 19th March (incidentally, a full seven weeks following the first confirmed case in the UK) by the time I arrived on 21st April the lab was capable of carrying out tens of thousands of tests per day. These samples, at first arriving only in the hundreds but soon growing to many thousands per day, came from all over the country; from care homes and NHS staff to drive-through testing centres and posted test-at-home kits.

Working alongside me at the lab were many other academics from across the country, working in a variety of biological science disciplines, from undergraduate students to principal investigators. Many were contributing their time for no reason other than to help the community in whatever way they could – in many ways a privilege which other people did not have. Meeting these

researchers and discussing their work, from studying human fungal pathogens to population genetics of rare marine species, gave me a fantastic opportunity to hear the perspectives of experts in other fields of biology and make contacts from outside my own area of study.

The lab operation itself involved the receipt of vials containing sterile swabs, used to sample the back of the nose and throat of tested individuals, double-bagged to protect the handlers from infection. These bags were opened in airflow cabinets to prevent the release of the virus. Media within the vials, potentially containing SARS-CoV-2 viral RNA, was transferred to 96 well plates using Tecan liquid handling robots in a high-throughput manner. Individual identification codes on each vial were simultaneously stored in an electronic system which followed the samples through the production line. Following transfer of the samples to plates, automated, high-throughput extraction of RNA was carried out using Kingfisher robots. The eluted RNA was then sampled to prepare qPCR plates with a pre-prepared multiplex qPCR mastermix (ThermoFisher), again automated using Tecan robots. Finally, RT-qPCRs were carried out using many qPCR machines provided by universities and commercial labs all over the country. The multiplex qPCR were designed to test for the presence of three viral genes encoding (1) the spike protein, (2) the nucleocapsid protein, and (3) nonstructural proteins encoded by the open reading frame ORF1ab that form a viral replication complex. In addition, an internal control was incorporated in each test allowing detection of MS2 RNA from a bacteriophage. The tests were classified as positive when the two or three of the three targeted viral genes were detected, whilst the detection of only one gene was considered an inconclusive result requiring a repeat testing. Tests in which none of the three viral genes detected were classified negative.

In order to maximise testing throughput, the lab was configured into a production line. As a worker on this line, I was primarily tasked with running the Tecan robotic liquid handlers transferring media from sample vials into the 96-well plates for subsequent RNA extraction. These robots were housed within large biosafety cabinets, as any viral particles would still be active at this stage of the process. The role mostly involved preparing samples for the robots, creating and checking the files for the storage of identification codes from each

sample vial, maintaining the robots and correcting any errors that occurred during the process. As the robots were running 24 hours a day, seven days a week – far above their originally conceived capacity, maintenance was an important task in keeping the production line going. The correct creation of the files to track individual samples through the rest of the system was also vital, to ensure that correct results would be returned to the tested individuals. As well as running the machines, I had the opportunity to train others in their use as the team grew and other volunteers left. This role also allowed me to be involved in processing many samples, normally 2000-2500 in each 12-hour shift. In total, I believe I will have helped carry out more than 70,000 tests over the course of my placement.

Working at the lab provided a unique experience to see inside the largest Covid-19 testing facility in the UK at that time. I learned to use new high-tech equipment and train others in its use as well as gaining new IT skills. I had also never previously worked in a diagnostic lab, so gained a feel for working in this environment. Whilst this work may not have resulted in my gaining many new skills or exposure to radically different work environments to those I was already experienced with, I can say that I am proud to have been able to contribute to the effort to fight the Covid-19 outbreak in the UK.

a

b

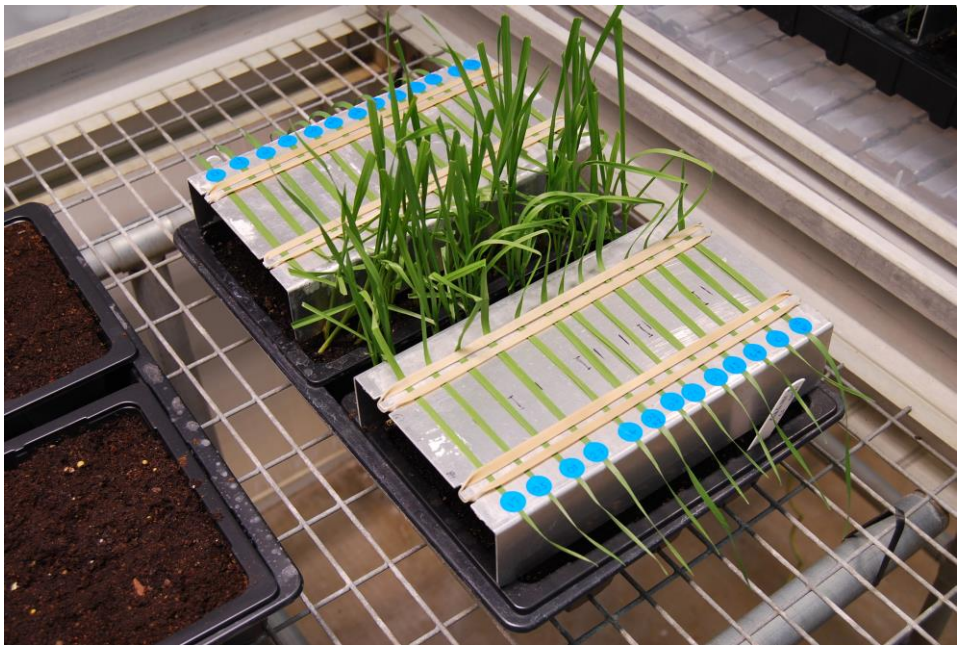

Figure S2.1: Images of plants utilised as part of project. **a)** Four-week-old *Nicotiana benthamiana* plant, with fully expanded leaves. **b)** Wheat leaves mounted on inoculation platform for inoculation bioassay.

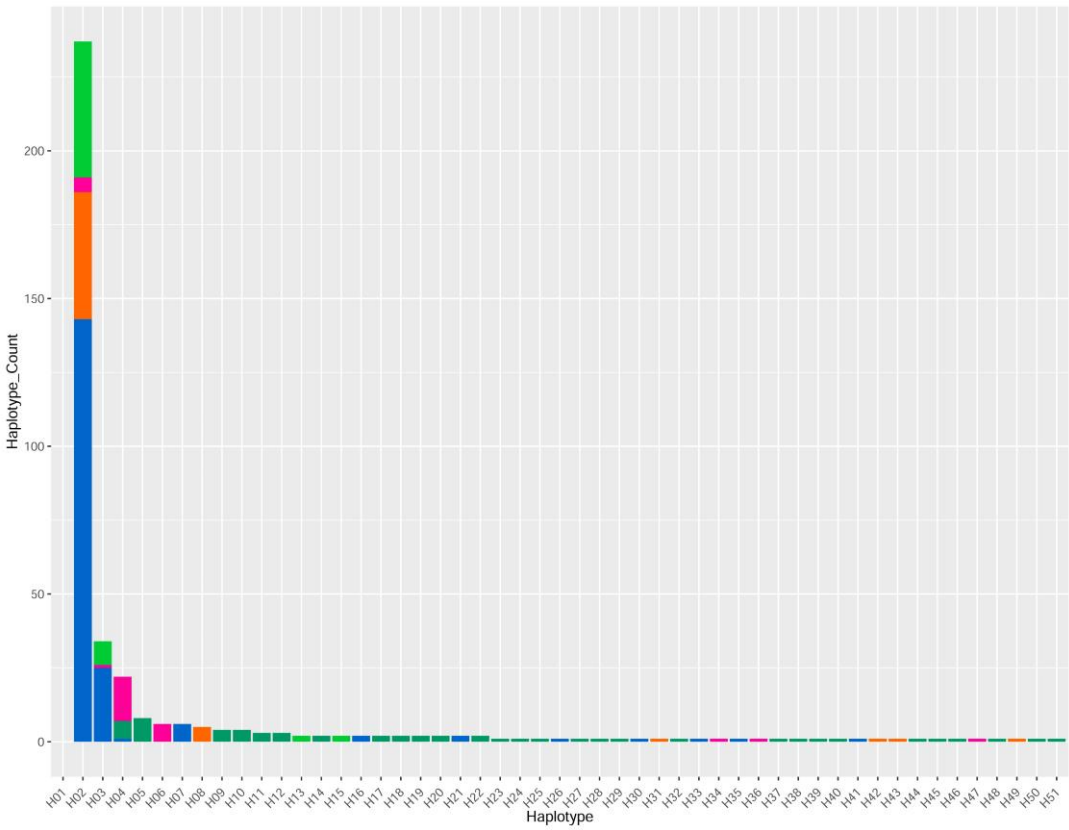

Figure S3.1. Frequency of each of the identified *AvrStb6* haplotypes along with their geographic origin

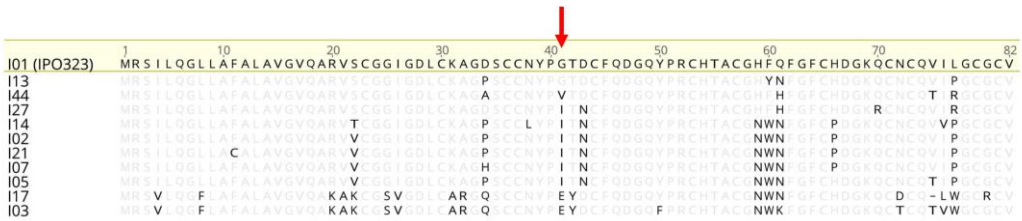

Figure S3.2: Alignment of AvrStb6 isoforms from *Z. tritici* isolates tested in pathoassays to determine virulence on Stb6 wheat. Red arrow indicates the amino acid (#41) hypothesised to determine the virulence/avirulence phenotype.

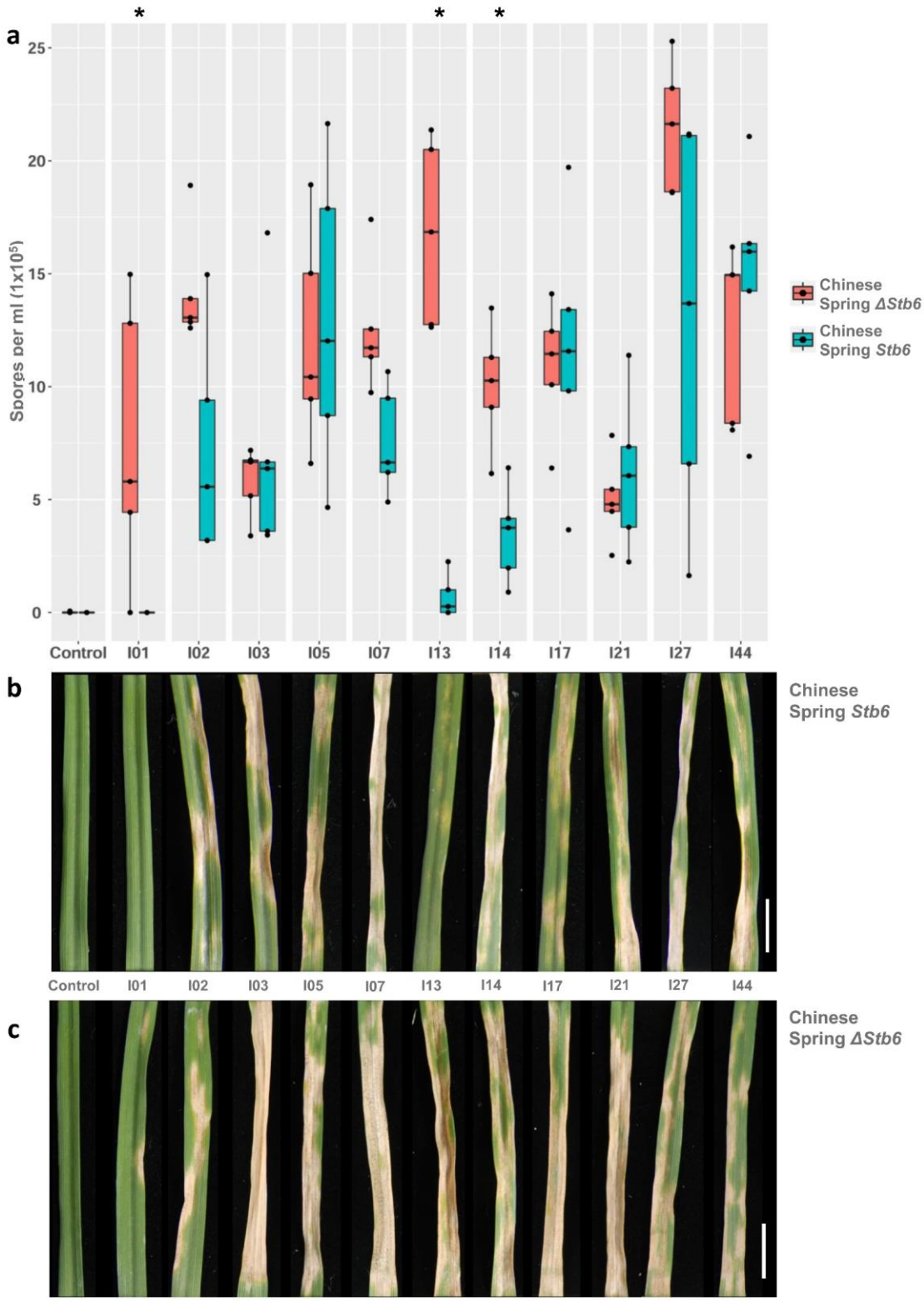

Figure S3.3: Plant inoculation bioassay using wheat near-isogenic lines of cultivar Chinese Spring

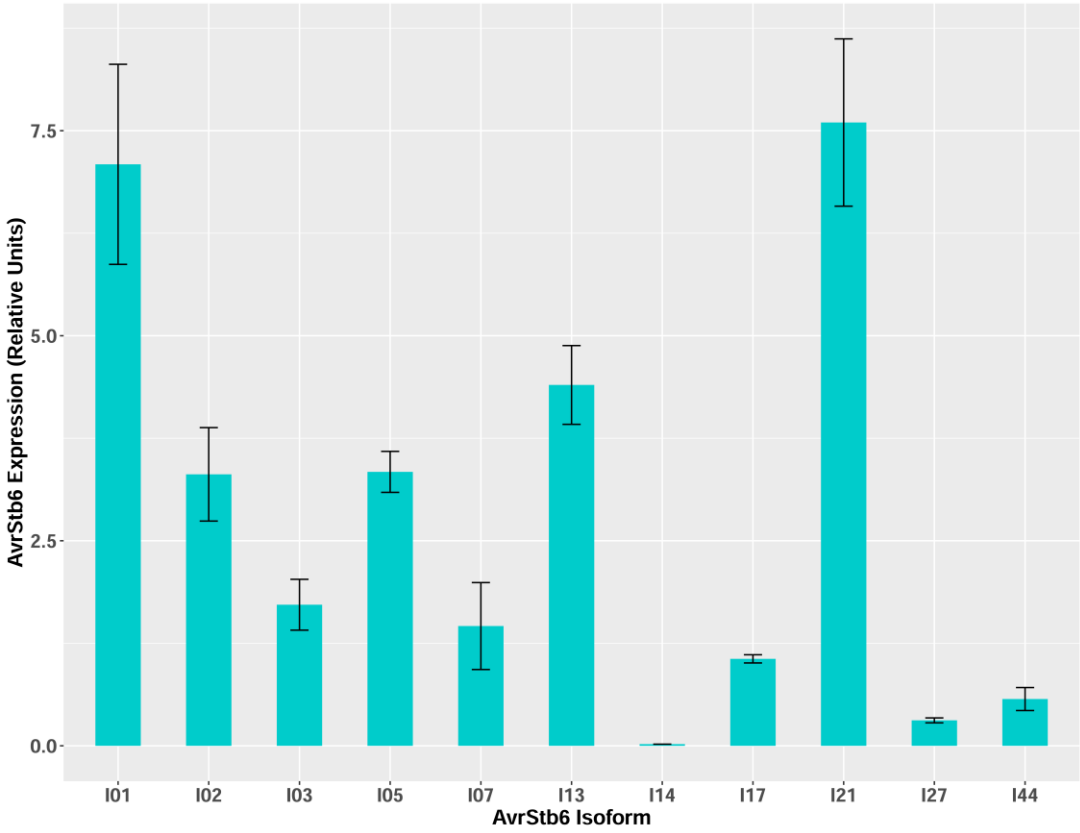

Figure S3.4: Expression levels of different *AvrStb6* haplotypes during *Zymoseptoria tritici* infection of wheat

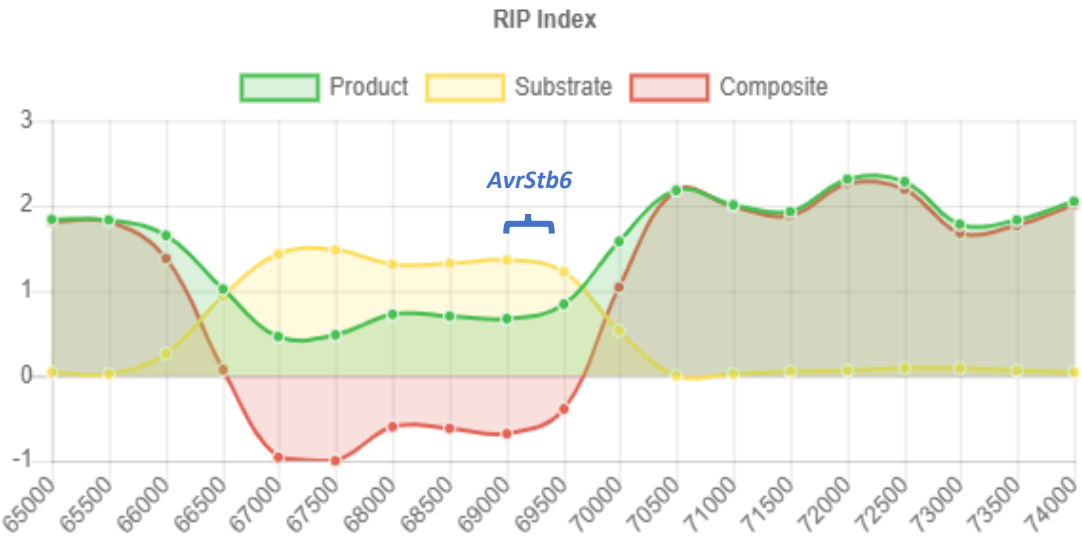

Figure S3.5: Analysis of repeat induced point mutation frequency at the *AvrStb6* locus on *Zymoseptoria tritici* chromosome 5 using RIPper (http://theripper.hawk.rocks)

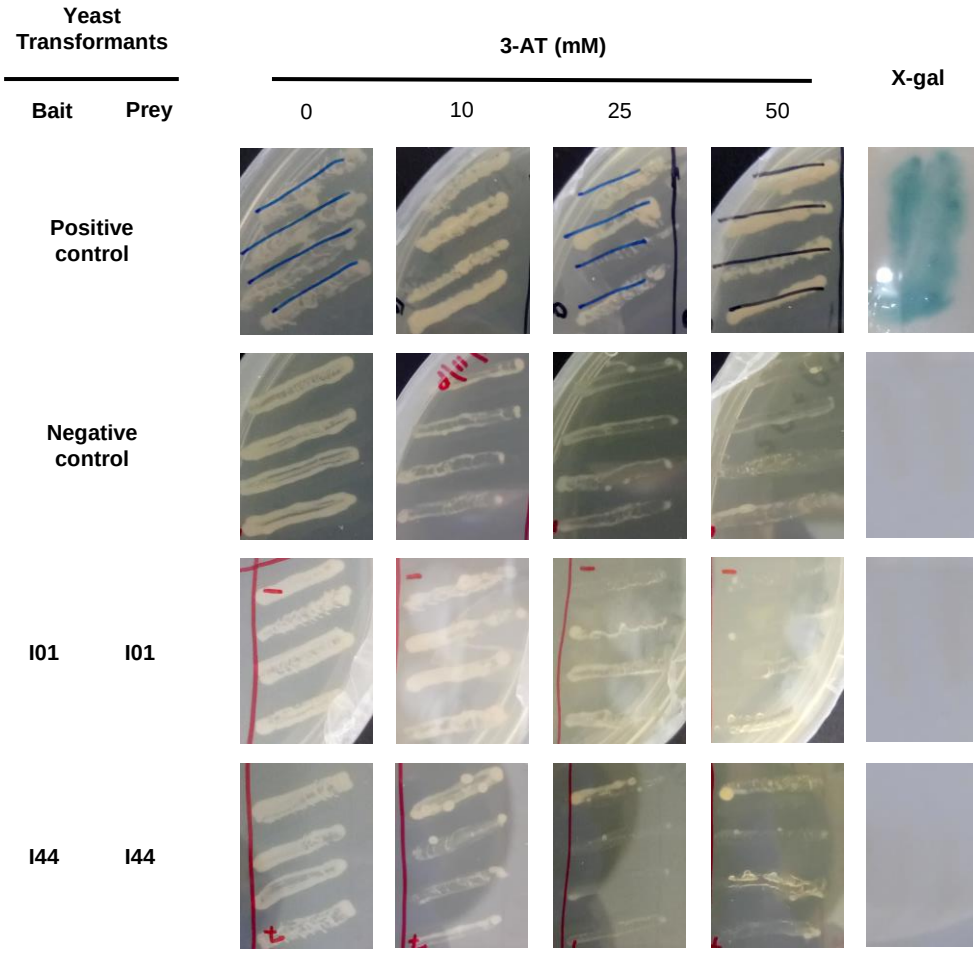

Figure S4.1: AvrStb6 shows no dimerization under yeast two-hybrid conditions. Test transformants possess AvrStb6 isoforms I01 (IPO323, avirulent) or I44 (IPO88004, virulent).

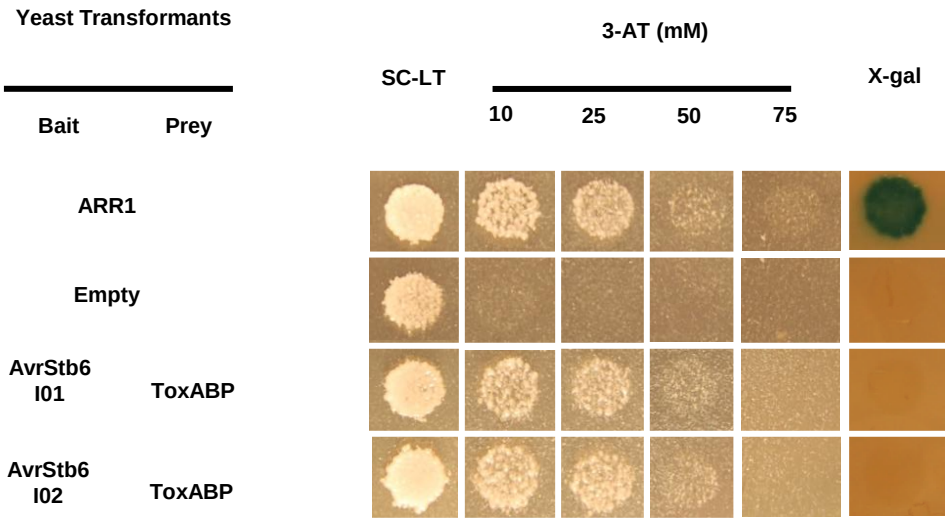

Figure S4.2 : Yeast two-hybrid assay testing the interaction between AvrStb6 (I01 and I02) and ToxABP/Thf1/Psb29.

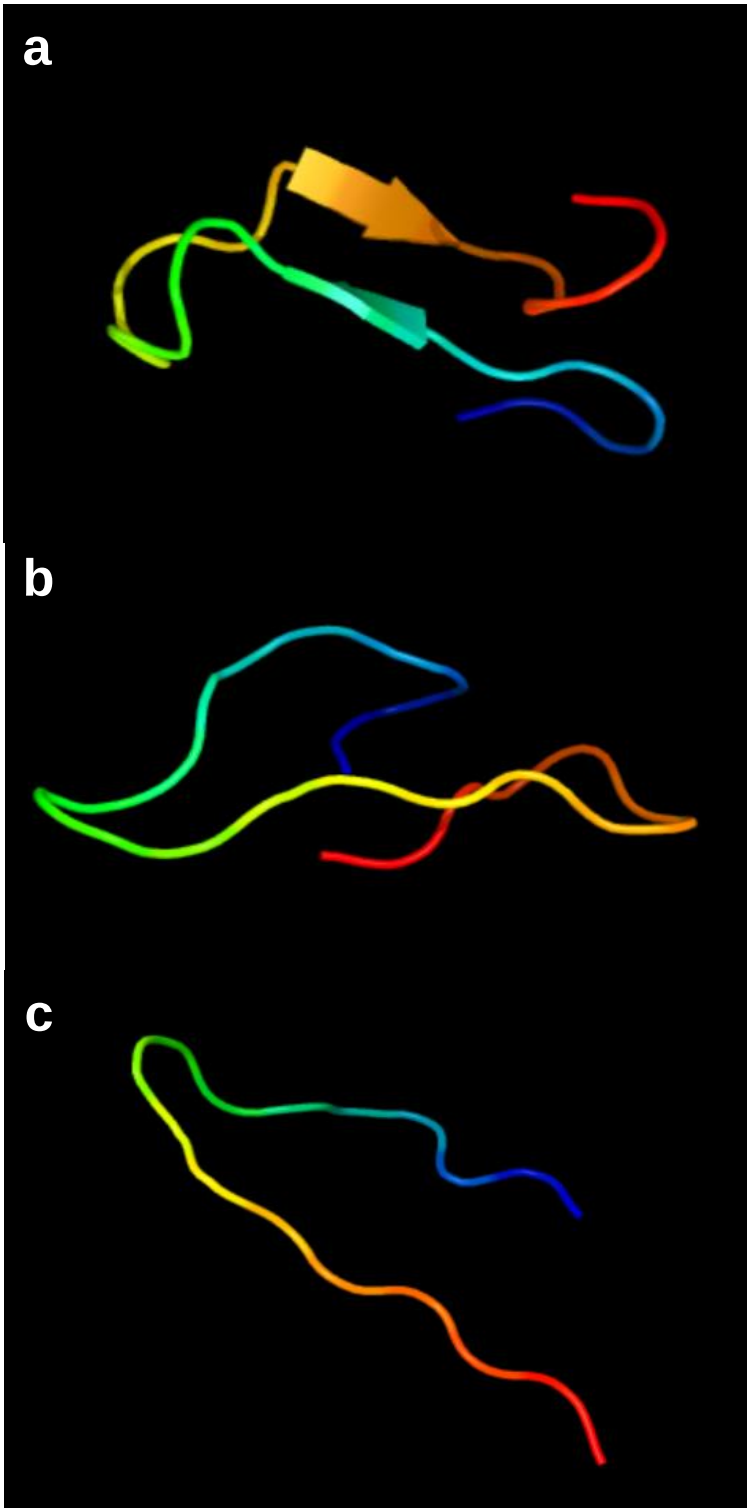

Figure S4.3 : AvrStb6 isoforms share no predicted structure. Images were created using Phyre2 (http://www.sbg.bio.ic.ac.uk/phyre2) **a)** AvrStb6 I01. Model confidence = 32.4%, coverage = 30% **b)** AvrStb6 I02. Model confidence = 58%, coverage = 40% **c)** AvrStb6 I44. Model confidence = 24%, coverage = 27%.

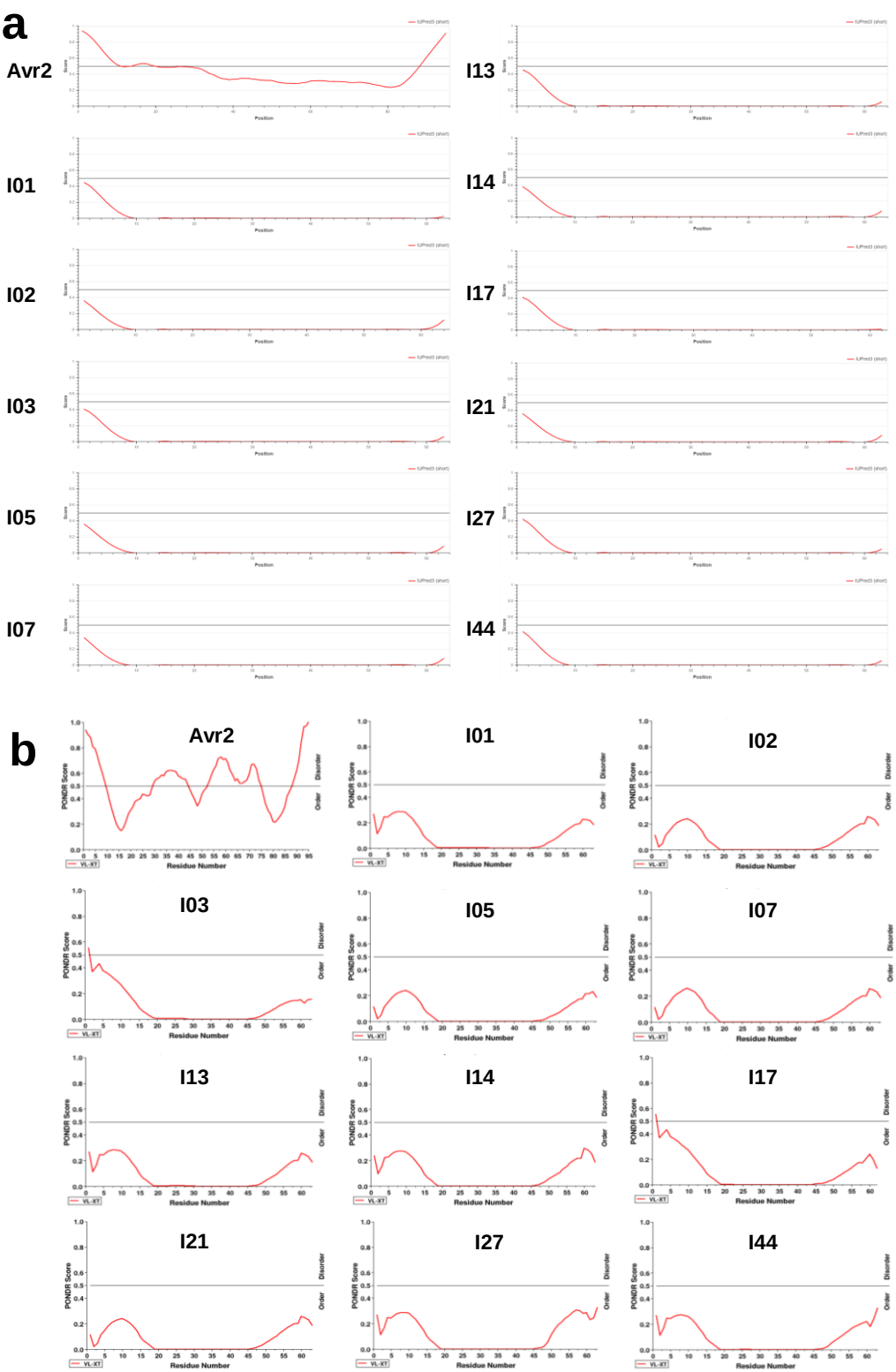

Figure S4.4: AvrStb6 isoforms show little disorder tendency. Graphical assessments of the disorder tendency of mature AvrStb6 protein regions. Mature Avr2 of *Phytophthora infestans*, previously found to show high levels of intrinsic disorder (Yang et al., 2020) was included for comparison. **a)** Predictions using the UIPred3 tool (short disorder, https://iupred.elte.hu/). **b)** Predictions using the PONDR VL-XT tool (http://www.pondr.com/).

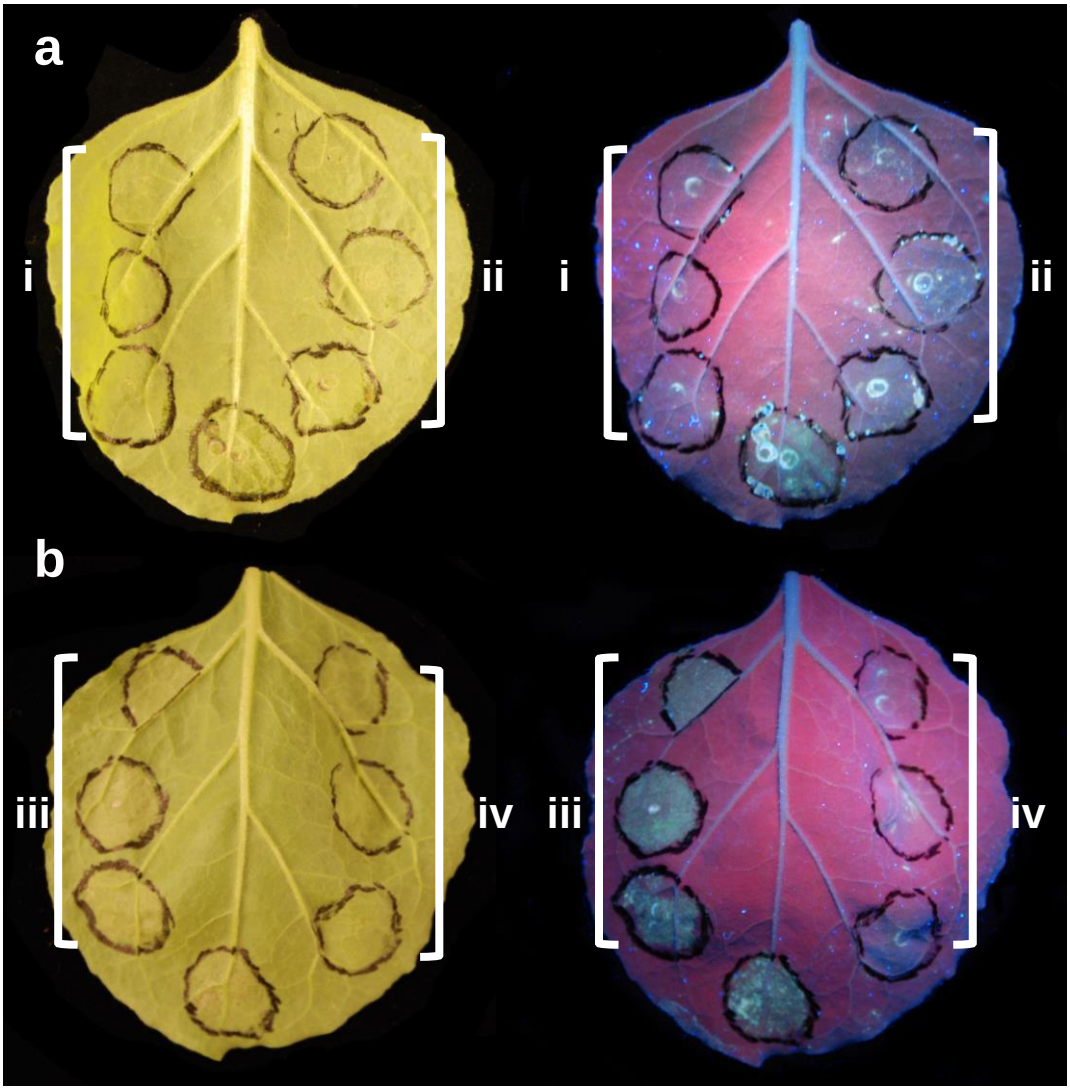

Figure S4.5: AvrStb6 does not induce or supress cell death. **a)** *N. benthamiana* leaf transiently expressing *AvrStb6* I01 (i) or I02 (ii), under normal light (left) or UV (right). **b)** Leaves transiently co-expressing *Stb6* from cv. Cadenza (functional kinase) and *AvrStb6* I01 (iii) or *AvrStb6* I01 alone (iv). Bottom infiltration zone on each leaf is transiently expressing *MgNLP*. Images were taken at 5 days post infiltration.

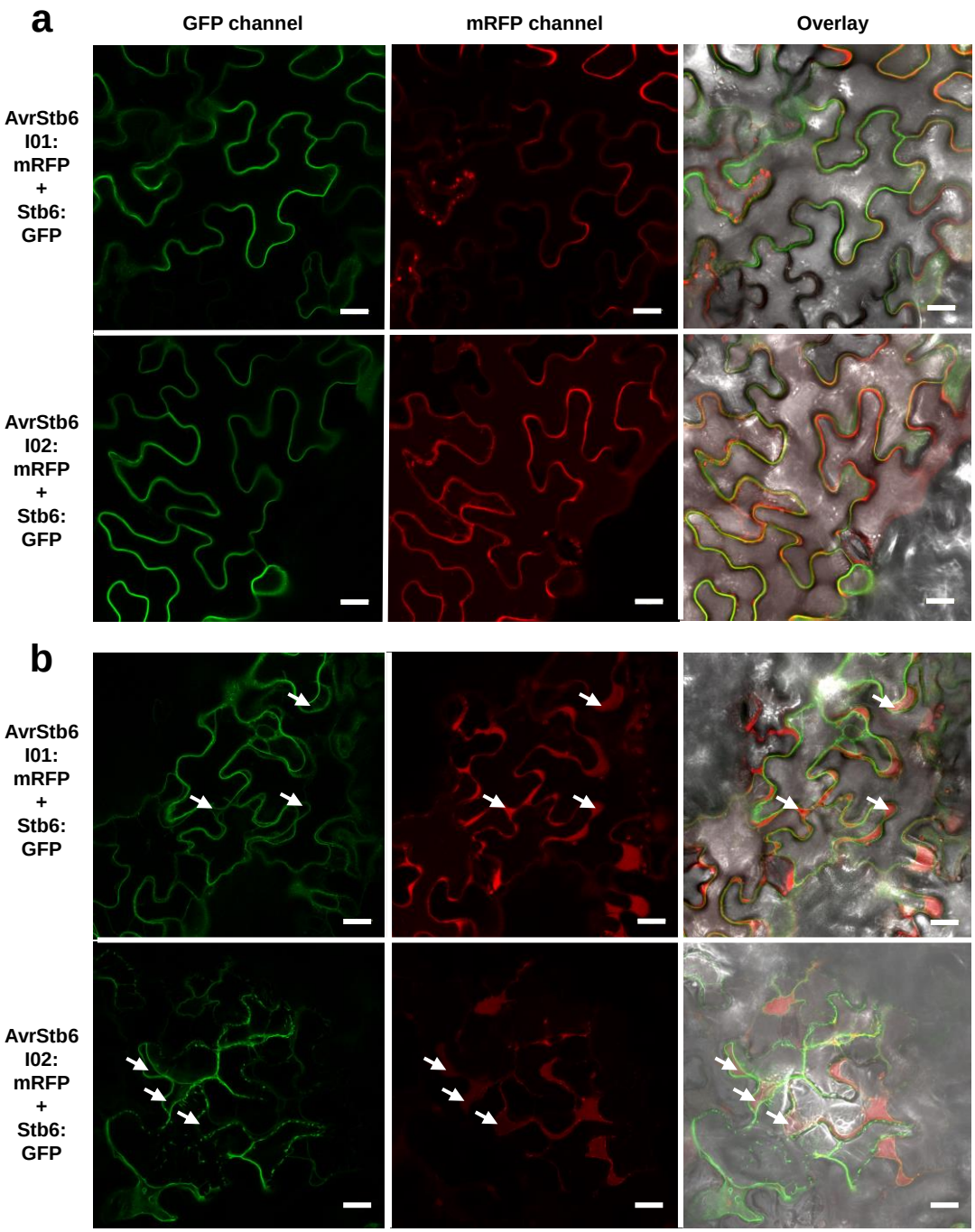

Figure S4.6: AvrStb6 isoforms I01 and I02 localise to the apoplast when expressed in *Nicotiana benthamiana*. Leaves were harvested at 5 days post infiltration (dpi). **a)** Leaf cells prior to plasmolysis **b)** Leaf cells after 30 minutes incubation with 0.8M mannitol solution. White arrows indicate example locations of the apoplastic space, following plasmolysis. White bars represent 20µm.

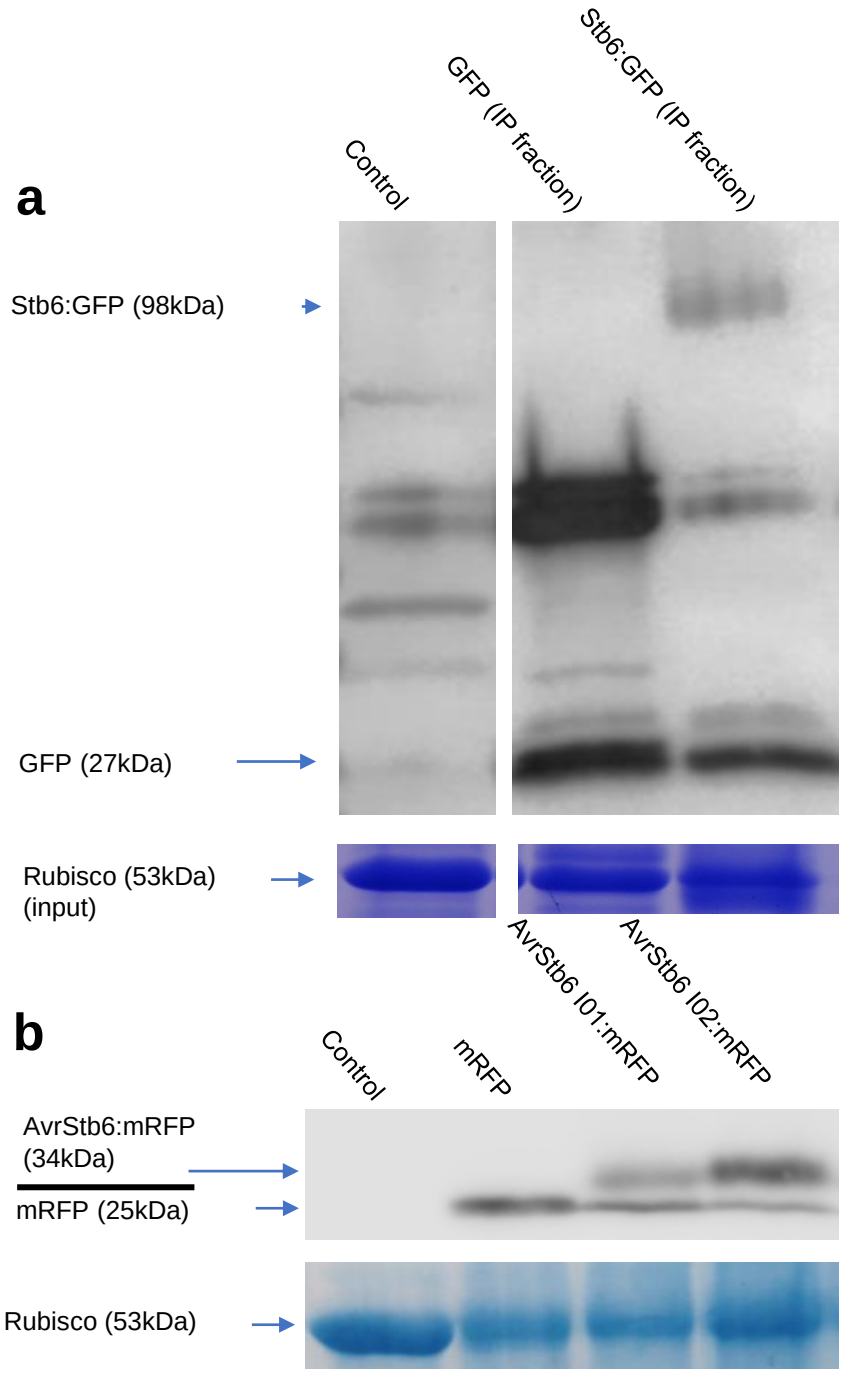

Figure S4.7: Cleavage of fluorophores observed during Stb6 and AvrStb6 construct expression. **a)** Top panels show anti-GFP western blots. Left shows control protein extract, from leaf infiltrated with untransformed *Agrobacterium tumefaciens.* Right panel shows test protein extracts, following immunoprecipitation using anti-GFP trap beads (IP fraction). Bottom two panels shows Coomassie blue staining of rubisco band for input protein. **b)** Top panel shows anti-RFP western blot. Bottom panel shows amido black stain of rubisco bands.

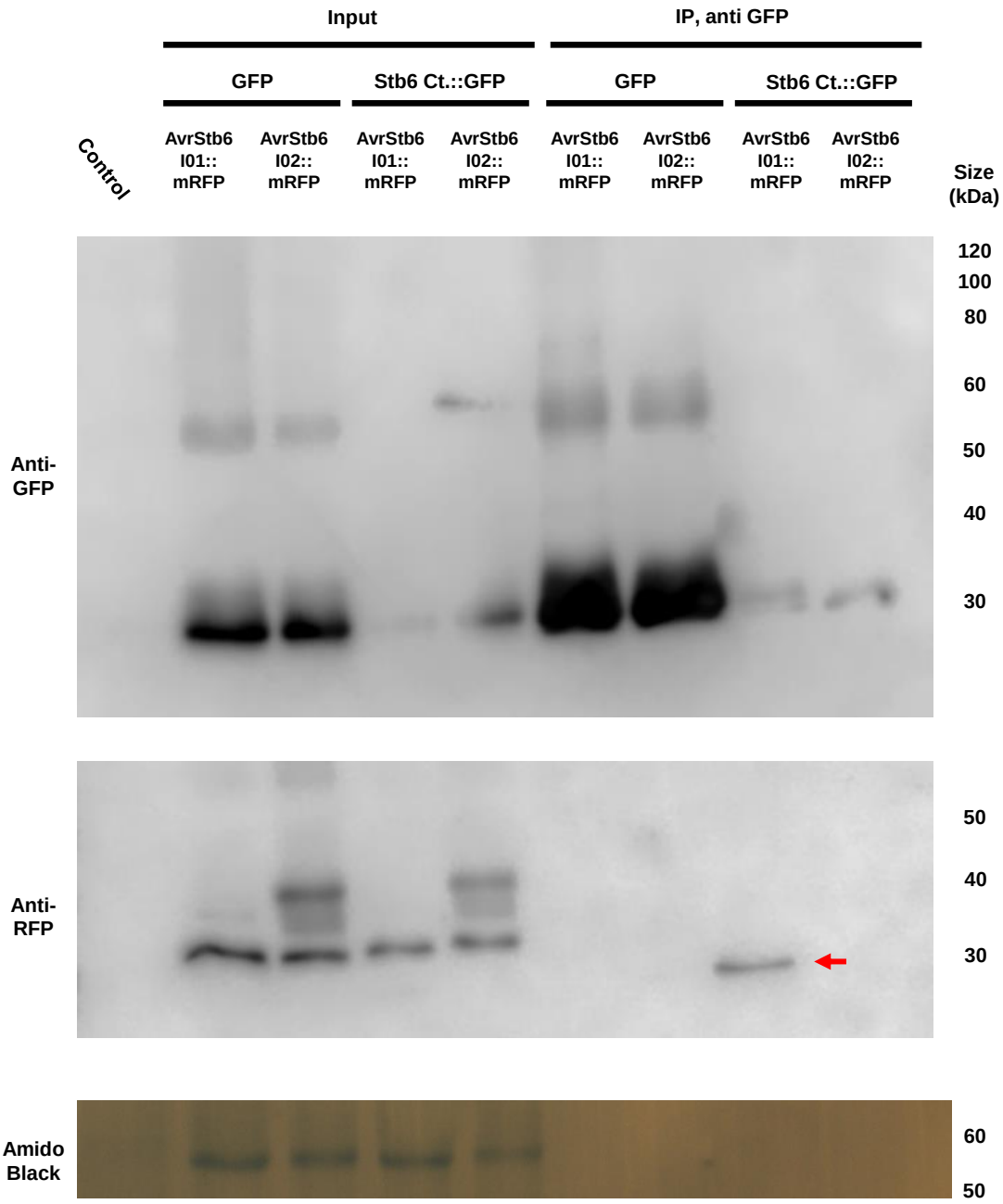

Figure S4.8: CoIP experiment to determine the interaction between Stb6 and AvrStb6. Stb6 (encoded by haplotype 3):GFP was used as bait and AvrStb6 (I01 or I02):mRFP as prey. Band corresponding to AvrStb6 I01:mRFP was observed in CoIP fraction, following anti-GFP IP (red arrow). However, this observation could not be replicated (Figure 4.4).

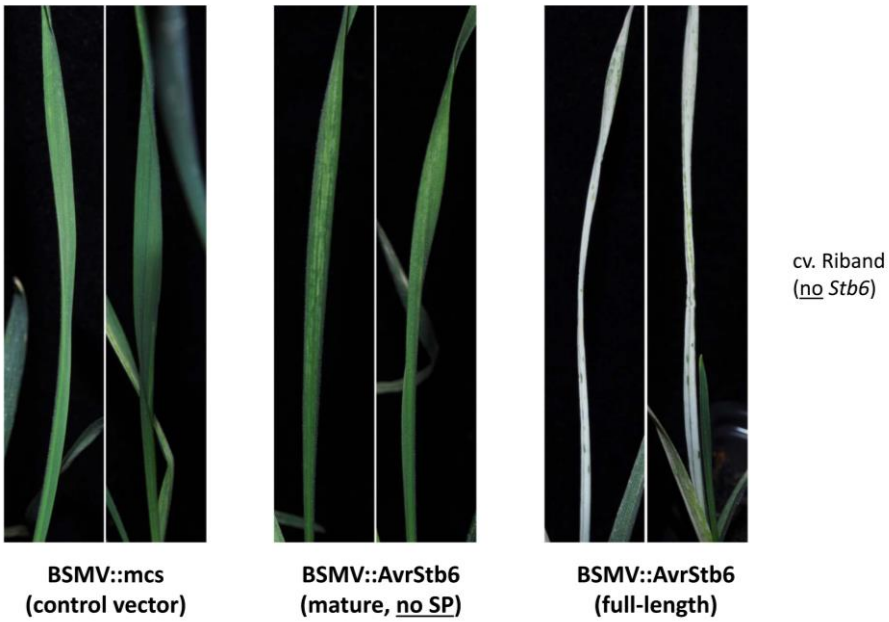

Figure S4.9: Virus-induced overexpression of AvrStb6 in wheat leaves induces bleaching phenotype. Wheat plants were treated with *Barley stripe mosaic virus* (BSMV) to overexpress AvrStb6 without its signal peptide (SP, central panel) or as a full-length protein (right). BSMV:mcs construct possesses an empty multiple cloning site (mcs). Figure provided by K Kanyuka.

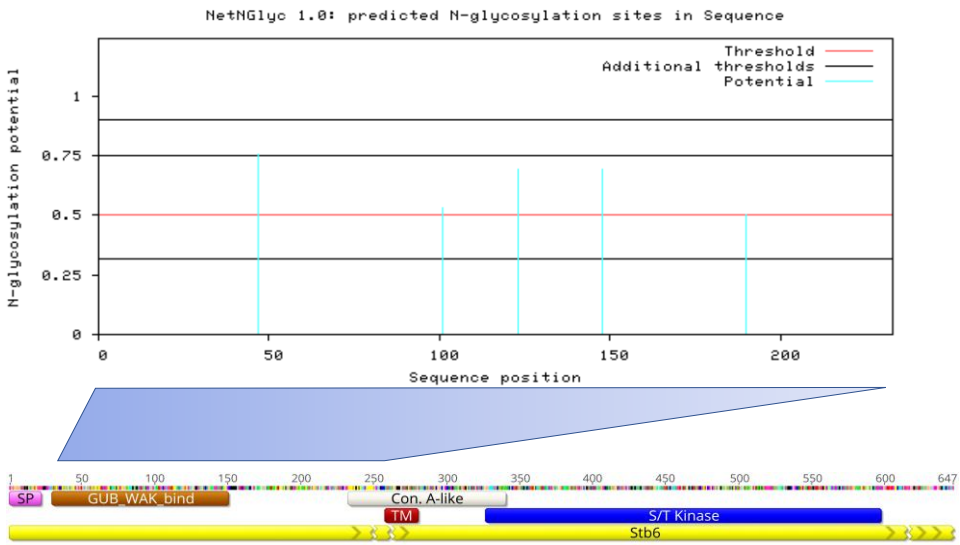

Figure S4.10: Several putative glycosylation sites predicted within the Stb6 ectodomain. The NetNGlyc 1.0 Server (www.cbs.dtu.dk/services/NetNGlyc/) was used to predict amino acid residues with high N-glycosylation potential, within the extracellular domain on Stb6. The amino acid sequence from the end of the signal peptide (SP, residue 23) to the transmembrane domain (TM, residue 257) was analysed. Residues meeting or exceeding the threshold for N-glycosylation potential are highlighted in cyan.

Figure S5.1: Alignment of Stb6 isoforms encoded by *Stb6* haplotype 1 (from wheat cultivar Cadenza, functional kinase) and haplotype 3 (from cv. Courtot, non-functional kinase). Highlighted in the kinase domain is the single amino acid variation between the isoforms. SP = signal peptide; GUB_WAK_bind = galacturonan-binding domain; TM = transmembrane domain; ST Kinase = serine/threonine kinase domain. Y2H testing region = the region used in all Stb6 kinase Y2H assays.

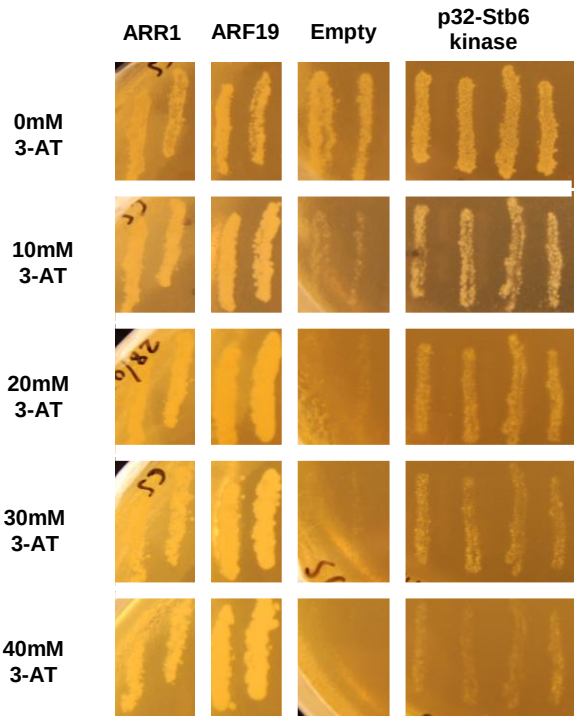

Figure S5.2: Yeast two-hybrid assay to determine the optimal 3-amino-1,2,4-triazol (3-AT) concentration for growth inhibition of yeast transformed with *Stb6* haplotype 1 (from cv. Cadenza) kinase in p32 (bait) plasmid and empty prey (p22) plasmid. “ARR1” and “ARF19” are positive interaction controls, “Empty” is a negative control, transformed with empty bait and prey vectors.

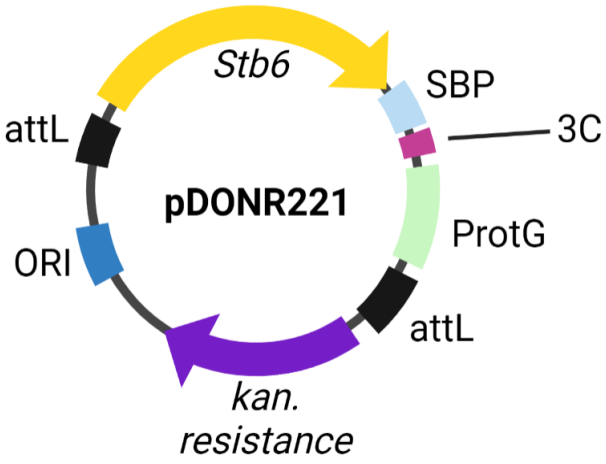

Figure S5.3: Schematic diagram of *Stb6* C-terminal GSRhino tag construct, generated in the pDONR221 vector. SBP = Streptavidin-binding protein; 3C = Rhinovirus 3C protease cleavage sites; ProtG = Protein G immunoglobulin-binding proteins; attL = Gateway recombination sites; kan. resistance = kanamycin resistance gene; ORI = origin of replication. Construct was generated using *Stb6* cDNA. Figure created using Biorender.

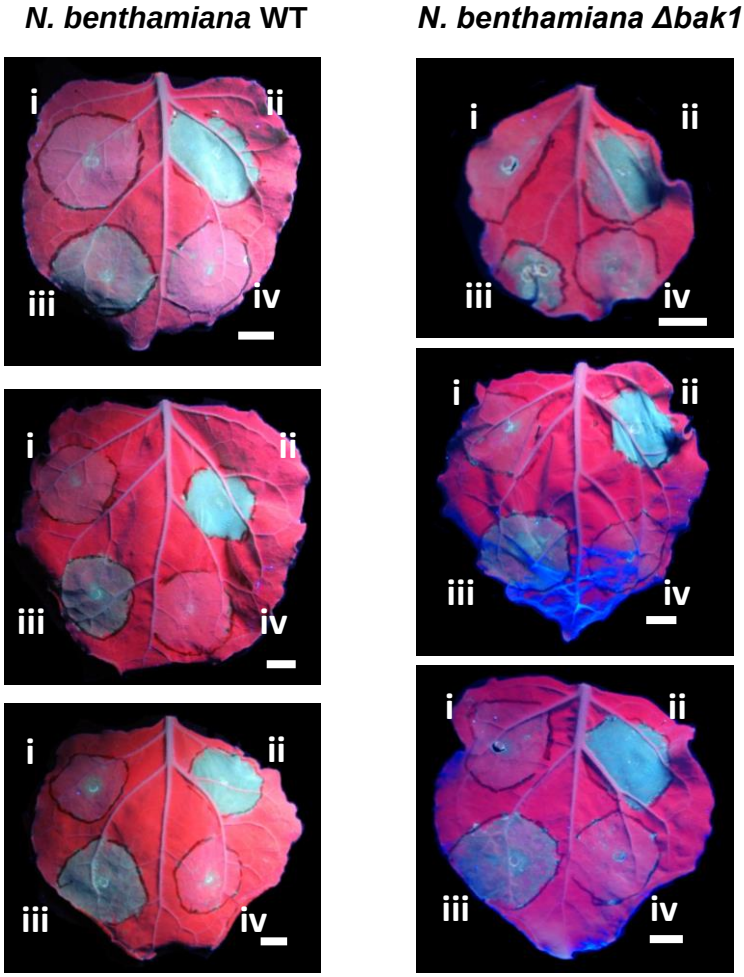

Figure S5.4: *Stb6*-induced cell death is independent of BAK1**.** Wild-type and *Δbak1 Nicotiana benthamiana* leaves were imaged under UV lamp at 5 days post infiltration with *Agrobacterium tumefaciens.* **i)** untransformed *Agrobacterium* **ii)** *Mycosphaerella graminicola* necrosis- and ethylene-inducing peptide 1 (Nep1)-like protein family (MgNLP) **iii)** *Stb6* haplotype 1 (cv. Cadenza, functional kinase) **iv)** *Stb6* haplotype 3 (cv. Courtot, non-functional kinase). White bars represent 10mm.

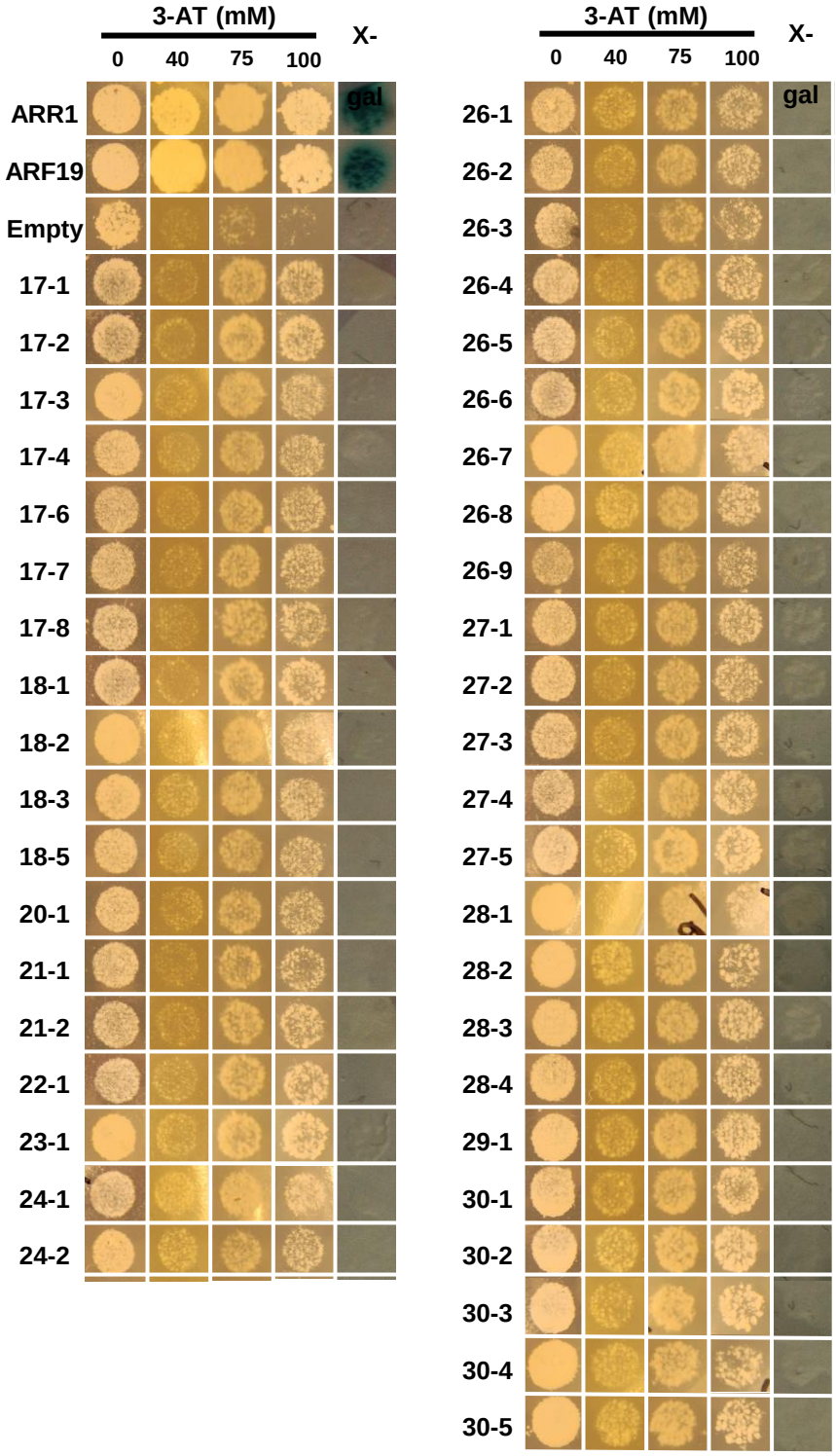

Figure S5.5: Retesting of HIS$^+$ colonies identified in yeast two-hybrid library assay with Stb6 kinase bait. Continued from Figure 5.3. “ARR1” and “ARF19” are positive control yeast transformants, “Empty” yeast strain is negative control, transformed with empty bait and prey vectors.

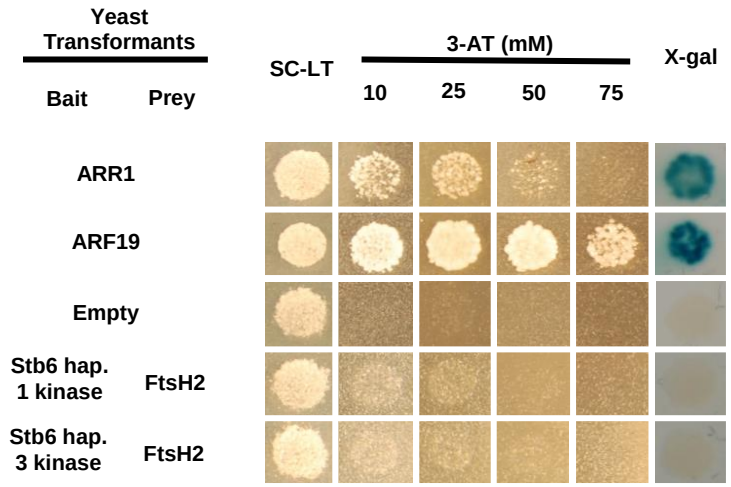

Figure S5.6: Yeast two-hybrid assay for detection of interaction between Stb6 kinase and FtsH2 peptidase. *Stb6* haplotype 1 encodes a functional kinase, haplotype 3 a non-functional kinase. “ARR1” and “ARF19” are positive control yeast transformants, “Empty” yeast strain is transformed with empty bait and prey vectors.

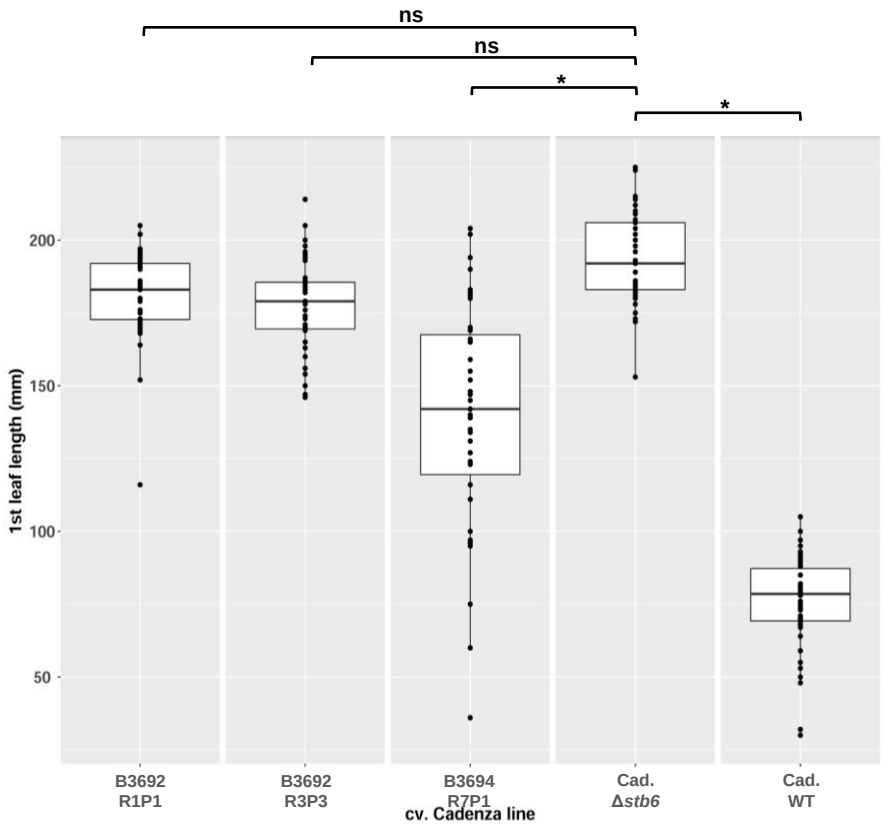

Figure S5.7: Length of first leaves from three-week-old wheat plants. B3692 R1P1, B3692 R3P3 and B3694 R7P1 are control Cadenza lines, recovered from tissue culture process. Lower and upper hinges of each boxplot correspond to the first and third quartiles, respectively. Whiskers extend to the largest value no further than 1.5 times the interquartile range from the hinge. “*” represents significant difference using Dunnett’s multiple comparison test (95% C.I. [175.0, 211.5]). “ns” represent non-significant differences.

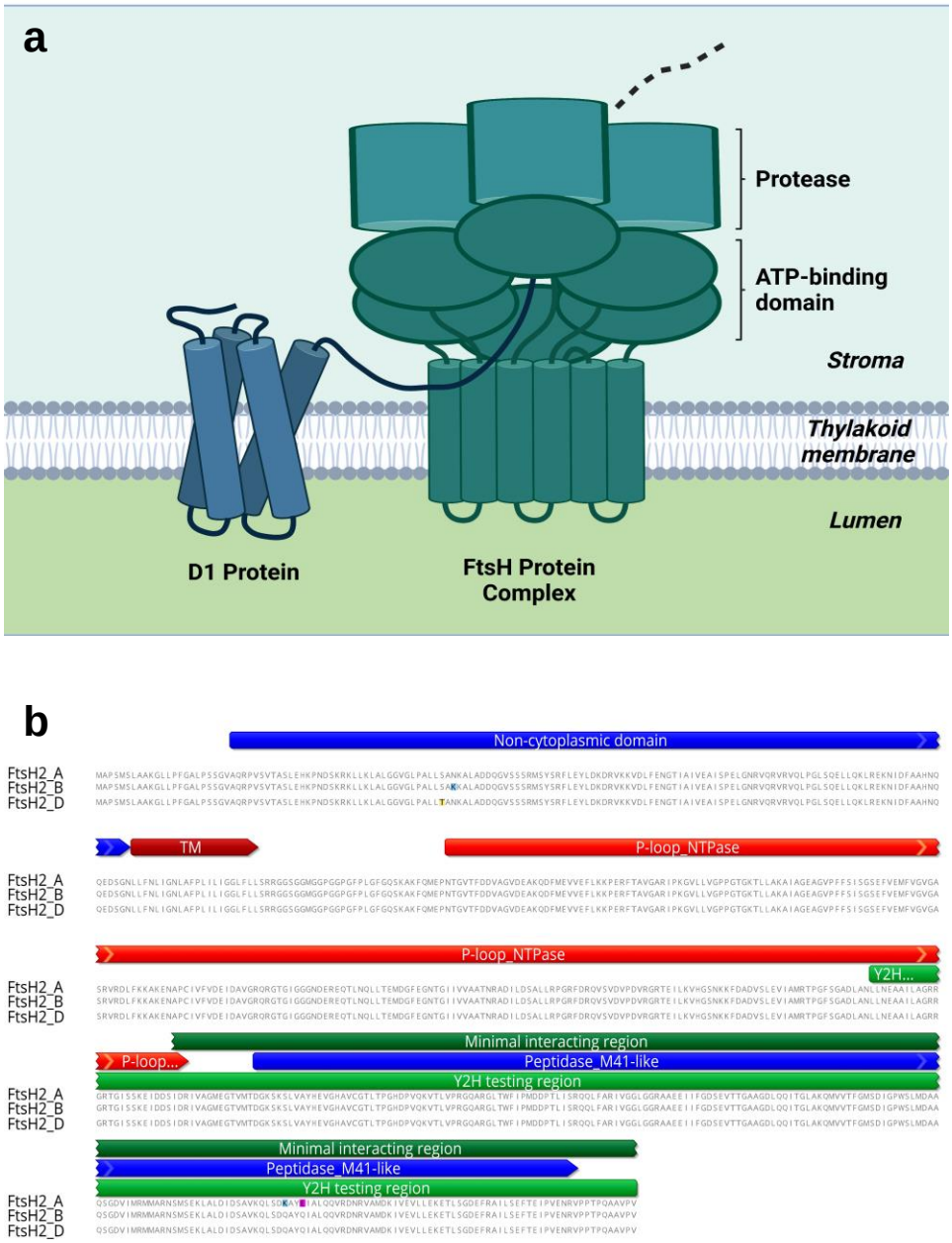

Figure S5.8: FtsH2 was identified as a strong candidate for interaction with Stb6 kinase. a) Schematic figure illustrating the FtsH protein hexameric complex, composed of three copies each of FtsH2 and FtsH5. The complex is embedded in the internal chloroplastic thylakoid membrane. The FtsH protein complex functions in degrading the photosystem protein D1. Figure adapted from Niwa *et al.,* 2002 and created using Biorender. b) Alignment of the protein products of the three homeologues of *FtsH2,* from the A genome (FtsH2_A), B genome (FtsH2_B) and D genome (FtsH2_D). Amino acid variations are highlighted. TM = transmembrane domain; P-loop NTPase = ATP-binding domain; Peptidase_M41-like = protease domain. “Minimal interacting domain” indicates the strongest candidate region for binding with Stb6 kinase. “Y2H testing region” indicates the gene fragment used in the generation of constructs for Y2H and coimmunoprecipitation.

Table S2.1: Split-Plot Experimental Design

Plot No.	Large tray	Small tray	Wheat line	*Z. tritici* isolate
1101			WT	Isolate 12
1102			WT	Isolate 8
1103			WT	Isolate 7
1104			WT	Isolate 6
1105			WT	Isolate 4
1106			WT	Isolate 2
1107		**Top**	WT	Isolate 3
1108			WT	Isolate 11
1109			WT	Isolate 9
1110			WT	Isolate 10
1111			WT	Isolate 5
1112			WT	Control
1113	**1**		WT	Isolate 1
1201			ΔStb6	Isolate 3
1202			ΔStb6	Isolate 11
1203			ΔStb6	Isolate 4
1204			ΔStb6	Isolate 10
1205			ΔStb6	Isolate 2
1206			ΔStb6	Control
1207		**Bottom**	ΔStb6	Isolate 12
1208			ΔStb6	Isolate 5
1209			ΔStb6	Isolate 7
1210			ΔStb6	Isolate 1
1211			ΔStb6	Isolate 6
1212			ΔStb6	Isolate 8
1213			ΔStb6	Isolate 9
2101			ΔStb6	Isolate 12
2102			ΔStb6	Isolate 1
2103			ΔStb6	Isolate 9
2104			ΔStb6	Isolate 2
2105			ΔStb6	Isolate 6
2106			ΔStb6	Isolate 5
2107		**Top**	ΔStb6	Isolate 3
2108			ΔStb6	Isolate 4
2109			ΔStb6	Control
2110			ΔStb6	Isolate 11
2111			ΔStb6	Isolate 8
2112			ΔStb6	Isolate 10
2113	**2**		ΔStb6	Isolate 7
2201			WT	Isolate 9
2202			WT	Isolate 12
2203			WT	Control
2204			WT	Isolate 5
2205			WT	Isolate 11
2206			WT	Isolate 3
2207		**Bottom**	WT	Isolate 6
2208			WT	Isolate 1
2209			WT	Isolate 8
2210			WT	Isolate 2
2211			WT	Isolate 7

2212			WT	Isolate 10
2213			WT	Isolate 4
3101			ΔStb6	Isolate 9
3102			ΔStb6	Isolate 1
3103			ΔStb6	Isolate 8
3104			ΔStb6	Isolate 2
3105			ΔStb6	Isolate 3
3106			ΔStb6	Isolate 7
3107		**Top**	ΔStb6	Isolate 11
3108			ΔStb6	Control
3109			ΔStb6	Isolate 5
3110			ΔStb6	Isolate 6
3111			ΔStb6	Isolate 10
3112			ΔStb6	Isolate 4
3113	**3**		ΔStb6	Isolate 12
3201			WT	Isolate 6
3202			WT	Isolate 7
3203			WT	Isolate 10
3204			WT	Isolate 5
3205			WT	Isolate 11
3206			WT	Isolate 9
3207		**Bottom**	WT	Isolate 4
3208			WT	Isolate 12
3209			WT	Isolate 8
3210			WT	Isolate 1
3211			WT	Isolate 2
3212			WT	Isolate 3
3213			WT	Control
4101			WT	Isolate 9
4102			WT	Isolate 4
4103			WT	Isolate 5
4104			WT	Isolate 12
4105			WT	Isolate 7
4106			WT	Isolate 10
4107		**Top**	WT	Isolate 3
4108			WT	Isolate 8
4109			WT	Isolate 2
4110			WT	Isolate 1
4111			WT	Isolate 11
4112			WT	Control
4113	**4**		WT	Isolate 6
4201			ΔStb6	Isolate 9
4202			ΔStb6	Isolate 5
4203			ΔStb6	Isolate 1
4204			ΔStb6	Control
4205			ΔStb6	Isolate 3
4206			ΔStb6	Isolate 8
4207		**Bottom**	ΔStb6	Isolate 6
4208			ΔStb6	Isolate 7
4209			ΔStb6	Isolate 11
4210			ΔStb6	Isolate 10
4211			ΔStb6	Isolate 2
4212			ΔStb6	Isolate 4
4213			ΔStb6	Isolate 12

5101			WT	Isolate 4
5102			WT	Control
5103			WT	Isolate 10
5104			WT	Isolate 8
5105			WT	Isolate 11
5106			WT	Isolate 3
5107		**Top**	WT	Isolate 5
5108			WT	Isolate 12
5109			WT	Isolate 6
5110			WT	Isolate 1
5111			WT	Isolate 9
5112			WT	Isolate 2
5113	**5**		WT	Isolate 7
5201			ΔStb6	Isolate 9
5202			ΔStb6	Isolate 5
5203			ΔStb6	Isolate 1
5204			ΔStb6	Isolate 11
5205			ΔStb6	Isolate 8
5206			ΔStb6	Isolate 3
5207		**Bottom**	ΔStb6	Isolate 6
5208			ΔStb6	Isolate 10
5209			ΔStb6	Isolate 4
5210			ΔStb6	Isolate 7
5211			ΔStb6	Isolate 12
5212			ΔStb6	Control
5213			ΔStb6	Isolate 2

Table S3.1. *Zymoseptoria tritici* isolates analysed as part of this study.

Isolate code	Region of origin	Country of origin	Year collected	Wheat cultivar source	Wheat cultivar *Stb6* haplotype	*AvrStb6* haplotype	AvrStb6 isoform	Genbank accession number
Zt_001	Tasmania	Australia	2014	ND*	ND	H13	I14	MT856842
Zt_002	Tasmania	Australia	2014	ND	ND	H13	I14	MT856842
Zt_003	Tasmania	Australia	2014	ND	ND	H03	I02	MT856832
Zt_004	Tasmania	Australia	2014	ND	ND	H03	I02	MT856832
Zt_005	Tasmania	Australia	2014	ND	ND	H03	I02	MT856832
Zt_006	Tasmania	Australia	2014	ND	ND	H03	I02	MT856832
Zt_007	Tasmania	Australia	2014	ND	ND	H03	I02	MT856832
Zt_008	Tasmania	Australia	2014	ND	ND	H03	I02	MT856832
Zt_009	Tasmania	Australia	2014	ND	ND	H03	I02	MT856832
Zt_010	Tasmania	Australia	2014	ND	ND	H03	I02	MT856832
Zt_011	Tasmania	Australia	2014	ND	ND	H02	I02	MT856831
Zt_012	Tasmania	Australia	2014	ND	ND	H02	I02	MT856831
Zt_013	Tasmania	Australia	2014	ND	ND	H02	I02	MT856831
Zt_014	Tasmania	Australia	2014	ND	ND	H02	I02	MT856831
Zt_015	Tasmania	Australia	2014	ND	ND	H02	I02	MT856831
Zt_016	Tasmania	Australia	2014	ND	ND	H02	I02	MT856831
Zt_017	Tasmania	Australia	2014	ND	ND	H02	I02	MT856831
Zt_018	Tasmania	Australia	2014	ND	ND	H02	I02	MT856831
Zt_019	Tasmania	Australia	2014	ND	ND	H02	I02	MT856831
Zt_020	Tasmania	Australia	2014	ND	ND	H02	I02	MT856831
Zt_021	Tasmania	Australia	2014	ND	ND	H02	I02	MT856831
Zt_022	Tasmania	Australia	2014	ND	ND	H02	I02	MT856831
Zt_023	Tasmania	Australia	2014	ND	ND	H02	I02	MT856831
Zt_024	Tasmania	Australia	2014	ND	ND	H02	I02	MT856831
Zt_025	Tasmania	Australia	2014	ND	ND	H02	I02	MT856831
Zt_026	Tasmania	Australia	2014	ND	ND	H02	I02	MT856831
Zt_027	Tasmania	Australia	2014	ND	ND	H02	I02	MT856831
Zt_028	Tasmania	Australia	2014	ND	ND	H02	I02	MT856831
Zt_029	Tasmania	Australia	2014	ND	ND	H02	I02	MT856831
Zt_030	Tasmania	Australia	2014	ND	ND	H02	I02	MT856831
Zt_031	Tasmania	Australia	2014	ND	ND	H02	I02	MT856831
Zt_032	Tasmania	Australia	2014	ND	ND	H02	I02	MT856831
Zt_033	Tasmania	Australia	2014	ND	ND	H02	I02	MT856831
Zt_034	Tasmania	Australia	2014	ND	ND	H02	I02	MT856831
Zt_035	Tasmania	Australia	2014	ND	ND	H02	I02	MT856831
Zt_036	Tasmania	Australia	2014	ND	ND	H02	I02	MT856831
Zt_037	Tasmania	Australia	2014	ND	ND	H02	I02	MT856831
Zt_038	Tasmania	Australia	2014	ND	ND	H02	I02	MT856831
Zt_039	Tasmania	Australia	2014	ND	ND	H02	I02	MT856831
Zt_040	Tasmania	Australia	2014	ND	ND	H02	I02	MT856831
Zt_041	Tasmania	Australia	2014	ND	ND	H02	I02	MT856831
Zt_042	Tasmania	Australia	2014	ND	ND	H02	I02	MT856831
Zt_043	Tasmania	Australia	2014	ND	ND	H02	I02	MT856831
Zt_044	Tasmania	Australia	2014	ND	ND	H02	I02	MT856831
Zt_045	Tasmania	Australia	2014	ND	ND	H02	I02	MT856831
Zt_046	Tasmania	Australia	2014	ND	ND	H02	I02	MT856831
Zt_047	Tasmania	Australia	2014	ND	ND	H02	I02	MT856831
Zt_048	Tasmania	Australia	2014	ND	ND	H02	I02	MT856831
Zt_049	Tasmania	Australia	2014	ND	ND	H02	I02	MT856831
Zt_050	Tasmania	Australia	2014	ND	ND	H02	I02	MT856831
Zt_051	Tasmania	Australia	2014	ND	ND	H02	I02	MT856831
Zt_052	Tasmania	Australia	2014	ND	ND	H02	I02	MT856831
Zt_053	Tasmania	Australia	2014	ND	ND	H02	I02	MT856831
Zt_054	Tasmania	Australia	2014	ND	ND	H02	I02	MT856831
Zt_055	Tasmania	Australia	2014	ND	ND	H02	I02	MT856831

Zt_056	Tasmania	Australia	2014	ND	ND	H02	I02	MT856831
Zt_057	Tasmania	Australia	2014	ND	ND	H15	I02	MT856844
Zt_058	Tasmania	Australia	2014	ND	ND	H15	I02	MT856844
Zt_059	S. America	Chile	2016	Crac-baer	ND	H06	I02	MT856835
Zt_060	S. America	Chile	2016	Crac-baer	ND	H06	I02	MT856835
Zt_061	S. America	Chile	2016	Crac-baer	ND	H06	I02	MT856835
Zt_062	S. America	Chile	2016	Crac-baer	ND	H06	I02	MT856835
Zt_063	S. America	Chile	2016	Crac-baer	ND	H06	I02	MT856835
Zt_064	S. America	Chile	2016	Crac-baer	ND	H06	I02	MT856835
Zt_065	S. America	Chile	2016	Crac-baer	ND	H03	I02	MT856832
Zt_066	S. America	Uruguay	2016	Genesis INIA 2375	3 (S)	H02	I02	MT856831
Zt_067	S. America	Uruguay	2016	Genesis INIA 2375	3 (S)	H34	I29	MT856861
Zt_068	S. America	Uruguay	2016	Genesis INIA 2375	3 (S)	H02	I02	MT856831
Zt_069	S. America	Chile	2016	Crac-baer	ND	H02	I02	MT856831
Zt_070	S. America	Argentina	2016	DM Fuste	ND	H02	I02	MT856831
Zt_071	S. America	Argentina	2016	DM Fuste	ND	H02	I02	MT856831
Zt_072	S. America	Chile	2016	Crac-baer	ND	H36	I37	MT856863
Zt_073	S. America	Argentina	2016	DM Fuste	ND	H47	I03	MT856873
Zt_074	S. America	Uruguay	2016	Genesis INIA 2375	3 (S)	H04	I03	MT856833
Zt_075	S. America	Uruguay	2016	Genesis INIA 2375	3 (S)	H04	I03	MT856833
Zt_076	S. America	Uruguay	2016	Genesis INIA 2375	3 (S)	H04	I03	MT856833
Zt_077	S. America	Uruguay	2016	Genesis INIA 2375	3 (S)	H04	I03	MT856833
Zt_078	S. America	Uruguay	2016	Genesis INIA 2375	3 (S)	H04	I03	MT856833
Zt_079	S. America	Uruguay	2016	Genesis INIA 2375	3 (S)	H04	I03	MT856833
Zt_080	S. America	Uruguay	2016	INIA 2375	3 (S)	H04	I03	MT856833
Zt_081	S. America	Chile	2016	Crac-baer	ND	H04	I03	MT856833
Zt_082	S. America	Argentina	2016	DM Fuste	ND	H04	I03	MT856833
Zt_083	S. America	Argentina	2016	DM Fuste	ND	H04	I03	MT856833
Zt_084	S. America	Argentina	2016	DM Fuste	ND	H04	I03	MT856833
Zt_085	S. America	Argentina	2016	DM Fuste	ND	H04	I03	MT856833
Zt_086	S. America	Argentina	2016	DM Fuste	ND	H04	I03	MT856833
Zt_087	S. America	Argentina	2016	DM Fuste	ND	H04	I03	MT856833
Zt_088	S. America	Argentina	2016	DM Fuste	ND	H04	I03	MT856833
Zt_089	Mediterranean	Turkey	2013-16	ND	ND	H24	I41	-
Zt_090	Mediterranean	Turkey	2013-16	ND	ND	H25	I28	MT856852
Zt_091	Mediterranean	Turkey	2013-16	ND	ND	H27	I30	MT856854
Zt_092	Mediterranean	Turkey	2013-16	ND	ND	H28	I34	MT856855
Zt_093	Mediterranean	Turkey	2013-16	ND	ND	H29	I31	MT856856
Zt_094	Mediterranean	Turkey	2013-16	ND	ND	H14	I15	MT856843
Zt_095	Mediterranean	Turkey	2013-16	ND	ND	H14	I15	MT856843
Zt_096	Mediterranean	Turkey	2013-16	ND	ND	H32	I26	MT856859
Zt_097	Mediterranean	Turkey	2013-16	ND	ND	H17	I12	-
Zt_098	Mediterranean	Turkey	2013-16	ND	ND	H17	I12	-
Zt_099	Mediterranean	Turkey	2013-16	ND	ND	H38	I23	MT856865
Zt_100	Mediterranean	Turkey	2013-16	ND	ND	H39	I19	MT856866
Zt_101	Mediterranean	Turkey	2013-16	ND	ND	H40	I22	MT856867
Zt_102	Mediterranean	Turkey	2013-16	ND	ND	H44	I25	MT856871
Zt_103	Mediterranean	Turkey	2013-16	ND	ND	H45	I06	MT856872
Zt_104	Mediterranean	Turkey	2013-16	ND	ND	H46	I42	-
Zt_105	Mediterranean	Turkey	2013-16	ND	ND	H11	I06	MT856840
Zt_106	Mediterranean	Turkey	2013-16	ND	ND	H11	I06	MT856840
Zt_107	Mediterranean	Turkey	2013-16	ND	ND	H11	I06	MT856840
Zt_108	Mediterranean	Turkey	2013-16	ND	ND	H18	I06	MT856846
Zt_109	Mediterranean	Turkey	2013-16	ND	ND	H18	I06	MT856846
Zt_110	Mediterranean	Turkey	2013-16	ND	ND	H19	I16	MT856847
Zt_111	Mediterranean	Turkey	2013-16	ND	ND	H19	I16	MT856847

Zt_112	Mediterranean	Turkey	2013-16	ND	ND	H04	I03	MT856833
Zt_113	Mediterranean	Turkey	2013-16	ND	ND	H04	I03	MT856833
Zt_114	Mediterranean	Turkey	2013-16	ND	ND	H04	I03	MT856833
Zt_115	Mediterranean	Turkey	2013-16	ND	ND	H04	I03	MT856833
Zt_116	Mediterranean	Turkey	2013-16	ND	ND	H04	I03	MT856833
Zt_117	Mediterranean	Turkey	2013-16	ND	ND	H04	I03	MT856833
Zt_118	Mediterranean	Turkey	2013-16	ND	ND	H20	I18	MT856848
Zt_119	Mediterranean	Turkey	2013-16	ND	ND	H20	I18	MT856848
Zt_120	Mediterranean	Turkey	2013-16	ND	ND	H48	I24	MT856874
Zt_121	Mediterranean	Turkey	2013-16	ND	ND	H05	I04	MT856834
Zt_122	Mediterranean	Turkey	2013-16	ND	ND	H05	I04	MT856834
Zt_123	Mediterranean	Turkey	2013-16	ND	ND	H05	I04	MT856834
Zt_124	Mediterranean	Turkey	2013-16	ND	ND	H05	I04	MT856834
Zt_125	Mediterranean	Turkey	2013-16	ND	ND	H05	I04	MT856834
Zt_126	Mediterranean	Turkey	2013-16	ND	ND	H05	I04	MT856834
Zt_127	Mediterranean	Turkey	2013-16	ND	ND	H05	I04	MT856834
Zt_128	Mediterranean	Turkey	2013-16	ND	ND	H05	I04	MT856834
Zt_129	Mediterranean	Turkey	2013-16	ND	ND	H50	I32	MT856876
Zt_130	Mediterranean	Turkey	2013-16	ND	ND	H51	I43	MT856877
Zt_131	Mediterranean	Turkey	2013-16	ND	ND	H09	I08	MT856838
Zt_132	Mediterranean	Turkey	2013-16	ND	ND	H09	I08	MT856838
Zt_133	Mediterranean	Turkey	2013-16	ND	ND	H09	I08	MT856838
Zt_134	Mediterranean	Turkey	2013-16	ND	ND	H09	I08	MT856838
Zt_135	Mediterranean	Turkey	2013-16	ND	ND	H37	I40	MT856864
Zt_136	Mediterranean	Turkey	2013-16	ND	ND	H10	I09	MT856839
Zt_137	Mediterranean	Turkey	2013-16	ND	ND	H10	I09	MT856839
Zt_138	Mediterranean	Turkey	2013-16	ND	ND	H10	I09	MT856839
Zt_139	Mediterranean	Turkey	2013-16	ND	ND	H10	I09	MT856839
Zt_140	Mediterranean	Turkey	2013-16	ND	ND	H12	I11	MT856841
Zt_141	Mediterranean	Turkey	2013-16	ND	ND	H12	I11	MT856841
Zt_142	Mediterranean	Turkey	2013-16	ND	ND	H12	I11	MT856841
Zt_143	Mediterranean	Turkey	2013-16	ND	ND	H22	I10	MT856850
Zt_144	Mediterranean	Turkey	2013-16	ND	ND	H22	I10	MT856850
Zt_145	Mediterranean	Turkey	2013-16	ND	ND	H23	I10	MT856851
Zt_146	Oregon	USA	2016	Kaseberg	7 (S)	H31	I39	MT856858
Zt_147	Oregon	USA	2016	Kaseberg	7 (S)	H02	I02	MT856831
Zt_148	Oregon	USA	2016	Kaseberg	7 (S)	H02	I02	MT856831
Zt_149	Oregon	USA	2016	Kaseberg	7 (S)	H02	I02	MT856831
Zt_150	Oregon	USA	2016	Kaseberg	7 (S)	H02	I02	MT856831
Zt_151	Oregon	USA	2016	Kaseberg	7 (S)	H02	I02	MT856831
Zt_152	Oregon	USA	2016	Kaseberg	7 (S)	H02	I02	MT856831
Zt_153	Oregon	USA	2016	Kaseberg	7 (S)	H02	I02	MT856831
Zt_154	Oregon	USA	2016	Kaseberg	7 (S)	H02	I02	MT856831
Zt_155	Oregon	USA	2016	Kaseberg	7 (S)	H02	I02	MT856831
Zt_156	Oregon	USA	2016	Kaseberg	7 (S)	H02	I02	MT856831
Zt_157	Oregon	USA	2016	Kaseberg	7 (S)	H02	I02	MT856831
Zt_158	Oregon	USA	2016	Kaseberg	7 (S)	H02	I02	MT856831
Zt_159	Oregon	USA	2016	Kaseberg	7 (S)	H02	I02	MT856831
Zt_160	Oregon	USA	2016	Kaseberg	7 (S)	H02	I02	MT856831
Zt_161	Oregon	USA	2016	Kaseberg	7 (S)	H02	I02	MT856831
Zt_162	Oregon	USA	2016	Kaseberg	7 (S)	H02	I02	MT856831
Zt_163	Oregon	USA	2016	Kaseberg	7 (S)	H02	I02	MT856831
Zt_164	Oregon	USA	2016	Kaseberg	7 (S)	H02	I02	MT856831
Zt_165	Oregon	USA	2016	Kaseberg	7 (S)	H02	I02	MT856831
Zt_166	Oregon	USA	2016	Kaseberg	7 (S)	H02	I02	MT856831
Zt_167	Oregon	USA	2016	Kaseberg	7 (S)	H02	I02	MT856831
Zt_168	Oregon	USA	2016	Kaseberg	7 (S)	H02	I02	MT856831
Zt_169	Oregon	USA	2016	Kaseberg	7 (S)	H02	I02	MT856831
Zt_170	Oregon	USA	2016	Kaseberg	7 (S)	H02	I02	MT856831
Zt_171	Oregon	USA	2016	Kaseberg	7 (S)	H02	I02	MT856831
Zt_172	Oregon	USA	2016	Kaseberg	7 (S)	H02	I02	MT856831

Zt_173	Oregon	USA	2016	Kaseberg	7 (S)	H02	I02	MT856831
Zt_174	Oregon	USA	2016	Kaseberg	7 (S)	H02	I02	MT856831
Zt_175	Oregon	USA	2016	Kaseberg	7 (S)	H02	I02	MT856831
Zt_176	Oregon	USA	2016	Kaseberg	7 (S)	H02	I02	MT856831
Zt_177	Oregon	USA	2016	Kaseberg	7 (S)	H02	I02	MT856831
Zt_178	Oregon	USA	2016	Kaseberg	7 (S)	H02	I02	MT856831
Zt_179	Oregon	USA	2016	Kaseberg	7 (S)	H02	I02	MT856831
Zt_180	Oregon	USA	2016	Kaseberg	7 (S)	H02	I02	MT856831
Zt_181	Oregon	USA	2016	Kaseberg	7 (S)	H02	I02	MT856831
Zt_182	Oregon	USA	2016	Kaseberg	7 (S)	H02	I02	MT856831
Zt_183	Oregon	USA	2016	Kaseberg	7 (S)	H02	I02	MT856831
Zt_184	Oregon	USA	2016	Kaseberg	7 (S)	H02	I02	MT856831
Zt_185	Oregon	USA	2016	Kaseberg	7 (S)	H02	I02	MT856831
Zt_186	Oregon	USA	2016	Kaseberg	7 (S)	H02	I02	MT856831
Zt_187	Oregon	USA	2016	Kaseberg	7 (S)	H02	I02	MT856831
Zt_188	Oregon	USA	2016	Kaseberg	7 (S)	H02	I02	MT856831
Zt_189	Oregon	USA	2016	Kaseberg	7 (S)	H02	I02	MT856831
Zt_190	Oregon	USA	2016	Kaseberg	7 (S)	H08	I07	MT856837
Zt_191	Oregon	USA	2016	Kaseberg	7 (S)	H08	I07	MT856837
Zt_192	Oregon	USA	2016	Kaseberg	7 (S)	H08	I07	MT856837
Zt_193	Oregon	USA	2016	Kaseberg	7 (S)	H08	I07	MT856837
Zt_194	Oregon	USA	2016	Kaseberg	7 (S)	H08	I07	MT856837
Zt_195	Oregon	USA	2016	Kaseberg	7 (S)	H42	I20	MT856869
Zt_196	Oregon	USA	2016	Kaseberg	7 (S)	H43	I38	MT856870
Zt_197	Oregon	USA	2016	Kaseberg	7 (S)	H49	I35	MT856875
Zt_198	W. Europe	Scotland	2015	Consort KWS	7 (S)	H26	I27	MT856853
Zt_199	W. Europe	England	2015	Cashel	3 (S)	H30	I36	MT856857
Zt_200	W. Europe	England	2016	Cougar	1 (R)	H33	I02	MT856860
Zt_201	W. Europe	England	2015	Cougar	1 (R)	H03	I02	MT856832
Zt_202	W. Europe	England	2015	Cougar	1 (R)	H03	I02	MT856832
Zt_203	W. Europe	England	2015	Cougar	1 (R)	H03	I02	MT856832
Zt_204	W. Europe	England	2015	Santiago KWS	1 (R)	H03	I02	MT856832
Zt_205	W. Europe	England	2015	Consort	7 (S)	H03	I02	MT856832
Zt_206	W. Europe	England	2015	Gallant	7 (S)	H03	I02	MT856832
Zt_207	W. Europe	England	2015	Gallant	7 (S)	H03	I02	MT856832
Zt_208	W. Europe	England	2015	Gallant	7 (S)	H03	I02	MT856832
Zt_209	W. Europe	England	2015	Cashel KWS	3 (S)	H03	I02	MT856832
Zt_210	W. Europe	England	2015	Cashel KWS	3 (S)	H03	I02	MT856832
Zt_211	W. Europe	England	2015	Cashel KWS	3 (S)	H03	I02	MT856832
Zt_212	W. Europe	France	2015	Cellule	ND	H03	I02	MT856832
Zt_213	W. Europe	Germany	2015	Tobac	ND	H03	I02	MT856832
Zt_214	W. Europe	Germany	2015	Tobac	ND	H03	I02	MT856832
Zt_215	W. Europe	England	2015	Zulu	1 (R)	H03	I02	MT856832
Zt_216	W. Europe	England	2016	Cougar	1 (R)	H03	I02	MT856832
Zt_217	W. Europe	England	2016	Cordiale	7 (S)	H03	I02	MT856832
Zt_218	W. Europe	England	2016	Consort	7 (S)	H03	I02	MT856832
Zt_219	W. Europe	England	2016	Dickens	1 (R)	H03	I02	MT856832
Zt_220	W. Europe	England	2016	Dickens	1 (R)	H03	I02	MT856832
Zt_221	W. Europe	Ireland	2017	Lumos	7 (S)	H03	I02	MT856832
Zt_222	W. Europe	Ireland	2017	Lumos	7 (S)	H03	I02	MT856832
Zt_223	W. Europe	Scotland	2017	ND	ND	H03	I02	MT856832
Zt_224	W. Europe	Scotland	2017	ND	ND	H03	I02	MT856832
Zt_225	W. Europe	Scotland	2017	ND	ND	H03	I02	MT856832
Zt_226	W. Europe	England	2015	Cougar	1 (R)	H02	I02	MT856831
Zt_227	W. Europe	England	2015	Cougar	1 (R)	H02	I02	MT856831
Zt_228	W. Europe	England	2015	Cougar	1 (R)	H02	I02	MT856831
Zt_229	W. Europe	England	2015	Cougar	1 (R)	H02	I02	MT856831
Zt_230	W. Europe	England	2015	Cougar	1 (R)	H02	I02	MT856831
Zt_231	W. Europe	England	2015	Cougar	1 (R)	H02	I02	MT856831

Zt_232	W. Europe	England	2015	Cougar	1 (R)	H02	I02	MT856831
Zt_233	W. Europe	England	2015	Cougar	1 (R)	H02	I02	MT856831
Zt_234	W. Europe	England	2015	Cougar	1 (R)	H02	I02	MT856831
Zt_235	W. Europe	England	2015	Cougar	1 (R)	H02	I02	MT856831
Zt_236	W. Europe	France	2015	Trapez	1 (R)	H02	I02	MT856831
Zt_237	W. Europe	England	2015	Crusoe	7 (S)	H02	I02	MT856831
Zt_238	W. Europe	England	2015	JB Diego	7 (S)	H02	I02	MT856831
Zt_239	W. Europe	Scotland	2015	Consort	7 (S)	H02	I02	MT856831
Zt_240	W. Europe	Scotland	2015	Consort	7 (S)	H02	I02	MT856831
Zt_241	W. Europe	England	2015	Dickens	1 (R)	H02	I02	MT856831
Zt_242	W. Europe	England	2015	Gallant	7 (S)	H02	I02	MT856831
Zt_243	W. Europe	England	2015	Gallant	7 (S)	H02	I02	MT856831
Zt_244	W. Europe	England	2015	Gallant	7 (S)	H02	I02	MT856831
Zt_245	W. Europe	England	2015	Gallant	7 (S)	H02	I02	MT856831
Zt_246	W. Europe	England	2015	KWS Cashel	3 (S)	H02	I02	MT856831
Zt_247	W. Europe	England	2015	KWS Cashel	3 (S)	H02	I02	MT856831
Zt_248	W. Europe	England	2015	KWS Cashel	3 (S)	H02	I02	MT856831
Zt_249	W. Europe	England	2015	KWS Cashel	3 (S)	H35	I21	MT856862
Zt_250	W. Europe	England	2015	KWS Cashel	3 (S)	H02	I02	MT856831
Zt_251	W. Europe	England	2015	KWS Cashel	3 (S)	H02	I02	MT856831
Zt_252	W. Europe	England	2015	KWS Cashel	3 (S)	H02	I02	MT856831
Zt_253	W. Europe	England	2015	KWS Cashel	3 (S)	H02	I02	MT856831
Zt_254	W. Europe	England	2015	KWS Cashel	3 (S)	H02	I02	MT856831
Zt_255	W. Europe	England	2015	KWS Cashel	3 (S)	H02	I02	MT856831
Zt_256	W. Europe	England	2015	KWS Cashel	3 (S)	H02	I02	MT856831
Zt_257	W. Europe	England	2015	KWS Cashel	3 (S)	H02	I02	MT856831
Zt_258	W. Europe	England	2015	KWS Cashel	3 (S)	H02	I02	MT856831
Zt_259	W. Europe	England	2015	KWS Cashel	3 (S)	H02	I02	MT856831
Zt_260	W. Europe	England	2015	Cashel	3 (S)	H02	I02	MT856831
Zt_261	W. Europe	France	2015	Cellule	ND	H02	I02	MT856831
Zt_262	W. Europe	France	2015	Cellule	ND	H02	I02	MT856831
Zt_263	W. Europe	France	2015	Cellule	ND	H02	I02	MT856831
Zt_264	W. Europe	France	2015	Cellule	ND	H02	I02	MT856831
Zt_265	W. Europe	France	2015	Cellule	ND	H02	I02	MT856831
Zt_266	W. Europe	France	2015	Cellule	ND	H02	I02	MT856831
Zt_267	W. Europe	Germany	2015	JB Asano	ND	H02	I02	MT856831
Zt_268	W. Europe	Germany	2015	Tobac	ND	H02	I02	MT856831
Zt_269	W. Europe	Germany	2015	Tobac	ND	H02	I02	MT856831
Zt_270	W. Europe	Germany	2015	Tobac	ND	H02	I02	MT856831
Zt_271	W. Europe	Germany	2015	Tobac	ND	H02	I02	MT856831
Zt_272	W. Europe	Germany	2015	Tobac	ND	H02	I02	MT856831
Zt_273	W. Europe	Germany	2015	Tobac	ND	H02	I02	MT856831
Zt_274	W. Europe	Germany	2015	Tobac	ND	H02	I02	MT856831
Zt_275	W. Europe	Germany	2015	Tobac	ND	H02	I02	MT856831
Zt_276	W. Europe	England	2016	Cougar	1 (R)	H02	I02	MT856831
Zt_277	W. Europe	England	2016	Cougar	1 (R)	H02	I02	MT856831
Zt_278	W. Europe	England	2016	Cougar	1 (R)	H02	I02	MT856831
Zt_279	W. Europe	England	2016	Cougar	1 (R)	H02	I02	MT856831
Zt_280	W. Europe	England	2016	Cougar	1 (R)	H02	I02	MT856831
Zt_281	W. Europe	England	2016	Cougar	1 (R)	H02	I02	MT856831
Zt_282	W. Europe	England	2016	Evolution	1 (R)	H02	I02	MT856831
Zt_283	W. Europe	England	2016	Evolution	1 (R)	H02	I02	MT856831
Zt_284	W. Europe	England	2016	Evolution	1 (R)	H02	I02	MT856831
Zt_285	W. Europe	England	2016	Evolution	1 (R)	H02	I02	MT856831

Zt_286	W. Europe	England	2016	Evolution	1 (R)	H02	I02	MT856831
Zt_287	W. Europe	England	2016	Evolution	1 (R)	H02	I02	MT856831
Zt_288	W. Europe	England	2016	KWS Santiago	1 (R)	H02	I02	MT856831
Zt_289	W. Europe	England	2016	KWS Santiago	1 (R)	H02	I02	MT856831
Zt_290	W. Europe	England	2016	KWS Santiago	1 (R)	H02	I02	MT856831
Zt_291	W. Europe	England	2016	Alchemy	7 (S)	H02	I02	MT856831
Zt_292	W. Europe	England	2016	Cordiale	7 (S)	H02	I02	MT856831
Zt_293	W. Europe	England	2016	Cordiale	7 (S)	H02	I02	MT856831
Zt_294	W. Europe	England	2016	Cordiale	7 (S)	H02	I02	MT856831
Zt_295	W. Europe	England	2016	Cordiale	7 (S)	H02	I02	MT856831
Zt_296	W. Europe	England	2016	Cordiale	7 (S)	H02	I02	MT856831
Zt_297	W. Europe	England	2016	Cordiale	7 (S)	H02	I02	MT856831
Zt_298	W. Europe	England	2016	Cordiale	7 (S)	H02	I02	MT856831
Zt_299	W. Europe	England	2016	Cordiale	7 (S)	H02	I02	MT856831
Zt_300	W. Europe	England	2016	Cordiale	7 (S)	H02	I02	MT856831
Zt_301	W. Europe	England	2016	Cordiale	7 (S)	H02	I02	MT856831
Zt_302	W. Europe	England	2016	Cordiale	7 (S)	H02	I02	MT856831
Zt_303	W. Europe	England	2016	JB Diego	7 (S)	H02	I02	MT856831
Zt_304	W. Europe	England	2016	Reflection	7 (S)	H02	I02	MT856831
Zt_305	W. Europe	England	2016	Reflection	7 (S)	H02	I02	MT856831
Zt_306	W. Europe	England	2016	Reflection	7 (S)	H02	I02	MT856831
Zt_307	W. Europe	England	2016	Reflection	7 (S)	H02	I02	MT856831
Zt_308	W. Europe	England	2016	Reflection	7 (S)	H02	I02	MT856831
Zt_309	W. Europe	England	2016	Consort	7 (S)	H02	I02	MT856831
Zt_310	W. Europe	England	2016	Consort	7 (S)	H02	I02	MT856831
Zt_311	W. Europe	England	2016	Consort	7 (S)	H02	I02	MT856831
Zt_312	W. Europe	England	2016	Consort	7 (S)	H02	I02	MT856831
Zt_313	W. Europe	England	2016	Consort	7 (S)	H02	I02	MT856831
Zt_314	W. Europe	England	2016	Consort	7 (S)	H02	I02	MT856831
Zt_315	W. Europe	England	2016	Consort	7 (S)	H02	I02	MT856831
Zt_316	W. Europe	England	2016	Consort	7 (S)	H02	I02	MT856831
Zt_317	W. Europe	England	2016	Consort	7 (S)	H02	I02	MT856831
Zt_318	W. Europe	Scotland	2016	Consort	7 (S)	H02	I02	MT856831
Zt_319	W. Europe	Scotland	2016	Consort	7 (S)	H02	I02	MT856831
Zt_320	W. Europe	Scotland	2016	Consort	7 (S)	H02	I02	MT856831
Zt_321	W. Europe	England	2016	Dickens	1 (R)	H02	I02	MT856831
Zt_322	W. Europe	England	2016	Dickens	1 (R)	H02	I02	MT856831
Zt_323	W. Europe	England	2016	Dickens	1 (R)	H02	I02	MT856831
Zt_324	W. Europe	England	2016	Dickens	1 (R)	H02	I02	MT856831
Zt_325	W. Europe	England	2016	Dickens	1 (R)	H02	I02	MT856831
Zt_326	W. Europe	England	2016	Dickens	1 (R)	H02	I02	MT856831
Zt_327	W. Europe	England	2016	Dickens	1 (R)	H02	I02	MT856831
Zt_328	W. Europe	England	2016	Dickens	1 (R)	H02	I02	MT856831
Zt_329	W. Europe	England	2016	Dickens	1 (R)	H02	I02	MT856831
Zt_330	W. Europe	England	2016	Dickens	1 (R)	H02	I02	MT856831
Zt_331	W. Europe	England	2016	Dickens	1 (R)	H02	I02	MT856831
Zt_332	W. Europe	England	2016	Dickens	1 (R)	H02	I02	MT856831
Zt_333	W. Europe	England	2016	Dickens	1 (R)	H02	I02	MT856831
Zt_334	W. Europe	England	2016	Dickens	1 (R)	H02	I02	MT856831
Zt_335	W. Europe	England	2016	Dickens	1 (R)	H02	I02	MT856831
Zt_336	W. Europe	England	2016	Dickens	1 (R)	H02	I02	MT856831
Zt_337	W. Europe	England	2016	Dickens	1 (R)	H02	I02	MT856831
Zt_338	W. Europe	England	2016	Dickens	1 (R)	H02	I02	MT856831
Zt_339	W. Europe	England	2016	Dickens	1 (R)	H02	I02	MT856831
Zt_340	W. Europe	England	2016	KWS Cashel	3 (S)	H02	I02	MT856831
Zt_341	W. Europe	England	2016	Marston	1 (R)	H02	I02	MT856831
Zt_342	W. Europe	England	2016	Zulu	1 (R)	H02	I02	MT856831
Zt_343	W. Europe	Unknown	2016	ND	ND	H02	I02	MT856831
Zt_344	W. Europe	Unknown	2016	ND	ND	H02	I02	MT856831

Zt_345	W. Europe	England	2017	Siskin	1 (R)	H02	I02	MT856831
Zt_346	W. Europe	England	2017	Siskin	1 (R)	H02	I02	MT856831
Zt_347	W. Europe	England	2017	Siskin	1 (R)	H02	I02	MT856831
Zt_348	W. Europe	England	2017	Siskin	1 (R)	H02	I02	MT856831
Zt_349	W. Europe	England	2017	Siskin	1 (R)	H02	I02	MT856831
Zt_350	W. Europe	England	2017	Siskin	1 (R)	H02	I02	MT856831
Zt_351	W. Europe	England	2017	Siskin	1 (R)	H02	I02	MT856831
Zt_352	W. Europe	England	2017	Siskin	1 (R)	H02	I02	MT856831
Zt_353	W. Europe	England	2017	Siskin	1 (R)	H02	I02	MT856831
Zt_354	W. Europe	England	2017	Siskin	1 (R)	H02	I02	MT856831
Zt_355	W. Europe	England	2017	Siskin	1 (R)	H02	I02	MT856831
Zt_356	W. Europe	England	2017	Siskin	1 (R)	H02	I02	MT856831
Zt_357	W. Europe	England	2017	Siskin	1 (R)	H02	I02	MT856831
Zt_358	W. Europe	Ireland	2017	Lumos	7 (S)	H02	I02	MT856831
Zt_359	W. Europe	Ireland	2017	Lumos	7 (S)	H02	I02	MT856831
Zt_360	W. Europe	Ireland	2017	Lumos	7 (S)	H02	I02	MT856831
Zt_361	W. Europe	Ireland	2017	Lumos	7 (S)	H02	I02	MT856831
Zt_362	W. Europe	Ireland	2017	Lumos	7 (S)	H02	I02	MT856831
Zt_363	W. Europe	Scotland	2017	ND	ND	H02	I02	MT856831
Zt_364	W. Europe	Scotland	2017	ND	ND	H02	I02	MT856831
Zt_365	W. Europe	Scotland	2017	ND	ND	H02	I02	MT856831
Zt_366	W. Europe	Scotland	2017	ND	ND	H02	I02	MT856831
Zt_367	W. Europe	Scotland	2017	ND	ND	H02	I02	MT856831
Zt_368	W. Europe	ND	ND	ND	ND	H02	I02	MT856831
Zt_369	W. Europe	England	2016	Cordiale	7 (S)	H02	I02	MT856831
Zt_370	W. Europe	England	2016	ND	ND	H16	I13	MT856845
Zt_371	W. Europe	Ireland	2017	Lumos	7 (S)	H16	I13	MT856845
Zt_372	W. Europe	France	2015	Trapez	1 (R)	H07	I05	MT856836
Zt_373	W. Europe	France	2015	Cellule	ND	H07	I05	MT856836
Zt_374	W. Europe	France	2015	Cellule	ND	H07	I05	MT856836
Zt_375	W. Europe	England	2016	Solace	1 (R)	H07	I05	MT856836
Zt_376	W. Europe	England	2016	Amplify	ND	H07	I05	MT856836
Zt_377	W. Europe	England	2016	Stratosphere	ND	H07	I05	MT856836
Zt_378	W. Europe	France	2015	Cellule	ND	H41	I33	MT856868
Zt_379	W. Europe	England	2015	Cougar	1 (R)	H04	I03	MT856833
Zt_380	W. Europe	England	2015	KWS Cashel	3 (S)	H21	I17	MT856849
Zt_381	W. Europe	Germany	2015	JB Asano	ND	H21	I17	MT856849

Table S4.1: List of putative AvrStb6 interactors from yeast two-hybrid library screen assay

Putative interactor name	Top *T. aestivum* BLAST hit	Alignment length, bp (query length, bp)	Alignment ID (%)	Identified domains	Domain description
P5C1	TraesCS1D02G404800	531 (543)	100	Glutaredoxin-like/Thioredoxin-like superfamily (GRX/TRX)	GRX/TRX is involved in many cellular functions including **DNA synthesis**, **signal transduction** and the defense against **oxidative stress**
P11C4	TraesCS3D02G517100	513 (750)	100	Abscisic acid/water deficit stress induced protein (ABA/WDS)	This is a family of plant proteins **induced by water deficit stress** (WDS), or **abscisic acid** (ABA) stress and ripening
P8C5	TraesCS7A02G198800	530 (633)	99.8	CAP protein superfamily	The cysteine-rich **secretory proteins**, antigen 5, and **pathogenesis-related** 1 proteins (CAP) superfamily of proteins
P4C2	TraesCS1D02G404800	408 (420)	100	Glutaredoxin-like/Thioredoxin-like superfamily	GRX/TRX is involved in many cellular functions including **DNA synthesis**, **signal transduction** and the defense against **oxidative stress**
P10C3	TraesCS5A02G524800	280 (600)	100	Dihydrodipicolinate reductase; NAD(P)-binding domain superfamily	Dihydrodipicolinate reductase (DHDPR), a product of an essential gene referred to as dapB, catalyzes the second step of **lysine biosynthesis**. Many different enzymes contain an NAD/NADP-binding domain, including **alcohol dehydrogenase**.
P9C3	TraesCS2A02G206100	219 (510)	100	Protein Thf1	Thf1 protein (also known as Psb29) is found in Cyanobacteria and in the plastids of vascular plants. They may

					function in the **biogenesis of Photosystem II complexes**
P3C4	TraesCS4B02G356100	112 (378)	100	NADH oxidase; Aldolase-type TIM barrel	TIM beta/alpha barrel found in aldolase and in related proteins - found in many enzyme families that catalyse completely unrelated reactions
P3C3	TraesCS2D02G141100	95 (192)	100	Mul1-like E3 Ubiquitin ligase; Zinc finger, RING type	Mul1 is an E3 ubiquitin ligase anchored in the outer **mitochondrial membrane** with its RING finger domain facing the cytoplasm. Plays a role in the control of mitochondrial morphology, promotes mitochondrial fragmentation and influences mitochondrial localisation
P11C1	TraesCS7D02G118100	93 (233)	100	Ubiquitin-associated protein	UBAP1 is a subunit of ESCRT-I, a complex facilitating endosomal sorting of ubiquitinated cargo
P6C4	TraesCS6B02G439600	83 (243)	98.8	Signal transduction histidine kinase; GAF domain	Phosphoacceptor domain superfamily found in some **histidine kinases**; GAF domains found in cGMP-specific phosphodiesterases, **adenylyl cyclases** and FhlA. It is also found in and **guanylyl cyclases** and **phytochromes**

Table S4.2: Protein alignment hits for AvrStb6 isoforms

Top Hit Description	Further Information	Confidence (%)	ID (%)	Shared with other Isoforms
AvrStb6 I01				
Plant protein	Kalata ("kb1[ghrw;23-28]")	32.4	53	I02, I44
Immunoglobulin-like beta-sandwich	RhoGDI-like	21.8	28	I44
Transcription	Zinc-finger domain in kiaa10642 protein	20.2	26	I02, I44
Signalling protein	Protein unc-119 homolog a	16.6	41	I44
Alpha-alpha superhelix	Clathrin heavy-chain linker domain	14.6	31	None
AvrStb6 I02				
Toxin	Insectidal toxin delta-paluit2-nh2	58	40	I01, I44
Resistin	Hormone/growth factor	33.3	47	None
Zinc Finger	CCCH zinc finger	26.5	60	I01
Transcription	Zinc-finger domain in kiaa10642 protein	24.5	26	I02, I44
Hydrolase	Endoglucanase eg-1	16.7	36	I01, I44
AvrStb6 I44				
Immunoglobulin-like beta-sandwich	RhoGDI-like	24	29	I01
Signalling protein	Protein unc-119 homolog a	17.5	47	I01
Transcription	Zinc-finger domain in kiaa10642 protein	10.1	26	I01, I02
Signalling protein	Granulin-a	10.1	67	I01
Toxin	Conotoxin gm9.1	9.1	75	I01, I02

Table S4.3: Predicted disulphide bridge formation in AvrStb6 isoforms

AvrStb6 Isoform	Predicted Connectivity (cysteine residue number)					
I01	1-4	2-5	3-8	6-7	9-12[1]	10-11
I02	1-3[1]	2-8	4-10	5-7	6-11	9-12[1]
I03	1-4	2-7	3-6	5-8	9-10	11-12
I05	1-3[1]	2-4	5-8	6-11	7-10	9-12[1]
I07	1-2	3-4	5-8	6-11	7-10	9-12[1]
I13	1-3[1]	2-8	4-10	5-7	6-11	9-12[1]
I14	1-3[1]	2-4	5-8	6-7	9-10	11-12
I17	1-11	2-7	3-9	4-10	5-6	8-12
I21	1-3[1]	2-8	4-10	5-7	6-11	9-12[1]
I27	1-3[1]	2-4	5-8	6-7	9-12[1]	10-11
I44	1-4	2-6	3-7	5-8	9-11	10-12

[1]Cysteine connections predicted for more than half of analysed isoforms.